INFORMATION TO USERS

This manuscript has been reproduced from the microfilm master. UMI films the text directly from the original or copy submitted. Thus, some thesis and dissertation copies are in typewriter face, while others may be from any type of computer printer.

The quality of this reproduction is dependent upon the quality of the copy submitted. Broken or indistinct print, colored or poor quality illustrations and photographs, print bleedthrough, substandard margins, and improper alignment can adversely affect reproduction.

In the unlikely event that the author did not send UMI a complete manuscript and there are missing pages, these will be noted. Also, if unauthorized copyright material had to be removed, a note will indicate the deletion.

Oversize materials (e.g., maps, drawings, charts) are reproduced by sectioning the original, beginning at the upper left-hand corner and continuing from left to right in equal sections with small overlaps. Each original is also photographed in one exposure and is included in reduced form at the back of the book.

Photographs included in the original manuscript have been reproduced xerographically in this copy. Higher quality 6" x 9" black and white photographic prints are available for any photographs or illustrations appearing in this copy for an additional charge. Contact UMI directly to order.

UMI®

Bell & Howell Information and Learning
300 North Zeeb Road, Ann Arbor, MI 48106-1346 USA
800-521-0600

EXCITED-STATE COORDINATION CHEMISTRY: A NEW QUENCHING MECHANISM

by
Charles Hicks

A dissertation submitted to the
Graduate Faculty in Chemistry
in partial fulfillment of the
requirements for the degree
of Doctor of Philosophy, the
City University of New York

2000

This Manuscript has been read and accepted by the Graduate Faculty in Chemistry in satisfaction of the dissertation requirement for the degree of Doctor of Philosophy.

9/13/00
Date

Chair of Examining Committee

9/18/00
Date

Executive Officer

Michael Drain

John Lombardi

Supervisory Committee

City University of New York

Abstract

EXCITED STATE COORDINATION CHEMISTRY:
A NEW QUENCHING MECHANISM

by

Charles Hicks

Advisor: Harry Gafney

Changes in Bronsted acid-base behavior in the excited state have been well established among organic molecules as well a transition metal complexes. Though the ideas of Lewis acid-base chemistry are well established in the ground state, no clear examples as such, exist in the excited state. Reported here are some examples of such interactions. There are a number of reasons that this type of interaction is more difficult to observe, including the time constraint due to the unquenched lifetime of the excited state, competitive relaxation by quenching pathways, and in many cases the formation of only transient products. Despite these difficulties, we present a number of cases where this type of interaction is apparent.

Diimine complexes of Ru(II) have been reported to have values of ΔpKa as large as 7.0. In this work evidence is presented for an excited state acid-base interaction between $[Ru(bpy)_2dpp](ClO_4)_2$ (bpy = 2,2'-bipyridine, dpp = 2,3-Bis(2-pyridyl)pyrazine), and a number of coordination complexes. In some cases the availability of a stable product allows an excited state interaction to lead to a net chemical change as in the case of $PtCl_6^{2-}$.

$$*Ru(bpy)_2dpp^{2+} + PtCl_6^{2-} \longrightarrow Ru(bpy)_2dppPtCl_4^{2+} + 2Cl^-$$

In other cases, such as the interaction of Ag^{+} with $^{*}Ru(bpy)_2dpp^{2+}$, a product can form between the donor and quencher and it does readily by thermal pathways. Therefore, though the equilibrium shifts in the excited state, it recedes to the ground state equilibrium position upon relaxation, resulting in no net chemical change.

These processes have been characterized by measurement of the lifetime and intensity quenching, as well as the decline in emission intensity associated with product accumulation, and correlation of the rate of product accumulation measured directly. The latter two methods serve as an independent check of the Stern-Volmer quenching model used. The family of quenchers studied have been chosen for a variety of reasons including, their likelihood to undergo, or fail to undergo other mechanisms of quenching. as well as their character as a chemical family with known similarities and differences.

Acknowledgement

To Harry Gafney, Dave Baker, and the memory of Dave Tischler. All of whom helped me get past difficult failures with their kind words of encouragement.

TABLE OF CONTENTS

List of Figures

List of Tables

Symbol Key

A_T – The total absorbance of a solution.

*D - An excited state species which is a potential energy donor.

ε - The molar absorptivity constant.

f - The fraction of I_a absorbed by a particular species.

f_{de}- The fraction of emitted light which reaches the detector.

f_D – The fraction total light absorbed by the solution which is absorbed by a particular component.

I^{em}- The emission intensity observed under conditions of steady state irradiation.

I_o^{em}- The emission intensity observed under conditions of steady state irradiation in the absence of any quencher.

I_a- The fraction of excitation light incident upon the sample window which is absorbed by a solution.

I_{de} - The fraction of the total emitted light which was incident upon the detector.

I_o- The incident light intensity.

I_o^{em}- The emission intensity observed under conditions of steady state irradiation in the absence of quencher.

*K_a – The equilibrium constant for excited state acid-base equilibrium.

k_{aq} – The rate constant for substitution of a ligand by water treated as a pseudo first-order process (s^{-1}).

k_{bim} - The rate constant for formation of a bimetallic species thermally.

k_{dif} - The diffusional rate constant for a particular solvent ($M^{-1}s^{-1}$).

*k_{dp} - The rate constant for deprotonation of an excited state species (s^{-1}).

K_{ep} - The equilibrium constant for formation of an encounter pair.

K_{ES} – The equilibrium constant for association of Ag^+ and $Ru(bpy)_2dpp^{2+}$ in the excited state.

K_1 - The first stepwise formation constant for ligation of a metal.

K_{GS} – The equilibrium constant for association of Ag^+ and $Ru(bpy)_2dpp^{2+}$ in the ground state.

K_{IP} - The equilibrium constant for formation of an ion pair.

k_{nr} - The non-radiative rate constant (s^{-1}).

$*k_p$- The rate constant for protonation of an excited state species treated as a pseudo first order process in aqueous solution (s^{-1}).

k_q - The rate constant for quenching of an excited state species ($M^{-1}s^{-1}$).

k_{qp} - The rate constant for quenching of an excited state species which results in product formation ($M^{-1}s^{-1}$).

k_r - The radiative rate constant (s^{-1}).

K_{S0} - The equilibrium constant for excited state acid base equilibrium involving the ground singlet state.

$*K_{S1}$ - The equilibrium constant for excited state acid base equilibrium involving the first excited singlet state.

$^PK_{sv}$, - The Stern-Volmer quenching constant for product formation quenching (M^{-1}).

$^QK_{sv}$ -The Stern-Volmer quenching constant for simple quenching (M^{-1}).

$^TK_{sv}$ - The total Stern-Volmer quenching constant (M^{-1}).

$*K_{T1}$ - The equilibrium constant for excited state acid base equilibrium involving the first triplet state.

λ - Wavelength of light.

μ - Ionic strength.

τ_o- The lifetime of a particular species in the absence of any quencher..

τ_{dp}- Lifetime of the deprotonated form of a particular species .

τ_p- Lifetime of the protonated form of a particular species .

P – A product species.

Q - A species which by interaction with an excited state species reduces the emission intensity.

ϕ_{em} - The quantum yield of emission.

ϕ_p- The quantum yield of product formation.

T- Temperature (K).

ν_A or ν_B - The wavenumber of the 0-0 transition in the absorption spectrum of the acid or conjugate base respectively (cm^{-1}).

η - Viscosity (poise).

V - Voltage

I Introduction

(1) General Introduction

The absorption of a photon by a molecule changes its chemical nature. The excited state produced differs from the ground state in possessing more energy, and often a wave function of lower symmetry. The effect of having more energy can be to simply facilitate processes that were available thermally. For instance, most excited state species are better oxidizing and reducing agents than the ground state of the molecule. Reactions that are endothermic from the ground state will be less so, or might be exothermic relative to the excited. The products of such a process are necessarily unstable with respect to the ground state starting materials and will undergo re-equilibration after relaxation to the ground state.

More striking however, is availability of new pathways. Thermal reactions proceed by pathways mediated by the availability of energy from the surroundings. These lowest energy pathways are a kinetic barrier to higher energy pathways, in the sense that molecules are funneled down them, before having the opportunity to achieve a high enough energy to enter a new mode of reaction. For instance, thermal substitution of H_20 in $Rh(NH_3)_5Br^{2+}$ proceeds exclusively with displacement of a bromide ion, the poorest ligand in the sense of binding to the metal.[1]

$$Rh(NH_3)_5Br^{2+} + H_2O \xrightarrow{\Delta} Rh(NH_3)_5(H_2O)^{3+} + Br^- \quad (1)$$

However, the photosubstitution, resulting from excitation into the LMCT state, proceeds predominantly with displacement of NH_3 The quantum yields for loss of $NH_3$and Br^- in water with 366 nm irradiation, are .18, and .02, respectively.[1]

Figure 1. Depiction of the energy scheme of a molecule D, in the ground and excited state (*D), as well as oxidized (D^+) and reduced (D^-) forms, showing that while the oxidized and reduced forms may be unstable with respect to the ground state, they may be stable with respect to the excited state.

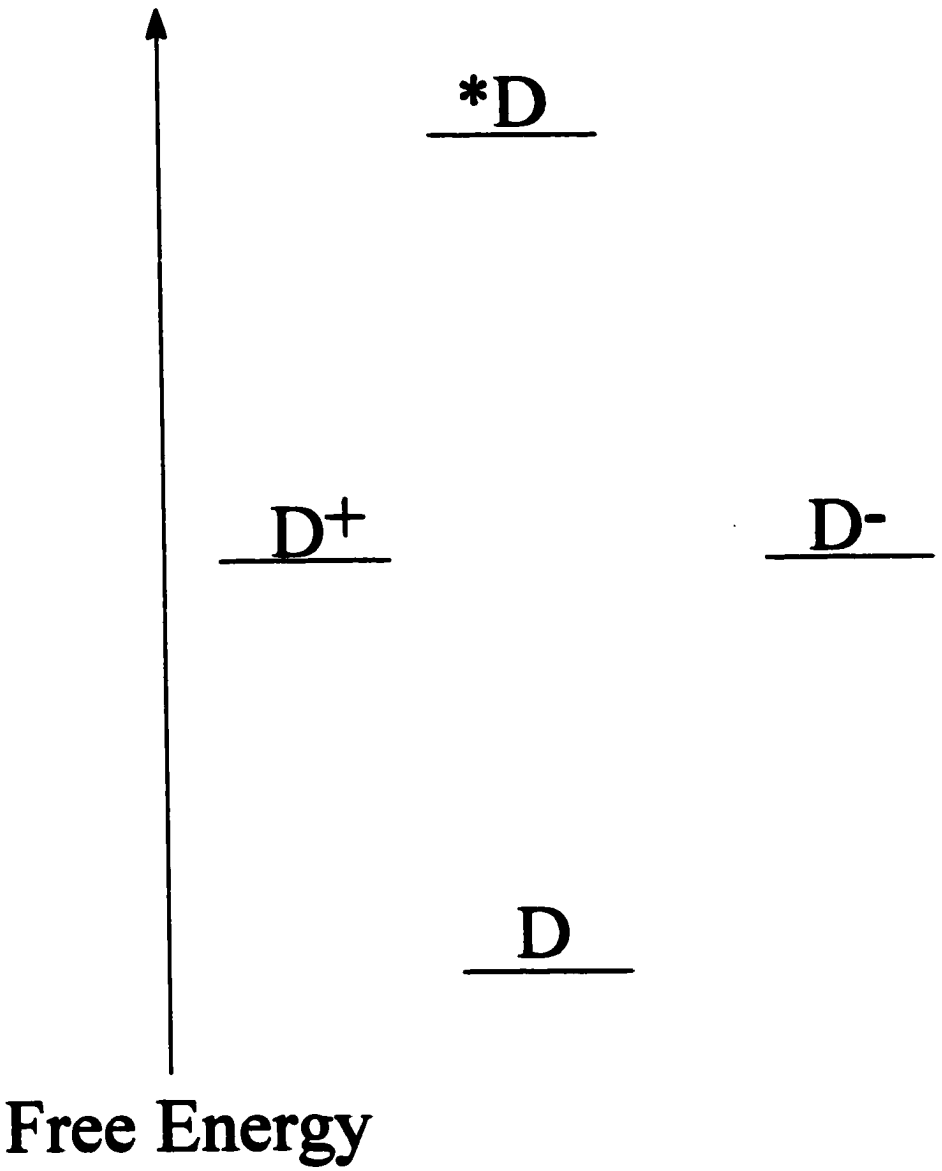

$$Rh(NH_3)_5Br^{2+} \xrightarrow{h\nu} Rh(NH_3)_4Br^{2+} + NH_3 \qquad (2)$$

The profound differences between ground and excited state chemistry are not due to energy considerations alone, but are also due to the differing symmetry between the ground and excited state. Among organic molecules, an excellent example of this concept exists in electrocyclic reactions, and is summarized in the Woodward-Hoffman rules.[2] These rules predict the stereochemistry observed, as a result of the disrotary or conrotary mode of reaction observed in electrocyclic reactions, based upon orbital symmetry considerations. As a result of the differing symmetry of the ground and excited states, a complementary chemistry is observed between them, in which a mode of reaction forbidden for the ground state, is allowed in the excited state and vice-versa. A similar set of rules have been shown to control the photosubstitution among some complexes of Cr(III).[3]

Though in both of these examples, new pathways lead to different products, new pathways might be created which lead to products also attainable thermally. This is observed in many ligand-photosubstition reactions, where the stereochemistry allows for only a single product. While the photochemical and thermal pathways might be very different, the availability of only a single product makes the photosubstitution appear simplistically to be an acceleration of the thermal reaction. For instance, Rh(III) amines have been heavily studied due to their slow thermal substitution chemistry. However, photoaquation

$$Rh(NH_3)_6^{3+} + H_2O \xrightarrow{h\nu} Rh(NH_3)_5(H_2O)^{3+} + Cl^- \qquad (3)$$

is relatively efficient, occurring with a quantum yields in the range .07-.09. Reaction of

eq 3 is believed to occur by intersystem crossing to the lowest energy triplet ligand-field state.[4] Although the products are the same, the pathways certainly are not.

The advent of high power pulsed lasers in the past thirty-five years, has radically improved the invasiveness of the techniques used in photochemistry. Before the availability of the nitrogen laser, flashlamps and stop-flow techniques were the most time invasive techniques available. They made accessible observation of events on the microsecond timescale. For instance, lifetimes of organic triplets that must undergo spin forbidden relaxation could be measured. However, events on the nanosecond or faster timescale were inaccessible. This controlled the scope of postulation of the chemistry of the excited state. With diffusion of a molecular distance on the order of a nanosecond, these techniques observed only an overall chemistry averaged over thousands of molecular events. The ability of pulsed laser techniques to probe chemical reactions on the timescale that they are happening, has shown, for instance, that electron transfer from a metal complex can take place within femtoseconds of excitation.[5] Whereas, 30 years ago whether or not excited state electron transfer even occurred in a simple coordination compound, was not established even though it was recognized to occur in photosynthesis. This was due to the fact that the resultant transient products had never been observed, and the simplest explanation consistent with the excited state quenching was that energy transfer was the operative mechanism.

Energy-transfer quenching was the first established quenching mechanism of the emission from transition metal complexes.[6] It has the distinction of being the simplest mechanistic explanation for overall transfer of energy from an excited donor to an acceptor. It postulates no chemical change, transitory or overall, only the migration of the

excitation energy from donor to acceptor. Its efficiency is therefore largely dependent upon the exothermicity of the process and is determined by the energy level spacings inherent to the donor and quencher.

(2) Models of Excited State Processes

After absorption of a photon (eq 4), the excited state produced can relinquish its energy by some of the pathways depicted in eqs 5-7

Process	Rate	
$D + h\nu \xrightarrow{k_1} {}^*D$	I_a	(4)
${}^*D \xrightarrow{k_r} D + h\nu'$	$[{}^*D]k_r$	(5)
${}^*D \xrightarrow{k_{nr}} D + \Delta$	$[{}^*D]k_{nr}$	(6)
${}^*D + Q \xrightarrow{k_q} D + Q$	$[{}^*D][Q]k_q$	(7)

where $h\nu'$ and Δ, represent emission, and dissipation of heat to the surroundings. The rate of formation of the excited state of the donor (*D), is equal to ${}^DI_a$ the rate of absorption of photons by the donor (D). ${}^DI_a$ can be expressed in terms of the incident light intensity I_o and the absorbance of the D.

$$I_a = I_o(1-10^{-\epsilon B[D]}) \tag{8}$$

In the absence of a *quencher* (Q), D decays by only first-order processes with rate constants k_r and k_{nr}, the *radiative*, and *non-radiative rate constants*, respectively.

$$\frac{d[{}^*D]}{dt} = I_a - [{}^*D](k_r + k_{nr}) \tag{9}$$

(3) Diffusion-Limited Processes

In fluid solution all *bimolecular processes* occur at a rate mediated by the solvent. The rate of bimolecular collision to form an *encounter pair* (EP), and reversible formation of A and B, the pre-encounter species,

$$A + B \underset{k_{-dif}}{\overset{k_{dif}}{\rightleftharpoons}} EP \qquad (10)$$

is characterized by k_{dif} and k_{-dif}, the rate constants for the forward and reverse steps of eq 10 . In contrast to gas phase reactions, bimolecular processes in solution are often treated as the formation of an encounter pair, as in eq 10. The advantage of this is that it allows for the introduction of a rate constant that depends upon the rate of diffusion within the solvent. Subsequent processes, such as quenching, are treated as first order processes in EC, characterized by the rate constant k_1.

$$EC \xrightarrow{k_1} C \qquad (11)$$

If the kinetics are cast in this way, the observed rate constant for a bimolecular process ($^{obs}k_2$) is a composition of rate constants.

$$^{obs}k_2 = \frac{k_1}{k_1 + k_{dif}} k_{dif} \qquad (12)$$

The coefficient of k_{dif} is sometimes represented by α, the probability that the event whose rate is characterized by k_2 will take place during the encounter. If k_2 is much smaller than k_{dif}, the observed rate is necessarily smaller than k_{dif}. If k_2 is much greater than k_{dif}, then the observed value will approach k_{dif}. The actual value for k_{dif} depends upon the

molecular size and shape of A and B, but it is useful that an upper limit can be placed on it equal to that observed for an aqueous proton, often taken to be 10^{10} $M^{-1}s^{-1}$. Processes whose values of ^{obs}k approach 10^{10} $M^{-1}s^{-1}$, in aqueous solution are said to be diffusion-limited, since the formation of EP is the rate determining step. Rate constants observed to be in excess of this upper limit, likely reflect the inclusion of non-diffusional processes. For example, the quenching which occurs between a donor and quencher that are ion-paired upon excitation are said to undergo static quenching, because the donor can undergo quenching by its ion-paired partner, without having to undergo diffusion first. Therefore, static quenching can occur more rapidly than the corresponding diffusional encounter.

Values of k_{dif} reflect the *viscosity* of the solvent (η), and in turn the difficulty with which diffusion occurs in it, due to steric interference and the intermolecular forces between the solvent and reactants. Though as a quantitative parameter, viscosity is not very precise, since properties other than the viscosity itself, such as solvent dielectric constant and the structure of the solvation shell, vary in even the most carefully chosen solvent series. Additionally, the mode of reaction itself might change as the solvation shell changes since this will change the probability of escape of the reactants from the solvent cage. Since the viscosity is really a bulk property, the model that relates it to the microenvironment at the molecular level cannot take account of the details of molecular shape and size. The variation of the rate constant with η has been postulated to be,[7]

$$k_{dif}(M^{-1}s^{-1}) = \frac{2.0\times10^{5}T}{\eta} \qquad (13)$$

with η in poise and T expressed in degrees Kelvin.

(4) Stern-Volmer Quenching

In the presence of a quencher acting in a diffusional encounter as depicted in eq 7, in addition to first order decay processes, the rate of decay is also mediated by the concentration of Q

$$\frac{d[^*D]}{dt} = I_a - [^*D](k_r + k_{nr} + [Q]k_q) \qquad (14)$$

Under conditions of constant concentration of quencher, after a pulsed excitation, *D undergoes a natural exponential decay. This allows measurement of the excited state lifetime (τ), from the intensity decay. It is assumed that the concentration of *D, is proportional to the emitted light intensity (I^{em}), and is often measured orthogonal to the excitation pathway. The emitted light can be used to generate a photocurrent in a photomultipler tube in proportion to the emitted intensity. The current can then be converted to a voltage drop across a load resistor, and voltage drop measured in the time domain by an oscilloscope. Such a setup was used in this laboratory to measure excited-state lifetimes. For a simple one component decay, $\tau = 1/(k_r + k_{nr} + k_q[Q])$, can be measured from oscilloscope traces, as the value of -1/slope of a plot of ln(V) versus time, since $\ln(V) \propto \ln[^*D]$.

$$\ln[^*D] = \ln[^*D_o] - t/\tau \qquad (15)$$

The determination of τ by this method is independent of the initial excitation intensity, and therefore $[^*D]_o$. It is also free of other artifacts, such as competitive absorption of the excitation or emitted light intensity. Competitive absorption of the excitation intensity occurs due to the overlap of the absorption spectra of the quencher

and donor at the excitation wavelength. Competitive absorption of light by the quencher reduces the initial intensity. This can be compensated for experimentally by increasing the excitation intensity or voltage across the photomultiplier, so as to obtain measurable emission intensity. Competitive absorption of the emitted light is also called trivial or radiative energy transfer, it is due to overlap of the absorption spectrum of the quencher and the emission spectrum of the donor. It occurs by a mechanism involving emission of light by the donor and subsequent absorption by the quencher. It does not involve an encounter between the two. In the case of trivial radiative energy transfer, the quencher can be thought of as an inner filter blocking the emission, effectively reducing the measured intensity at all points by a factor equal to the fraction of light it absorbs. This fraction can be related to the total absorbance of the solution and its components using a modified version of Beers Law,

$$A = \varepsilon BC \tag{16}$$

where A is the absorbance measured, ε is the molar absorptivity of the absorbing species, B is the pathlength the light must traverse, and C is the concentration of the absorbing species. The average path through the sample for an emitted photon to the detector is taken to be 1/2 the path length of the cell used in the experiment, which faces the detector. The fraction of light blocked by this inner filter is therefore $1\text{-}10^{-(\varepsilon B[Q]/2)}$.

While both mechanisms act to reduce the observed intensities, neither affects the decay kinetics. Therefore, evaluation of τ is independent of both of these trivial effects. The Stern-Volmer equation applicable to lifetime data is the most reliable method by which to evaluate diffusional quenching.

$$\frac{\tau_o}{\tau} = K_{sv}[Q] + 1 \qquad (17)$$

In this equation τ_o, is the lifetime of the donor in the absence of quencher, τ, is the lifetime of the donor as a function of quencher concentration and K_{sv} is the *Stern-Volmer constant* defined in terms of the various rate constants for deactivation of the excited state as

$$K_{sv} = \frac{k_q}{(k_r + k_{nr})} \qquad (18)$$

Generally speaking K_{sv} is the ratio of the bimolecular quenching rate constant to the sum of the first-order rate constants. Its inverse is the concentration of quencher required to reduce τ, or I by a factor of two.

Under conditions of constant irradiation, in the absence of quencher, after a period of time much greater than τ, the concentration of excited donor (*D), becomes independent of time. A steady-state approximation for this concentration allows $[^*D]_{ss}$ to be expressed in terms of the rate constants for the decay processes and the rate of light absorption.

$$\frac{d[^*D]}{dt} = I_a - [^*D]_{ss}(k_r + k_{nr}) = 0 \qquad (19)$$

$$[D]_{ss} = \frac{^D I_a}{k_r + k_{nr}} \qquad (20)$$

The *unquenched emission intensity* (I_o^{em}) depends upon the fraction of emitted light that reached the detector (f_{de}), as well as the fraction of the incident radiation absorbed by the ground state of the D (^DI_a).

$$I_o^{em} = \frac{dhv'}{dt} = \frac{f_{de} I_a k_r}{k_r + k_{nr}} \tag{21}$$

Equation 20 can be used to measure the quantum yield of emission (ϕ_{em}), the ratio of first-order rate constants,

$$\phi_{em} = \frac{k_r}{k_r + k_{nr}} \tag{22}$$

without measuring either I_a, or f_{dc}. This is done by measuring the emission intensity of the molecule in question, as well as the intensity of a material for which ϕ_{em} is known. These solutions must have either the same absorbance at the excitation wavelength, or else the emission intensity must be corrected by dividing each solution's emission intensity by the factor ($1-10^{-A}$), which is the fraction of the incident light absorbed by the solution. Use of a standard for which the value of ϕ_{em}, is known allows for elimination of the factor $f_{dc}I_o$ from eq 21.

$$\frac{\phi_1}{\phi_2} = \frac{I_1^{em}}{I_2^{em}} \tag{23}$$

In the presence of quencher, the emission intensity is given by

$$I^{em} = \frac{I_a k_r}{(k_r + k_{nr}) + [Q]k_q} \tag{24}$$

Dividing eqs 21 and 24, gives the Stern-Volmer equation applicable to steady-state emission intensity data

$$\frac{I_o^{em}}{I^{em}} = 1 + K_{sv}[Q] \tag{25}$$

Stern-Volmer analysis of lifetime and intensity quenching data uses equations 17 and 25. Plots of τ_o/τ and I_o/I versus [Q] will have slopes equal to the Stern-Volmer constant (K_{sv}), if all quenching is diffusional. Otherwise, the intensity data will reflect other modes of reaction, such as static quenching. The intercept of both plots should be within experimental error of unity.

(5) Static Quenching

If the simple scheme outlined in eqs 4-7 holds, then Stern-Volmer plots, I_o/I or τ_o/τ versus [Q] will have the same slopes within experimental error. Deviations from this behavior are often encountered if the donor and quencher are of opposite charge. In this case, a tendency to form ion pairs leads to a two component, time-resolved intensity decay, and an increase in the apparent values of K_{sv} obtained from intensity data with increasing quencher concentration. The relatively rapid rate of decay of a donor ion paired to a quencher molecule makes it easily separable from the diffusional component in the time domain. If the detection system's bandwidth limits the time resolution to a few nanoseconds, effectively filtering out this component by its inability to resolve it. The true value of K_{sv} is then only obtained from Stern-Volmer plots of lifetime data. In this case, the emission data can be used to extract the equilibrium constant for ion pairing by fitting it to[8]

$$\frac{I_o^{ss}}{I^{ss}} = 1 + (K_{sv} + \beta K_{eq})[Q] + \beta K_{sv} K_{eq}[Q]^2 \qquad (26)$$

In this equation, β is equal to1 if the solutions are optically dilute, otherwise it is equal to the ratio of the molar absorptivity of the ion-pair to the donor,$\varepsilon_{DQ}/\varepsilon_D$, at excitation wavelength.

In some cases reported in this work, quenching is associated with formation of a bond, so that instead of, or in addition to, simple quenching (eq 7), a step such as

$$*D + Q \xrightarrow{k_{qp}} P \qquad \frac{d[P]}{dt} = k_{qp}[*D][Q] \tag{27}$$

can be considered. Under conditions of constant irradiation, a steady-state approximation is valid for *D, and substitution into eq 27 yields

$$\frac{d[P]}{dt}_{ss} = \frac{I_a[Q]k_q}{k_r + k_{nr} + [Q]k_q} \tag{28}$$

Since the quantum yield of product formation (ϕ_p), is measured under conditions of constant irradiation, this equation can be rearranged yielding,

$$\phi_p = \frac{d[P]/dt}{I_a} = \frac{[Q]k_{qp}}{k_r + k_{nr} + [Q]k_{qp}} \tag{29}$$

This equation can be rearranged to give a linear dependence if the dependent and independent variables are taken to be $1/\phi_p$ and 1/[Q]. It is most often expressed in terms of K_{sv}, which was defined earlier yielding

$$\frac{1}{\phi_p} = 1 + \frac{1}{K_{sv}[Q]} \tag{30}$$

A plot of 1/slope of $1/\phi_p$ versus 1/[Q] will have slope equal to $1/K_{sv}$. If the intercept is not within experimental error of unity, or the value of K_{sv} obtained is not in agreement with the value obtained from lifetime quenching, then inclusion of both simple and product forming quenching steps yields,

$$\frac{1}{\phi_p} = \frac{k_r + k_{nr}}{k_{qp}[Q]} + \frac{k_{qp} + k_q}{k_{qp}} \tag{31}$$

The introduction of a second bimolecular quenching process forces distinctions to be made between 3 possible designations of K_{sv}:

$$^{T}K_{sv} = \frac{k_q + k_{qp}}{k_r + k_{nr}} \tag{32}$$

$$^{P}K_{sv} = \frac{k_{qp}}{k_r + k_{nr}} \tag{33}$$

$$^{Q}K_{sv} = \frac{k_q}{k_r + k_{nr}} \tag{34}$$

$^{T}K_{sv}$ is the total Stern-Volmer constant, $^{P}K_{sv}$ is the Stern-Volmer constant for product formation, and $^{Q}K_{sv}$ is the Stern-Volmer constant for simple quenching. Examination of eq 31 shows that plots of $1/\phi_p$ versus 1/[Q] will have a slope equal to $1/^{P}K_{sv}$, and the ratio of intercept to slope will be equal to $^{T}K_{sv}$. Since each of the Stern-Volmer constants have the same denominator they are of course simply additive, $^{T}K_{sv} = {}^{P}K_{sv} + {}^{Q}K_{sv}$.

With the inclusion of the step shown in eq 27, in addition to directly monitoring product formation, steady-state emission intensity should be time dependent. This is due to the decrease in the concentration of D, and resulting decrease in the concentration of *D. However eqs 35 and 36 are coupled, so that they must be solved numerically for [*D] and [P], before the time dependence of the decline in steady-state emission can be predicted.

$$\frac{d[P]}{dt} = [^*D]([Q]_o - [P])k_{qp} \tag{35}$$

$$\frac{d[^*D]}{dt} = I_a - (k_r + k_{nr})[^*D] - [^*D]([Q]_o - [P](k_q + k_{qp}) \tag{36}$$

$$\frac{dh\nu'}{dt} = k_r[^*D] \tag{37}$$

In practice, the methodology implemented in our laboratory was to collect the lifetime and intensity (steady-state irradiation) quenching data as well as the time dependence of the steady-state emission intensity. The Stern-Volmer quenching law for intensity quenching becomes the theory that accounts for the initial intensities in the experiments in which the steady-state intensity decays with time. These experiments must be analyzed obtaining numerical solutions to eqs 35 - 37. In order to eliminate the need to measure an instrumental parameter that determines the fraction (f_{de}) of emitted light that reaches the detector (I_{de}),

$$I_{de} = f_{de}[^*D]k_r \tag{38}$$

the following procedure was used. The initial intensities for a series of trials initial intensities were checked for consistency with the Stern-Volmer quenching law (i.e. $I_o/I = 1 + {}^{T}K_{sv}[Q]$). In the case of static quenching by ion-pairs the data was checked for agreement between lifetime quenching and intensity quenching data under conditions of low quencher concentration. If the initial intensities were consistent, the data was normalized to the same arbitrary initial value, as the experimental data. Effectively this is equivalent to measuring a relative quantum yield, since all the factors that determine the

observed intensity that are instrumental, can be eliminated by comparison to a standard under the same instrumental conditions.

The contribution of ion pairing leads to larger apparent values of ${}^{T}K_{s}$, as concentration of quencher increases. This is because an ion-paired donor and acceptor, upon excitation, are in such close proximity, that they do not need to diffuse into an encounter pair in order to undergo quenching. Therefore, this fraction of excited states decays much more rapidly than the fraction free in solution.

Treating the ion-pair with a simple equilibrium model,

$$D + Q \longrightarrow IP \tag{39}$$

leads to the solution,

$$[IP] = \frac{1}{2}\left[[Q]_o + [D]_o + \frac{1}{K_{IP}} - \sqrt{\left([Q]_o + [D]_o + \frac{1}{K_{IP}}\right)^2 - 4[Q]_o[D]_o}\right] \tag{40}$$

where $[D]_o$ and $[Q]_o$ are the initial concentrations of donor and quencher, respectively. The negative root must be the solution in this system, since the stoichiometry dictates

$$[IP] \leq [D] \text{ or } [IP] \leq [Q] \tag{41}$$

and choice of the positive root can yield values of [IP] as large as $[D] + [Q] + 1/K_{IP}$. The term $4[Q]_o[R]_o$ is always positive making the expression within the square root sign smaller than $[Q]_o+[R]_o+1/K_{IP}$. Taking the limit of [IP] as $[Q]_o$ approaches zero shows that in the infinite dilution limit, the fraction of donor that is ion-paired must approach zero. This limit of zero ion pairing at infinite dilution is used to estimate the ${}^{P}K_{sv}$, from data complicated by ion pairing, by an extrapolation technique that is discussed in greater detail later.

(6) Mechanisms of quenching

The process depicted by eq 7 represents a number of potential mechanisms, including collisional energy transfer, oxidative or reductive electron transfer, and proton or atom transfer.

(6.1) Collisional Energy Transfer

Collisional energy transfer consists of transfer of energy during a diffusional collision, in which an excited state of the quencher is produced while the donor is relaxed to its ground state. It is the simplest scheme kinetically, since no chemical change takes place in deactivating the excited state. At 25° C the efficiency of collisional energy transfer for processes endothermic by more than a few kJ, is very low. The rate of collisional energy transfer depends on the degree of overlap of resonant states of the excited donor and the acceptor. This overlap integral, denoted J, is the relative overlap of the donors emission, and acceptor's absorption spectrum, after being suitably normalized such that complete overlap would correspond to J equal to one, in a domain proportional to energy (Figure 2).

(6.2) Electron Transfer

The mechanism of electron-transfer quenching requires that a reduction-oxidation reaction occur between the donor and acceptor pair resulting in deactivation of the donor. This pair can undergo back reaction prior to diffusing apart or diffuse apart and undergo the back reaction in a subsequent encounter. In the latter case, the rate constant of the back reaction is less than k_{dif}, whereas in the former case, it can be significantly larger. Electron transfer can occur reductively or oxidatively, specified with respect to the donor.

Figure 2. The spectral overlap integral between the absorption spectrum of $PtCl_6^{2-}$ and the emission spectrum of $Ru(bpy)_2dpp^{2+}$ used to estimate the efficiency of energy transfer from $Ru(bpy)_2dpp^{2+}$ to $PtCl_6^{2-}$.

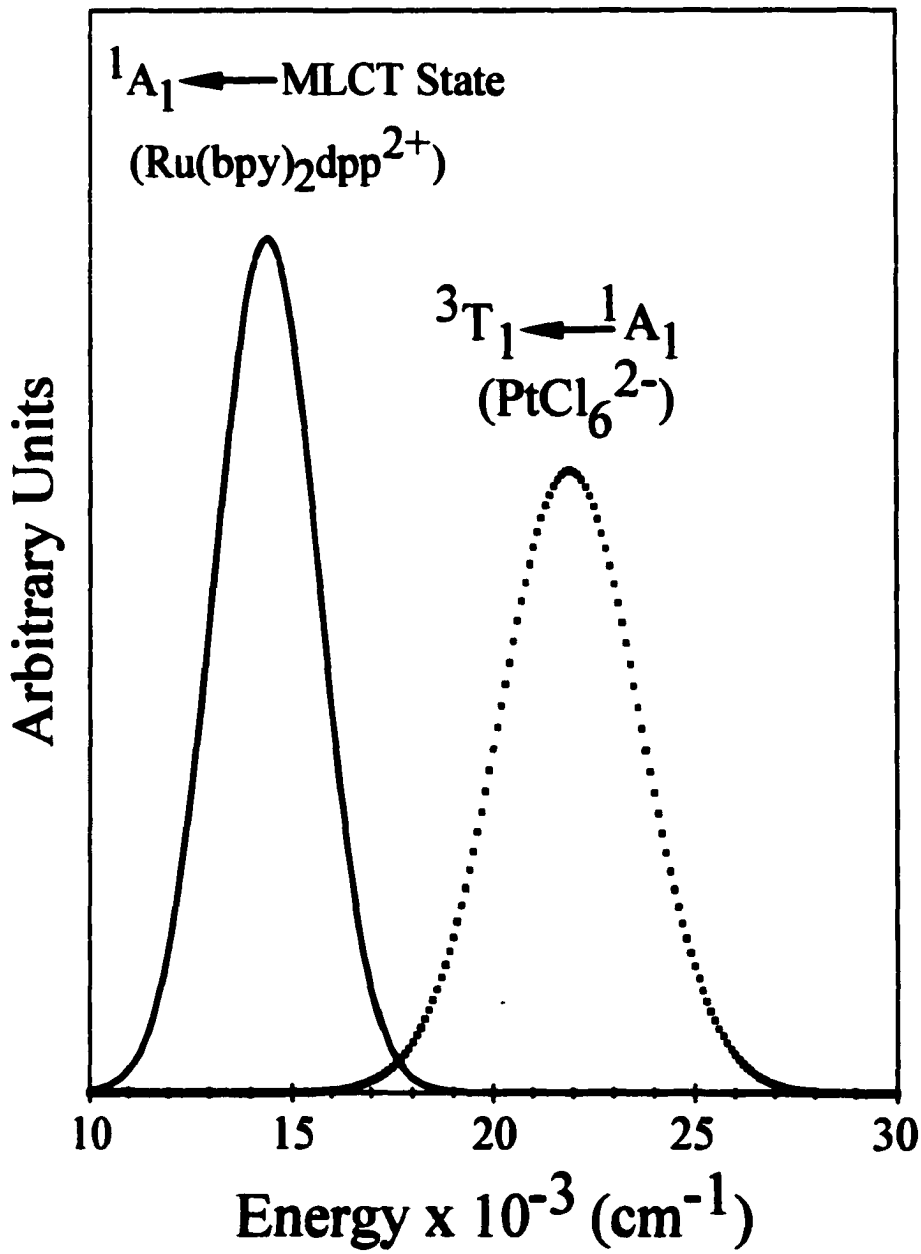

The intensive study of thermal electron transfer, in the context of Marcus theory, has elucidated much information. The most startling being the experimental confirmation of an inverted region (i.e. a range over which increases in driving force actually slow the rate of reaction). Many factors influence the rate, including solvent atmosphere, magnitude of bond length changes for the process, and inherent self-exchange rate. However, the best predictor of the feasibility of an electron transfer as a quenching mechanism is its overall thermodynamic driving force.[9]

The mechanism of electron-transfer quenching involves a reduction-oxidation reaction that does not have a favorable free energy change in the ground state. Since the excited state is meta-stable with respect to the ground state, any overall process which effects its deactivation has in its favor a free energy term equal to the energy of the excited state. The free energy for the redox pair that formed from electron transfer quenching, to escape from the encounter pair to a solvent separated ion-pair (ssip), without reforming the starting materials, can be estimated from the Weller equation, neglecting entropy differences between the ground and excited states. The Weller equation for reductive quenching is

$$\Delta G_{ssip} = E(A/A^-) - E(D^+/D) - E(^*D) - e^2/\varepsilon_r d_{ssip} \qquad (42)$$

In this equation: ΔG_{ssip} is the free energy change to form a solvent separated ion-pair, $E(A/A^-)$ and $E(D^+/D)$ are the reversible ground state reduction potentials for the acceptor and donor, respectively. $E(^*D)$ is the energy of the excited state of the donor while the latter term, $e^2/\varepsilon d_{ssip}$, is a coulombic term for the separation of the pair. In this term ε_r is the dielectric constant of the solvent and d_{ssip} is the charge separation distance of the solvent-separated ion-pair. In solvents with high dielectric constant, such as water,

this term is can be neglected. The potentials are often expressed in volts, and since all known mechanisms involve single electron transfers, these potentials coincide with the energy values expressed in electron volts.

The Weller equation can be expressed for oxidative quenching, though regardless of whether oxidative or reductive quenching is considered the term for the energy of the excited state makes a negative contribution to the overall driving force. This is an indication that all excited states are potentially stronger oxidizing and reducing agents. The coulombic term, $e^2/\varepsilon_r d_{ssip}$, is often neglected in water with its large dielectric constant, $\varepsilon_r = 80$. In this case, escape from the solvent cage is not considered at all as a pathway, and the free energy term calculated is for the formation of the redox pair. Under these conditions it is termed an electron exchange mechanism.

If escape from the ion pair occurs, the products then undergo recombination by diffusional processes to reform the starting materials. In either case, the overall result of the process is transfer of energy from donor to acceptor, with at most transitory chemical change. This of course is due to the fact that the favorable driving force for the redox reaction only exists in the excited state.

(6.3) Atom Transfer

Atom transfer quenching has been observed in aromatic ketones. For instance, Benzophenone,

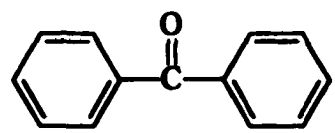

Benzophenone

is luminescent in fully halogenated solvents at room temperature, and has τ equal to 700μs.[10] However, in alcohol no luminescence can be detected and the lifetime of the triplet state estimated from competitive energy-transfer experiments is 10 ns. Rapid intermolecular H atom transfer quenches the phosphorescence.[11]

$$^3(Ar_2CO)^* + ROH \longrightarrow (Ar_2COH) + RO^{\cdot} \qquad (43)$$

(6.4) Proton Transfer

Because the proton is a zero electron species it does not possess excited-electronic states. It also is very difficult to reduce to a hydrogen atom, so the observation that the emission intensity of different molecules is dependent upon proton concentration led to the realization that excited molecules can possess acid-base properties quite different from those of the ground state. Subsequent studies of organic molecules in particular, have shown that optical excitation can dramatically increase or decrease the acid-base properties of a molecule. More recent studies show that metal complexes, can exhibit similar changes in acid-base properties, although in these molecules, the change in properties arise from a charge transfer transition, which literally rearrange the electron density between ligand and metal.

Proton transfer has been determined to be the mechanism of quenching, in many systems wherein the donor exhibits excited-state enhancement of basicity. This pathway of quenching can be the result of greater efficiency of deactivation, if protonation improves solvent coupling, thereby enhancing the non-radiative rate constant. Certainly coupling to the solvent has an effect on k_{nr}, as suggested by comparing complexes with ligands containing carboxy functional groups. Esterification of carboxylated diimine

ligands raises the values of both τ and ϕ_{em}, of the corresponding Ru(II)complex[12] This implies that k_{nr} must have decreased since increasing ϕ_{em} requires either increasing k_r or decreasing k_{nr}. However, τ also increases implying that $k_r + k_{nr}$ must get smaller, which can only happen by k_{nr} diminishing. In contrast to this situation however, quenching can also occur as a result of chemical quenching (i.e. production of a new species). In the case of proton quenching, the new species produced is just the protonated form of the molecule. Although this is a small structural change, its effect on the electronic structure can be profound. Take for example any well-known acid-base indicator, the change in electronic structure upon exchange of a proton is so clear it can be detected in trace amounts by the naked eye. In fact, the Forster cycle uses this change in electronic structure to predict the change in the ionization constants, between the ground and excited states. The inherent emission properties of a new species must be viewed as potentially very different, and this point is borne out well in the case of $Ru(bpy)_2(dcbxy\text{-}bpy)^{2+}$ (dcbxy-bpy = 2,2'-bipyridine-4,4'-dicarboxylic acid). The protonated and twice deprotonated forms have been shown to have been shown to have lifetimes of to τ_p = 320 ns, and τ_{dp} =395.[13] (there has been some difference of opinion on the precise values[14]) the relative emission intensity of the protonated form is ca. 1% that of the deprotonated form.[12] Solving for the ratio of radiative rate constants for the protonated and deprotonated form

$$\frac{\frac{^{dp}\phi_{em}}{^{dp}\tau}}{\frac{^{p}\phi_{em}}{^{p}\tau}} = \frac{^{dp}k_r}{^{p}k_r} = 82 \qquad (44)$$

Figure 3. Structure and photophysical properties of $Ru(bpy)_2(4,4'\text{-dcbxy})^{2+}$ and its twice deprotonated form.

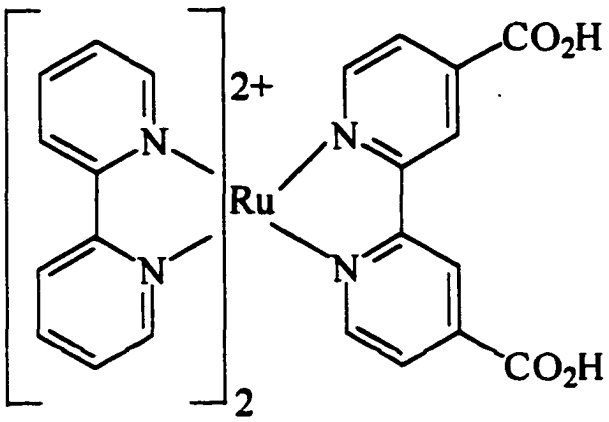

$\tau = 320$ ns.

$^{rel}\phi_{em} = .010$

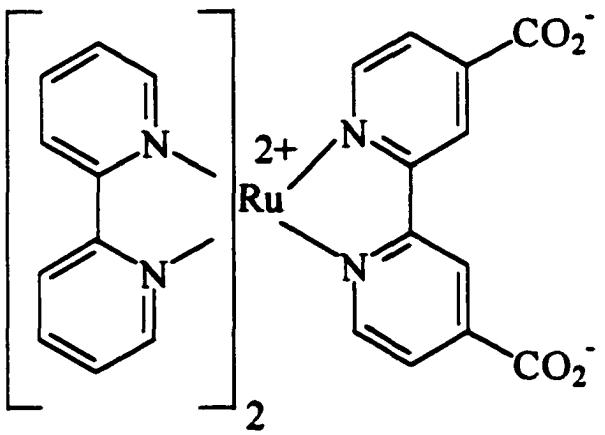

$\tau = 395$ ns.

$^{rel}\phi_{em} = 1.0$

shows that k_r declines by a factor of 82, going from protonated to the twice deprotonated form. This suggests that 82% of the difference between the two form's emission properties can be attributed to a decline in the radiative rate constant, while only 12% is due to an increase in the efficiency of non-radiative pathways. (Figure 3). It is well known that the radiative rate constant is independent or at best weakly dependent upon the medium. Rather, it depends on the internal properties of the molecule itself. Therefore the differences observed, at least in this case, have little do due with solvent coupling, but rather the production of a new species with different inherent emission properties. The observation of quenching of protonable molecules in the presence of acid is not necessarily a result of deactivation of the excited state, since it might also reflect a reduction in the efficiency of radiative pathways. These two examples considered together show the importance of measuring of both τ and ϕ_{em} to understand the nature of quenching processes.

Proton quenching has been reported for both organic and inorganic compounds, though many of the organics that do emit, do so from both protonated and deprotonated forms. On the other hand, there are few examples of inorganics, where both forms emit. The only additional examples of complexes where both forms emit in aqueous solution, that we are aware of, are $Ru(TAP)_3^{2+}$ for which both the monoprotonated and hexaprotonated forms are emissive,[15] and $Ru(bpz)_3^{2+}$ for which all six protonated forms are emissive[16]

(7) Excited State Acid-Base Properties of Organic Molecules

Absorption of a photon changes the acid-base properties of many molecules. The first observation of changes in acid-base properties in the excited state was made by

Weber,[17] who observed the pH dependence of the emission from 1-napthylamine-4-sulphonate. More quantitative work performed subsequently by Weller[18] on β-napthol revealed a decline in pK_a of 6.3 units in going from the ground to the first excited-state singlet.

However, much more moderate changes were observed between the ground and excited triplet states. For example in the case of β-naptholamine,

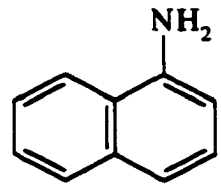

β-Naptholamine

for the triplet and singlet excited states respectively, values of ΔpK_a equal to .9[19] and -6.1[20] were obtained. The triplets were generated by energy transfer and the value represents an average values of $^*pK_a$ determination from two methods; phosphorescence and transient absorbance. The equilibrium for the conjugate acids of the protonated amines being,

$$^1RNH_3^+ + H_2O \rightleftharpoons {}^1RNH_2 + H_3O^+ \qquad pK_{S0} = -4.1 \qquad (45)$$

$$^{1*}RNH_3^+ + H_2O \rightleftharpoons {}^{1*}RNH_2 + H_3O^+ \qquad pK_{S1} = 1.9 \qquad (46)$$

$$^{3*}RNH_3^+ + H_2O \rightleftharpoons {}^{3*}RNH_2 + H_3O^+ \qquad pK_T = -3.2 \qquad (47)$$

where pK_{S0}, pK_{S1}, and pK_T are the pK_a's for the ground state, first excited singlet and triplet state species, respectively.

Within the model used in these systems, four forms are assumed to be present in equilibrium, the protonated and deprotonated forms, of both the ground and excited state (Figure 4) The work of both Weller and Forster assumed equilibration was rapid relative to the lifetime of all species involved.

Equilibration must be at least partially obtained within the lifetime of the excited state, in order to see any change in pK_a. A criterion often taken for the attainment of excited-state equilibrium requires that the rate of deactivation of the excited species be assumed to be much slower than the rate of protonation or deprotonation.[21] Therefore in the case of the deprotonated form we require,

$$[B^-]({}^{dp}k_r + {}^{dp}k_{nr}) \ll [B^-][H^+]k_p \tag{48}$$

$$1/\tau_{dp} \ll k_p[H^+] \tag{49}$$

and for the protonated form,

$$[BH]({}^{p}k_r + {}^{p}k_{nr}) \ll [BH]k_{dp} \tag{50}$$

$$1/\tau_p \ll k_{dp} \tag{51}$$

where the superscipts p and dp denote the protonated and deprotonated forms, respectively. In addition, it should be noted that in the excited state, equilibrium must be defined differently than it is in the ground state, since differing lifetimes of the protonated and deprotonated forms lead to a time dependent ratio of the various species. The position of equilibrium constantly shifts since the concentrations of faster decaying components, are declining more rapidly than slower components, by decay processes unrelated to the acid-base equilibrium.

Figure 4. Scheme showing the four species assumed to be involved in the equilibrium established in the excited state.

In the case that excited state equilibrium is not established, the values that are obtained represent only a partial equilibration, since the system's ground state equilibrium position was unable to shift far enough to be at excited-state equilibrium within its time in the excited state. Therefore, the failure to approach excited-state equilibrium leads to underestimates of ΔpK_a. Though it has been suggested that equilibration can be assured athigh buffer concentrations[22], most data available in the literature is obtained under conditions of moderate buffer concentration, including that obtained in strong acid and base. Therefore, the magnitude of reported values of ΔpK_a are generally reported as lower limits for the true value.

Experimental values of $^*pK_a$ can be obtained from fluorometric titration curves. The emission intensity I^{em}, at the wavelength of maximum intensity of either or both protonated and deprotonated forms is monitored as a function of pH through a series of buffer solutions. Under sufficiently acidic and basic conditions the intensity of the protonated and deprotonated forms becomes independent of pH. This intensity is taken as the inherent emission of that form, and in the Stern-Volmer convention is designated I_o^{em}. Plots of I^{em}/I_o^{em}, for protonated and deprotonated forms have an "S" shape, similar to ground state titration curves. While the differences in lifetime play a role in determining the steady-state concentrations, the concentrations themselves are time independent after $t >> \tau_p$ or τ_{ϕ} if eqs 49 and 51 are satisfied then

$$K_a = \frac{[H_3O][^*B^-]}{[BH\ ]} \tag{52}$$

If the two emissions overlap significantly, the intensity values should be corrected for overlap of each. The correction used in this work was taken from the literature.[21]

$$ {}^{p}I_{corr} = \frac{{}^{p}I_{obs} - c'\,{}^{dp}I_{obs}}{1 - cc'} \tag{53} $$

$$ {}^{dp}I_{corr} = \frac{{}^{dp}I_{obs} - c\,{}^{p}I_{obs}}{1 - cc'} \tag{54} $$

In these equations, the superscipts p and dp denote protonated and deprotonated forms, the subscripts obs and corr denote observed and corrected emission intensities. The constants c and c' refer are the values of the protonated and deprotonated forms emission intensities at the wavelength used for determination of the other form. The values of c and c', must be measured under conditions where each is considered to be the only form present

The value of $*pK_a$, uncorrected for differences in lifetime of the excited state species, is taken to be the inflection point of a fluorometric titration curve, assuming that excited state equilibrium is attained. Data for the protonated and deprotonated forms will obey eqs 55 and 56. ^{p}I and ^{dp}I refer to the emission intensity of the protonated and deprotonated forms, respectively.[23]

$$ \frac{{}^{p}I}{{}^{p}I_{o}} = \frac{1 + k_{p}[H_3O^{+}]\tau_{p}}{1 + k_{dp}\tau_{dp} + k_{p}\tau_{p}[H_3O^{+}]} \tag{55} $$

$$ \frac{{}^{dp}I}{{}^{dp}I_{o}} = \frac{k_{dp}\tau_{dp}}{1 + k_{dp}\tau_{dp} + k_{p}\tau_{p}[H_3O^{+}]} \tag{56} $$

The relationship between the pH at the inflection point, the $*pK_a$ value, and the lifetimes of both protonated and deprotonated forms is given by[21]

$$ pH = *pK_a - \log(\tau_p/\tau_{dp}) \tag{57} $$

If both forms emit, the agreement of the values of pK_a obtained from the two fluormetric titration curves is an indication that equilibrium is attained and confirms the validity of the model. In the case that only one form emits, the flourometric titration curve must be treated with caution.

If the lifetime of the non-emissive form is very short, excited state equilibrium will never be approached, since this form is removed by deactivation more rapidly than the system can adjust. A rule of thumb is that the apparent ΔpK_a value is an underestimates, since failure to equilibrate results in equilibrium concentrations that are less shifted relative to the initial ground state values than the excited-state equilibrium constant would dictate. In this case, the fluorometric titration curve reflects the rate constants, and the proton donor or acceptor ability of the solvent. This can be visualized as a two step process, depicted in eqs 58-59 for the case of enhancement of basicity in the excited-state. The first step, autoionization of the solvent, is slow relative to the second step, which is acceptance of a proton by the excited species

$$H_3O^+ \rightleftharpoons H^+ + H_2O \qquad \text{(slow)} \qquad (58)$$

$$^*D + H^+ \rightleftharpoons {}^*DH^+ \qquad \text{(fast)} \qquad (59)$$

Therefore, the ability of the solvent to autoionize becomes the limitation on the rate at which the equilibrium can shift. In the ground state this leveling effect prevents the differentiation of acids stronger than the conjugate acid of the solvent. In the excited state, a leveling effect is observed in the sense that the actual rate of protonation is limiting. All that can be definitively concluded is that the equilibrium is shifting in the excited state at a rate limited by the solvent itself. In dilute solution, virtually all

protonations and deprotonations take place between the acid or base and the solvent. In the case that protonation leads to rapid deactivation of the excited state, the rate constant for deprotonation of the excited state ($^*k_{dp}$) is undefined. If the deprotonation is considered to occur from the ground state then ΔpK_a,

$$\Delta pK_a = {}^*pK_a - pK_a \tag{60}$$

$$\Delta pK_a = -\log\left(\frac{^*k_{dp}}{^*k_p}\right) - \log\left(\frac{k_p}{k_{dp}}\right) \tag{61}$$

is equal to the ratio of rate constants for protonation in the ground (k_p), and excited states ($^*k_p$). In other words, the enhancement of the forward rate constant in the excited state, is the apparent ΔpK_a, rather than a value of the excited state equilibrium constant.

$$\Delta pK_a(\text{apparent}) = -\log\left(\frac{k_{dp}}{^*k_p}\right) - \log\left(\frac{k_p}{k_{dp}}\right) \tag{62}$$

$$\Delta pK_a(\text{apparent}) = \log\left(\frac{^*k_p}{k_p}\right) \tag{63}$$

Generally the interpretation of a lone fluorometric titration curve requires knowledge that the lifetime of both species involved satisfy the inequalities of eqs 49 and 51. This is necessary in order to determine whether the data reflects establishment of an excited-state equilibrium, or the kinetically controlled phenomena described above. Values of τ are often extracted from intensity decay measurement, but in the case that only one form emits, measurement of τ must be accomplished by other methods, such as transient absorption. If τ cannot be evaluated a lower limit of $^*pK_a$ can still be made, that being the pK_a of the solvent in which the material was dissolved.

The assumption that the rate of proton transfer does not limit the attainment of excited-state equilibrium is well supported in many cases by its rapid diffusion in aqueous solution. This is due of course to its small size, as well as the availability of a hopping mechanism. However, if significant solvent reorganization must occur equilibration might still not be obtained even after hundreds of nanoseconds. It has been suggested that the variation in $^*pK_a$ observed as a function of lifetime for a number inorganic compounds, could be due to an inability to reorganize the solvent within the lifetime of the excited state (Figure 5).[24]

Large changes in acidity or basicity observed in the excited state, are due to redistribution of electron density. This is not surprising given the known sensitivity of ground state acidity constants to attached electron donating or withdrawing substituents. For instance, the difference between acetic acid with pK_a equal to 4.75 and trifluoroacetic acid with pK_a equal to .3, this due to differences in electron distribution. However the principle effect is due to entropy of solvent reorganization, rather than enthalpy of dissociation. [25]

A value of $^*pK_a$ can also be estimated from fluorescence data using the Forster equation.

$$^*pK_a = pK_a + \frac{0.625}{T}(\nu_B - \nu_A) \qquad (64)$$

In this equation ν_A and ν_B refer to the wavenumber of the 0-0 transition in the absorption spectrum of the acid and its conjugate base, respectively and K_a is the acid ionization constant of the protonated form in the ground state. Use of the 0-0 transition is the most desirable way to assign the energy of the excited state, particularly that from low

Figure 5. Variation of *pKa with the excited state lifetime for several families of Ru(II) diimines

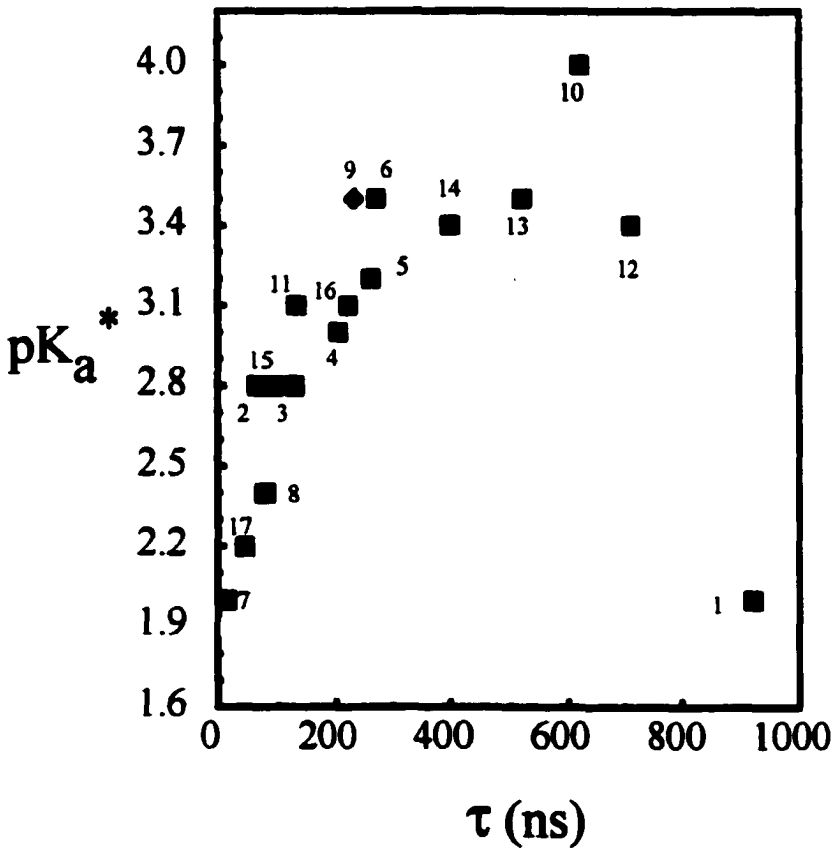

Table 1. Variation of $*pK_a$ with the excited state lifetime for several families of Ru(II) diimines.

Complex	pKa	*pK_a	ΔpKa	τ (ns)	Reference
1. $Ru(bpz)_3^{2+}$	-2.2	2.0	4.2	900	16
2. $Ru(Me_2bpy)_2(dpp)^{2+}$	-3.7	2.8	6.5	64	12
3. $Ru(bpy)_2(dpp)^{2+}$	-3.8	2.8	6.6	127	12
4. $Ru(phen)_2(dpp)^{2+}$	-4.0	3.0	7.0	202	12
5. $Ru(5\text{-}Cl\text{-}phen)_2(dpp)^{2+}$	-	3.2	-	260	12
6. $Ru(dpp)_3^{2+}$	-4.8	3.5	8.3	270	12
7. $Ru(bpy)_2(bpm)^{2+}$	-2.9	2.0	4.9	13	12
8. $Ru(bpm)_3^{2+}$	-1.0	2.2	3.2	83	88
9. $Ru(TAP)_3^{2+}$	-3.0	3.5	6.5	230	15
10. $Ru(TAP)_2(bpy)^{2+}$	-2.6	4.0	6.6	620	15
11. $Ru(bpy)_2(TAP)^{2+}$	-2.0	3.1	5.1	130	15
12. $Ru(bpz)_2(bpm)^{2+}$	-	3.4	-	710	34
13. $Ru(bpm)_2(bpz)^{2+}$	-	3.5	-	520	34
14. $Ru(bpz)_2(bpy)^{2+}$	-	3.4	-	400	92
15. $Ru(bpy)_2(bpz)^{2+}$	-	2.8	-	92	34
16. $Ru(bpy)_2(bpm)(bpz)^{2+}$	-	2.2	-	44	34
17. $Ru(bpm)_2(bpy)^{2+}$	-	3.1	-	220	92

bpz = 2,2'bipyrazine; Me2bpy = 4,4'-dimethyl-2,2'bipyridine; dpp = 2,3-bis(2-pyridyl)-pyrazine; bpy = 2,2'-bipyridine; phen = phenanthroline; 5-Cl-phen = 5-chloro-phenanthroline; bpm = 2,2'-bipyrimidine; TAP = 1,4,5,8-tetraazaphenanthrene

* The *pK_a value of 6.6 reported in this reference, is not corrected for differences in lifetimes between the protonated and deprotonated forms.

** This Reference reports ΔpKa ≥ 3.0.

temperature emission data. In the case of metal complexes, however, the absence of a well defined 0-0 transition, has led to the necessity that an estimated value be used. One method is to take the point of intersection of the absorption and corrected emission spectra for each form as the energy of its 0-0 transition. Another method is to take the average of the absorption and fluorescence maxima ($\nu_{abs} + \nu_f$)/2, as an estimate of the 0-0 transition. If the linewidths are comparable these maxima can be used, since the differences between the Franck-Condon and 0-0 transitions will be very similar.[15]

The largest contribution to the error, in applying the Forster equation, is the location of the 0-0 transition. In partucular, since the error is amplified as these energy values are scaled exponentially from the standpoint of calculating $^*K_a$. This analysis uses the enthalpy change between the acid-base pair in the ground and excited states, (Figure 6) and neglects differences in entropy, in assuming that values in ground and excited states are negligibly different. This has been shown to be a questionable assumption in the ground state[25] and might well be in the excited state.

The ground state pK_a is usually obtained by performing a ground state titration, using a spectrophotometer to monitor the protonation. If more than one protonation is possible, these spectra may indicate whether the ground state pK_a's differ significantly enough for resolution, by the existence of isosbestic points. An isosbestic point is a stationary point in the absorption spectrum, which is maintained during a chemical change. It suggests a quantitative conversion of starting materials to products, although it can also reflect an invariant ratio of a mixture of products.

From the spectral change observed, a plot of absorption versus acidity function is constructed with the absorption measured at a single wavelength where the change is to

Figure 6. Relative enthalpy differences between the ground and excited state forms of a typical acid-base pair that undergoes a change pK_a in the excited state

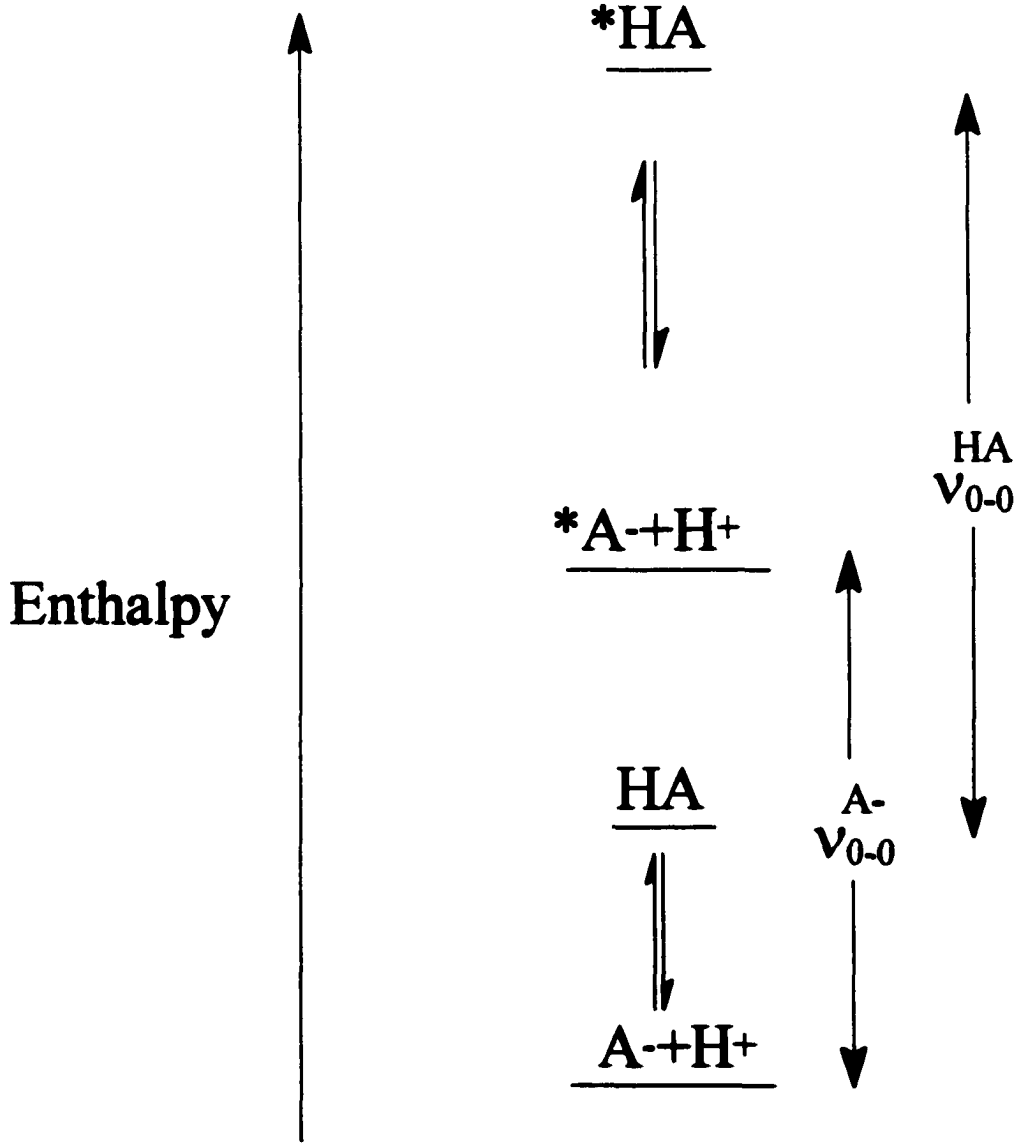

be monitored. The inflection point of this curve is the ground state pK_a. In choosing the wavelength at which to monitor the titration, a determination must be made as to whether the spectral change corresponds to a single protonation. If this is the case, as in molecules with only one protonation site, the optimum wavelength is that corresponding to the largest spectral change. This will be the wavelength at which the magnitude of the difference between the values of the ε's, of the protonated and deprotonated forms, is the largest.

If the spectral changes are associated with successive protonations, two factors must be considered. First, are the spectral changes far enough apart in the region of the absorption spectrum they affect, to be monitored simultaneously? If they are then two optimum wavelengths can be chosen and each will yield a titration curve for a separate pK_a. The second consideration is whether the pKa values are sufficiently different that their inflection points occur at pH values that were widely enough separated to distinguish. If this is the case, the position of the spectral changes for each step need not be very different. If either criterion can be met, the separation in either the wavelength or pH domains allows for the construction of independent titration curves. If the absorptions overlap in both pH and wavelength domains, the titration curves will distort each other throughout the titration, in both pH and wavelength. A method has been suggested for disentangling this type of spectral data by Lever.[16]

(8) Excited State Acid-Base Properties of Metal Complexes

The first reports of excited-state proton transfer for a metal complex were made by Demas[26] and Wrighton.[13] Demas observed that $(bpy)_2Ru(CN)_2$ (bpy = 2,2'-bipyridine) emitted only in the deprotonated form and that the luminescence yields were independent of the relative fractions of $(bpy)_2Ru(CN)_2$,$(bpy)_2Ru(CN)(CNH)^+$, $bpy)_2Ru(CNH)(CNH)^{2+}$

in the ground state which underwent excitation. In other words, irradiation of solutions that had virtually all of the complex protonated in the ground state, resulted in emission from the fully deprotonated form. This lead to the realization that rapid deprotonation must take place in the excited state. His interpretation of the data involved assumption of an equilibrium between $(bpy)_2Ru(CN)_2$, $(bpy)_2Ru(CN)(CNH)^+$, $(bpy)_2Ru(CNH)(CNH)^{2+}$, where the protonation occurred without deactivation. The protonated species were assumed to be intrinsically non-emissive, but present and therefore involved in the excited state equilibrium.

Wrighton and co-workers observed an enhancement of basicity for $(bpy)_2Ru(dcbxy\text{-}bpy)^{2+}$. At a pH value of 3.5 excitation of exclusively deprotonated form resulted in emission from predominatly the fully protonated form. The monoprotonated form was not detected in either the ground state titration or the fluorescence titration, leading to the assumption that the ground state pK_a's were too close to resolve. It was also taken to mean that the monoprotonated form did not emit, and was long enough lived to undergo a protonation before and without its own deactivation. The details of this molecule have been the subject of some difference of opinion upon reinvestigation,[14] though Wrighton's observations remain the first report of emission from both protonated and deprotonated forms of a metal complex.

The observations of both Demas and Wrighton of enhanced acidity and basicity in the excited state can be rationalized by the same principal. Both changes are due to the charge transfer being delocalized on the most easily reduced ligand. Demas observed an enhancement of acidity in the excited state, this due to the localization of the charge transfer on the bpy ligands.[27] The redistribution of electron density away from the metal

center, making it formally Ru(III), inductively reduces the electron density on the CN ligands, resulting in a reduction in the value of $^*K_a$ by five orders of magnitude relative to the ground state. The charge transfer for $(bpy)_2Ru(dicarbxy\text{-}bpy)$ is delocalized on the functionalized bpy ligand, thereby directly enhancing the electron density of both carboxylate groups, and increasing their basicity.

Many examples of emissive metal complexes are molecules for which spin-orbit coupling cannot be neglected. The mixed singlet-triplet nature of these excited states is responsible for the lengthening of the lifetimes relative to organic singlet states, and makes them very attractive to study. However a drawback of this is that, the assignment of pure singlet and triplet states is impossible, and the distinctions that are so significant between these states in organic molecules, cannot be made at all. For instance lack of a well defined 0-0 transiton, even at low temperatures introduces a great deal of uncertainty into Forster cycle calculations on these molecules. Another difficulty in quantifying enhancements of acid-base properties in the excited state, is the failure of both protonated and deprotonated forms to emit in many cases. As discussed earlier it is very difficult to distinguish between proton transfer with and without deactivation, since in many cases the protonated form fails to emit, even if it is the form that is directly excited. Regardless of these difficulties, metal complexes present new possibilities in possessing large changes in acid-base properties, without short fluorescent lifetimes, the drawback inherent in organic systems with comparable changes.

(9) Exciplexes

An exciplex is a complex formed between an excited and a ground state molecule. In the case that the donor and acceptor are identical molecules, the complex is referred to

as an eximer, a term coined from it being an excited-dimer. A classic example of an organic eximer occurs with pyrene.[28] The emission spectrum of pyrene in n-heptane at a concentration of 10^{-5} M, shows a structured peak centered at 25,000 cm^{-1} due to the monomer fluorescence. With increasing concentration a broad structureless band appears 5000 cm^{-1} lower in energy with maintenance of an isoemissive point, suggesting two species are involved. The absorption spectrum of pyrene shows no evidence of a new species formed in the ground state over this same range of concentration. The formation of an exciplex by a diffusional process is further supported by measurement of the time dependence of the emission spectrum. After picosecond excitation, the emission spectrum is that of the monomer, but within 100 ns the spectrum evolves into that observed in the steady-state measurement (i.e. shifted to lower energy). At room temperature, the eximer is thought to form with ΔG of approximately -4 kcal/mole.[28]

While numerous examples of organic exciplexes exist, fewer cases are known among transition metal complexes. The majority of current data in the literature of exciplex formation with excited metal complexes, involves interaction with a ground state metal ion having an $ns^0(n-1)d^{10}$ configuration, such as Ag^+ or $HgCl_2$. It is thought that the diffuse "ns"orbital plays a role as an acceptor in forming the exciplex. A simplified MO explanation using the orbital configuration of the excited state interacting with the ground state molecule is often invoked to visualize the orientation of the interaction. The exciplexes of transition metal complexes have been classified based upon distinctions of the excited or ground state species being an electron donor or acceptor and the nature of the orbitals involved, being ligand or metal centered.

The dependence of τ and ϕ_{em} on the concentration of the ground state ion in most examples of transition metal exciplexes, can not be adequately modeled using only a bimolecular collision leading to formation of the exciplex. For example, in order to account for the dependence of τ and ϕ_{em} on the concentration of Ag^+, for formation of an exciplex between $Ru(bpy)_3^{2+}$ and Ag^+, Demas inferred the formation of both bimolecular and termolecular species, in the first report of an inorganic exciplex.[29] The formation of these species was later supported by a polarized luminescence study. This study proved exciplex formation using the dissymetry factors for emission (g_{em}) and absorption (g_{abs}) defined as

$$g_{em} = \frac{2(I_L - I_R)}{I_L + I_R} \tag{65}$$

$$g_{abs} = \frac{2(\varepsilon_L - \varepsilon_R)}{\varepsilon_L + \varepsilon_R} \tag{66}$$

While g_{abs} remained unchanged by addition of silver, g_{em} showed a strong dependence on the concentration of Ag^+, establishing that the new species formed existed only in the excited state.[30]

In a study of the interaction between $Ru(bpz)_3^{2+}$ and Ag^+, Lever and co-workers suggest that exciplexes involving as many as 6 Ag^+ per $Ru(bpz)_3^{2+}$ may exist.[31] However, $Ru(bpz)_3^{2+}$ differs from $Ru(bpy)_3^{2+}$ in that the bpz ligand has two peripheral nitrogens,

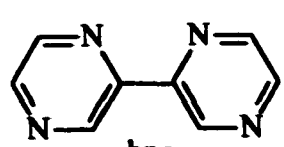

bpz

which can act as coordination sites. Consequently this system may involve a different mechanism of formation of an exciplex that is not available to $Ru(bpy)_3^{2+}$, since it does not have coordination sites on its periphery.

Another characteristic of exciplex formation, among organics or transition metal exciplexes, is a strong solvent dependence. Among transition metal complexes solvent effects are more profound due to the fact that charged species are more likely involved and the coulombic terms for interaction are more sensitive to a solvent to either shield or compete via ion-dipole interactions. Typically stabilization of the exciplex relative to the free pair is a few kcals per mole, which is on the order of solvation energy differences between solvents. Therefore, the formation of an exciplex might altogether become unfavorable in one solvent, while being viable in another. Solvent effects can also change the degree of charge transfer achieved in the formation of the exciplex. It is thought that formation of more highly charged or separated species is favored with increasing solvent polarity. Therefore, a change in mode from an exciplex which is a contact ion-pair, to one which is a solvent-separated ion-pair might take place in going from less to more polar solvents. For instance, exciplex formation between $Ir(phen)_3^{3+}$ and $HgCl_2$ shows a complex dependence on the solvent, the ionic strength μ, and the identity of the particular ions used to control μ . The lifetime of $Ir(phen)_3^{3+}$ in DMF rises ten-fold between 0.0 and 1.0 mM of $HgCl_2$ and then becomes independent of the amount of $HgCl_2$. Throughout the same experiment, a decline in the values of τ_o/τ of a similar magnitude to that observed for the values of I_o/I takes place. The changes in τ_o/τ occur more slowly with the change in concentration of $HgCl_2$ than the changes in I_o/I. The extent of these changes for τ_o/τ does not appear to saturate at a ten-fold increase, in contrast to the corresponding changes

in I_o/I. These two pieces of data show two effects. The first effect is the formation of the exciplex in an equilibrium process in the excited state suggested by the saturation of the change in emission intensity. The second effect is suggested simply by the independence of the lifetime data from the intensity data. Whatever interaction leads to the formation of the exciplex, a second interaction must account for lifetime data. Considering the same system, in water at high perchlorate concentration, exciplex formation appears be almost non-existent. On the other hand, use of chloride ion results in a decline in τ at concentrations higher than the concentration $HgCl_2$, without any change in the shape of the emission spectrum. This suggests that the interaction of the chloride ions with $HgCl_2$ does quench the lifetime of the exciplex without forming a new exciplex. It has been suggested that the inhibition of the emisive exciplex formation with increase in concentration of ClO_4^-, occurs by preferential formation of an ion-pair that is not emissive, with the ClO_4^-. It was postulated that the ion pair formed to the exclusion of the chloride exciplex, and that the Cl^- dependence reflects coordination of one or more Cl^- to $HgCl_2$ to form tri- and tetrachloro Hg species.[32]

The observed chemistry of exciplex formation is very complex. It is only known to be this complex however, because it is a type of excited-state chemistry, which lends itself to easy measurement in the case that an emissive exciplex is formed. The interactions of non-emissive species in solution are much harder to observe. Although, this does not mean that processes involving non-emissive species are any less chemically complex.

(10) Photochemistry of Ruthenium(II) Diimines

Intensive study of Ru(II) diimines was spurred by the realization that $Ru(bpy)_3^{2+}$ can undergo photoinduced electron transfer.[33] The excited state is believed to be ligand localized, often represented as an oxidized-metal, reduced-ligand species, $Ru(III)\text{-}L^{-}$.[34] Its strong absorption of visible light, its long lifetime, $\tau = 600 \pm 20$ ns, high quantum yield of emission, $\phi_{em} = .042$, in water, and its tremendous stability (its quantum yield of decomposition, ϕ_{dec}, is not measureable at room temperature and is less than 10^{-6} at 80 °C), make it attractive to study. The exploitation of it's photo-redox properties in solar energy storage schemes, was considered in numerous studies. Its use in photocatalyzing multi-electron reductions, such as the conversion of carbon dioxide to methane, was also investigated. In attempts to gain the ability to transfer multiple electrons from a single excited state, polymetallic complexes were considered. Maintenance of a similar microsymmetry and chemical environment about the metal center, lead to the design of number ligands, one of which was 2,3-dipyridyl-2'2'-pyrazine (dpp).

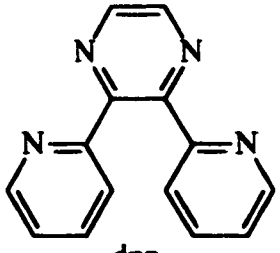

dpp

The monometallic complex, $Ru(bpy)_2dpp^{2+}$ is strongly emissive in water with $\phi_{em} = .05$, fairly long lived with $\tau = 125 \pm 10$ ns,[35] and very stable with $\phi_{dec} < 10^{-5}$. Resonance Raman studies have shown that the MLCT transition is strongly coupled to vibrations on the dpp associated with the peripheral immine nitrogens, establishing a ligand localized

Figure 7. Molar absorptivity and emission spectrum of $Ru(bpy)_2dpp^{2+}$ in water.

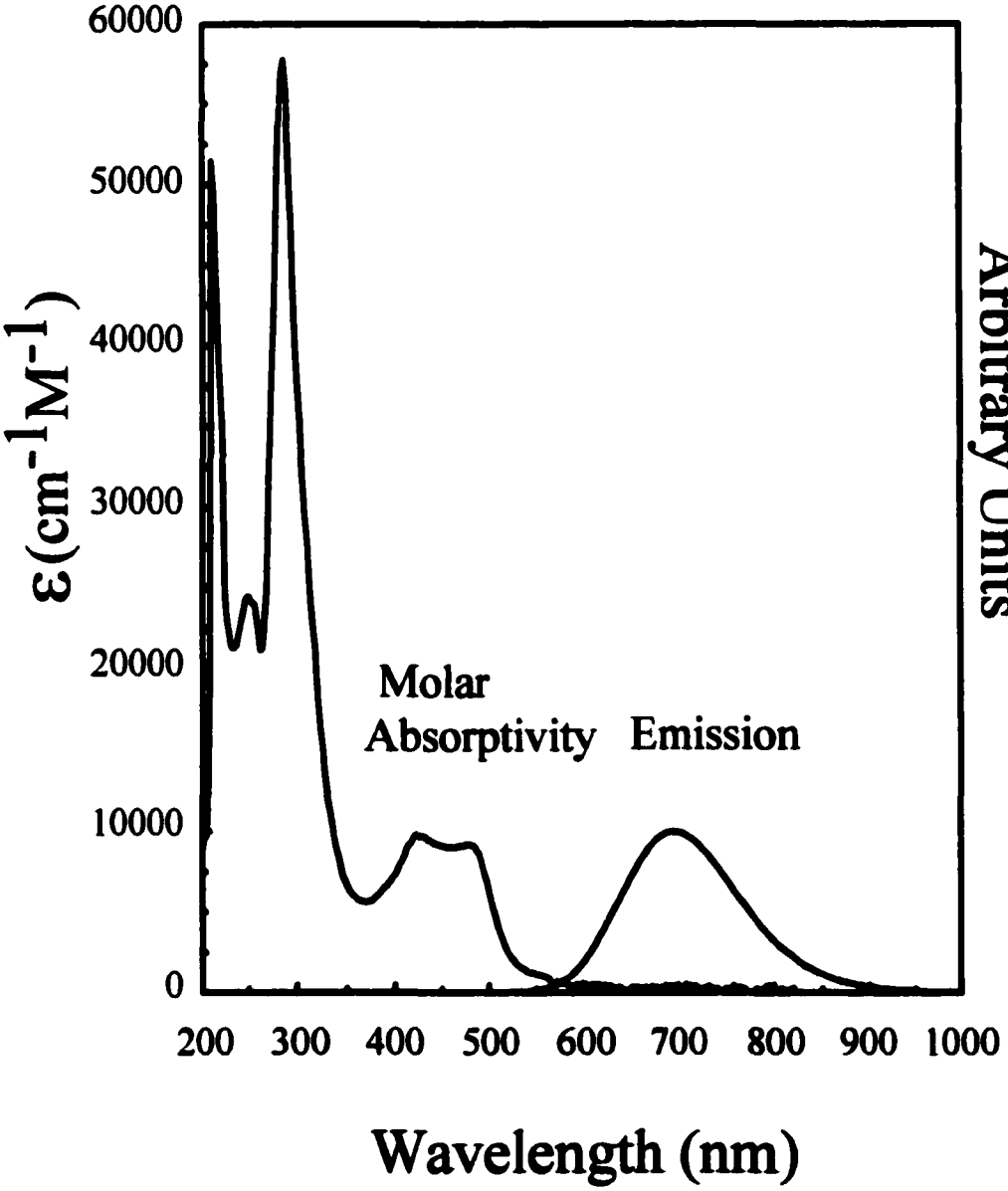

excited state.[35] Investigation of its acid-base properties has shown $Ru(bpy)_2dpp^{2+}$ to undergo a tremendous change in basicity in the excited state, characterized by a $\Delta pKa \geq 3$.[35] The redistribution of electron density in the excited state increases the basicity of the nitrogens on the periphery of dpp. The excited state also undergoes efficient proton quenching with $K_{sv} = 767\ M^{-1}$.[35] The photosensitivity and thermal lability of all the coordination complexes used as quenchers, was carefully considered throughout this work. The absorption of light by the quenchers was minimized, by adjustment of the experimental conditions, while still being able to measure the desired effect. Very high values of μ (3.0-5.0 M NaCl) were used both to minimize formation of ion-pairs between $Ru(bpy)_2dpp^{2+}$ and the quenchers used, and to retard any equilibrium releasing coordinated chloride ion. The thermal pathways of aquation and chelation by $Ru(bpy)_2dpp^{2+}$, were characterized under the same experimental conditions that the photochemical measurements were made. Despite these efforts to optimize the experimental conditions, substantial extents of interference from these competing pathways was a nagging concern in some cases. However, consideration of all the data, paints a picture that cannot be accounted for by any trivial effect derived from thermal or photoinduced processes initiated on the quenchers used.

(11) Photosubsititution and Ligand Exchange Reactions of the $Na_2[PtCl_6]$

The thermal substitution chemistry of low-spin d^6 octahedral complexes is known to be very slow at room temperature in aqueous solution.[36] In contrast, excitation into either LMCT or LF states has been shown to lead to measurable quantum yields of photosubstitution.[37] The photochemistry of has $PtCl_6^{2-}$, which has long been noted as complex, has been the most intensively studied of the platinum triad hexachlorides. The

thermal chloride exchange reaction was studied by Taube, who found that the Cl- exchange reaction proceeded via a five-coordinate Pt(III) intermediate formed in a bimolecular process[38]

$$Pt(IV)Cl_6^{2-} + Pt(II)Cl_4^{2-} \rightleftharpoons 2Pt(III)Cl_5^{2-} \quad (67)$$

$$*Pt(III)Cl_5^{2-} + PtCl_6^{2-} \rightleftharpoons *Pt(IV)Cl_6^{2-} + Pt(III)Cl_5^{2-} \quad (68)$$

Reaction rates were observed to be very sensitive to even ambient light exposure which was presumed to generate $PtCl_5^{2-}$.

Later work by Wright and Laurence,[39] using UV flash photolysis and transient absorption, showed that Cl_2^- radicals could be detected. They suggested that a Pt(III) intermediate formed by photolytic homolyis, and that it was the chain carrier Taube had suggested to explain the sensitivity to light of the interconversion and chloride exchange reactions of $PtCl_6^{2-}$ and $PtCl_4^{2-}$. From the ionic strength dependence of the of the transients rate constant for quenching by Fe^{2+}, he deduced that its charge was −1. He proposed that the Pt(III) transient was four coordinate with the argument that Pt(III), a d^7 system would prefer a square planar geometry so that, after homolyis to a five coordinate species, loss of a chloride to form a square planar four coordinate species would occur rapidly. He proposed the mechanism

$$PtCl_6^{2-} \xrightarrow{h\nu} PtCl_5^{2-} + Cl \quad (69)$$

$$PtCl_5^{2-} \longrightarrow PtCl_4^- + Cl^- \quad \text{(fast)} \quad (70)$$

$$Cl + Cl^- \longrightarrow Cl_2^- \quad (71)$$

for the photoreduction. For the photoaquation he suggested that after excitation and intersystem crossing to the lowest energy triplet state, aquation promptly occurred by a pseudo-first order process.

$$PtCl_6^{2-} + H_2O + h\nu \longrightarrow PtCl_5(OH)^{2-} + Cl^- + H^+ \quad (72)$$

Wright and Laurence suggested that the ratio of quantum yields of about 10:1 for photoaquation to photoreduction, reflected the fraction of excited states produced which underwent conversion to the lowest energy triplet state, from which aquation occurred. The Pt(III) transient was found to decay by second-order kinetics with k_2 equal to 4.6×10^{-6} $M^{-1}s^{-1}$.

$$2Pt(III) \xrightarrow{k_2} Pt(IV) + Pt(II) \quad (73)$$

The photosensitivity and thermal lability of all the coordination complexes used as quenchers was carefully considered throughout this work. The absorption of light by the quenchers was minimized by adjustment of the experimental conditions, while still being able to measure the desired effect. Very high values of μ (3.0-5.0 M NaCl), were used both to minimize formation of ion pairs between $Ru(bpy)_2dpp^{2+}$ and the quenchers used, and to retard any equilibrium releasing coordinated chloride ion. The thermal pathways of aquation and chelation by $Ru(bpy)_2dpp^{2+}$, were characterized under the same experimental conditions that which the photochemical measurements were made. Despite these efforts to optimize the experimental conditions, substantial interference from these competing pathways was a nagging concern in some cases. However, consideration of all the data, paints a picture that cannot be accounted for by any trivial effect derived from thermal or photoinduced processes initiated on the quenchers used.

II Experimental

(1) Materials

$Na_2[PtCl_6]$, $Na_2[PtCl_4]$, $Na_3[RhCl_6]$, K_2PdCl_6, $K_3[RuCl_6]$, $K_2[OsCl_6]$, $K_3[IrCl_6]$, cis-$Ru(bpy)_2Cl_2$ and dpp, were obtained from Aldrich Chemical Company, and used without further purification

(2) Preparations

(2.1) $[Ru(bpy)_2dpp](ClO_4)_2$

$[Ru(bpy)_2dpp](ClO_4)_2$ was prepared by refluxing one equivalent, of dpp and one equivalent of cis-$Ru(bpy)_2Cl_2$ in ethanol for 8 hours. The reaction mixture was filtered, evaporated to dryness, and redissolved in water. The aqueous solution was treated with solid sodium perchlorate to precipitate $[Ru(bpy)_2dpp](ClO_4)_2$, which was then collected by suction filtration. The crude product was then redissolved in a minimal volume of acetonitrile and eluted down an alumina column with acetonitrile. Unreacted dpp, which is almost colorless, eluted first and was detected in the fractions by its UV absorbance spectrum. The purified $[Ru(bpy)_2dpp](ClO_4)_2$, which was orange, eluted second. The purple unreacted $Ru(bpy)_2Cl_2$ remained essentially immobile at the top of the column. Fractions were collected and their absorption spectrum compared for traces of the starting material.

$[Ru(bpy)_2dpp](ClO_4)_2$ was characterized by ^{13}C, and ^1H NMR spectra. Visible absorption spectra and emission spectra were found to be in good agreement with reported spectra. The ^1H NMR was also in good agreement with the reported spectrum.

(2.2) $[Ru(bpy)_2dppPtCl_4]PtCl_6$

$[Ru(bpy)_2dppPtCl_4]ClPtCl_6$ was prepared both thermally and photochemically. Thermally it was prepared by reflux of one equivalent of $[Ru(bpy)_2dpp](ClO_4)_2$ with one equivalent of $Na_2[PtCl_6]$ in water. After 8 hours reflux the solution was evaporated to dryness. The red product was insoluble or slightly soluble, in virtually all common solvents. Successive rinsing of the solid residue with water, and ethanol, to aid in drying, was performed to remove both starting materials. The thermal product was characterized by UV-vis absorption spectroscopy.

Photochemically $[Ru(bpy)_2dppPtCl_4]PtCl_6$ was prepared by dissolving 200 mg of $[Ru(bpy)_2dpp](ClO_4)_2$ (one equivalent), and 663 mg of $Na_2[PtCl_6]$ (five equivalents), in a minimal volume of water. This solution was placed in an ice bath in a 600-milliliter glass beaker with a magnetic stirring bar, and irradiated with 488-nm line of an Ar-ion laser. The extent of reaction was monitored by absorption spectroscopy. The estimated value of $\varepsilon_{488} = 12000\ M^{-1}cm^{-1}$, for the product, calculated as described earlier, was used. The reaction was stopped at approximately 70% conversion, the maximum extent of reaction for which the isosbestic points were maintained. The solution was then evaporated to dryness. For both syntheses similar purification steps were used. Unreacted starting material was extracted from the solid residue into absolute ethanol. The efficiency of extraction was monitored by absorption spectroscopy, until neither starting material could be detected. The remaining solid was dried under reduced pressure and stored under vacuum.

The photochemical product was characterized by UV-Vis Absorption Spectroscopy. Combustion analysis for C, H, N, Pt, and Ru, suggested a partial empirical

formula, $C_{34}H_{29.1}N_{6.7}Pt_{1.9}Ru_{0.7}$, compared to $C_{34}H_{28}N_8Pt_2Ru$, expected for formation of $[Ru(bpy)_2dppPtCl_4]PtCl_6 \cdot 3H_20$. The product was also analyzed by FAB Mass Spectroscopy (Figure 8). Attempts to characterize the photochemical product by ^{13}C, and ^1H and ^{195}Pt NMR spectroscopy, were hindered by its poor solubility. Atomic absorption measurements were attempted to determine the relative ratio of Ru to Pt in the product. However, Pt and Ru levels in a saturated solution of the product in water are below detection limits of 1 ppm. Atomic absorption measurements indicated a measurable Ru content though Pt was not detected. This was determined to be due to a failure to separate unreacted $Ru(bpy)_2dpp^{2+}$ from the thermal product. This was inferred from extracting $Ru(bpy)_2dpp^{2+}$ with ethanol and comparing the emission spectrum of the extract to that of $Ru(bpy)_2dpp^{2+}$.

(2.3) $K_2[RhCl_5H_20]$

$K_2[RhCl_5(H_2O)]$ was prepared by a modified version of a procedure previously reported. $Na_3[RhCl_6]$, obtained commercially from Strem Chemical Company, was dissolved in a minimal volume of an aqueous solution, .25 M in KCl and .25 M in HCl. This mixture was allowed to react at room temperature for 30 minutes. The reaction was quenched by immersion in an ice bath at which point an equal volume of ice-cold absolute ethanol was added. The pink and amorphous looking precipitate, was suction filtered and washed three times with ice cold ethanol on the filter. This solid was then dried and stored under vacuum. The absorption spectrum in water displayed maxima at 404 and 508 with ε values of 95 $M^{-1}cm^{-1}$ for both, in good agreement with the reported values of 99 $M^{-1}cm^{-1}$.

Figure 8. FAB-MS spectrum of $[Ru(bpy)_2dppPtCl_4]PtCl_6$.

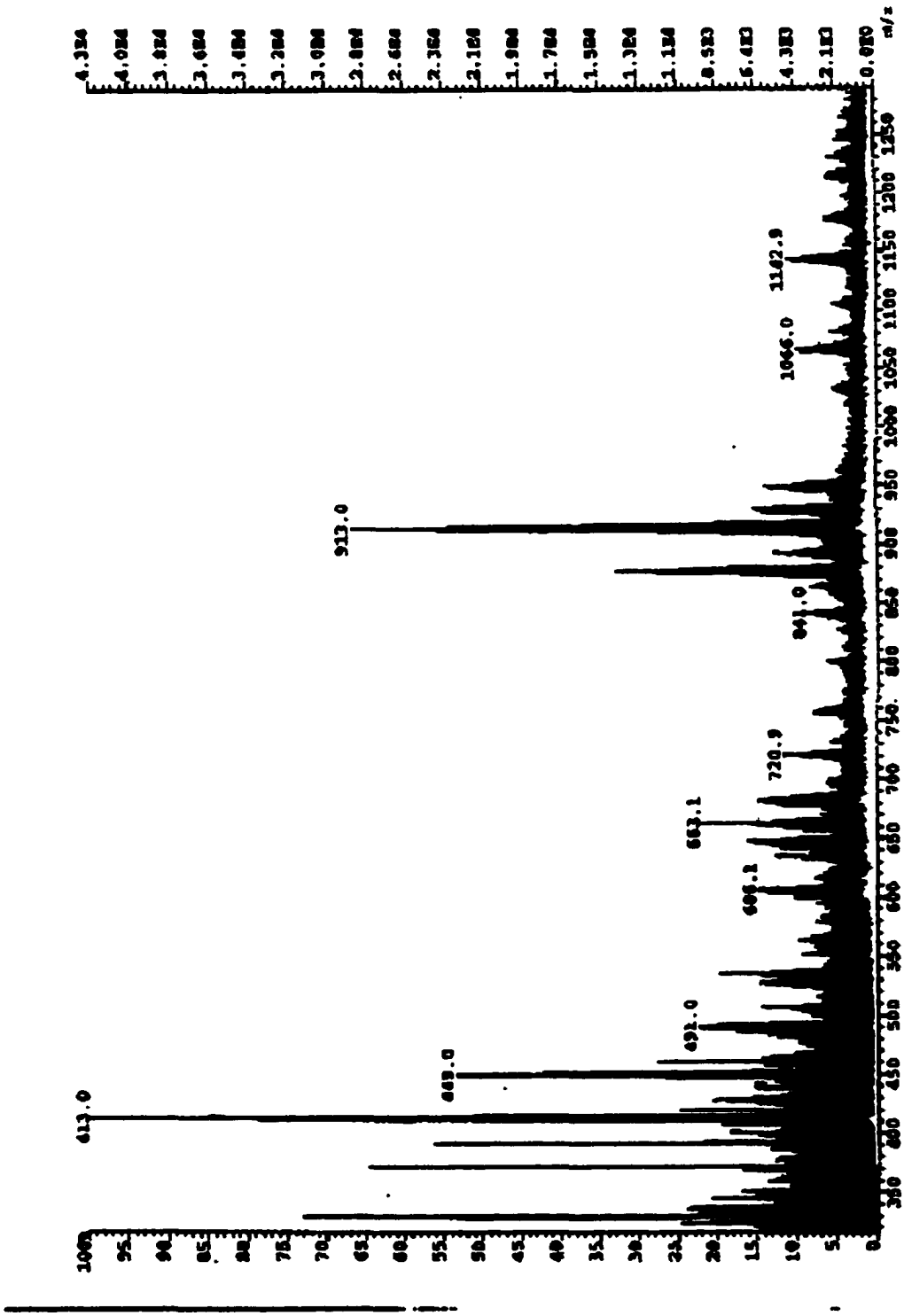

Table 2. Fragment assignments for the FAB-MS of $[Ru(bpy)_2dppPtCl_4]PtCl_6$.

m/z	Fragment Assignment
491	$Ru(bpy)_2dppPtCl_4^{2+}$
948	$Ru(bpy)_2dppPtCl_3^{+}$
413	$Ru(bpy)_2^{+}$
429	$PtCl_4dpp^{+}$
913	$Ru(bpy)_2dppPtCl_2^{2+}$

(3) Physical Measurements

(3.1) Measurement of Excited-State Lifetimes

Excited-state lifetimes (τ), were measured by conventional pulse excitation techniques, using the system outlined in Figure 9. A Q-switched Nd-YAG laser, Quanta-Ray DCR-2A, with a SHG crystal, producing pulses with 8-9 ns width at half-height, was used as the excitation source. The second harmonic 532 nm, was selected with a Pellin-Brocha prism and then directed onto a quartz cuvette. The emission, collected orthogonal to the excitation, was resolved with a 0.25 m Bausch & Lomb High Intensity Grating Monochromator, with 1350 grooves/mm and a 500 nm blaze. The slits were attenuated such that emission sampled was $\leq$ 10 nm, about the emission maximum. The emitted light transmitted through the monochromator was measured with an RCA model 31034A photomultiplier tube, which was operated at 1100 Volts. The photocathode current was fed into the vertical input of a Techtronics 7834 Storage Oscilloscope, which has an input impedance of 50Ω. This instrument was equipped with a 7B85 Time Base, and has a 400 MHz bandwidth with a 1.0 ns risetime. The scope was triggered on the positive slope portion of the emission decay, so that pulse jitter was not a concern. It was used in storage mode and the decays were photographed and subsequently digitized manually. The RC time constant of the detection circuit, principally the result of inductive capacitance, and the impedance of the oscilloscope, was determined to be less than seven ns by direct measurement of the excitation pulse scattered from a microscope slide. The broadening of this pulse was found to be negligible, when compared to the technical specifications for the laser pulse width. Consequently, it was concluded that the RC time

Figure 9. Experimental setup used to measure intensity decays.

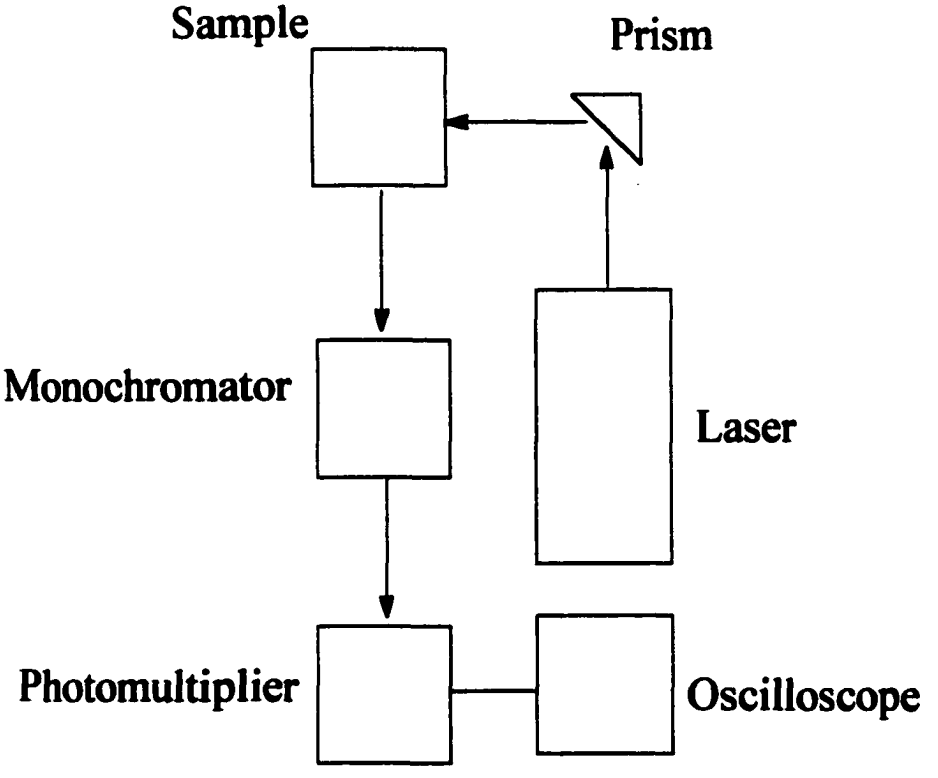

constant broadening of the measured emission was smaller than the pulse width and therefore negligible. Attenuation of the experimental setup to obtain measurable intensity was done by lowering the intensity of the excitation source, rather than the monochromator slits or photomultiplier voltage. After digitizing the decay traces (Figure 10), the intensity in arbitrary units of voltage, and relative time, then was manipulated in Psiplot. The time domain was converted to absolute units by multiplication by the appropriate conversion factors given the time scale that was chosen for each measurement. For instance, the relative data from a decay trace taken with a 100 ns/box time scale, was converted to nanoseconds by multiplication by the factor of (100ns/box)×(1box/.730 cm). Plots of ln(Intensity) versus time were constructed and checked for linearity. Typically, data could be collected over at least 2 lifetimes and shown to agree well with a first-order model over this range. Values of τ were extracted from plots of Ln(Intensity) versus time, as the negative of the inverse of the slope (Figure 11). Due to the limitations in time resolution, τ_o/τ values in excess of 10 were inaccessible for $Ru(bpy)_2dpp^{2+}$, with τ equal to 135 ± 10 ns.

(3.2) Absorption spectrometer setup for kinetics

Absorbance measurements to obtain values of the molar absorptivity (ε), for subsequent absorbance and quantum yield of product (ϕ_p) measurements, were done on a Hewlett-Packard 8452 Diode Array Spectrometer. All values of ε's, were calculated from solutions freshly prepared from solids, and promptly diluted to obtain accurately measurable absorbance values between .1 and 1.6.

Figure 10. Oscilloscope trace, showing the decay in emission intensity at 695 nm with time, after a seven-nanosecond 532-nm laser pulse.

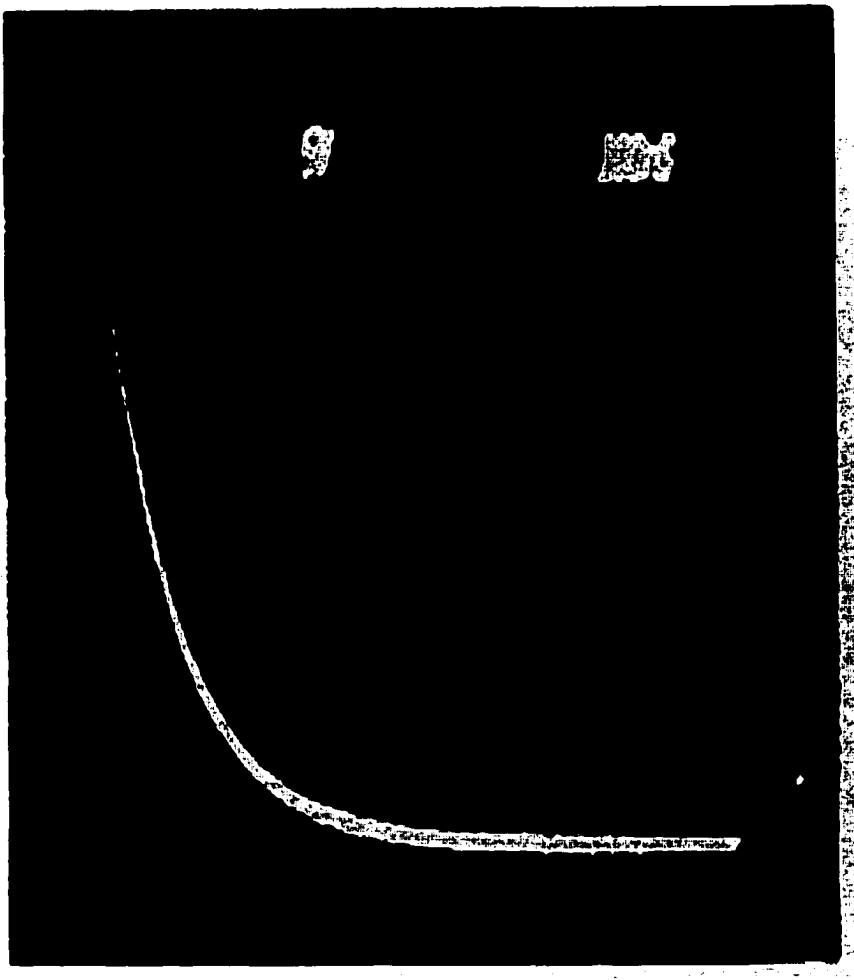

Figure 11. Typical plot used to extract the excited state lifetime (τ), from an oscilloscope trace.

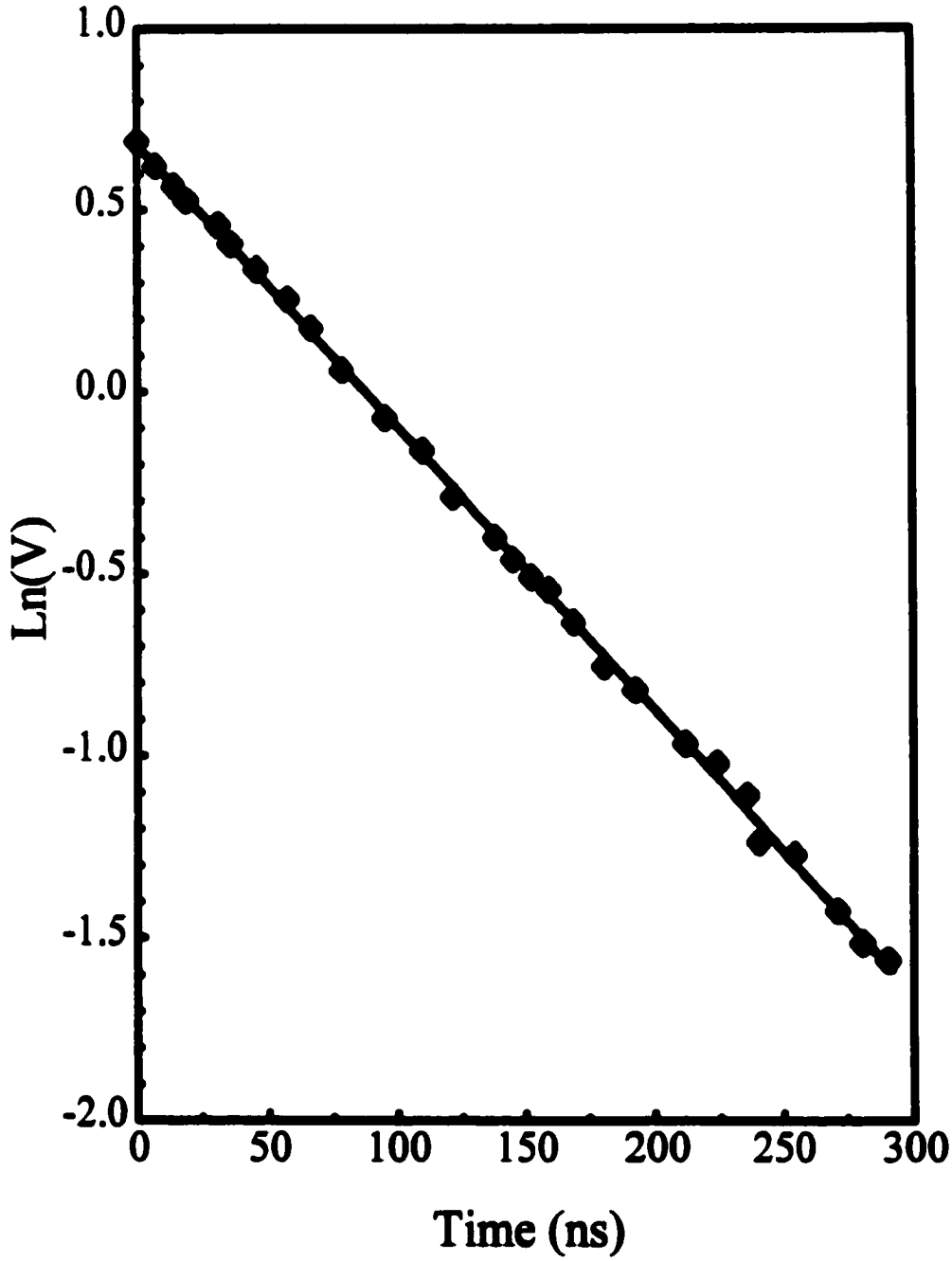

A cell holder was constructed consisting of a hollow brass temperature block with a straight through path for absorbance measurement, and a window perpendicular to this path for irradiation. The block was mounted on a water-driven stirrer attached to a constant-temperature bath. Two hose cocks attached to the block allowed water from a Haake model-FK2 constant-temperature bath, to flow through the block. A small cell-stirring bar, which sat below both light paths, was used at all times to ensure uniformity of the solution. (Figure 12.) The setup was used for the collection of all absorbance kinetic data for photochemical and thermal reactions.

In the photochemical experiments, the 488-nm line of an Ar-ion laser was used as the light source for each irradiation. The beam was spread with a convex lens and dispersed on the cell holder window perpendicular to the path of absorbance measurement. All data were collected with the HP 8452 diode array spectrometer, with the instrument in kinetics mode.

(3.3) Use of Spectral Changes in Measuring Reaction Rates

If the interaction of dissolved species with each other perturbs their absorbance negligibly, then Beers Law (eq 16) can be extended to multiple components. For instance, in the reaction

$$D + Q \longrightarrow P \tag{74}$$

$$A = \varepsilon_D B[D] + \varepsilon_Q B[Q] + \varepsilon_p B[P] \tag{75}$$

The stoichiometric relation between D, Q, and P, can be written

$$[D]=[D]o - [P](t) \tag{76}$$

$$[Q] = [Q]o - [P](t) \tag{77}$$

Figure 12. Experimental setup used for measurement of absorbance during 488-nm photolysis.

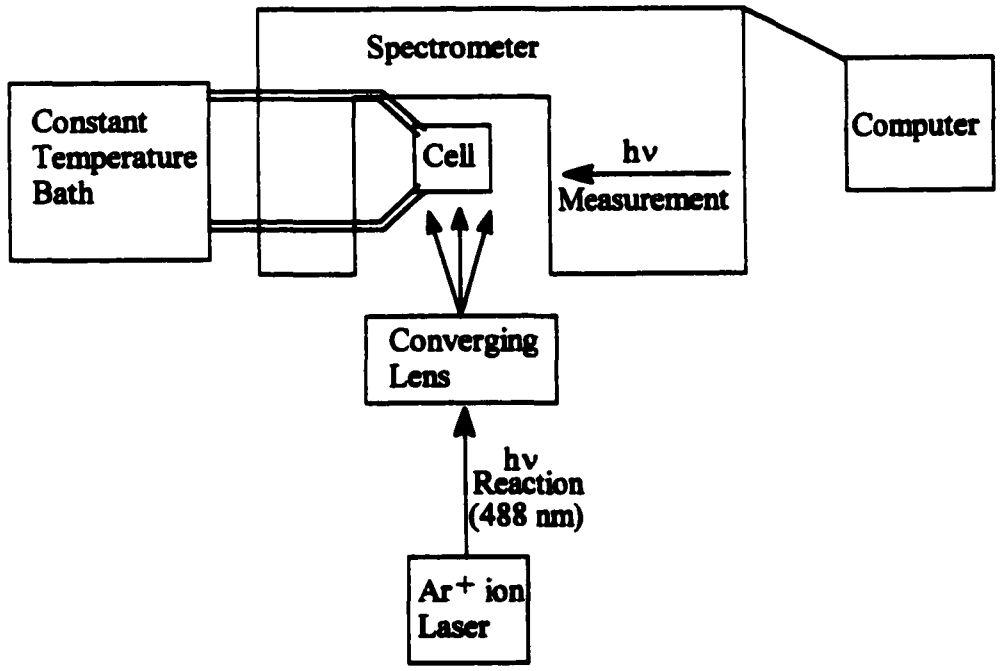

The spectral data, absorption versus time, can be related to the concentration of products by differentiating eq 75 with respect to time, and rearranging

$$\frac{d[P]}{dt} = \frac{dA/dt}{B(\varepsilon_p - \varepsilon_D - \varepsilon_Q)} \tag{78}$$

In practice, plots of $A/B(\varepsilon_p-\varepsilon_D - \varepsilon_Q)$ versus time were constructed and were taken to be equivalent to plots of [P] versus time. If all the ε's which appear in eq 75 are not available, particularly ε_P, they can be estimated from kinetic data. This is done by assuming that a spectral change for a long reaction time, can be assigned to complete reaction (i.e. the concentration of P after a long reaction time, is close to that which would be obtained if the limiting reagent was largely depleted),

$$\varepsilon_p = \frac{A - \varepsilon_D B[D]_f - \varepsilon_Q B[Q]_f}{[P]} \tag{79}$$

where $[Q]_f$, $[D]_f$ and [P], refer to the final concentrations of the donor, quencher, and product respectively. Either D or Q could be the limiting reagent, making its value zero in eq 79. In the case that the reactions mixture is actually far from complete reaction, this leads to an overestimation of the rate, which is not bounded by any measured quantity, since there is no precise upper limit for the value of the unknown epsilon value.

$$\frac{d[P]}{dt}(apparent) \geq \frac{d[P]}{dt} \geq 0 \tag{80}$$

Alternately, rather than estimating the unknown ε, a decreasing spectral change ($\varepsilon p < \varepsilon_D + \varepsilon_Q$) can be used, and ε_p neglected. In this case an inequality is introduced. This makes use of the fact that a lower bound of zero can be placed on the value of the epsilon.

$$\frac{d[P]}{dt}(apparent) \leq \frac{d[P]}{dt} \leq 0 \qquad (81)$$

This inequality holds since the ε's are all positive, and neglecting ε_p increases the magnitude of the denominator in eq 78. While the validity of this technique cannot be confirmed without an independent measurement of the value of molar absorptivity of the product that is being neglected (ε_p), the direction of the inequality at least places an upper limit on the error introduced by this procedure.

Usually the data were collected at a single wavelength. The optimum wavelengths were determined from difference spectra. This analysis uses very small spectral changes and a spectral subtraction method. To implement this method, a mixture of reactants was prepared and its spectra taken immediately. For every wavelength, this initial spectrum (A_o), can be expressed in terms of the independent contributions from each absorbing species using Beers law,

$$A_o = A_D + A_Q = \varepsilon_D B[D]_o + \varepsilon_Q B[Q]_o \qquad (82)$$

The difference spectrum were constructed by subtraction of A_o from each spectra taken at a later time(A_1), after the reaction had proceeded,

$$A_1 = \varepsilon_D B([D]_o - [P]_1) + \varepsilon_Q B([Q]_o - [P]_1) + \varepsilon_P B[P]_1 \qquad (83)$$

For small extents of reaction (i.e. $[P]_1 << [D]_o$ and $[Q]_o$), eq 83 can be written,

$$A_1 \approx \varepsilon_D B[D]_o + \varepsilon_Q B[Q]_o + \varepsilon_P B[P]_1 \qquad (84)$$

and the result of the spectral subtraction,

$$A_1 - A_o \approx \varepsilon_P B[P]_1 \qquad (85)$$

is a relative absorption spectra of the products, which can be used to identify the maxima in the ε spectra of the products. Since $[P]_1$ remains unknown, the values of the epsilons themselves cannot be extracted. However, this allows for assignment of the wavelength at which a new maximum is growing in, from a very small change in absorbance. In effect, the sensitivity of this method is weighted by the epsilon difference spectra. This was because it was used only on data representing the smallest detectable change in absorbance, which coincides with the wavelengths where the epsilon spectra have maxima. Other regions are obscured by the fact that spectral change in these regions is so small that it is indistinguishable from noise. A wavelength at which the difference spectra exhibited a maximum was chosen as the optimum single wavelength for monitoring the reaction, since these were the points of greatest sensitivity. In other words, this wavelength is the point of greatest difference between the epsilons of the product and starting materials, which appear in the denominator of eq. 77, making dA/d[P] at this wavelength, largest for any given extent of reaction. An example of a difference spectrum used to determine the optimum wavelength to monitor the $Ru(bpy)_2dpp^{2+}$, $PtCl_6^{2-}$, and $Ru(bpy)_2dppPtCl_4^{2+}$ reaction system is shown in Figure 13.

The maintenance of an isosbestic point, a wavelength at which the absorbance of the reaction mixture does not change as the reaction proceeds, is suggestive of the formation of a single product. It corresponds to a point at which the ε's, for both product and starting materials are equal. Equation 9 can be factored to make this clear.

$$A(\lambda,t_o) = \varepsilon_p B[P] - (\varepsilon_D+\varepsilon_Q)B[P] + \text{constants} \qquad (86)$$

If there is a value of λ at which ε_p is equal to $(\varepsilon_D+\varepsilon_Q)$ the absorbance will remain constant, regardless of the extent of reaction.

Figure 13. Difference spectrum obtained from the photochemical reaction of $Ru(bpy)_2dpp^{2+}$ with $PtCl_6^{2-}$.

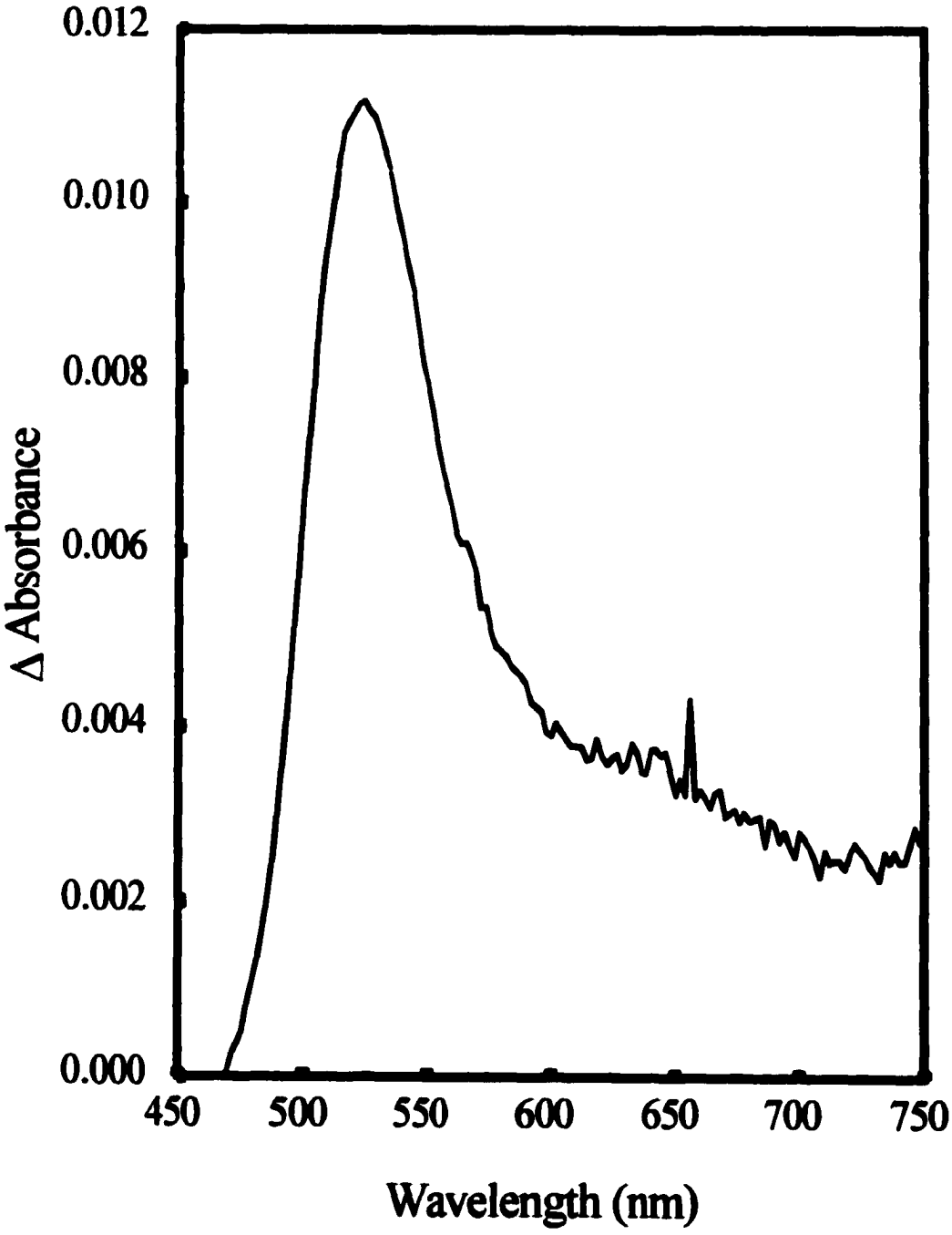

The maintenance of an isosbestic point in a spectral change is suggestive of formation of a single product, though it can also reflect an invariant ratio of products. Consider the two competing reactions

$$D + Q \longrightarrow P_1 \tag{87}$$

$$D + Q \longrightarrow P_2 \tag{88}$$

The absorbance of the reaction mixture is given by

$$A = \varepsilon_D(\lambda)B([D]_o - [P_1] - [P_2]) + \varepsilon_Q(\lambda)B([Q]_o - [P_1] - [P_2]) + \varepsilon_{P1}(\lambda)B[P_1] + \varepsilon_{P2}(\lambda)B[P_2] \tag{89}$$

where ε_{p1}, and ε_{p2}, refer to the molar absorptivity of P_1 and P_2, respectively, and λ is the wavelength. In principle, P_1 and P_2 are both independent variables, so there might not be any value of λ that has $dA/dt = 0$. As the reaction proceeds, changes in the composition of the reaction mixture might begin to favor one product over another. This would lead to different yields of each product at different extents of reaction, with the average of these yields being the final yield of each product from the reaction. However, as long as the product yields remain invariant, then a relation linking P_1 and P_2 exists.

$$P_1 / P_2 = \text{constant} \tag{90}$$

If there is a value of λ for which $(\varepsilon_D + \varepsilon_Q)$ is equal to $(\varepsilon_{P1} + \varepsilon_{P2})$ this will be a stationery point in the absorption spectrum regardless of extent of reaction, as long as the ratio of products remains invariant. This isosbestic point does not reflect the formation of a single product.

(3.4) Intensity Quenching

Intensity quenching data was obtained on a Spex Fluorolog-2 emission spectrometer, outfitted with a Hammatsu R928P red sensitive photomultiplier tube.

Corrections for the inner filter effect due to overlap of the absorption spectra of the donor and quencher were calculated from absorbance data as follows. For a series of solutions with the same concentration of donor species, but with increasing quencher concentration, the fraction of light that is absorbed by the donor declines as the fraction of light competitively absorbed by the quencher increases. This effect can be corrected for within the scope of Beers Law. If I_o is the light intensity incident upon the cell, and A_T is the total absorbance of the solution, then I_a, the fraction of I_o absorbed, is given by,

$$I_a=I_o(1-10^{-A_T}) \tag{91}$$

The partitioning of the absorbed light amongst each particular component is proportional to that component's fraction of the total absorbance. If A_Q is the absorbance of the quencher measured in a solution by itself, then F_Q, the fraction of the total absorbance of a solution which has Q as one of its components at the same concentration A_Q was measured, is

$$F_Q = A_Q / A_T \tag{92}$$

where A_Q is rthe absorbance of the quencher. The correction factor to convert solutions with competitive absorption to a footing as if the effect was absent can be solved for by introducing it as an unknown and equating the corrected and unperturbed fractions.

$$(1-10^{-A_T})F_DC = (1- 10^{-A_D}) \tag{93}$$

$$C = \frac{1-10^{-A_D}}{F_D(1-10^{-A_T})} \tag{94}$$

This factor was used to correct steady-state emission spectra, since the steady-state concentrations of the excited-state are proportional to the fraction of light absorbed, regardless of the various decay pathways.

Solutions optically dilute at the emission maximum of $[Ru(bpy)_2dpp](ClO_4)_2$ (i.e. I_a less than .02), were not corrected for the inner filter. The concentration of $Ru(bpy)_2dpp^{2+}$ was in all cases small enough that its inner filter distortion was negligible. In the few cases where the absorption of the donor's emission by the quencher (i.e. trivial radiative energy transfer), was not negligible, a correction for the inner filter effect due to the overlap of the quencher's absorption spectrum with the emission spectra of the donor was used. Since the emitted light must pass through an average pathlength of ½ the cell path, the emitted light intensity is reduced by a factor of $10^{-A_Q/2}$.

$$I_{em}(\text{observed}) = I_{em}(\text{actual})10^{-A_Q/2} \tag{95}$$

Therefore, dividing the spectra point by point, by the factor $10^{-A_Q/2}$, which varies with wavelength, corrects the spectra for the quencher absorption of the donor emission.

In addition to the trivial effects arising from the spectral properties of the individual components in solution, the sensitivity of these quenching experiments is dependent upon the noise inherent in the detection circuitry under the conditions of the measurement. In these measurements, the metal complexes emit in the red end of the spectrum, where sensitivity is limited by the dark current of the tube. At room temperature the dark current output of the tube was less than 500 cps. All measurements

were made with a signal to noise ratio of greater than 30. The slitwidths were adjusted to attenuate the bandpass to be less than 20 nm. The dispersion of the 1681 single grating spectrometer is 3.77 nm/mm. Therefore, the slits were always kept less than 20/3.77 = 5.35 mm wide. O_2 quenching was negligible at 25 °C in an air-saturated solution, hence the solutions were not degassed.

(3.5) Analysis of the Time Dependence of the Steady-State Emission Intensity

These experiments were undertaken in order to exploit the unique characteristic of the quenching observed for some of the metal complexes that form products photochemically, as an event associated with quenching. The emission intensity under conditions of constant irradiation does not usually vary, if no net chemical change occurs. However, with the formation of a product, the concentration of emitting species in solution declines, leading to a decline in emission intensity. In addition, competitive absorption of the excitation intensity by the product(s) also contributes to the reduction in emission intensity, at sufficient extents of reaction.

Experiments examining the time dependence of the steady-state emission were performed on the previously described emission spectrometer. For these experiments the cell compartment was modified to accommodate the magnetic stirrer, cell stir bar, and temperature controlled cell used for kinetic absorbance measurements. The quencher stock solutions were prepared directly from solids for each trial and were used immediately. The instrument collected data in kinetics mode, at a rate in accord with the particular experiment's rate of change in aqueous solutions of the reagents. The excitation of $Ru(bpy)_2dpp^{2+}$ was always centered at 488 nm, and the emission monitored at 695 nm, when the experiments were performed in aqueous solution. Absolute light intensities,

for both quantum yield and steady-state emission with time experiments, were measured using ferrioxalate actinometry.[10]

The experimental data was first checked for consistency with the Stern-Volmer quenching law, using the initial concentration of quencher and initial intensity. In all cases the values obtained were in good agreement with the independently measured values obtained from earlier intensity quenching experiments. At a quencher concentration less than 10^{-3} M, where ion pairing had been shown to be negligible, the initial intensity values agreed well with values obtained from lifetime quenching. The intensity decays were then normalized to one. Numerical solutions to eqs 35 and 36 were generated using the ordinary differential equation solver.[40] A representative set of data, taken directly from the software in Appendix I.

The model shown in Appendix I generated the data in Figure 14. The value of (k_q+k_{qp}) was taken to be 3.2×10^9 $M^{-1}s^{-1}$. This was the value calculated using ${}^{T}K_{sv}$, obtained from lifetime quenching data and use of the relation

$$(k_q+k_{qp})\tau = {}^{T}K_{sv} \qquad (96)$$

The value of k_{qp} was varied to obtain agreement between the calculated and experimental data. Since no minimization routine was available within the software, the values successively improved by repetitive calculation, and comparison to the experimental data. The numerical solutions generated were found to be very stable with respect to step size, and particular solution method. The data set shown was generated using a Runga-Kutta method.

Figure 14. Experimental (♦) and best fit (—) data, obtained from numerical solution of eqs 35-37, for the reaction between $Ru(bpy)_2dpp^{2+}$ and $PtCl_6^{2-}$.

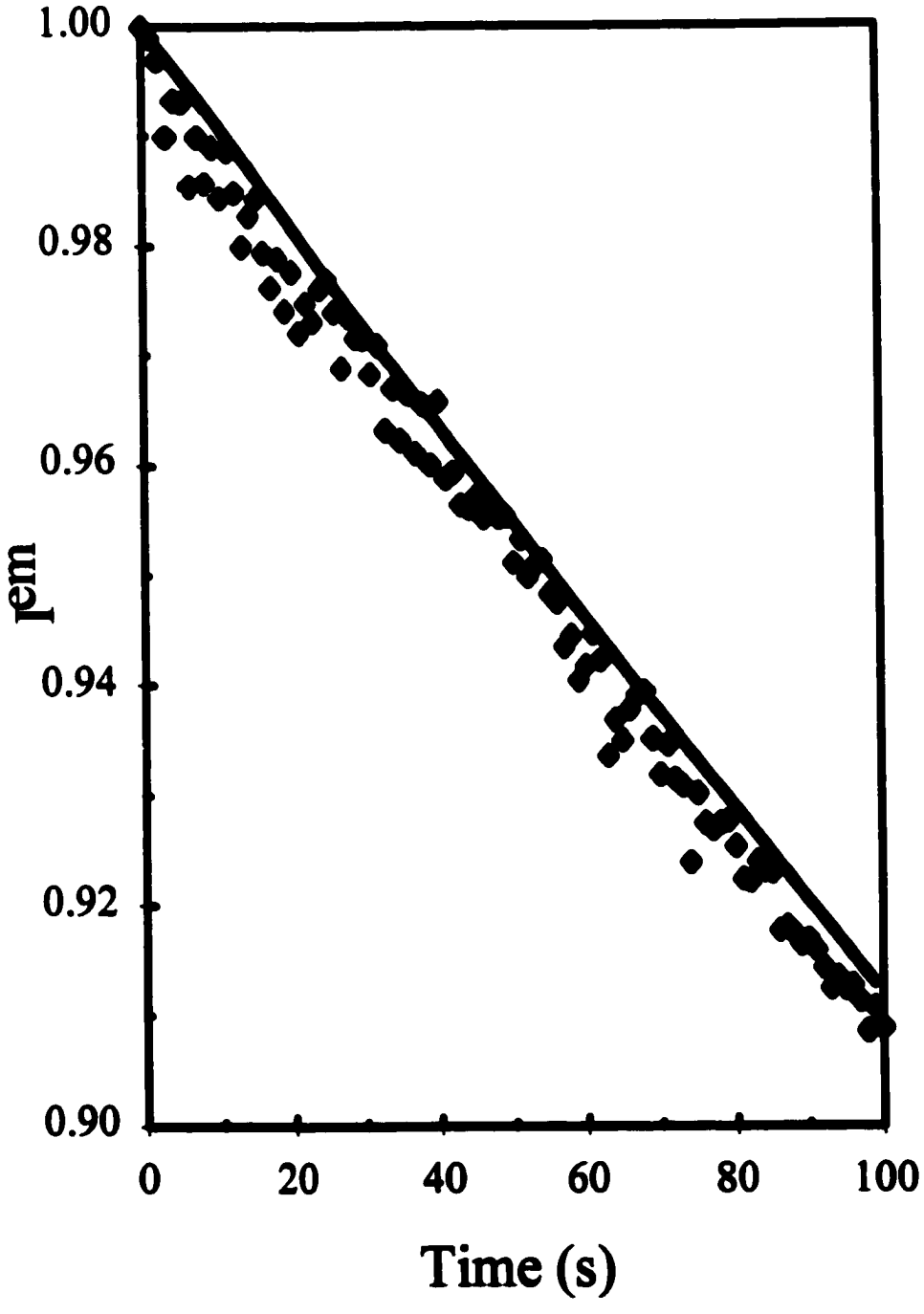

The values obtained from these solutions are not true values, but rather apparent values of ${}^{P}K_{sv}$, because they reflect ion pairing in addition to diffusion limited quenching. Since the fraction of donors that are ion paired varies with concentration of Q, therefore the apparent value of the ${}^{T}K_{sv}$, does also. Plots of ${}^{T}K_{sv}$(apparent) versus concentration of Q, were used to extrapolate back to the value of K_{sv} at infinite dilution of Q. The justification for this is that the extent of ion pairing must approach zero, as the concentration of quencher approaches zero, so the apparent value of ${}^{P}K_{sv}$ must approach the true value.

(3.6) Measurement of the Quantum Yield of Product Formation

Measurement of the quantum yields of product formation, were made using absorption spectroscopy to monitor the formation of products. The excitation source was the 488-nm emission of an Argon-Ion laser. Absorbance at ε_{max} for the products was monitored, and Beers law, (eq 16) was applied to the data. The absorbances were assumed to be additive,

$$A_T = A_{products} + A_{reactants} \tag{97}$$

$$A_T = \varepsilon_p B[P] + \varepsilon_{Ru} B([Ru(bpy)_2dpp^{2+}]_o - [P]) \tag{98}$$

where the square brackets indicate the concentration of the particular species. The absorbance of the quencher was in many cases negligible at the wavelength used to monitor product formation, and was therefore neglected. P is the bimetallic product.

$$[P] = \frac{A_T - \varepsilon_{Ru} B[Ru(bpy)_2dpp^{2+}]_o}{(\varepsilon_p - \varepsilon_{Ru})B} \tag{99}$$

With $Na_2[PtCl_6]$ and $Na_3[RhCl_6]$, the stock solutions were prepared in a 35 mm-film photocanister made of black plastic, by weighing the solid on an analytical scale, and syringing in solvent through a tiny hole punctured in the lid. Aliquots were then taken from this stock solution with glass syringe. In the case of $K_2RhCl_5H_20$ the solutions for each trial were prepared directly from solids in a cuvette. The absorption spectrum was taken immediately after mixing in order to establish its concentration and the solution was promptly used. In all cases, this rate data was treated with an initial rate assumption in order to extract the rates used calculate the quantum yield of product formation. The value of ε_p was estimated from a long irradiation assuming complete product conversion, as described earlier. The absorbance change used represented a signal to noise ratio of greater than 20. The standard deviation of the noise obtained from a trial where data was collected om a blank for 60 seconds is 0.005. Two standard deviations of the noise were considered, to give a 95% confidence level. Therefore the changes in absorbance used to measure the rate of reaction were no less than 0.01.

(3.7) Instrumentation

All NMR spectra were obtained on a Bruker 400MHz NMR spectrometer, outfitted with a fixed frequency probe for ^{13}C, and ^{1}H. Absorbance measurements were made on a Hewlett-Packard Model 8452 diode array absorption spectrometer, with a modified cell compartment as outlined earlier. Measurement of emission intensity was performed on a Spex-Fluorolog-2 emission spectrometer, outfitted with a Hammamatsu model R2658 red sensitive photomultiplier tube. In the case of the measurements of the time dependence of the steady-state emission intensity, the cell compartment was

modified as outlined earlier. The emission intensity decays were obtained from the detection system described earlier.

III. Results

(1) Reactions of $Na_2[PtCl_6]$

Measurement of the stability constant of $PtCl_6^{2-}$, as a function the concentration of HCl, has shown that in 3.0 M HCl no aquated products are detectable.[41] Since $Ru(bpy)_2dpp^{2+}$ is completely proton quenched at concentrations of acid greater than .10 M, high NaCl concentrations were used instead of HCl. The extent of aquation was evaluated by monitoring changes in the UV absorption spectrum. An estimate of the rate in 3.0 M NaCl at 25 °C, was made by monitoring two declining spectral changes centered at 216 and 264 nm. Having no knowledge of ε's of the aquated products made it necessary to use a declining change, and neglect the absorbance of the aquated products (Figure 15). The slope of this plot is 2.2×10^{-9} M/s. Using this data and the initial concentration of $PtCl_6^{2-}$, it was found that $PtCl_6^{2-}$ undergoes aquation with a pseudo first-order rate constant no greater than 2.6×10^{-5} s^{-1}. This was consistent with a value of 5.0×10^{-7} s^{-1} estimated[42] from Archibald's data.[43] Therefore, a freshly prepared solution could be expected to be no more than 3.0% aquated within 2 minutes by the most conservative estimates.

Reflux of an aqueous solutions of the $PtCl_6^{2-}$ and $Ru(bpy)_2dpp^{2+}$ in the dark for several hours, leads to formation of the corresponding bimetallic complex produced by substitution of two chlorides by the free imine nitrogens of dpp. (Figure 16). In contrast, 488 nm irradiation of $Ru(bpy)_2dpp^{2+}$ in the presence of $PtCl_6^{2-}$, leads to the formation of the bimetallic complex $Ru(bpy)_2dppPtCl_4^{2+}$ to a measurable extent within seconds (Figure 17) Thin layer chromatography using an alumina plate and eluting with

Figure 15. Plot of concentration versus time used to estimate the rate of aquation of $PtCl_6^{2-}$.

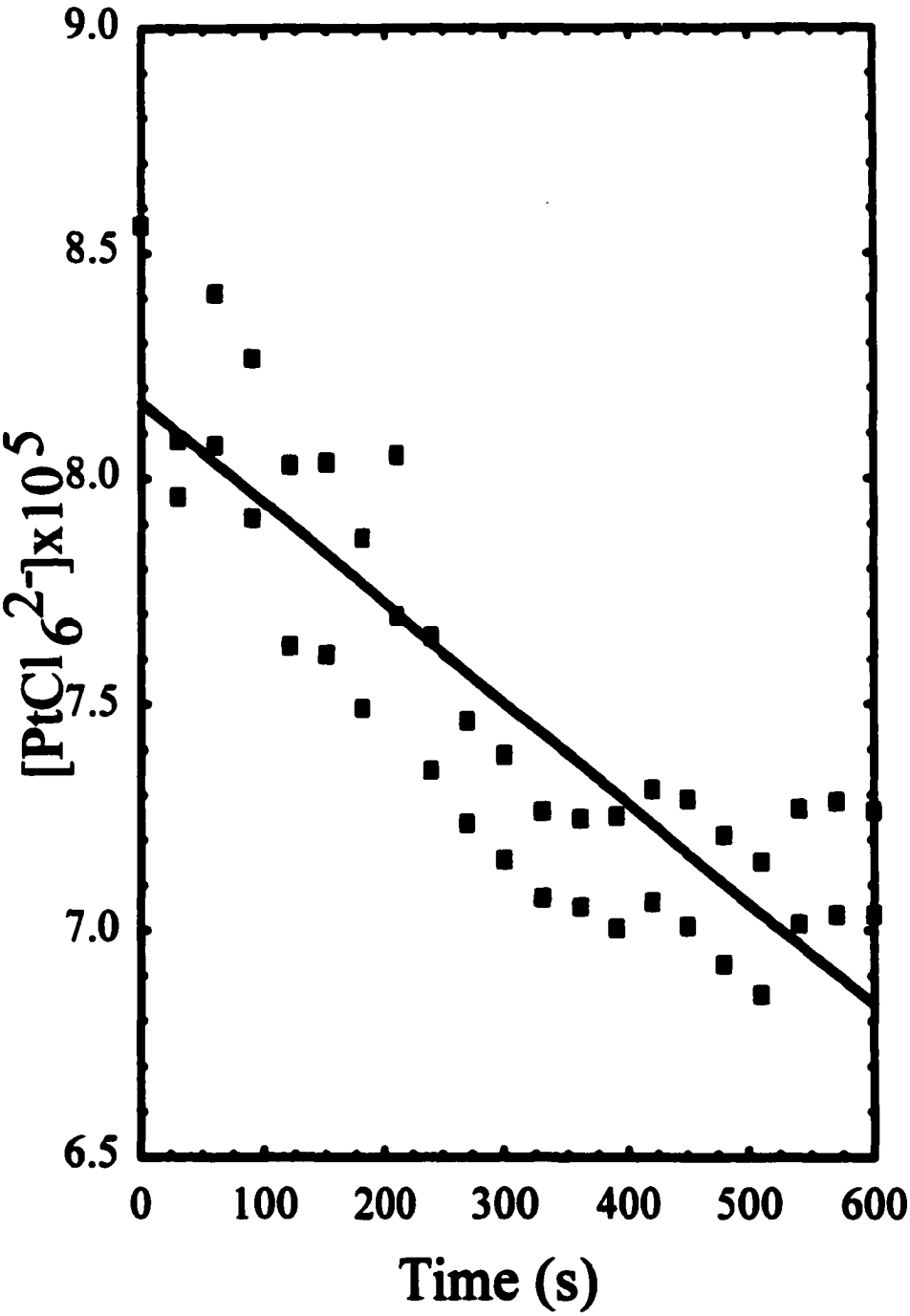

Figure 16. Absorbance spectra taken of a reaction mixture 10^{-4} M in $Ru(bpy)_2dpp^{2+}$ and 5.0×10^{-4} M in $PtCl_6^{2-}$ after reaction in the dark at 100 °C indicating chelation at the peripheral imine nitrogens of $Ru(bpy)_2dpp^{2+}$.

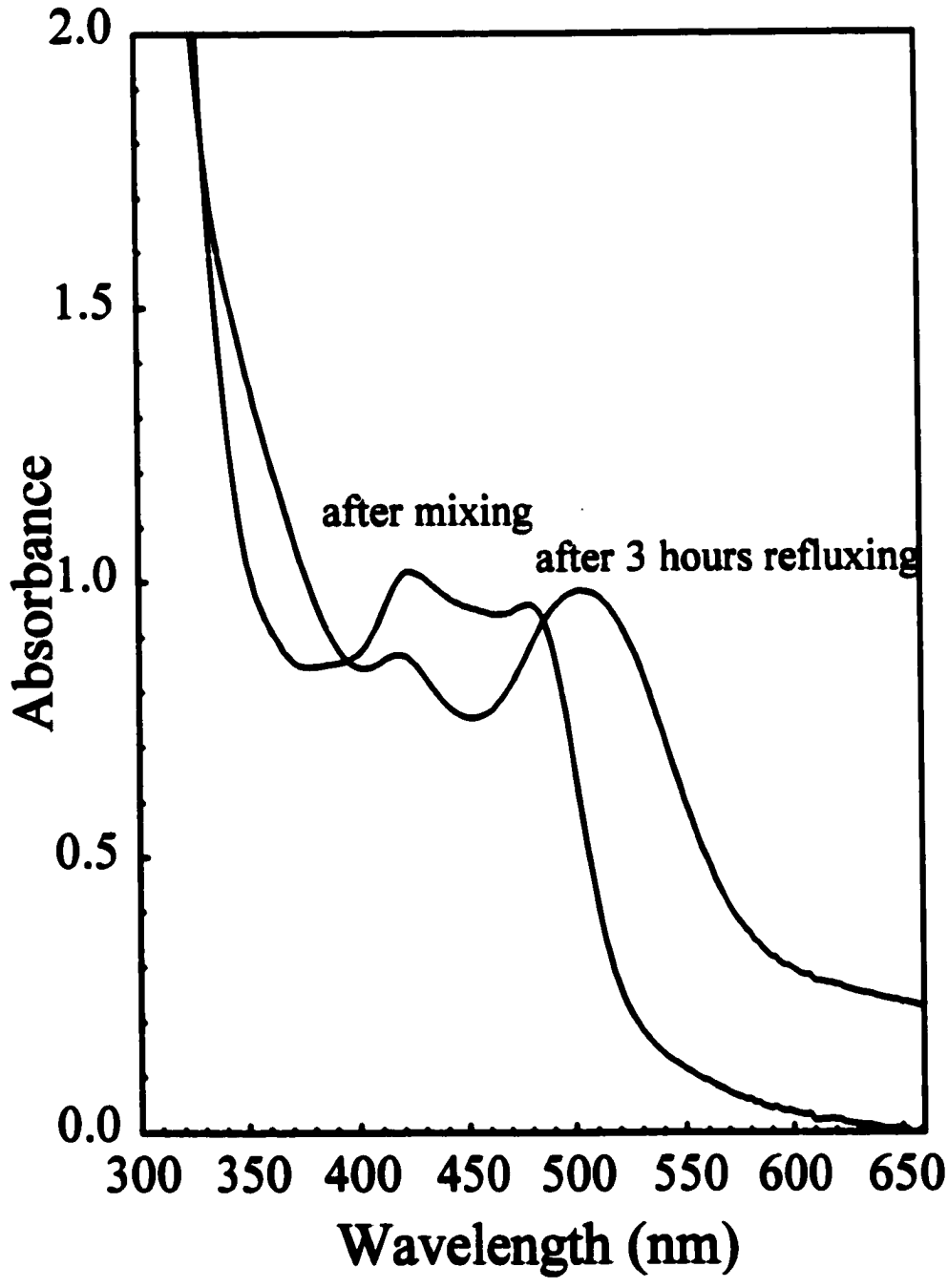

Figure 17. Absorption spectra taken of a reaction mixture 10^{-4} M in $Ru(bpy)_2dpp^{2+}$ and 5.0×10^{-4} M in $PtCl_6^{2-}$ as the solution was irradiated with the 488-nm laser line of an argon ion laser. Spectra shown are taken every 30 seconds.

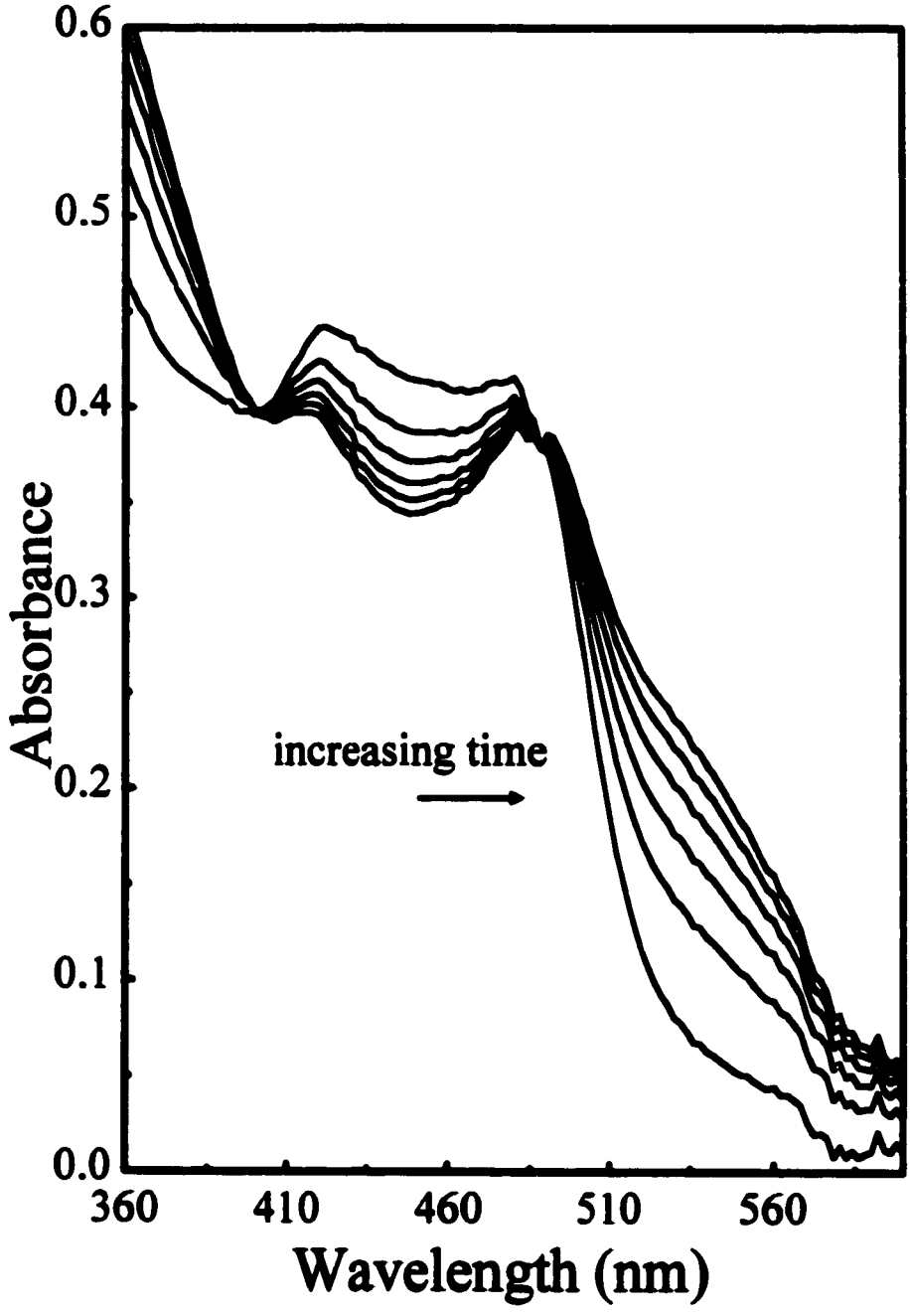

acetonitrile indicated the formation of single product. Attempts to purify this product on a larger scale were unsuccessful. Decomposition during elution was significant enough to make column chromatography impractical.

$PtCl_6^{2-}$ quenches the emission of $Ru(bpy)_2dpp^{2+}$ (Figure 18). Most of the experimental data in this work uses the sodium salts of $PtCl_6^{2-}$. However, no measurable difference between potassium and sodium salts was observed and a K_{sv} value of 403 ± 16 M^{-1} was obtained from the lifetime quenching data. Use of platinic acid, H_2PtCl_6, yielded values of K_{sv} larger than other counterions due to proton quenching, and was for this reason not used. The data in Table 3 illustrates the decline in lifetime with increased concentration of quencher. In 3.0 M NaCl, values of ${}^{T}K_{sv}$ obtained from intensity and lifetime quenching agree within experimental error, over the range restricted to a concentration of $PtCl_6^{2-}$ less than 1.0×10^{-2} (Figure 19). Outside this range, intensity data shows an upward curvature, attributed to ion pairing of $Ru(bpy)_2dpp^{2+}$ with $PtCl_6^{2-}$, even at this high ionic strength. Fitting this data to eq 26, using a nonlinear parameter optimization, yield a value of 55 ± 3 M^{-1}, for the equilibrium constant for the formation of $[Ru(bpy)_2dpp^{2+}\text{-}PtCl_6^{2-}]$ ion pair.

The spectral change for both the thermal and photochemical reactions is identical. Based on these results and other data presented below, the product was identified as the bimetallic $Ru(bpy)_2dppPtCl_4^{2+}$. An estimate of the absorption spectrum of the product was obtained by irradiating a solution 5.0×10^{-5} M in $Ru(bpy)_2dpp^{2+}$ and 10^{-3} M in $PtCl_6^{2-}$ until no further change occurred. Under the assumption that all of the $Ru(bpy)_2dpp^{2+}$ had reacted, the remaining starting material was subtracted and the

Figure 18. Stern-Volmer plots for intensity (●) and lifetime (◆) quenching of $Ru(bpy)_2dpp^{2+}$ by $PtCl_6^{2-}$ in 3.0 M NaCl.

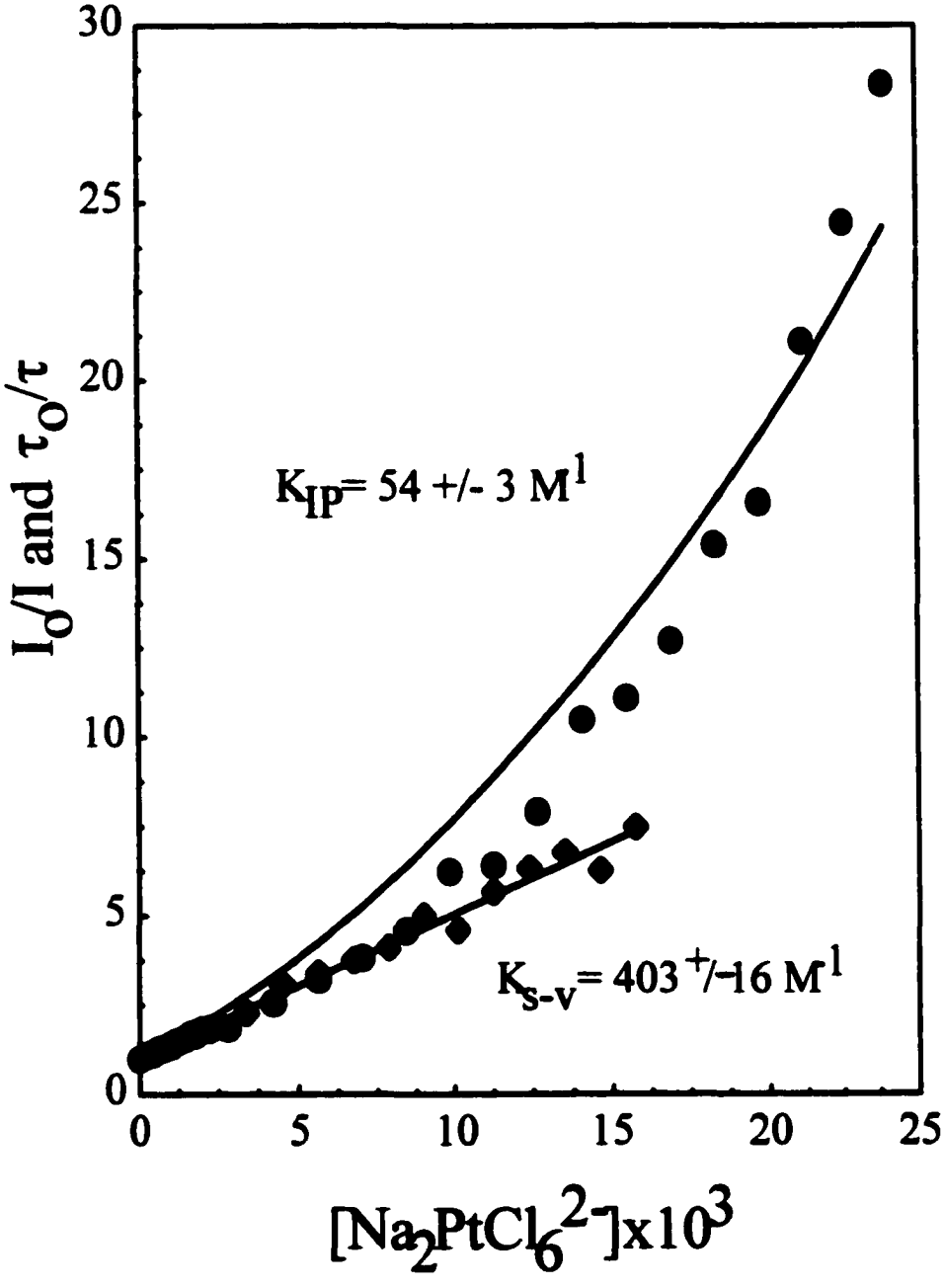

Figure 19. Stern-Volmer plot for the quenching of $Ru(bpy)_2dpp^{2+}$ by $PtCl_6^{2-}$ in 3.0 M NaCl over a range of quencher less than 10^{-2} M.

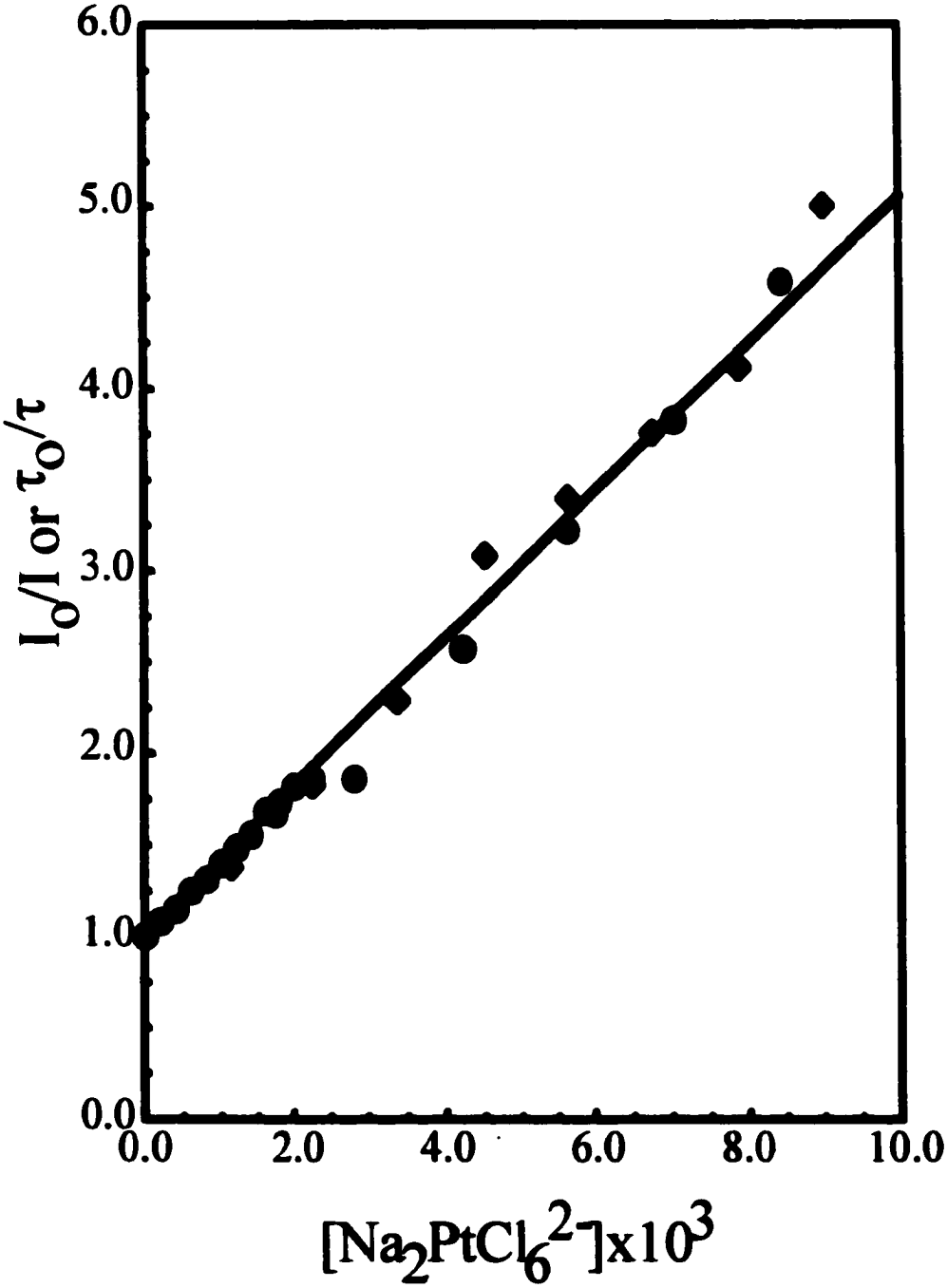

Table 3. Lifetime quenching data for $PtCl_6^{2-}$ quenching $Ru(bpy)_2dpp^{2+}$ in 3.0 M NaCl.

$[PtCl_6^{2-}]x10^3$ (M)	τ (ns)	τ_o/τ
0.00	131	1
1.13	95	1.38
2.25	72	1.83
3.38	58	2.29
4.50	43	3.08
5.63	39	3.39
6.75	35	3.76
7.88	32	4.12
9.00	26	5.00
10.13	28	4.60
11.25	23	5.67
12.38	21	6.33
13.50	19	6.78
14.63	21	6.27
15.75	18	7.49

resulting spectrum had a maximum at 525 nm with ε equal to 12,000 $M^{-1}cm^{-1}$. This was found to be in reasonable agreement with the value of 12,125 $M^{-1}cm^{-1}$ that was obtained later, when mg amounts of the product were isolated (Figure 20).

A plot of $1/\phi_p$ versus $1/[PtCl_6^{2-}]$ is quite linear and the inverse of the slope gives the ${}^{P}K_{sv}$, yielding a value of $20 \pm 1\ M^{-1}$ (Figure 21 and Table 4). The data for dependence of quantum yield of product formation as a function of concentration of $PtCl_6^{2-}$, is shown in Table 4. The ratio of intercept to slope gives a value of ${}^{T}K_{sv}$, equal to $417 \pm 250\ M^{-1}$, which is within experimental error of the values obtained from the lifetime and intensity quenching. The intercept redundantly gives the limiting yield of product formation as .05 -.11 or the ratio of the product formation ${}^{P}K_{sv}/{}^{T}K_{sv}$. The value of ${}^{T}K_{sv}$ was found to be independent of the concentration of the donor, $Ru(bpy)2dpp^{2+}$, as predicted by the Stern-Volmer quenching law (Figure 22).

Relative values of the quantum yield of product formation, were also measured as a function of the concentration of $Ru(bpy)_2dpp^{2+}$. Under conditions where greater than 98% of the light was absorbed by $Ru(bpy)_2dpp^{2+}$, the quantum yield was independent of the concentration of $Ru(bpy)_2dpp^{2+}$ (Figure 23). The concentration of $PtCl_6^{2-}$ was 2.0×10^{-4} M in all of these trials. The quantum yield of product and data from which it was calculated from are shown in Table 5. Under conditions where $PtCl_6^{2-}$ absorbance accounted for fractions of the absorbed light greater than 5%, the quantum yield was found to be strongly dependent upon the concentration of $Ru(bpy)_2dpp^{2+}$ (Figure 24). In all of these trials, the concentration of $PtCl_6^{2-}$ was 1.86×10^{-3} M, causing a non-negligible fraction of light be absorbed by the $PtCl_6^{2-}$.

Figure 20. Plot of the values of the molar absorptivity (ε), for the bimetallic product, $Ru(bpy)_2dppPtCl_4^{2+}$.

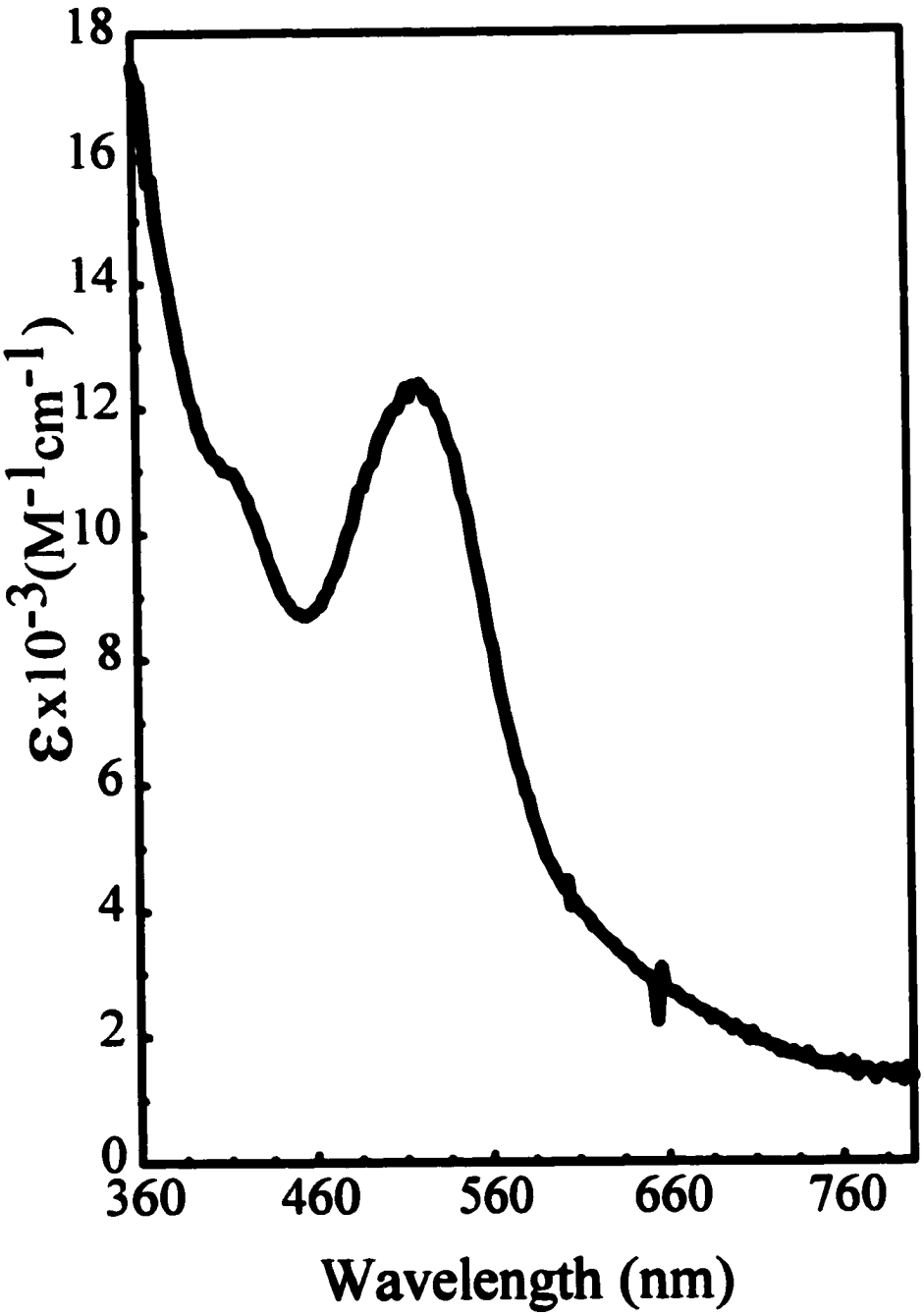

Table 4. Values of the quantum yield of formation of [$Ru(bpy)_2dppPtCl_4^{2+}$] at 488 nm, as a function of the concentration of $PtCl_6^{2-}$, in 3.0 M NaCl.

$[PtCl_6^{2-}]x10^4$ (M)	$\phi_n x10^3$
2.0	3.68
1.9	3.24
1.8	3.24
1.7	3.09
1.6	2.76
1.5	2.60
1.4	2.21
1.3	2.11
1.2	2.21
1.1	2.08
1.0	1.90
0.90	1.65
0.80	1.49
0.70	1.56
0.60	1.27
0.50	1.04
0.40	1.00
0.30	0.56
0.20	0.39
0.10	0.19

Figure 21. Plot of inverse of quantum yield of product formation vs. inverse of concentration of $PtCl_6^{2-}$, used to evaluate ${}^{T}K_{sv}$ and ${}^{P}K_{sv}$, from the rate photochemical product formation.

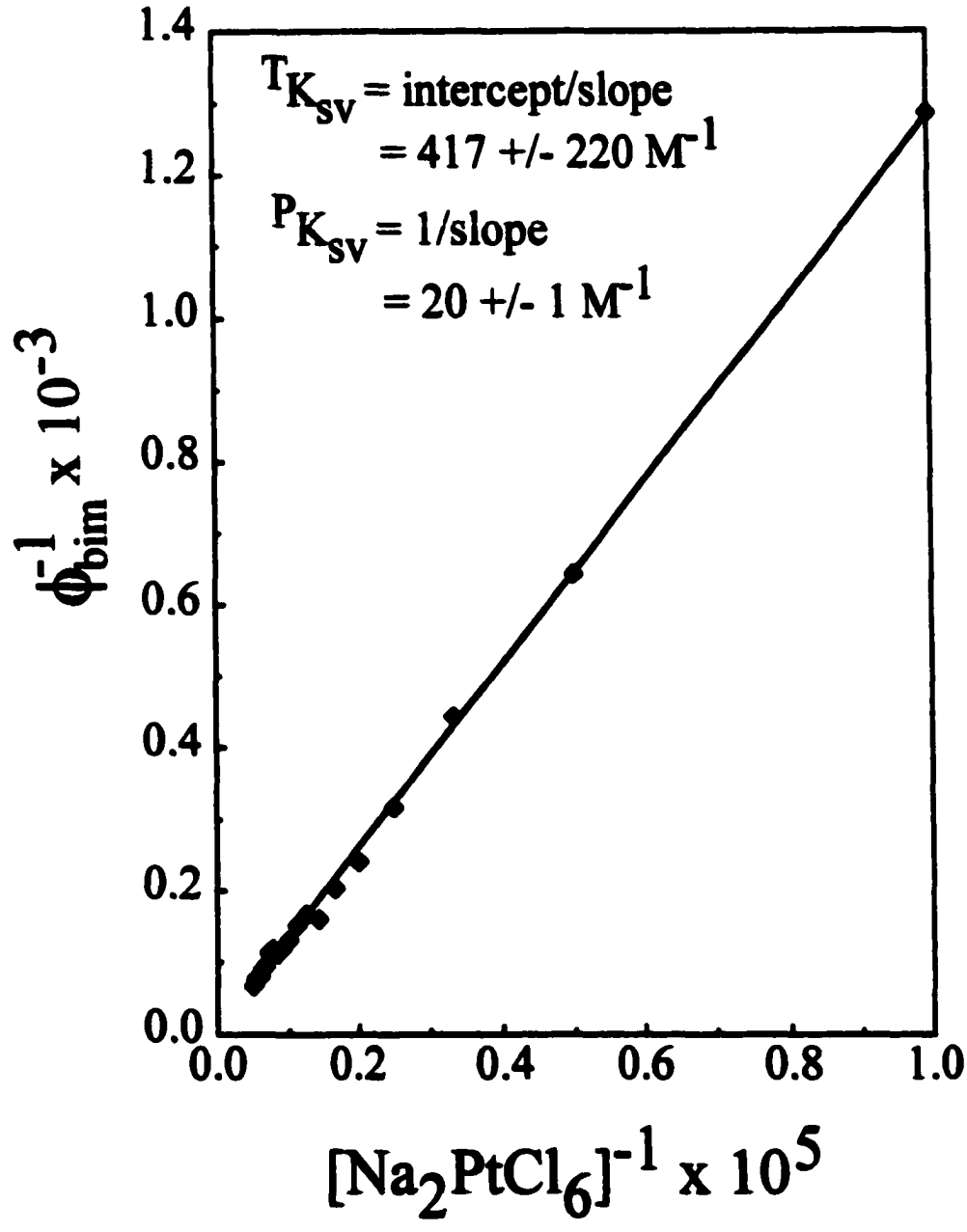

Figure 22. The dependence of the total Stern-Volmer constant ($^{T}K_{sv}$) on the concentration of $Ru(bpy)_2dpp^{2+}$.

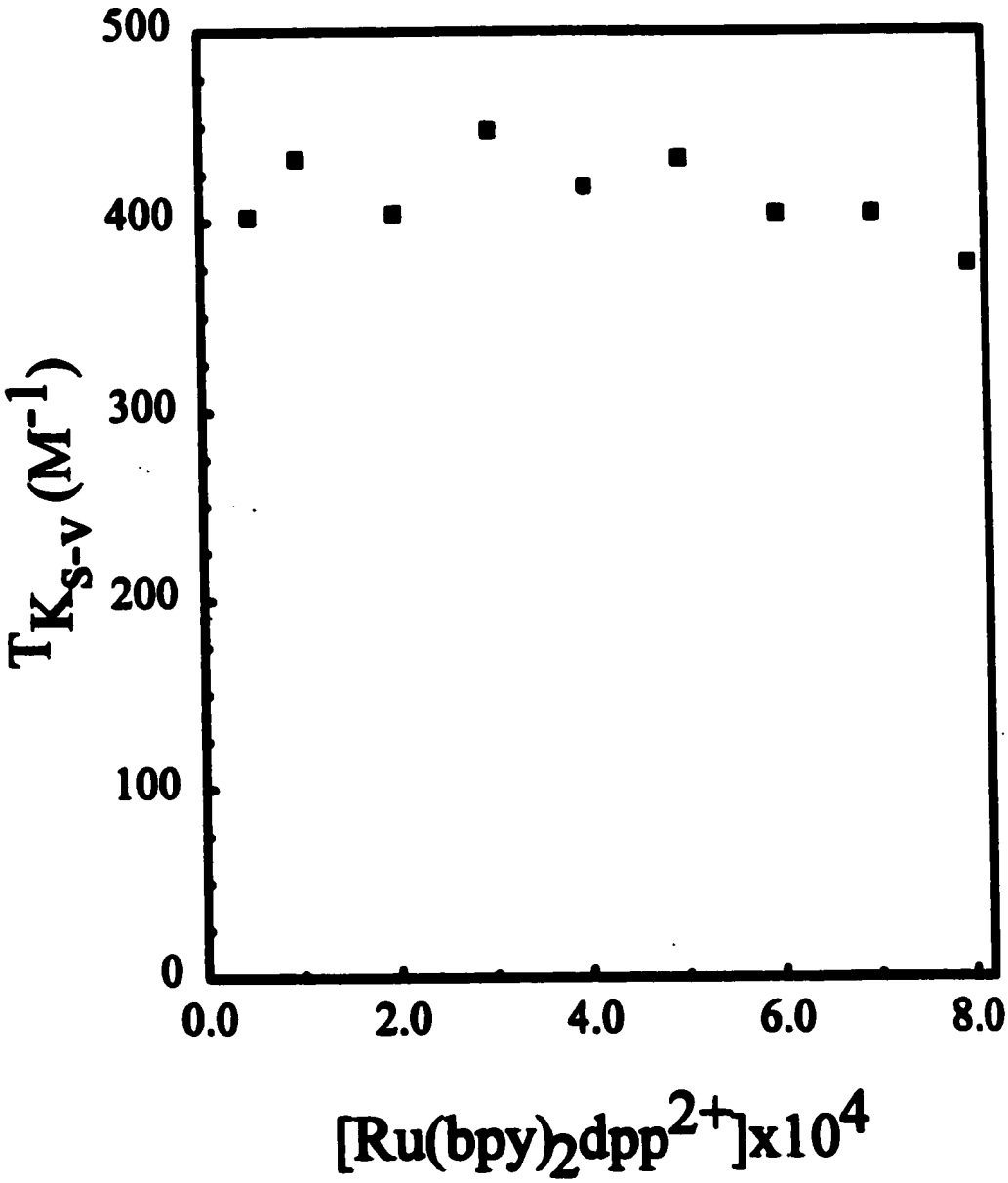

Figure 23. Relative quantum yield of formation of $Ru(bpy)_2dppPtCl_4^{2+}$ as a function of the concentration of $Ru(bpy)_2dpp^{2+}$ in 3.0 M NaCl. Concentration of $PtCl_6^{2-} = 2.0 \times 10^{-4}$ M.

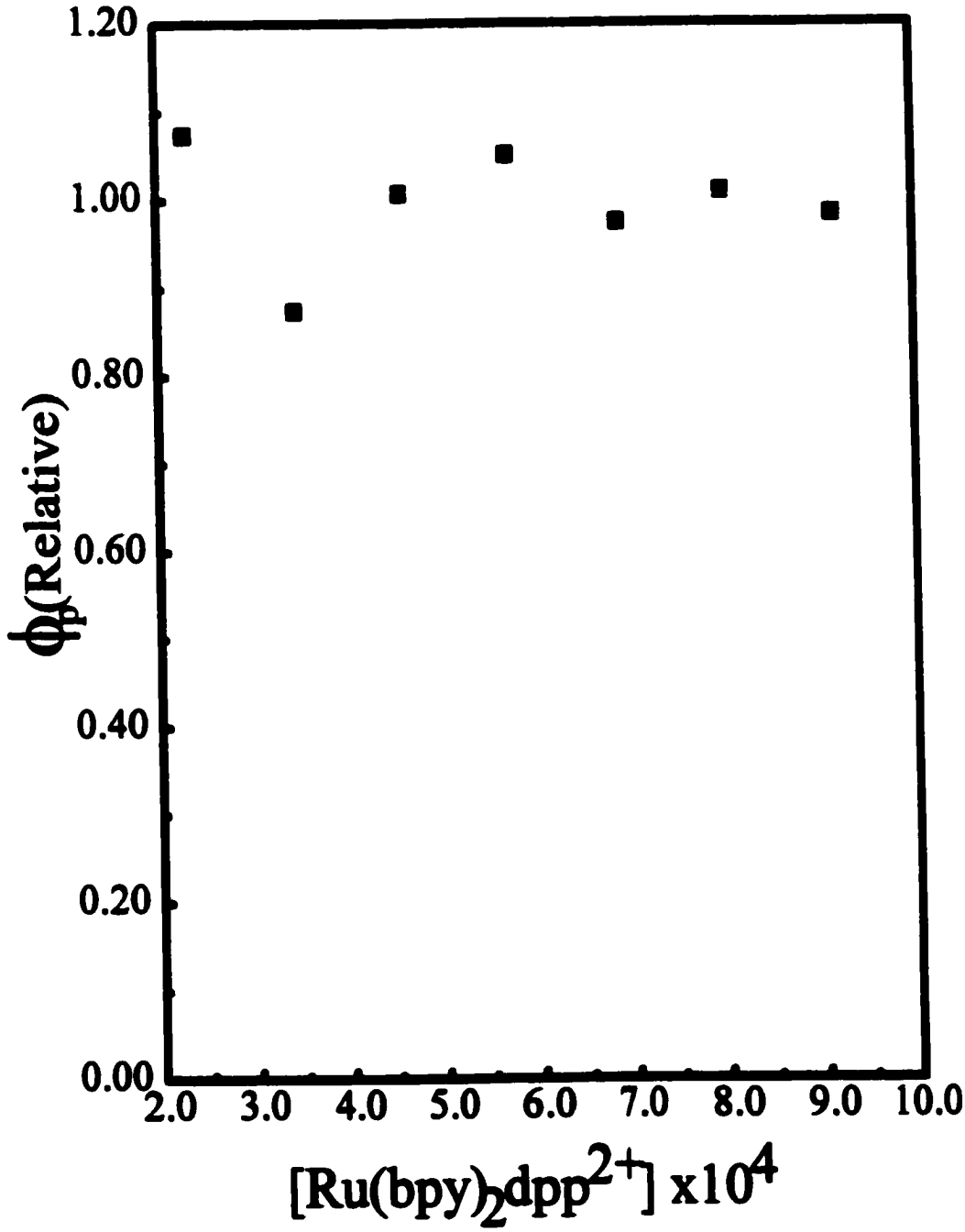

Table 5. Quantum yield of product formation as a function of the concentration of $Ru(bpy)_2dpp^{2+}$, with a concentration of $PtCl_6^{2-}$ of 2.0×10^{-4} M

$[Ru(bpy)_2dpp^{2+}] \times 10^4$	Relative rate	A_{Ru}/A_{tot}	ϕ_p (relative)
9.13	0.98	0.9991	0.98
7.99	1.01	0.9989	1.00
6.85	0.97	0.9988	0.97
5.70	1.05	0.9986	1.04
4.56	1.00	0.9982	0.99
3.42	0.87	0.9967	0.87
2.28	1.06	0.9866	1.06

Figure 24. Relative quantum yield of formation of $Ru(bpy)_2dppPtCl_4^{2+}$ as a function of the concentration of $Ru(bpy)_2dpp^{2+}$ in 3.0 M NaCl. Concentration of $PtCl_6^{2-}$ = 1.86×10^{-3} M.

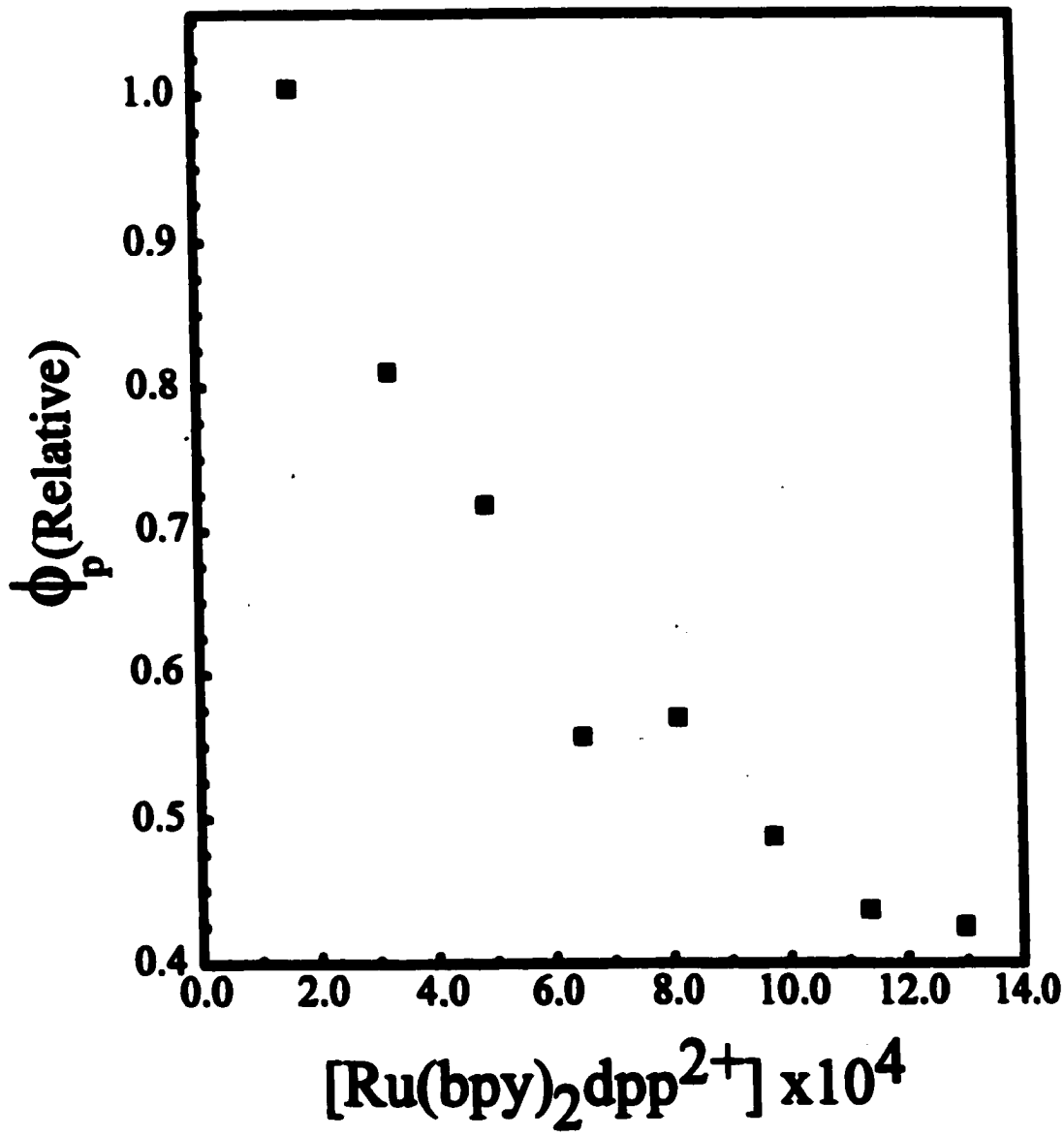

Attempts to numerically integrate the equations governing decline in emission intensity under conditions of constant irradiation, as a function of one input the parameter k_{qp},yielded values dependent upon the concentration of the hexachloride (Table 6).This is due to ion-pair quenching, since the intensity quenching reflects static as well as diffusional events. At higher concentrations of quencher, greater fractions of become ion-paired in the ground state. Upon excitation these ion-pairs require no diffusion for quenching to occur, since they are already in close enough proximity. Therefore, this fraction of the excited species decays very rapidly.

A value of K_{sv} was extracted by numerical solution of eqs 35-37, varying the value of k_{qp}, as outlined in the experimental section. In order to extract $^{P}K_{sv}$ from this data, it is necessary to extrapolate back to infinite dilution. A plot of the apparent value of the Stern-Volmer constant for product formation ($^{P}K_{sv}$(apparent)) versus concentration of $PtCl_6^{2-}$, had an intercept, at zero $PtCl_6^{2-}$ concentration, equal to 25 ± 10 M^{-1} (Figure 25). This is the limiting value, reflecting diffusion limited quenching only. This value is within experimental error of the value of 20 ± 1 M^{-1}, obtained from the quantum yield data.

A competitive quenching experiment was performed, where $FeCl_3$, a known quencher of $Ru(bpy)_2dpp^{2+}$ with K_{sv} equal to 650 ± 68 M^{-1} (Figure 26), was used to intercept increasing fractions of the excited-state population of $Ru(bpy)_2dpp^{2+}$. Quantum yield of product formation ϕ_p, for $Ru(bpy)_2dppPtCl_4^{2+}$, was measured as a function of [$FeCl_3$] and was found to be sharply reduced with increasing [$FeCl_3$]. (Figure 27)

Table 6. Values of $^{P}K_{sv}$, obtained from numerical integration of the equations governing the decline in emission intensity, under conditions of constant irradiation.

$[PtCl_6^{2-}]x10^3$	Apparent ${}^{P}K_{s-v}$ (M^{-1})
0.0976	23
0.184	30
1.192	87
1.31	36
3.089	111
3.712	111
5.428	169

Figure 25. Plot of $^{P}K_{rv}$(apparent), vs. concentration of $PtCl_6^{2-}$ used to extrapolate back to infinite dilution. Values generated from a numerical integration.

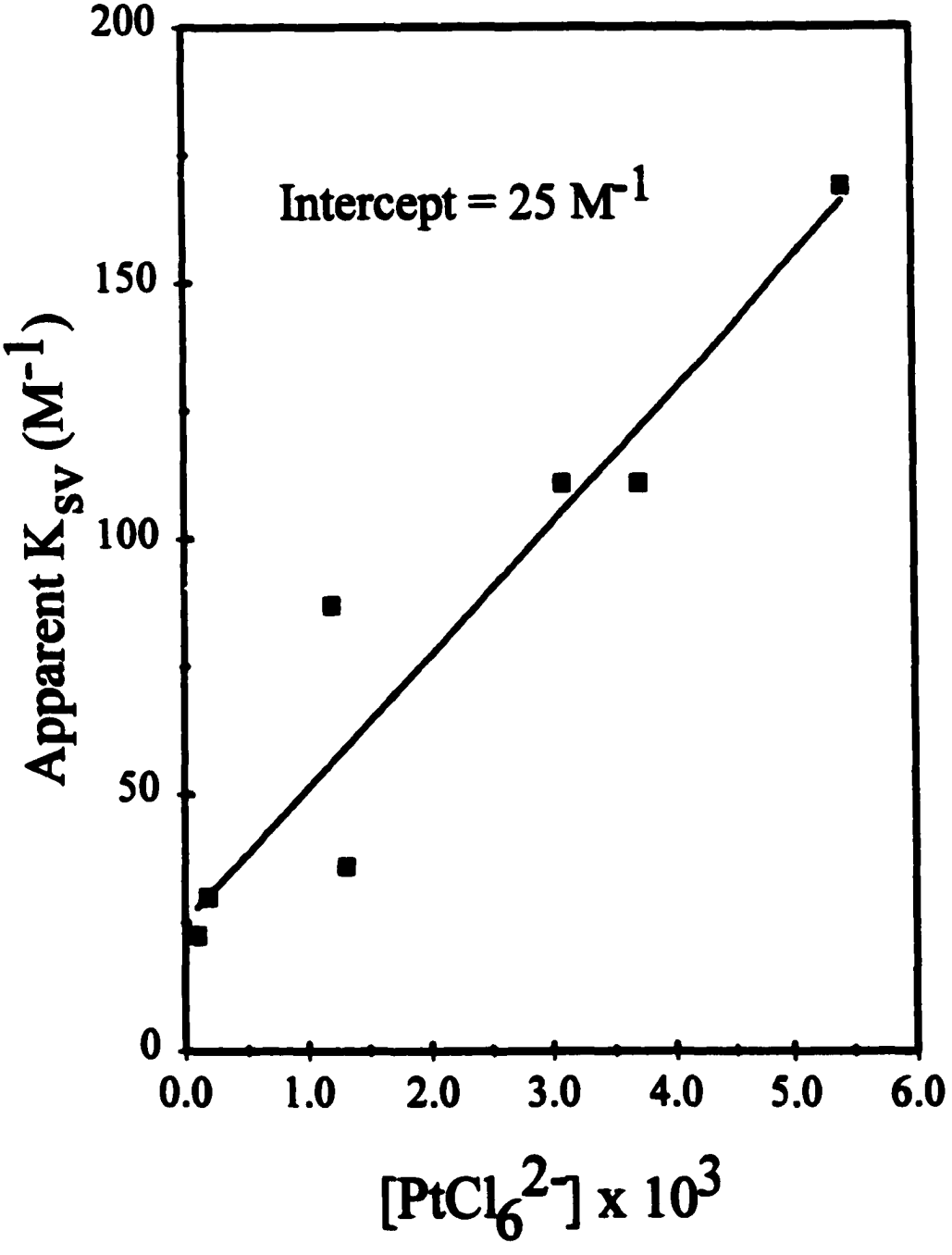

Figure 26. Stern-Volmer intensity quenching plot, for the quenching of $Ru(bpy)_2dpp^{2+}$ by $FeCl_3$ in 3.0 M NaCl.

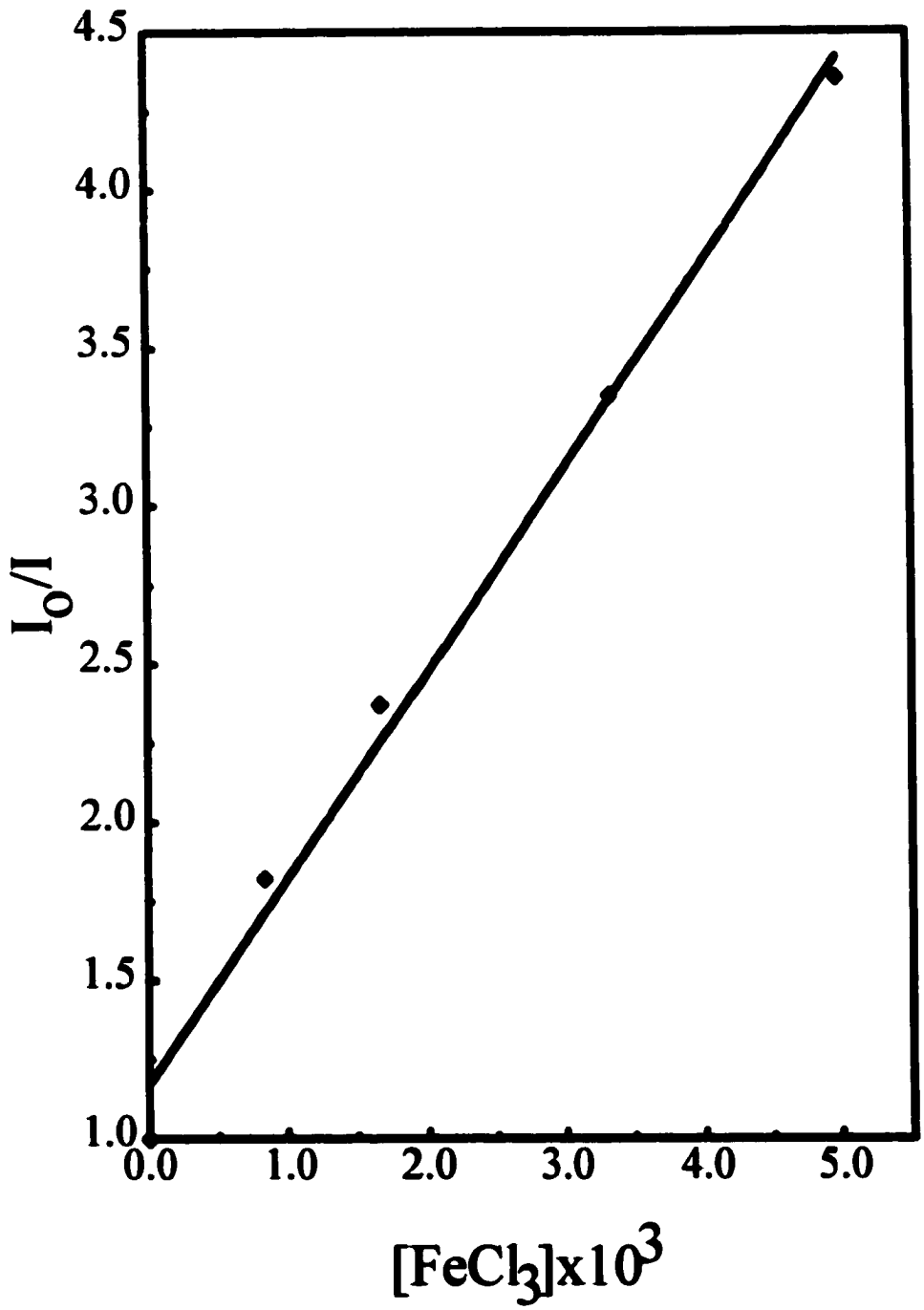

Figure 27. Quantum yield of formation of $Ru(bpy)_2dppPtCl_4^{2+}$ (ϕ_p) with increasing concentration of a competitive quencher $FeCl_3$.

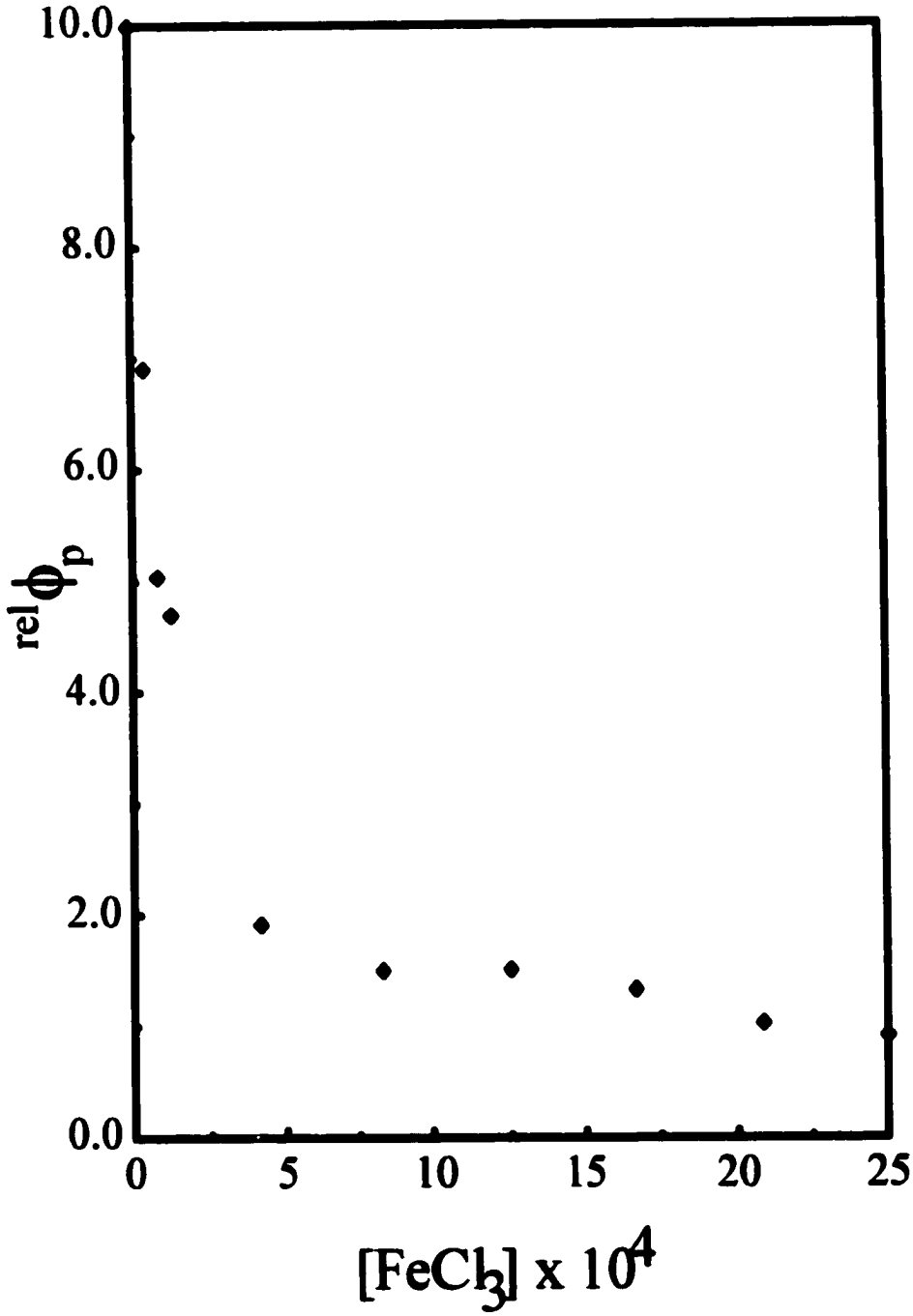

The quantum yield of bimetallic formation was measured as a function of $[PtCl_4^{2-}]$ to determine if any of the known chemistry linking $PtCl_4^{2-}$ and $PtCl_6^{2-}$ might play a role in photochemical product formation (Figure 28) The concentration range was limited so that $PtCl_4^{2-}$ absorbed less than 5% of the incoming light. Within experimental error, the rate of bimetallic formation was independent of the amount of $PtCl_4^{2-}$ present.

(2) Reactions of $K_3[RuCl_6]$

In aqueous 5.0 M NaCl, $K_3[RuCl_6]$ appears to monoaquate rapidly, consistent with reports in the literature, that it is substitution labile.[44] The absorption spectrum of a freshly prepared solution with $K_3[RuCl_6]$ equal to 5.1×10^{-4}, was monitored every 60 seconds. Significant monoaquation is apparent from the maintenance of 5 isosbestic points at 327, 364, 384, 472, and 526 nm.(Figure 29) Within 400 seconds, the solution reached equilibrium, as shown by (Figure 30) These spectra and one other taken one hour after mixing, when the spectra had ceased to significantly change, were used to estimate the pseudo first-order rate constant for aquation. Assuming the equilibration after one hour represented complete monoaquation, this implies a value of k_{aq} greater than 5.6×10^{-3} s^{-1}. While the first aquation has been previously reported to very rapid, the second aquation step to form either isomer of $RuCl_4(H_2O)_2^-$, has been reported to have a half life of about a year.[45] Therefore, stock solutions prepared from $K_3[RuCl_6]$ were predominantly the monoaqua species, $RuCl_4(H_2O)_2^-$. On the qualitative side, these solutions displayed changes apparent to the eye within 30 minutes, growing darker and forming a muddy precipitate.

Stock solutions of $RuCl_6^{3-}$ displayed reaction with $Ru(bpy)_2dpp^{2+}$ to form a bimetallic complex thermally (Figure 31), though not photochemically over a period of

Figure 28. Quantum yield of formation of $Ru(bpy)_2dppPtCl_4^{2+}$ (ϕ_p) with increasing concentration of $PtCl_4$

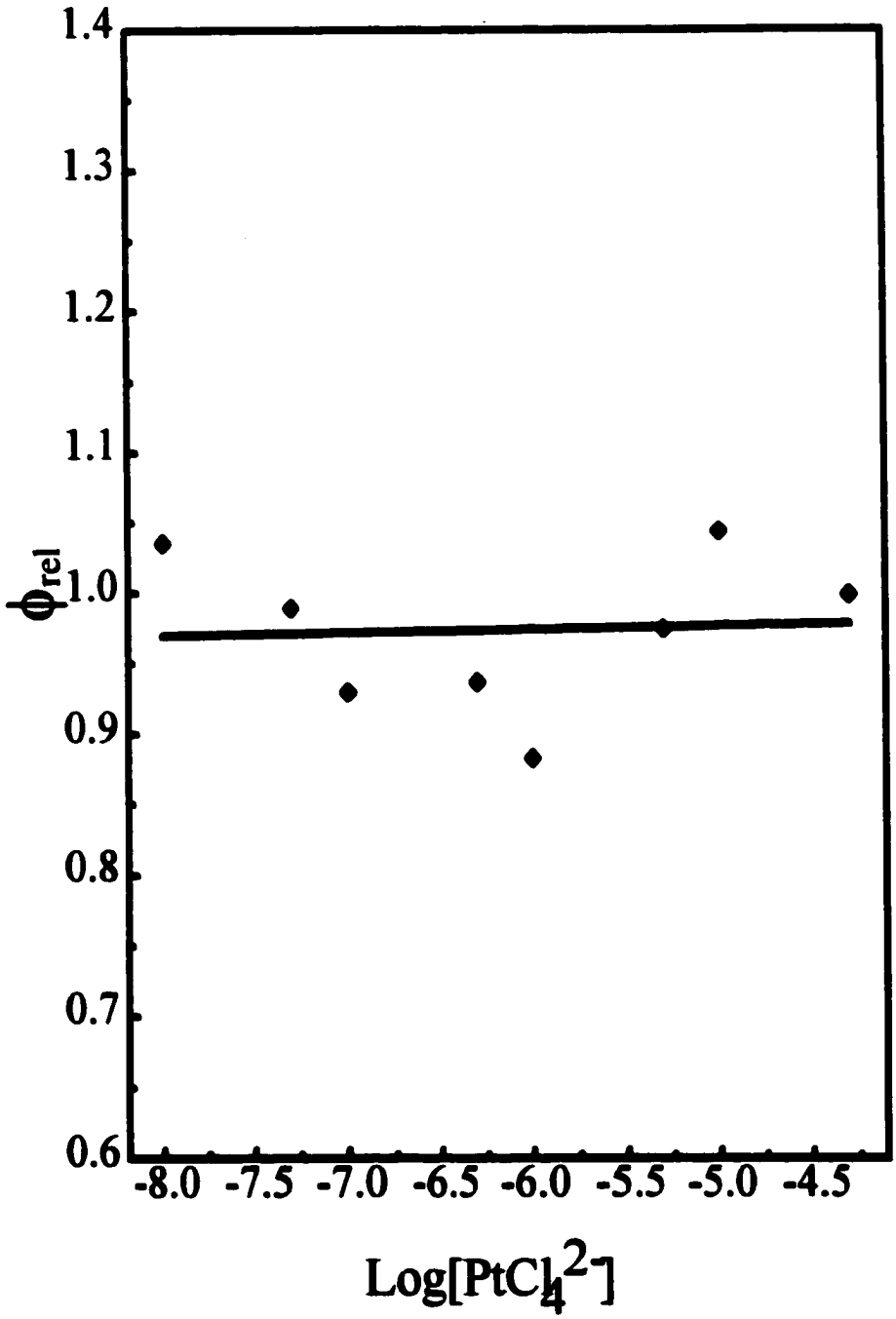

Figure 29. Spectral change obtained upon dissolving K_3RuCl_6 in 5.0 M NaCl. Spectra shown were taken every 60 seconds.

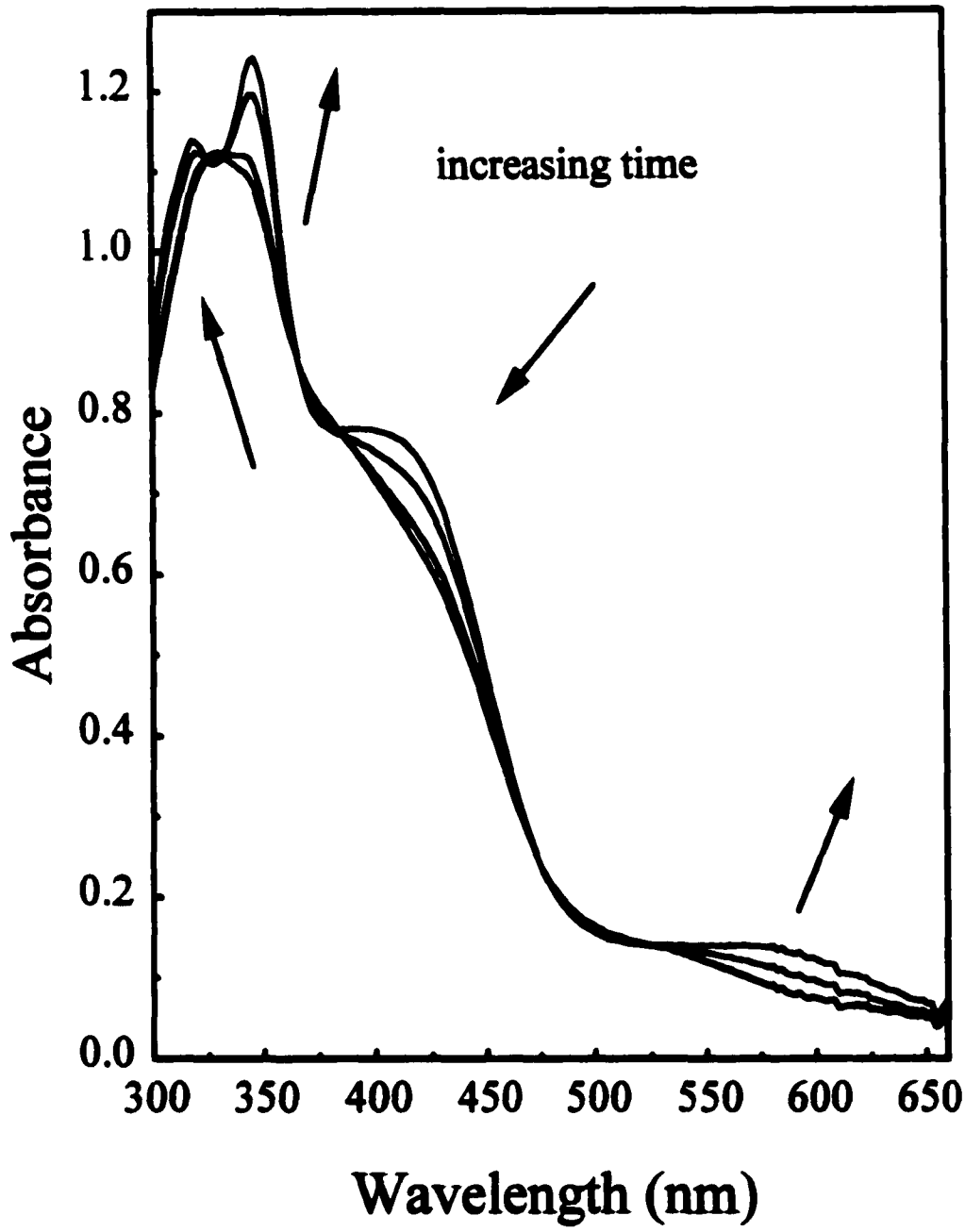

Figure 30. Plot of absorbance at 596 nm vs. time for a freshly prepared solution 5.1×10^{-4} M in $RuCl_6^{3-}$.

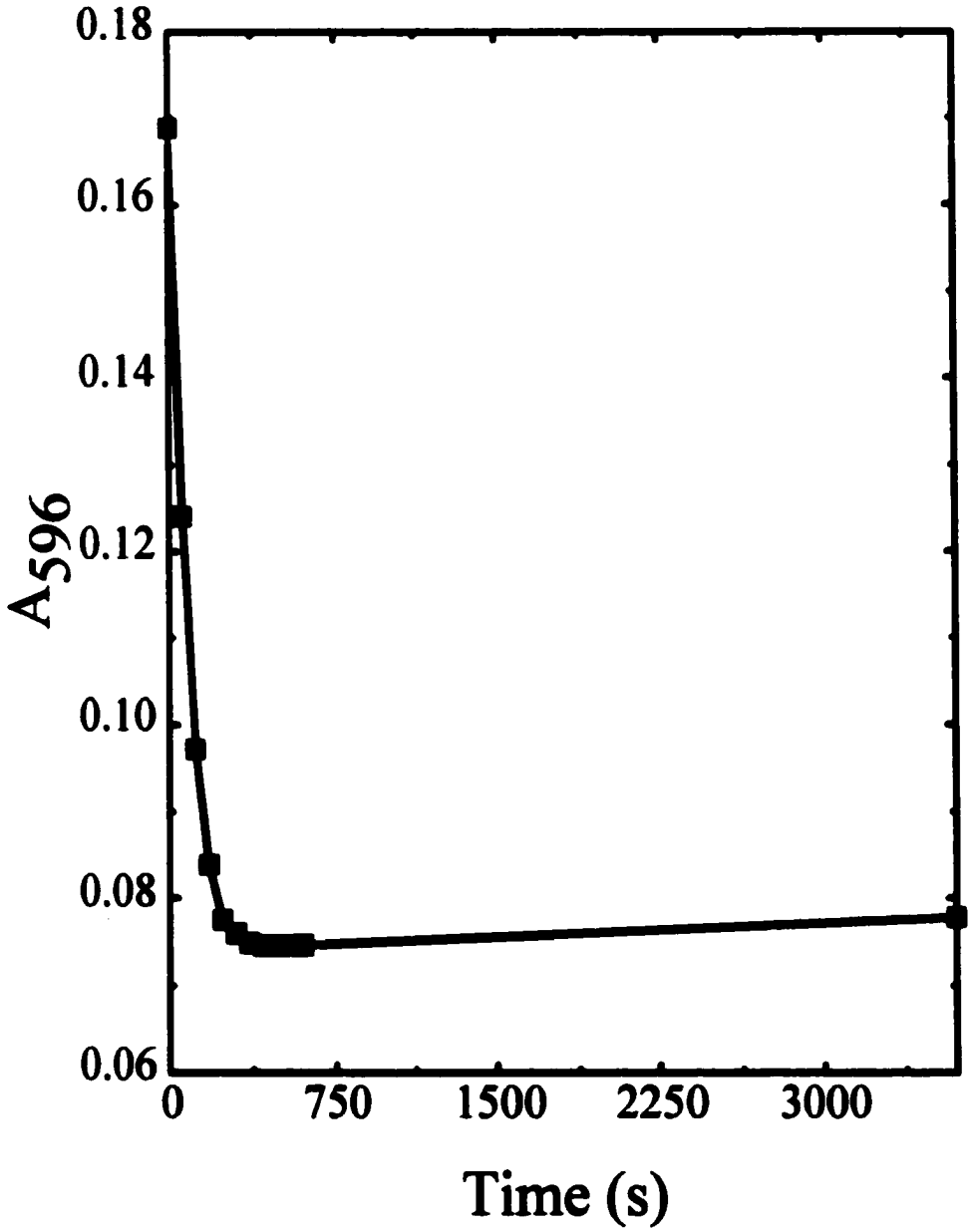

Figure 31. Spectral change obtained for a solution 10^{-4} M in $RuCl_6^{3-}$ and 1.2×10^{-4} M in $Ru(bpy)_2dpp^{2+}$ over three days in the dark at room temperature.

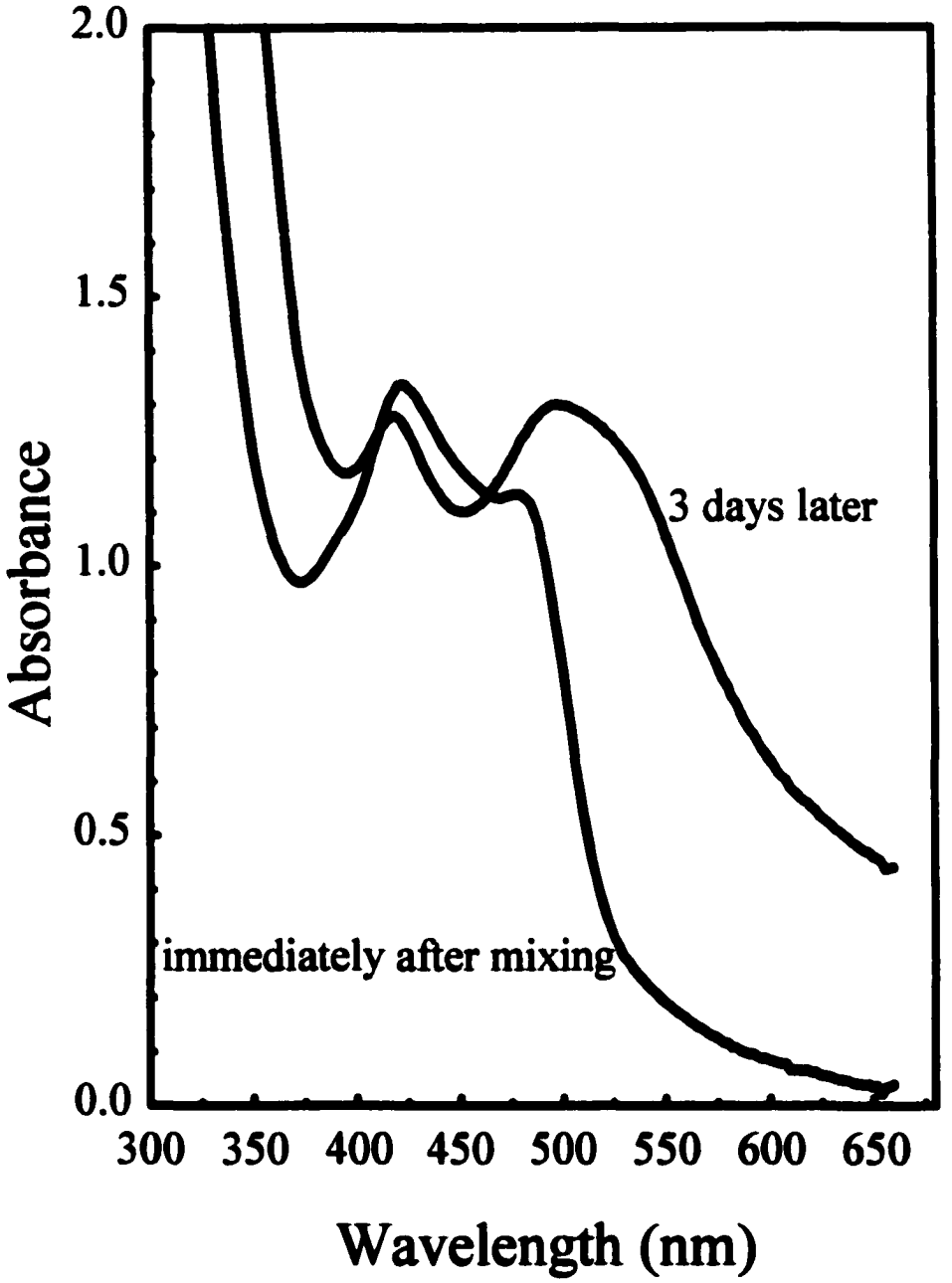

Figure 32. Stern-Volmer plots for intensity (●), and lifetime (■) quenching of $Ru(bpy)_2dpp^{2+}$ by $RuCl_6^{3-}$ in 5.0 M NaCl.

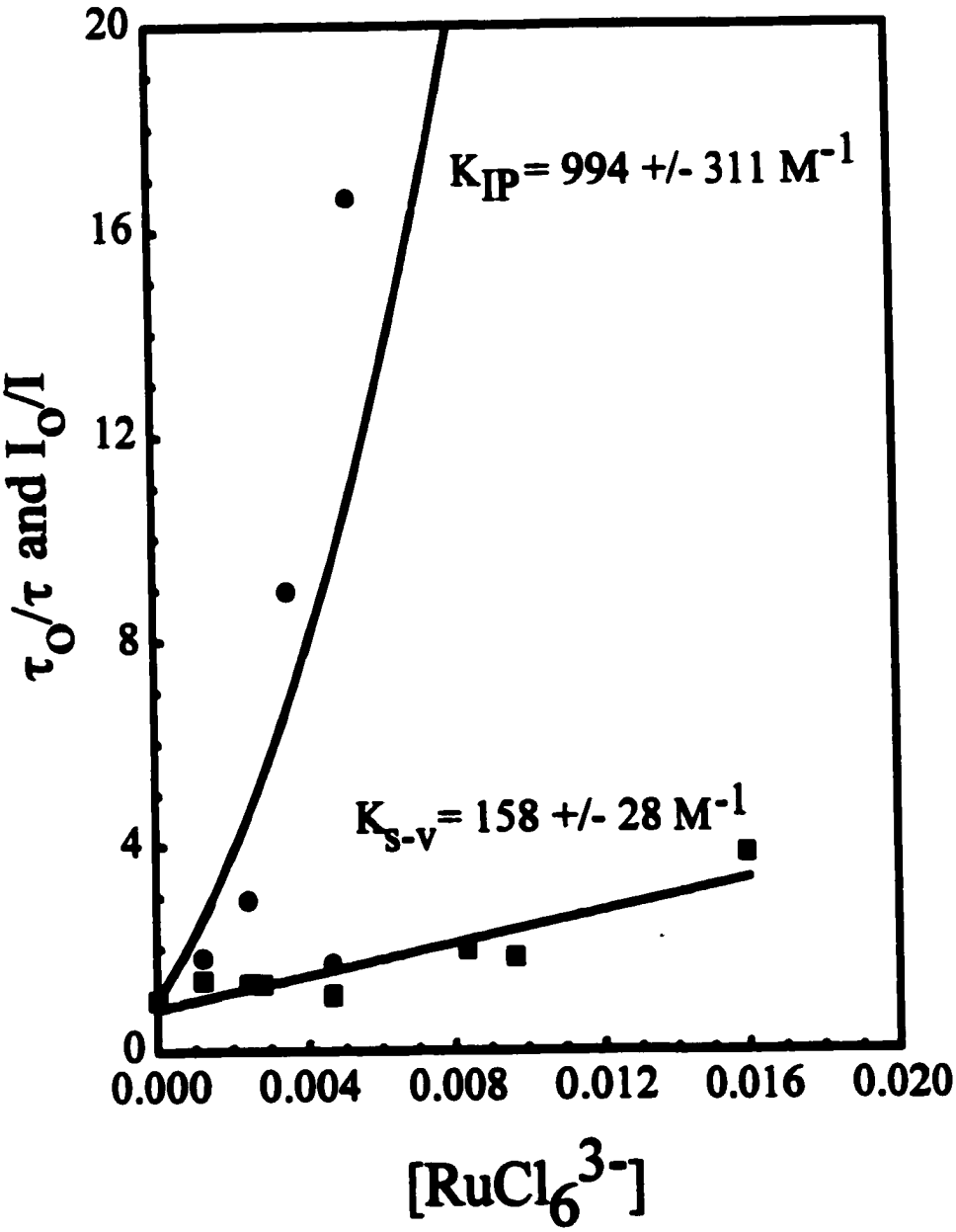

days in the dark at room temperature. In light of the rapid thermally induced aquation of the hexachloride, quenching data was obtained by freshly preparing each trial solution directly from the solid and using it promptly. Under these conditions, it was found that $K_3[RuCl_6]$ quenches the emission of $Ru(bpy)_2dpp^{2+}$ with a K_{sv} equal to $158 \pm 28\ M^{-1}$, obtained from lifetime data (Figure 32). However, comparison of the lifetime and intensity data show that ion pairing is significant even at the lowest concentrations of $K_3[RuCl_6]$ used, 1.4×10^{-3} M. Fitting the I_o/I data to eq 26, yields a value of K_{IP} equal to 944 ± 311

Measurement of the time dependence of the steady-state emission shows a decline suggesting that the aquated species quenches the emission of $Ru(bpy)_2dpp^{2+}$ more effectively than the hexachloride. This was determined by comparison of a freshly prepared solution of $RuCl_6^{3-}$ and $Ru(bpy)_2dpp^{2+}$, with an identical solution prepared from the same stock solution that was kept in the dark. Using the freshly prepared $RuCl_6^{3-}$ stock solution, a solution 10^{-5} M in $Ru(bpy)_2dpp^{2+}$ and 5.0 × 10-4 M in $RuCl_6^{3-}$ was prepared and the time dependence of the emission under conditions of steady-state emission was measured. After a significant decline in emission intensity had been achieved, an identical solution was prepared and measured form the portion of $RuCl_6^{3-}$ stock kept in the dark. The initial intensity of this solution was comparable to the value first solution had declined to over the measurement period, suggesting that chemistry centered on the hexachloride was responsible for the time dependence of the emission intensity, rather than reaction a with $Ru(bpy)_2dpp^{2+}$. An attempt was made to evaluate the change in pH during this time period, to determine if proton quenching via the monoaqua complex, could be responsible. This seemed possible since $Ru(bpy)_2dpp^{2+}$ is

proton quenched quite effectively with K_{sv} equal to 737 M^{-1}. However, the high ionic strength and presence of the other Lewis acids made the referencing of the pH electrode itself questionable since the stock solutions exhibited a pH of 3.0 relative to a pH 7.0 standard. This seemed unreasonable and was probably due to interference from other ions, at this high ionic strength. Though, from our independent measurement of the rate of aquation, with k_{aq} less than 5.6×10^{-3} s^{-1}, and assuming the monoaqua species to be a strong acid, the proton concentrations could have risen as high as 10^{-3} M during this time. This would imply a value of I_o/I of 1.7, which is higher than the observed value of 1.2. Therefore, proton quenching alone could account for the decline in intensity.

(3) Reactions of $Na_3[RhCl_6]$

In 5.0 M NaCl, freshly prepared solutions 1.9×10^{-3} M in $Na_3[RhCl_6]$ to change over time (Figure 33). The spectral change, a shift towards the blue end of the visible spectrum of the lowest energy spin allowed absorption band, is consistent with formation of aquated species. The reaction reaches equilibrium in about an hour (Figure 33). Use of the epsilons of the starting material and the monoaqua complex, suggest that at equilibrium 97% of the Rhodium species are aquated. Assuming a pseudo first-order rate law,

$$\text{rate} = k_{aq}[RhCl_6^{3-}] \qquad (100)$$

for the reaction,

$$RhCl_6^{3-} + H_20 \xrightarrow{k_{aq}} RhCl_5H_20^{2-} + Cl^- \qquad (101)$$

Figure 33. Absorption spectral change obtained from a freshly prepared solution 1.9×10^{-3} M in $RhCl_6^{3-}$, in 5.0 M NaCl. Specta shown were taken immediately after mixing, and at 5, 15, 30, and 55 minutes.

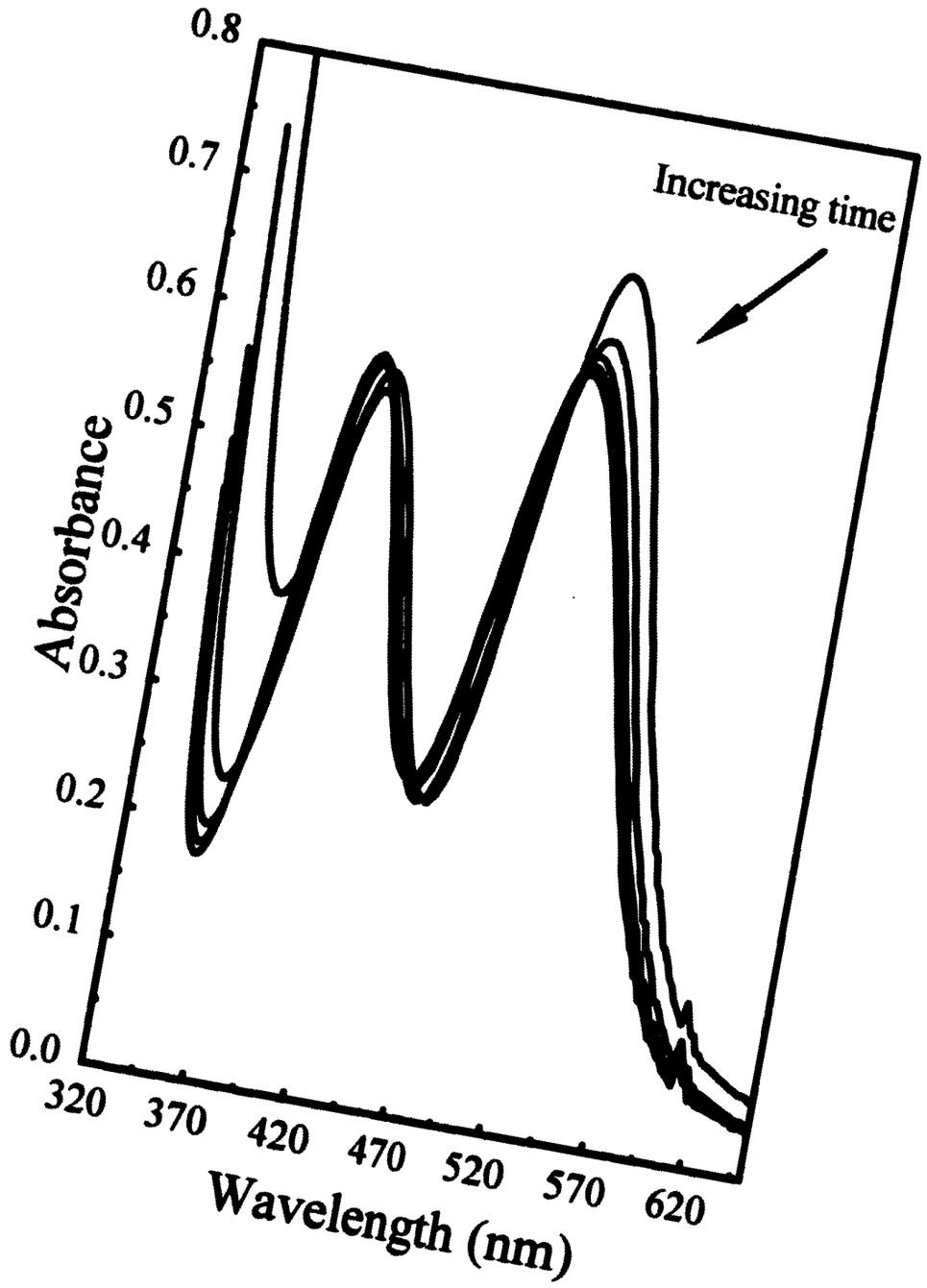

Figure 34. Absorbance at 530 nm as a function of time, for a freshly prepared solution 1.9×10^{-3} M in $RhCl_6^{3-}$, in 5.0 M NaCl.

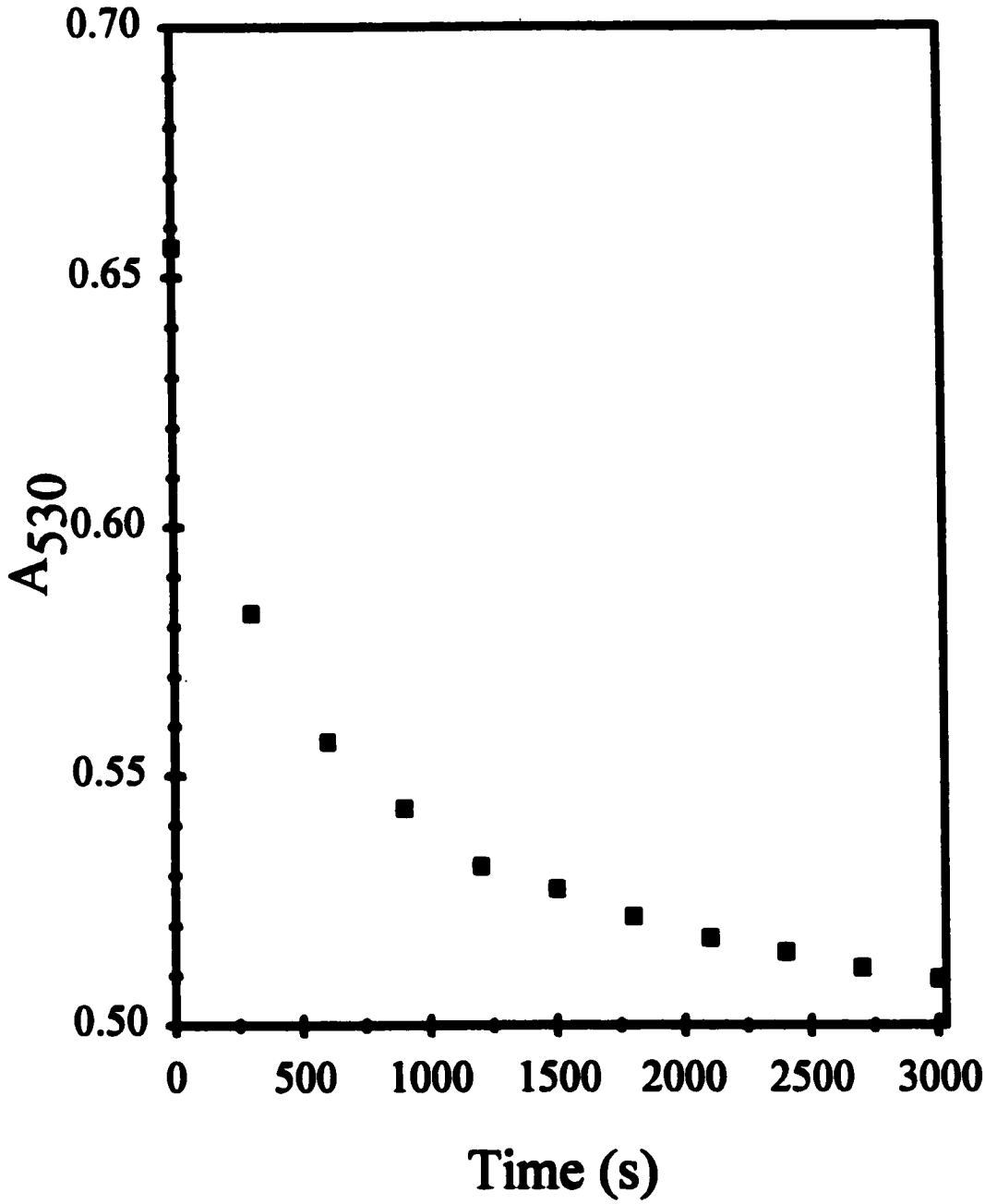

this data yields a value of k equal to 5.5×10^{-4} s^{-1}. Judging from the reaction solution of (Figure 34), equilibrium appears to be established within about an hour. This is also consistent with integration of the rate law proposed by Robb,

$$-d[RhCl_6^{3-}]/dt = k_1[RhCl_6^{3-}]-k_2[RhCl_5H_2O^{2-}][Cl^-] \quad (102)$$

with k_1 equal to 1.11×10^{-3} s^{-1} and k_2 equal to 2.17×10^{-4} $M^{-1}s^{-1}$, measured over a much lower range of chloride concentrations Using even the larger value of the rate constant, this suggests that in water within 30 seconds of mixing, as much as 5% of the nominal concentration of $RhCl_6^{3-}$ could be monoaquated.

Irradiation of an aqueous solution 5.0×10^{-3} M in $RhCl_6^{3-}$ and 4.0×10^{-5} M in $Ru(bpy)_2dpp^{2+}$ with 488-nm light, results in the appearance of a new band centered at 524 nm. Isosbestic points at 398 and 470 nm are maintained throughout the extent of reaction observed (Figure 35) and the spectral changes are equivalent to those occurring in the dark under reflux conditions (Figure 36). In both photochemical and thermal reactions the spectral change is consistent with the formation of the bimetallic $Ru(bpy)_2dppRhCl_4^+$.

Steady-state emission quenching data obtained in 3.0 M NaCl, show an increase in the apparent total Stern-Volmer constant with increased concentration of quencher (Figure 37). Fitting this data to eq. 26, yields an ion-pairing constant of 37 ± 2 M^{-1}. In aqueous solution, with no counterions added to control the ionic strength, a value of 880 ± 99 was obtained from the variation of initial intensity data observed after excitation with a seven-nanosecond laser pulse. In this experiment, a series of solutions with a constant concentration of $Ru(bpy)_2dpp^{2+}$ equal to 5.0×10^{-5} M were prepared with concentrations of $RhCl_6^{3-}$ varying from 10^{-4} to 10^{-2} M. The initial intensity of the decay

Figure 35. Spectral change obtained upon 488-nm irradiation of a reaction mixture 5.0×10^{-5} M in $Ru(bpy)_2dpp^{2+}$ and 5.0×10^{-4} M in $RhCl_6^{3-}$.

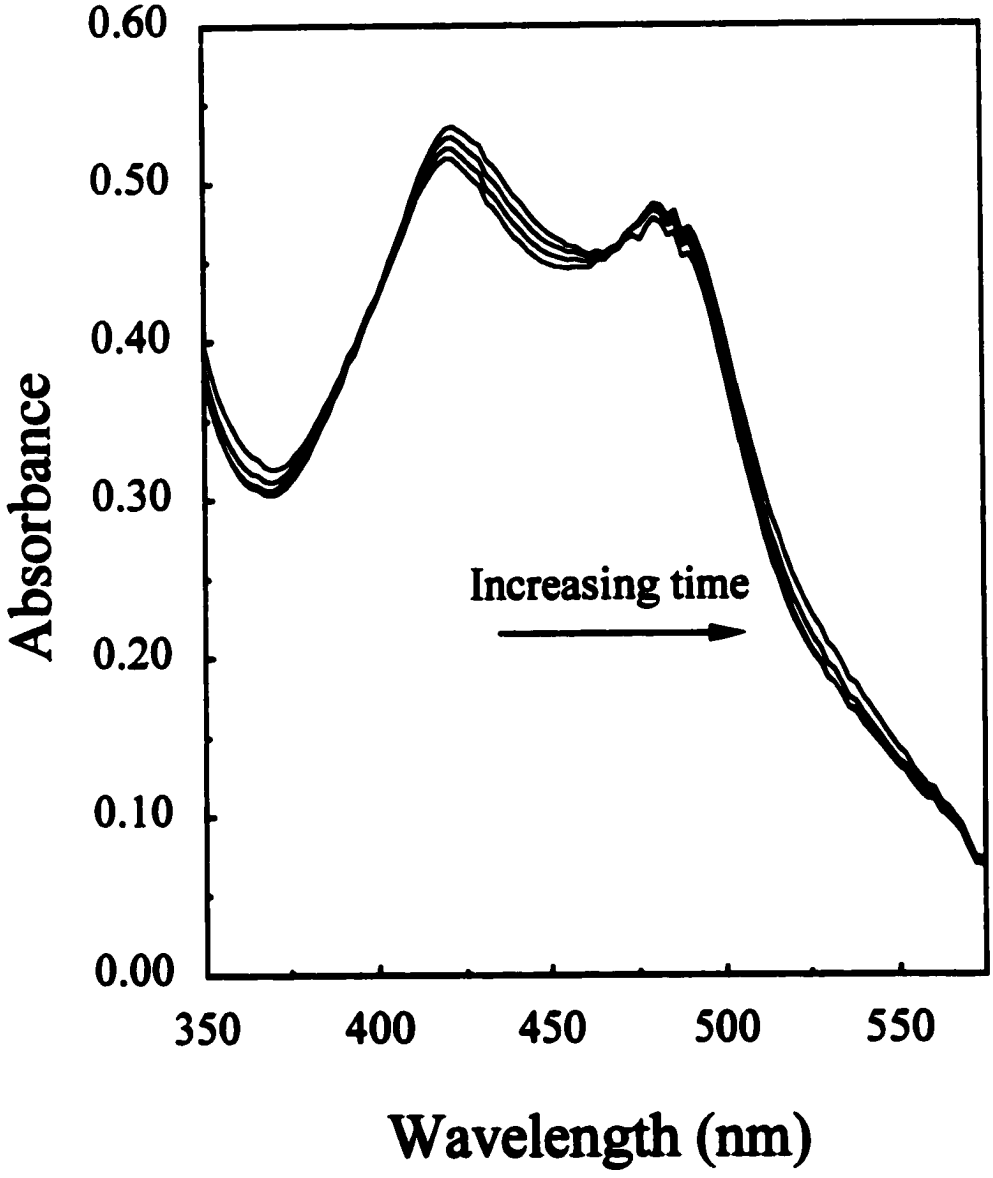

Figure 36. Spectral change obtained for a reaction mixture 1.4×10^{-4} M in $Ru(bpy)_2dpp^{2+}$ and 4.70×10^{-4} M in $RhCl_6^{3-}$ kept in the dark for three days.

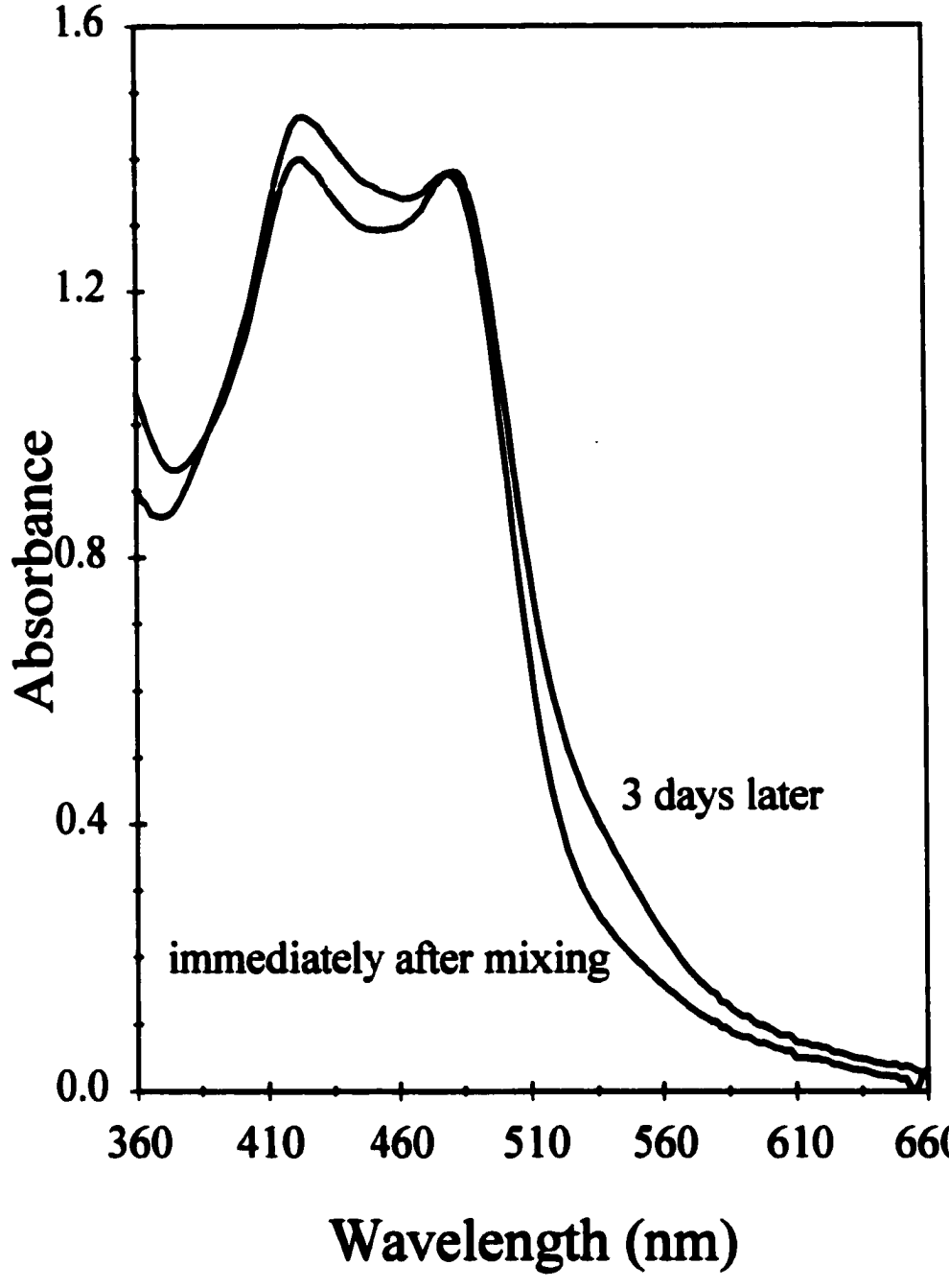

Figure 37. Stern-Volmer plot of intensity (■), and lifetime (●), quenching of $Ru(bpy)_2dpp^{2+}$ by $RhCl_6^{3-}$ in 5.0 M NaCl.

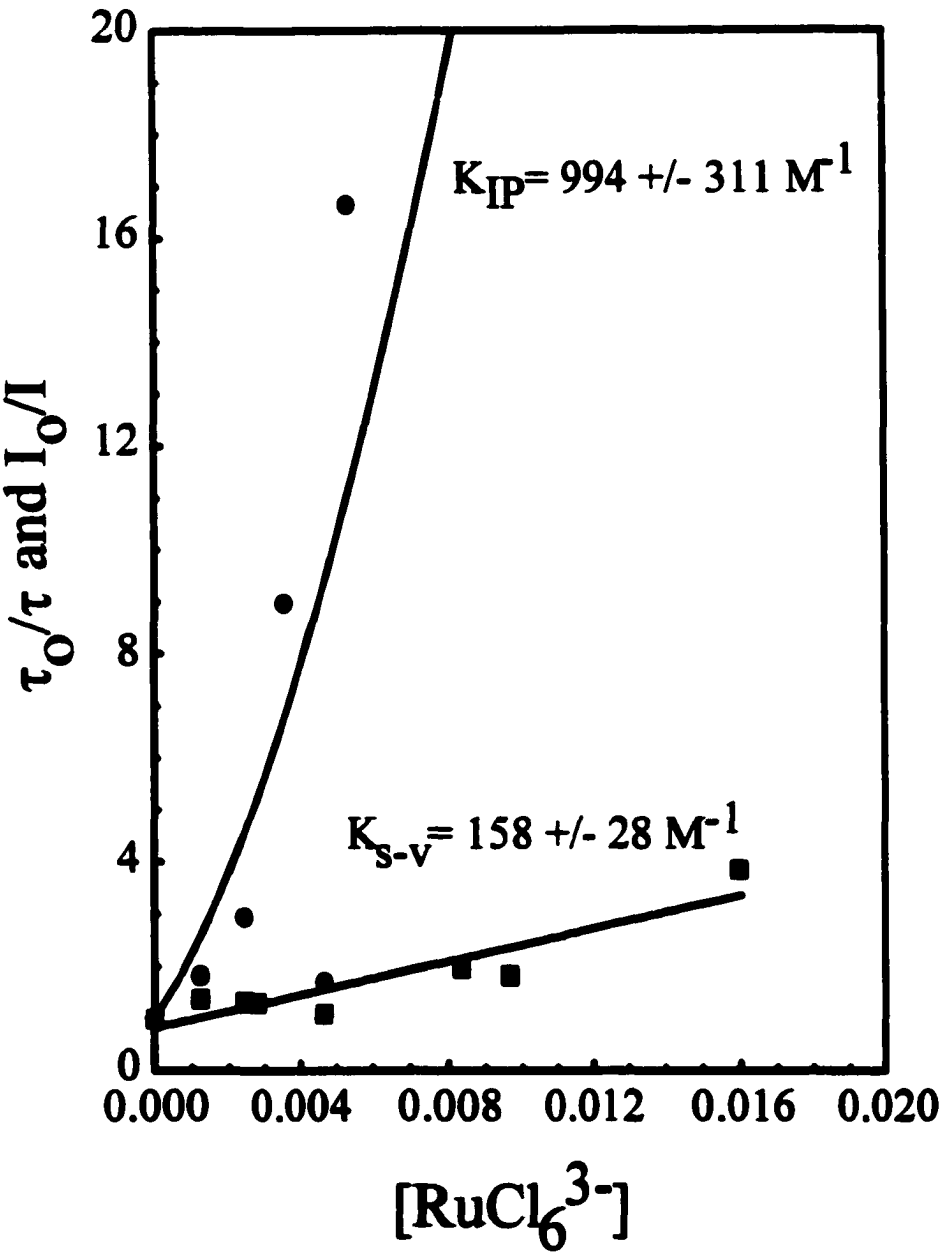

trace was taken to reflect the fraction of the excited states not ion-paired. The assumption being made here is that after the seven-nanosecond laser pulse the $Ru(bpy)_2dpp^{2+}$-$RhCl_6^{3-}$ ion-pairs decay more rapidly than our detection equipment can resolve. Therefore, the initial intensity of the single component exponential intensity decays reflected the fraction that was ion paired upon excitation. It is also assumed in this analysis, that the variation of the intensity from pulse to pulse, was a small percentage of the total pulseintensity, so that each trial received equivalent excitation. This seemed justified since the standard deviation of the pulses is reported to be 5%.[46]The equilibrium constant for ion-pair formation K_{IP}, was extracted assuming the model below.

$$D + Q \rightleftharpoons DQ \qquad (103)$$

Lifetime quenching data give the ${}^{T}K_{sv}$ equal to 417 ± 12 M^{-1}, a value within experimental error of that obtained from the I_o/I data if it is restricted to the range less than 5.0×10^{-3}, establishing that within this range quenching is diffusion controlled. (Figure 38). Data for the quantum yield of formation of $Ru(bpy)_2dppRhCl_4^{+}$ is shown in (Table 7). Plots of $1/\phi_p$ versus $1/[RhCl_6^{3-}]$ made within this restricted range, with the further restriction that the fraction of light absorbed by $RhCl_6^{3-}$ be less than 5% of the total light absorbed yield a value of 1/slope equal to .041 M^{-1}, which is negligibly small, compared to the value of ${}^{T}K_{sv}$ = 417 M^{-1}, obtained from quenching data.(Figure 39) The kinetic data used to obtain ϕ_p was treated within an initial rate assumption in order to calculate a reaction rate. However, this data showed an increase in rate with time. (Figure 40). This induction period seemed in accord with the rate of aquation for the

Figure 38. Stern-Volmer plot for intensity (●), and lifetime quenching (■), of $Ru(bpy)_2dpp^{2+}$ by $RhCl_6^{3-}$ in 5.0 M NaCl restricted to the range of $RhCl_6^{3-}$ less than 5.0×10^{-3} M.

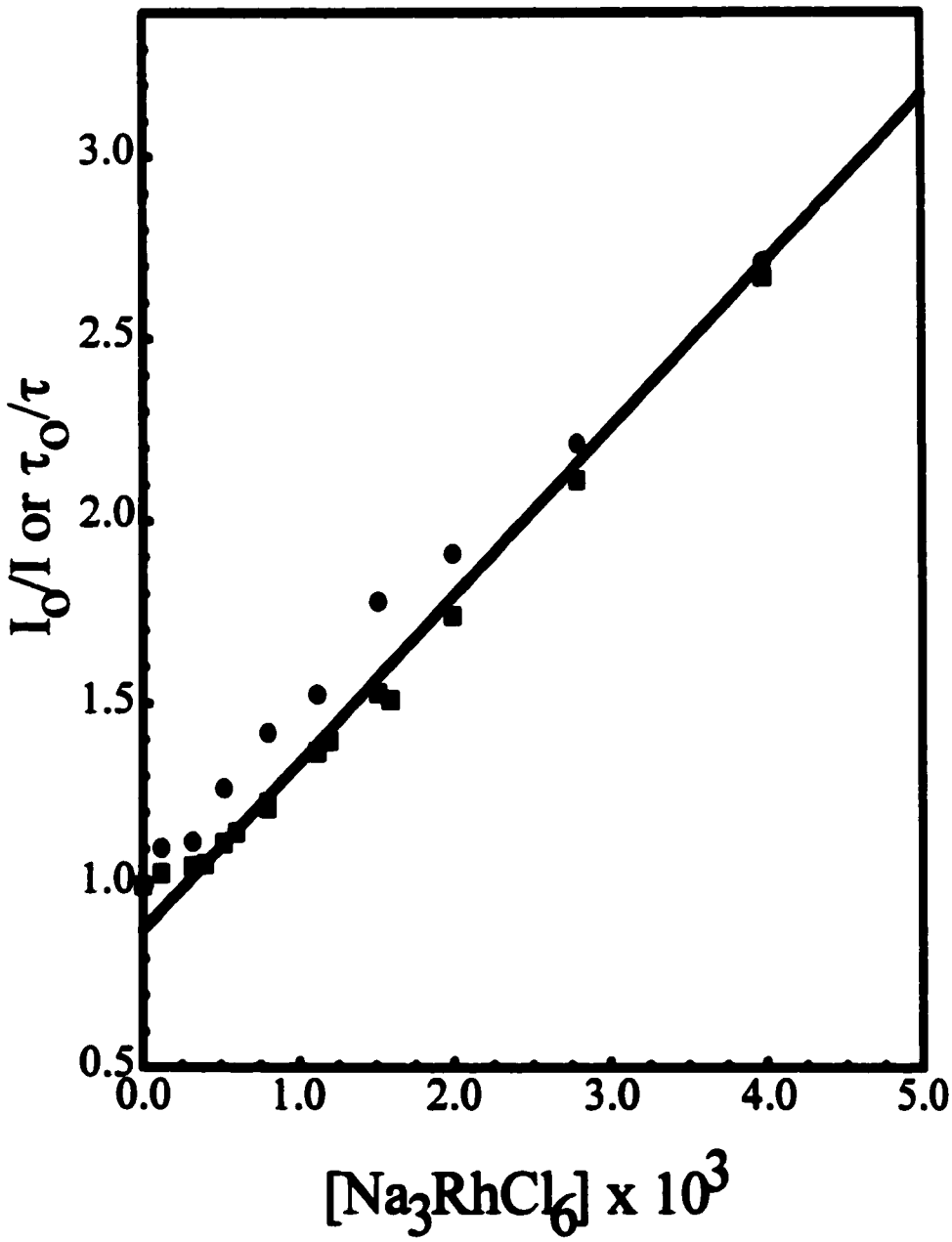

Table 7. Quantum yield of formation of [$Ru(bpy)_2dppRhCl_4^+$] as a function of concentration of $RhCl_6^{3-}$.

$[RhCl_6^{3-}]x10^4$	$\phi_p x10^3$
2.01	1.40
1.96	1.20
1.91	1.07
1.81	0.99
1.60	0.87
1.42	0.79
1.21	0.68
1.11	0.54
0.90	0.51
0.58	0.46

Figure 39. Plot of inverse of quantum yield of product formation of $Ru(bpy)_2dpp\ RhCl_4^+$ vs. inverse of concentration of $RhCl_6^{3-}$.

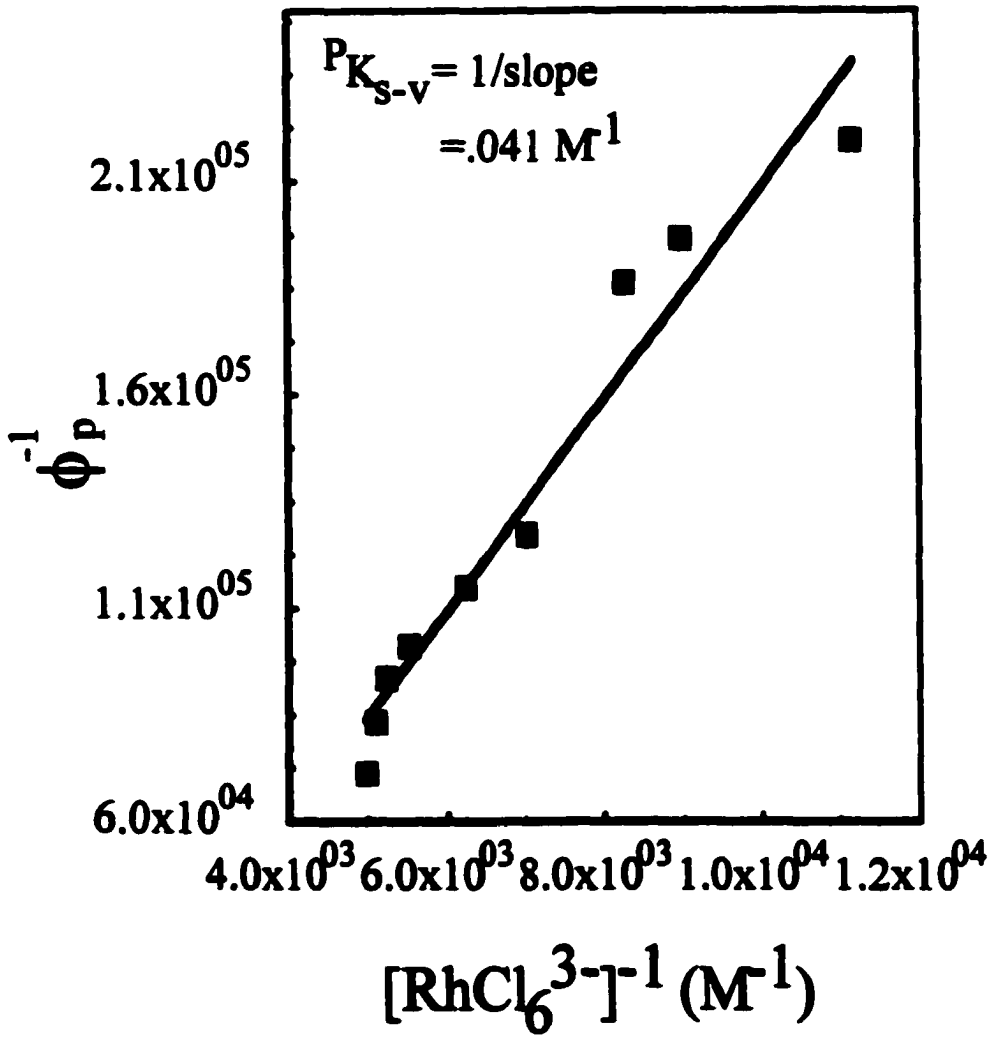

Figure 40. a) Spectral change observed at 525 nm for a solution 5.0×10^{-5} M in $Ru(bpy)_2dpp^{2+}$ and 8.4×10^{-4} M in $RhCl_6^{3-}$, irradiated immediately after preparation data set b) Spectral change measured at 525 nm for a solution 5.0×10^{-5} M in $Ru(bpy)_2dpp^{2+}$ and 8.4×10^{-4} M in $RhCl_6^{3-}$, pre-irradiated before addition of $Ru(bpy)_2dpp^{2+}$.

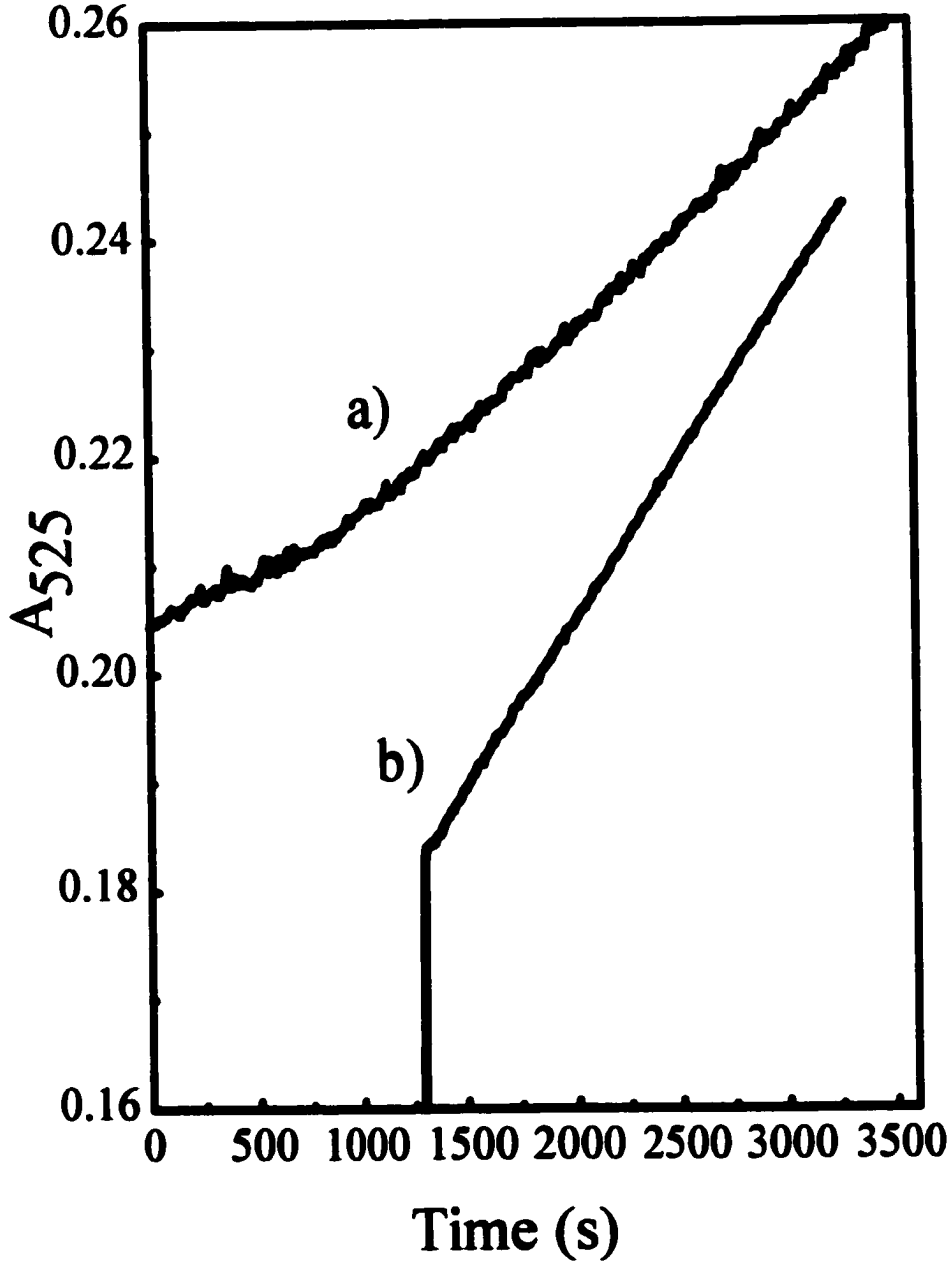

Figure 41. Values of the molar absorptivity (ε), for $K_2RhCl_5(H_20)$ in 3.0 M NaCl.

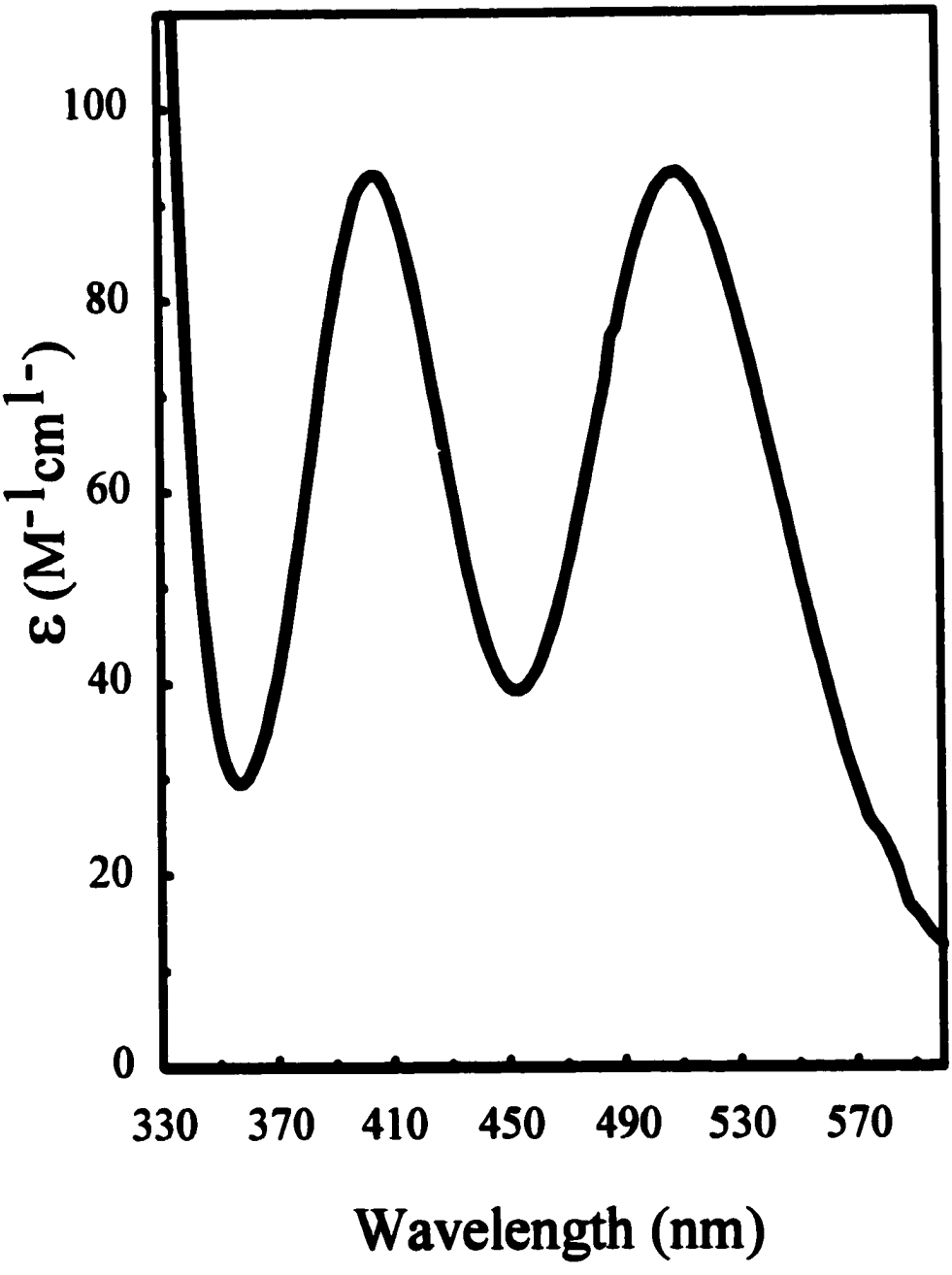

hexachloride by itself. Therefore, an experiment was performed in which an aliquot of $RhCl_6^{3-}$ stock was first pre-irradiated before addition of $Ru(bpy)_2dpp^{2+}$ this solution showed much less deviation from linearity suggesting an intermediate is produced either thermally or photochemically, which reacts much more efficiently with $^*Ru(bpy)_2dpp^{2+}$ or $Ru(bpy)_2dpp^{2+}$, than $RhCl_6^{3-}$ does.

(4) Reactions of $K_2[RhCl_5H_20]$

$K_2[RhCl_5H_20]$ was prepared by the method reported by Robb.[47] It was recrystallized twice from 0.5 M HCl with ice-cold ethanol and values of ε, at the maxima of 402 and 507 nm, were both to be 93 $M^{-1}cm^{-1}$, (Figure 41). This agrees well with the same maxima and values of the absorptivity equal to 99 $M^{-1}cm^{-1}$ for both, reported by Robb.[47] A freshly prepared solution of $RhCl_5(H_20)^{2-}$ in 5.0 M NaCl shows shift of the lowest energy spin allowed electronic transition to higher energy consistent with the formation of di-aquated products (Figure 42). The lowest energy absorption band shifts to higher energy with time. An equilibrium appears to be reached in about an hour as indicated by (Figure 43), suggesting replacement of a chloride for a water molecule.

Steady-state emission and lifetime data obtained in 5.0 M NaCl yield $^TK_{sv} = 75 \pm 5\ M^{-1}$ and equilibrium constant for ion-pairing K_{IP} equal to 20 ± 3 (Figure 44). Photolysis with 488 nm light of a freshly prepared solution 5.0×10^{-5} M in $[Ru(bpy)_2dpp^{2+}]$ and 2.0×10^{-4} M in $[RhCl_5(H_20)^{2-}]$, results in no change in the absorption spectrum.

(5) Reactions of $Na_2[PdCl_6]$

In 5.0 M NaCl the $PdCl_6^{2-}$ ion was stable, based on the lack of any change in the UV-vis absorption spectrum of freshly prepared solutions 10^{-3} M solutions of $PdCl_6^{2-}$.

Figure 42. Spectral change obtained upon dissolving $K_2RhCl_5(H_2O)$ in 5.0 M NaCl. Spectra shown were taken at 0, 1800, and 7200 seconds.

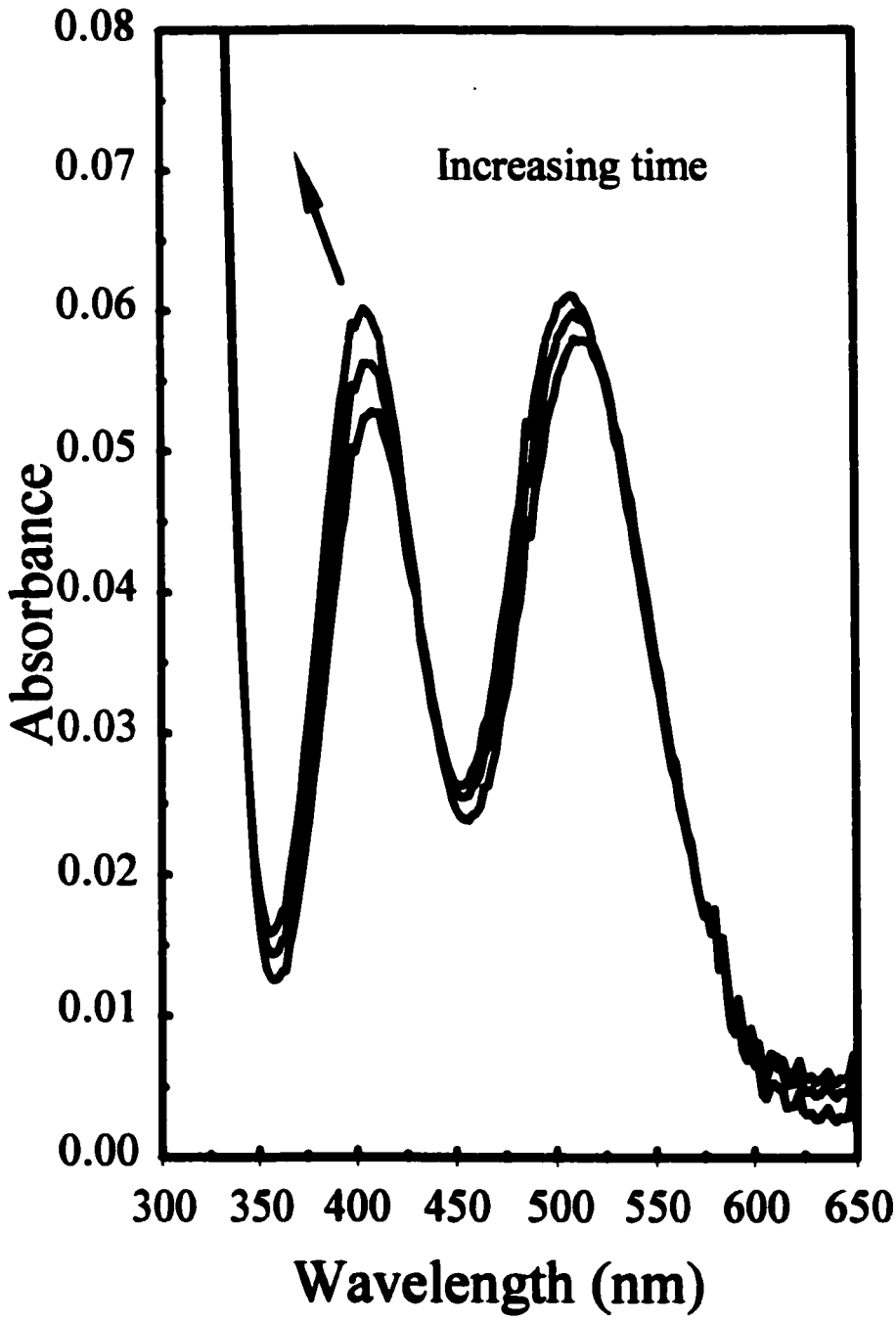

Figure 43. Plot of absorbance at 406 nm vs. time for a freshly prepared solution 6.45×10^{-3} M in $RhCl_5(H_2O)^{2-}$, in 5.0 M NaCl.

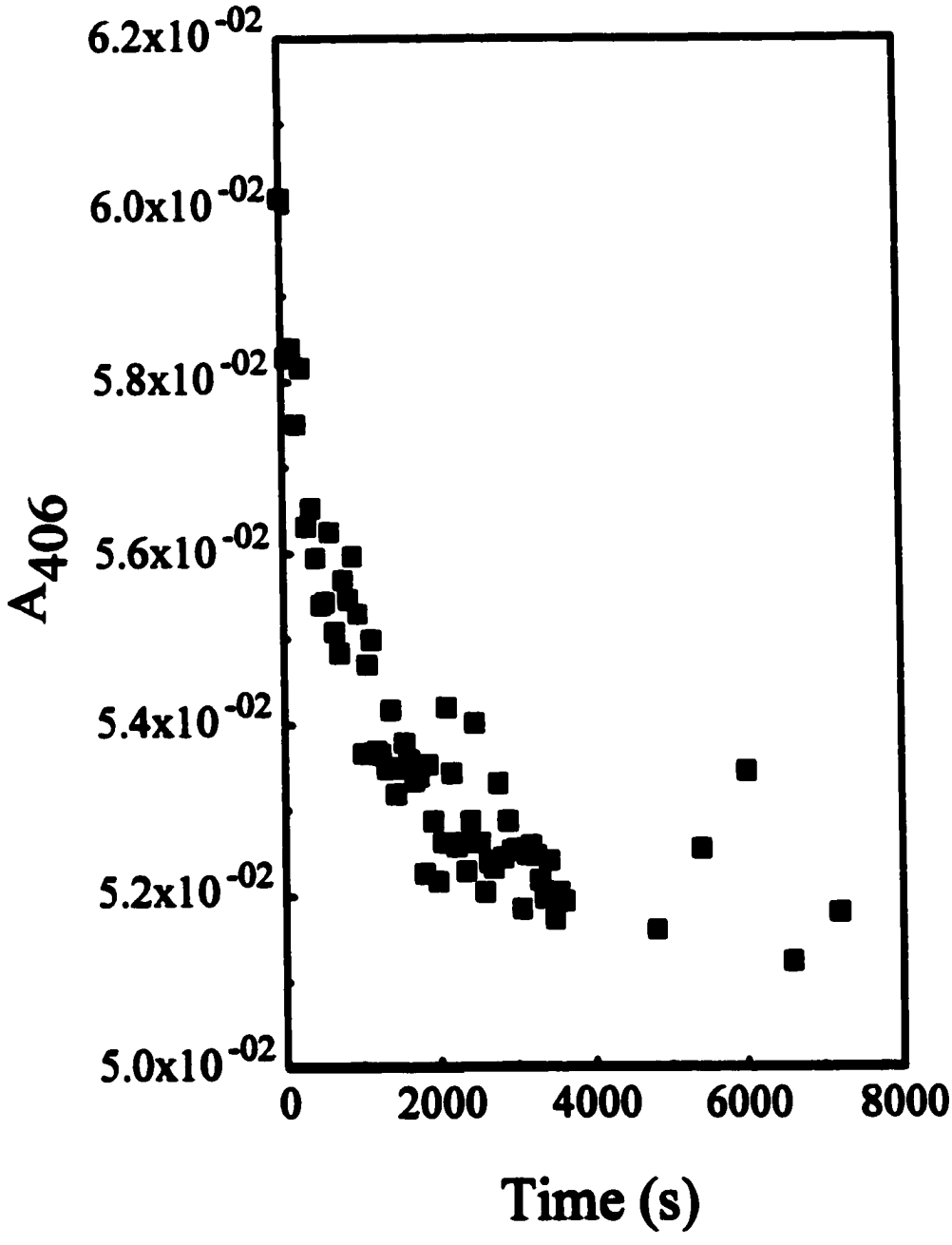

Figure 44. Stern-Volmer plot for intensity (●), and lifetime (■) quenching of $Ru(bpy)_2dpp^{2+}$ by $RhCl_5(H_2O)^{2-}$ in 5.0 M NaCl.

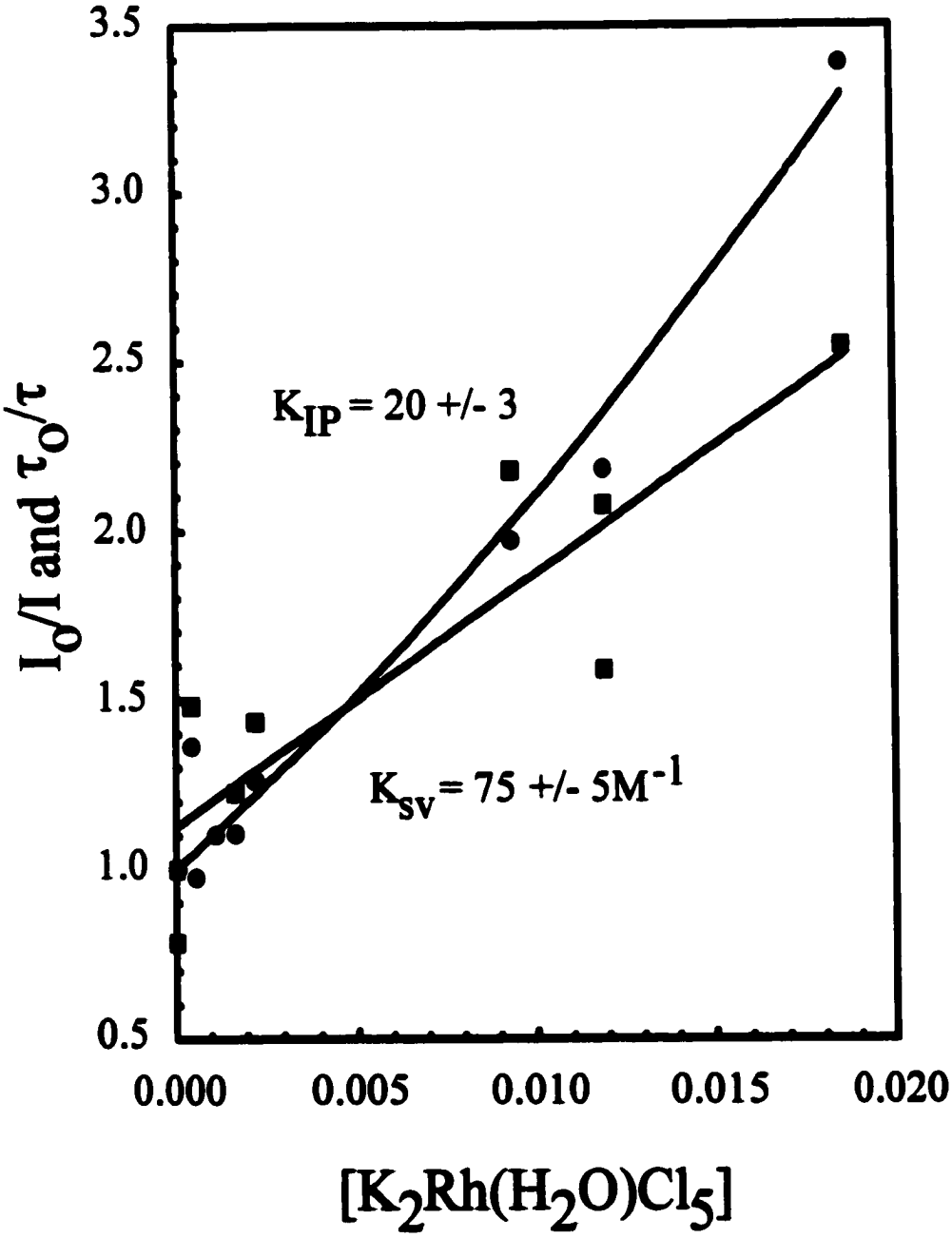

Figure 45. Spectral change observed for a solution 5.0×10^{-5} M in $Ru(bpy)_2dpp^{2+}$ and 5.0×10^{-4} M in $PdCl_6^{2-}$. Spectra taken immediately after preparation and after 20 minutes in the dark.

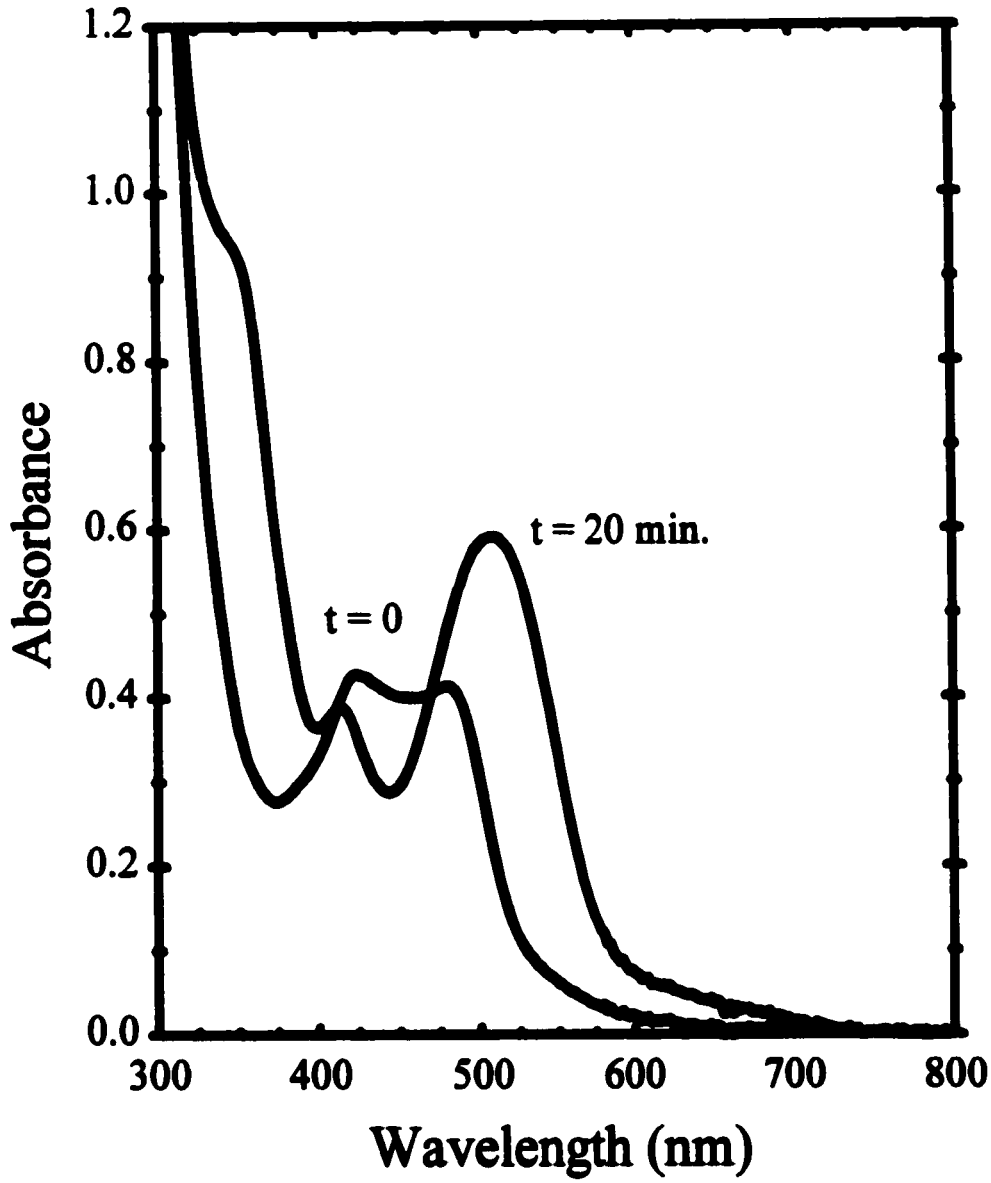

Figure 46. Logarithmic plot used to determine the order with respect to concentration of $PdCl_6^{2-}$ for the thermal reaction with $Ru(bpy)_2dpp^{2+}$.

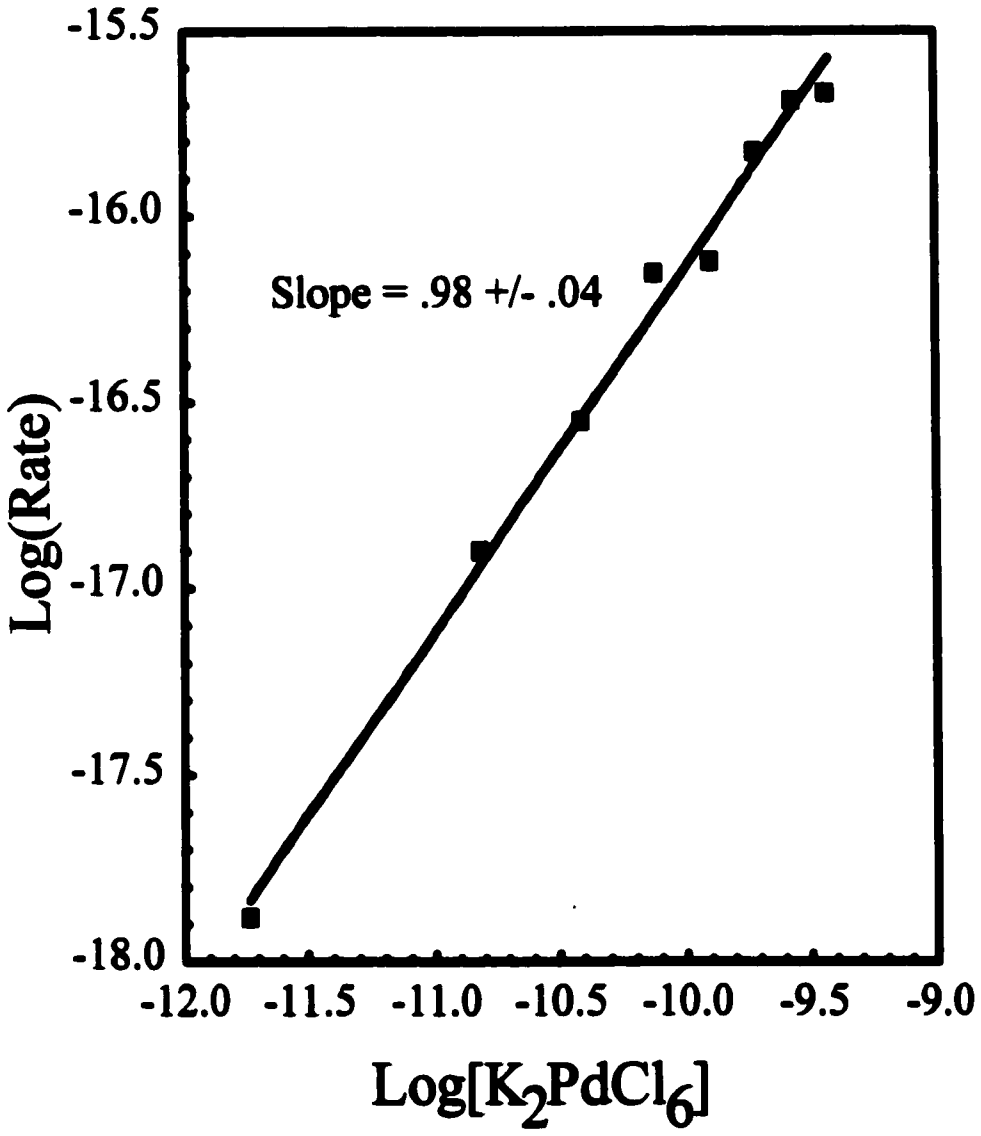

Figure 47. Logarithmic plot used to determine the order with respect to concentration of $Ru(bpy)_2dpp^{2+}$ for the thermal reaction with $PdCl_6^{2-}$.

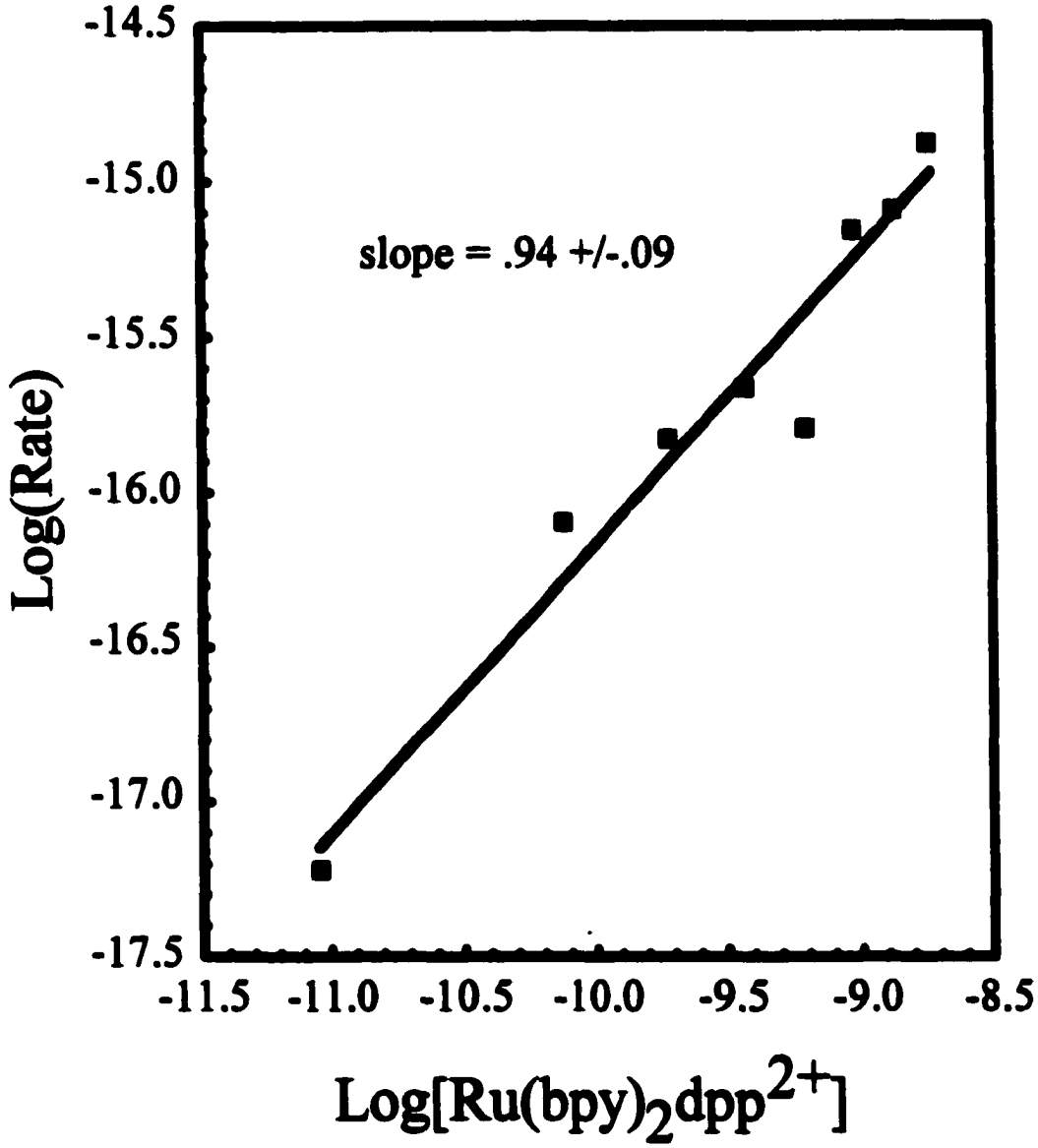

Figure 48. Arrhenius plot for the reaction between $Ru(bpy)_2dpp^{2+}$ and $PdCl_6^{2-}$.

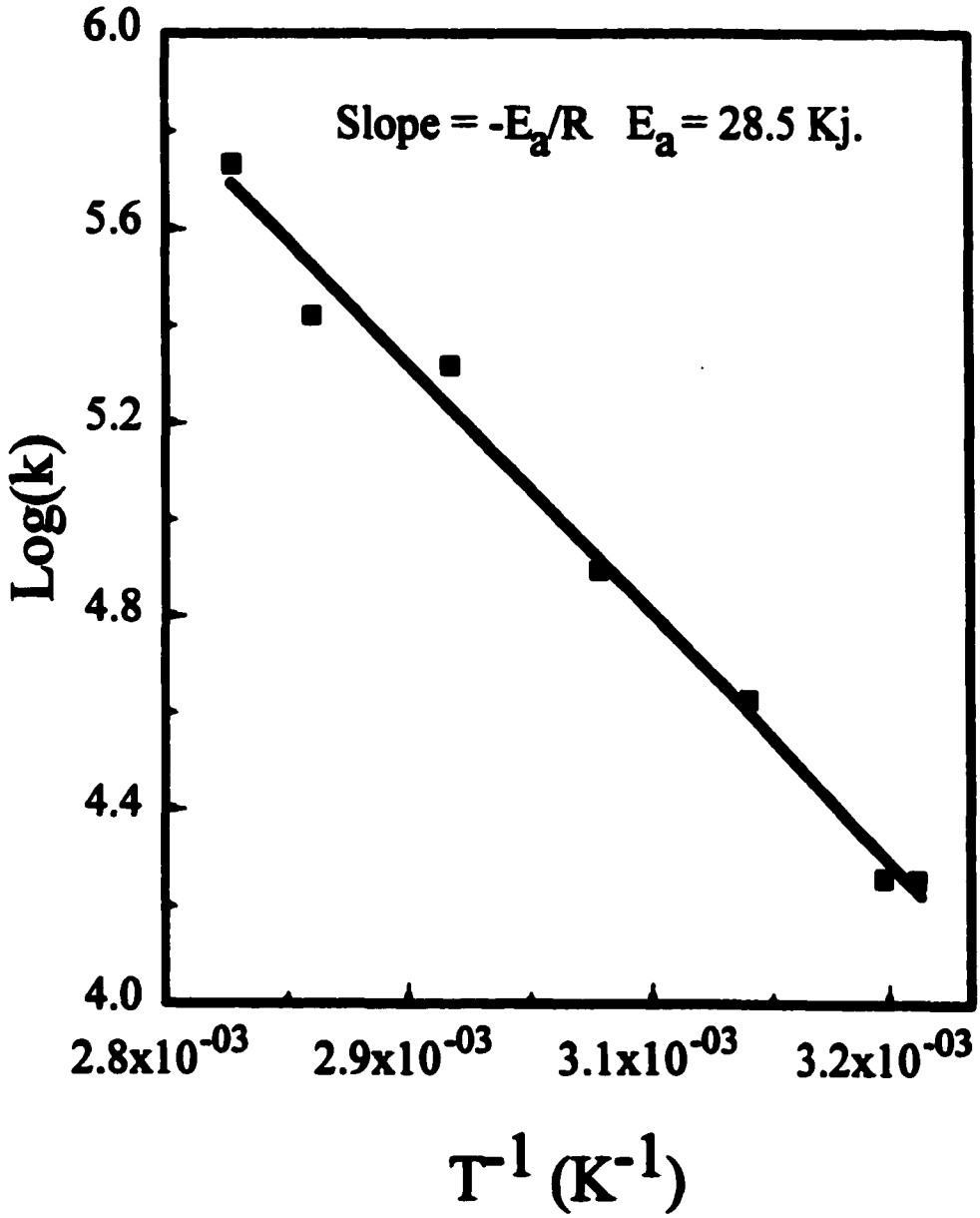

Solutions 2.5×10^{-5} M in $PdCl_6^{2-}$ and 5.0×10^{-5} M in $Ru(bpy)_2dpp^{2+}$, were prepared and found to react to completion within minutes (Figure 45). The spectral changes were similar to those observed for other hexachlorides, a shift to lower energy of the MLCT terminating on the dpp ligand. The kinetics of the thermal reaction was measured using the spectral change at 525 nm. The rate law was determined to be

$$\frac{d[PdCl_6^{2-}]}{dt} = -k[PdCl_6^{2-}]^{.98 \pm .04}[Ru(bpy)_2dpp^{2+}]^{.94 \pm .09} \qquad (104)$$

(Figures 46 and 47) with a rate constant at 25 °C of 75 $M^{-1}s^{-1}$ in 5.0 M NaCl. Measurement of the temperature dependence yielded an Arrhenius activation energy of 6.8Kcal/mol (Figure 48). At 0 °C the rate of the thermal reaction was found to be to fast to reproducibly measure a photochemical rate in competition with the thermal rate. A comparison of data collected during a 488 nm irradiation of a solution with $[PdCl_6^{2-}]$ equal to 5.0×10^{-4} M and $[Ru(bpy)_2dpp^{2+}]$ equal to 5.0×10^{-5} M, showed initial rates within experimental error, however attainment of a greater extent of reaction for the irradiated solution suggests some photochemical component to the reaction (Figure 49).

(6) Reactions of Na_2PtCl_4

The equilibrium constants for the first 2 aquation steps of $PtCl_4^{2-}$,

$$PtCl_4^{2-} + H_20 \longrightarrow PtCl_3H_20^- + Cl^- \qquad (105)$$

$$PtCl_3H_20^- + H_20 \longrightarrow PtCl_2(H_20)_2 + Cl^- \qquad (106)$$

have been reported to be K_1 equal to 1.34×10^{-2} and K_2 equal to 1.1×10^{-3} at 25 °C suggesting extensive solvolysis though the rate is reported to be slow.[48] Monitoring a

declining spectral change at 270 nm, suggests that k_{eq} for the first chloride displacement shown in eq 105, is less than 8.2×10^{-5}. (Figure 50)

Thermally, $PtCl_4^{2-}$ reacts relatively quickly with $Ru(bpy)_2dpp^{2+}$ (Figure 51). Using the data shown in Figure 51, with a second-order rate law yields a rate constant of 6.3×10^{-1} $M^{-1}s^{-1}$ It also reacts photochemically (Figure 52) to form a bimetallic complex. Both the thermal and photochemical reactions have identical spectral changes, with isosbestic points at 408 nm and 486 nm. Under the most intense 488-nm photolysis possible, a thermal and photochemical trial each 10^{-4} M in $Ru(bpy)_2dpp^{2+}$ and 7.3×10^{-4} M in $PtCl_4^{2-}$, displayed indistinguishable initial rates (Figure 53). A photochemical pathway of reaction is apparent though from the greater rate and extent of reaction after about 100 seconds. Due to the very fast thermal pathway leading to bimetallic formation, all solutions were prepared directly from solids and the solvent was pipetted into the cuvette immediately before measurement. It was found that $PtCl_4^{2-}$ quenches the emission of $Ru(bpy)_2dpp^{2+}$ with $K_{sv} = 282 \pm 28$ M^{-1} obtained from the lifetime data shown in Figure 54. Analysis as outlined earlier, of the intensity quenching data in Figure 54, which exhibits upward curvature, suggests $K_{IP} = 104 \pm 20$.

(7) Reactions of $K_2[OsCl_6]$

$K_2[OsCl_6]$does not appear to aquate very rapidly in 5.0 M NaCl, as indicated by no measurable spectral change within ten minutes of preparing a solution that had a concentration of $OsCl_6^{2-}$ equal to 8.7×10^{-5} M, in 5.0 M NaCl. However, stock solutions allowed to stand more than an hour did display some change evident from the formation of a dark insoluble material. This material has been proposed to be an Os-Os

Figure 49. Plot of absorbance at 525 nm vs. time for thermal and photochemical reactions at 25 °C. Both solutions were prepared 5.0×10^{-4} M in $PdCl_6^{2-}$ and 5.0×10^{-5} M in $Ru(bpy)_2dpp^{2+}$.

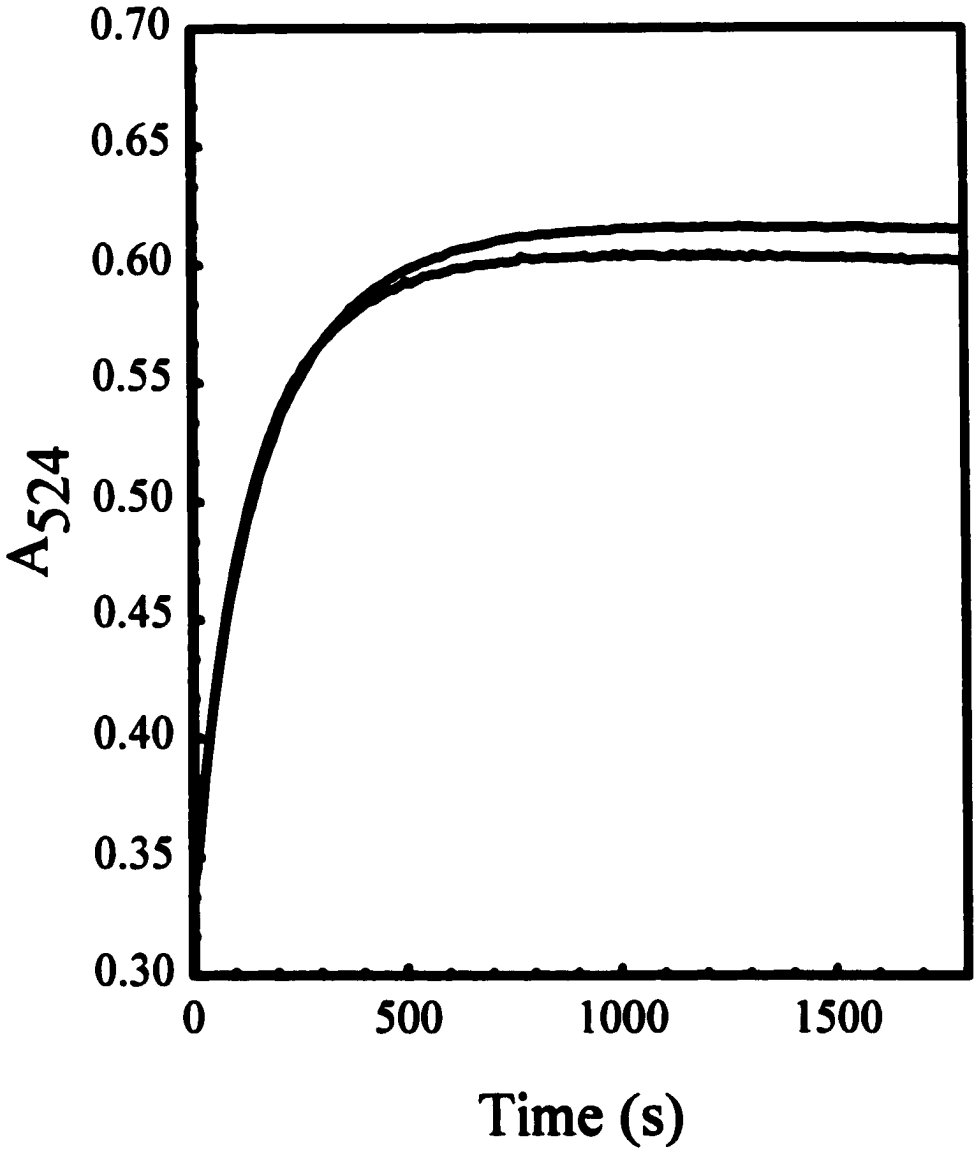

Figure 50. Spectral change observed at 270 nm for a freshly prepared solution of Na_2PtCl_4 in 3.0 M NaCl.

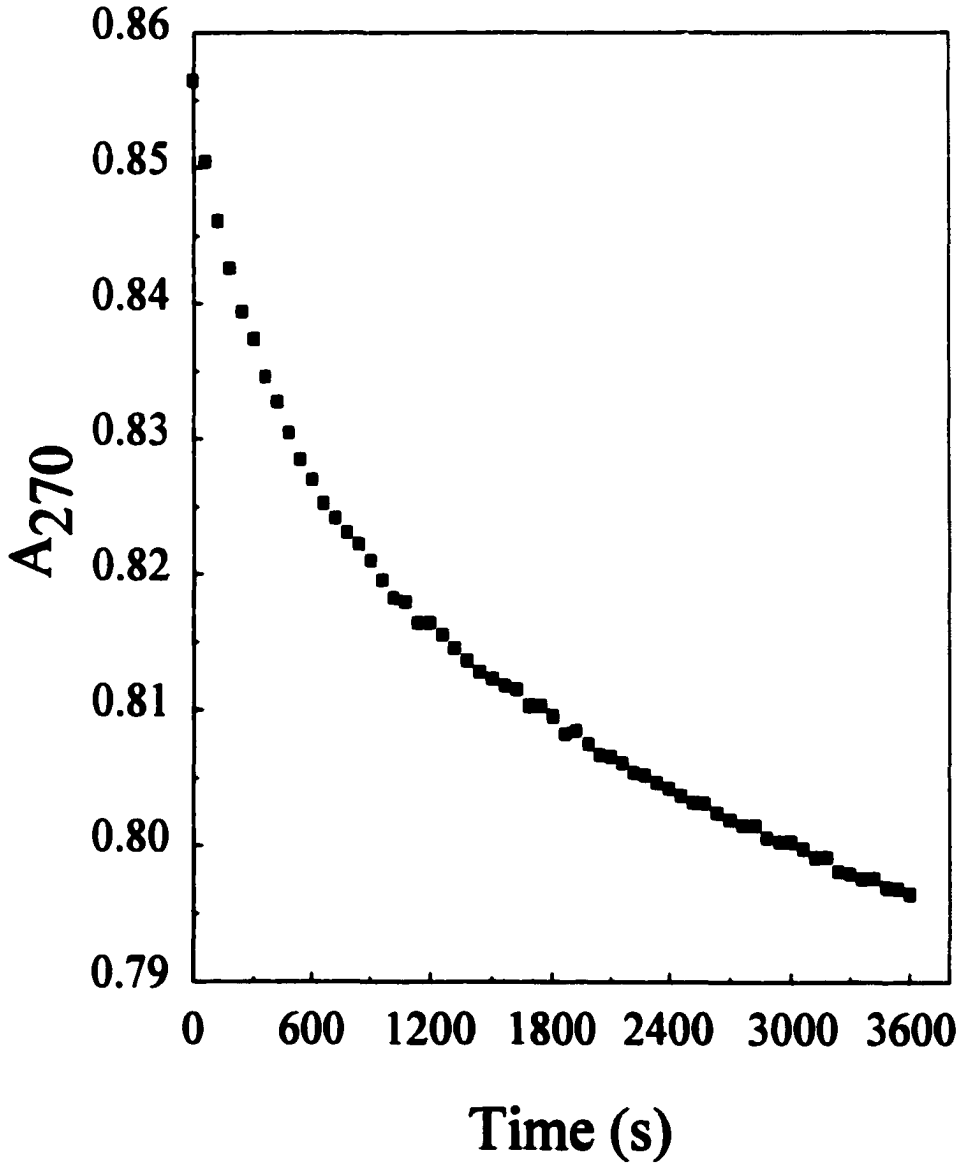

Figure 51. Spectral change observed during the thermal reaction of a solution 5.0×10^{-5} M in $Ru(bpy)_2dpp^{2+}$ and 10^{-3} M $PtCl_4^{2-}$ in 3.0 M NaCl. Shown are reaction times of 0, 60, 150, 270 and 570 seconds after mixing.

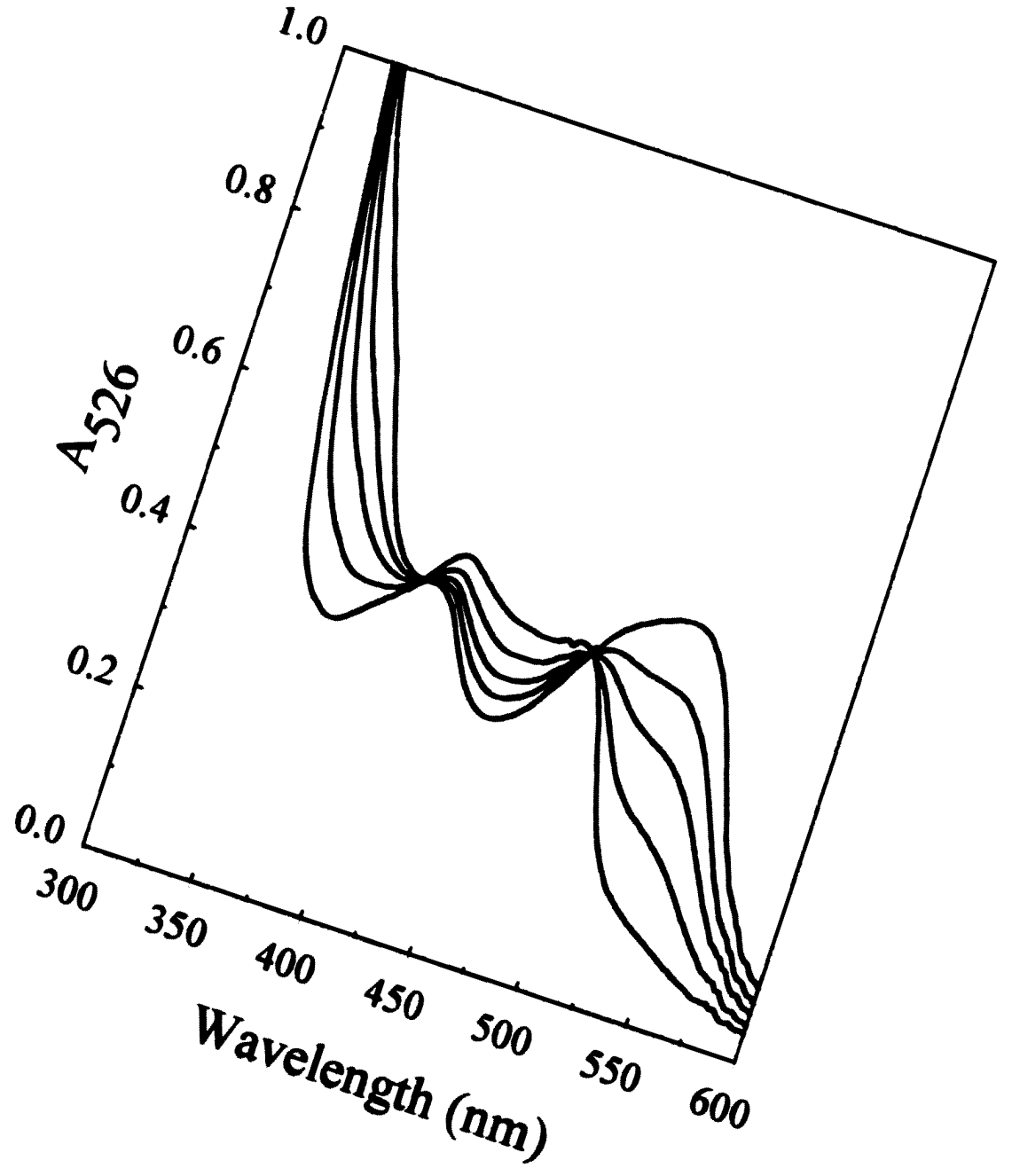

Figure 52. Spectral change observed at 532 nm, during 488 nm photolysis of a solution 4.0×10^{-5} M in $Ru(bpy)_2dpp^{2+}$ and 10^{-4} M in $PtCl_4^{2-}$ in 3.0 M NaCl. Irradiation times indicated in seconds.

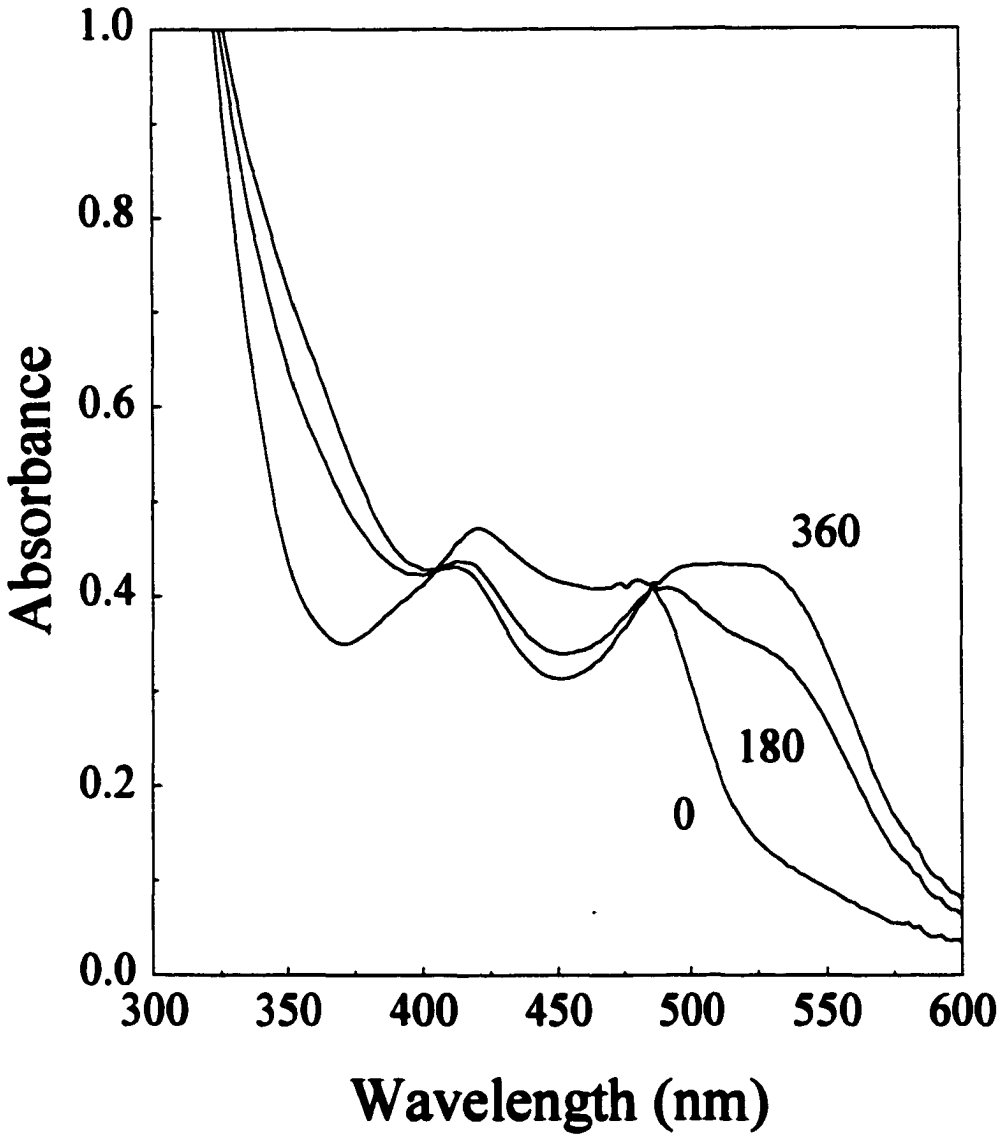

Figure 53. Plot of absorbance at 525 nm vs. time for thermal and photochemical reactions at 25 °C. Both solutions were prepared was 5.0×10^{-4} M in $PtCl_4^{2-}$ and 10^{-4} M in $Ru(bpy)_2dpp^{2+}$.

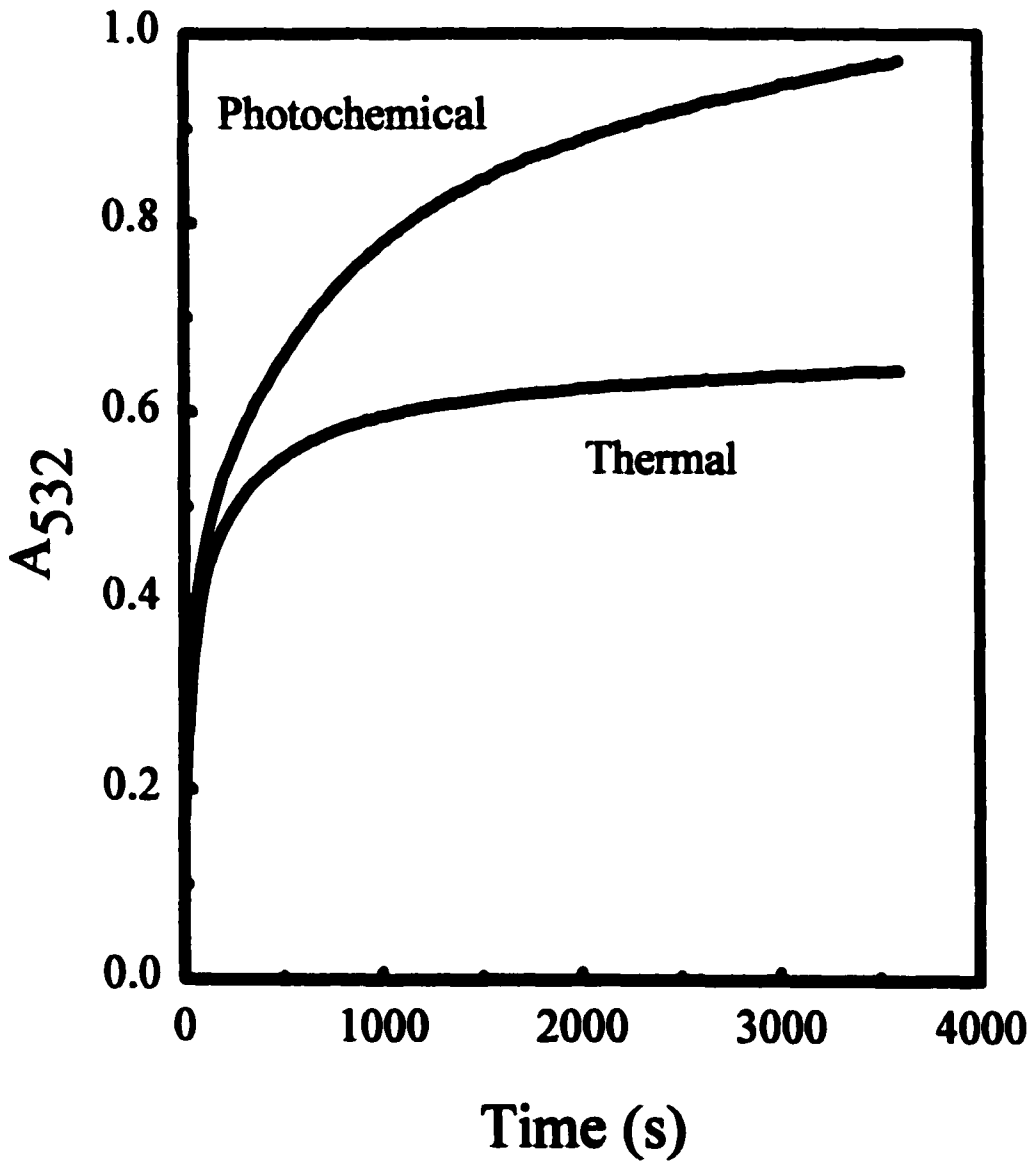

Figure 54. Stern-Volmer plot for intensity (●), and lifetime (■) quenching of $Ru(bpy)_2dpp^{2+}$ by $PtCl_4^{3-}$ in 5.0 M NaCl.

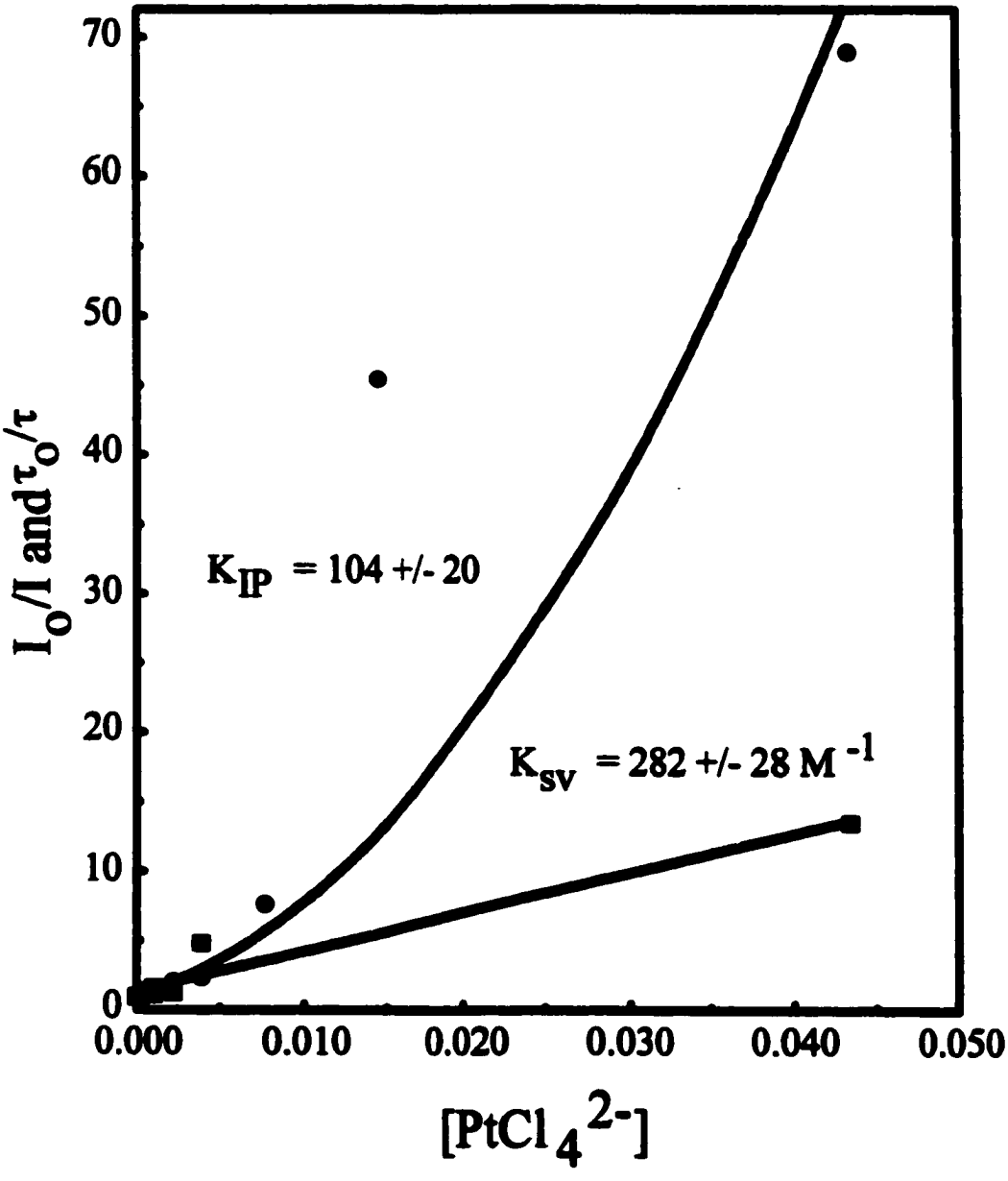

bimetallic.[49] Therefore, fresh stock solutions were prepared directly from solids and used immediately.

$OsCl_6^{2-}$ appears to form a bimetallic complex with $Ru(bpy)_2dpp^{2+}$ thermally (Figure 55), though it fails to react photochemically. It quenches the emission of $Ru(bpy)_2dpp^{2+}$ with K_{sv} equal to 603 M^{-1} (Figure 56) Surprisingly this di-cation does not appear to ion-pair significantly up to concentrations of $K_2[OsCl_6]$ equal to 6.0×10^{-3} M with the concentration of $Ru(bpy)_2dpp^{2+}$] equal to 5×10^{-5} M in 5.0 M NaCl. This might indicate that in fact it had undergone rapid mono or di-aquation resulting in a −1 charged anion or an uncharged species. Or it might suggest that the ion-pair has a structure that determines significantly different values for hexachlorides with different central metal ions. Fitting this data yields value of the ion-pairing constant of $K_{IP} = 21 + 4$

(8) Reactions of $K_3[IrCl_6]$

$IrCl_6^{3-}$ is stable in water as well as aqueous 5.0 M NaCl solution. This agreed well with literature available on its rates of aquation, and with it being regarded as substitution inert.[50] $K_3[IrCl_6]$ does react thermally under reflux in aqueous solution to form a bimetallic complex with $Ru(bpy)_2dpp^{2+}$. The extent of reaction is limited and the only evidence of reaction is a slight spectral change (Figure 57). A limited amount of quenching data has been collected, based on only a few lifetime and intensity quenching data points K_{sv} equal to ~10 M^{-1}.

(9) Interaction of $[Ru(bpy)_2dpp](ClO_4)_2$ with $AgNO_3$

$AgNO_3$ was observed to form an exciplex with $Ru(bpy)_2dpp^{2+}$ in aqueous solution. Upon titration of solid $AgNO_3$, into a single solution of a 5.0×10^{-5} M in

$Ru(bpy)_2dpp^{2+}$, a new emission peak centered at 732 nm begins to appear. (Figure 58). Changes in the absorption spectrum are also apparent in the ground state suggesting coordination at the peripheral nitrogens of the dpp ligand occurs thermally (Figure 59). This was supported by ^1H NMR spectra of $Ru(bpy)_2dpp^{2+}$ in the presence of Ag^+, which shows a downfield shift of five doublets, peaks 6, 9, 12, 13, and a bipyridine doublet at 7.75 ppm, with addition of silver. (Figures 60 and 61). An absolute assignment of the whole spectrum was not possible, since six of the seven spin systems are similar in having the same numbers of spins, and expected multiplicities. Figure 60 has the peaks labeled in reference to Figure 63. The peaks labeled with "*" are assigned to bipyridine resonance's. In parentheses the number of protons that the integration indicates for each resonance is included.

The spin systems that are affected by the addition of Ag^+ have been examined by COSY ^1H NMR spectrum (Figure 62). An assignment of the spectra has been made based upon examination of similar spectra, and the specificity of the interactions observed with Ag^+ (Figure 63).^1H NMR and absorption spectral changes were both analyzed using the simple association model shown below.

$$Ag^+ + Ru(bpy)_2dpp^{2+} \longrightarrow Ag\text{-}Ru(bpy)_2dpp^{3+} \qquad (107)$$

Both types of spectral data show saturation behavior at sufficiently high concentrations of Ag^+. The endpoint in the ^1H NMR spectral change was assigned to complete conversion to the bimetallic product. Though both ^1H NMR and absorbance data appeared to approach becoming independent of the concentration of Ag^+ (Figure 64), the absorbance data was handled differently, since acceptable fits to the

Figure 55. Spectral change observed during the thermal reaction of a solution 1.4×10^{-4} M in $Ru(bpy)_2dpp^{2+}$ and 10^{-4} M $OsCl_6^{2-}$ in 5.0 M NaCl. Shown are the spectrum of the solution immediately after mixing, and after two days in the dark at room temperature.

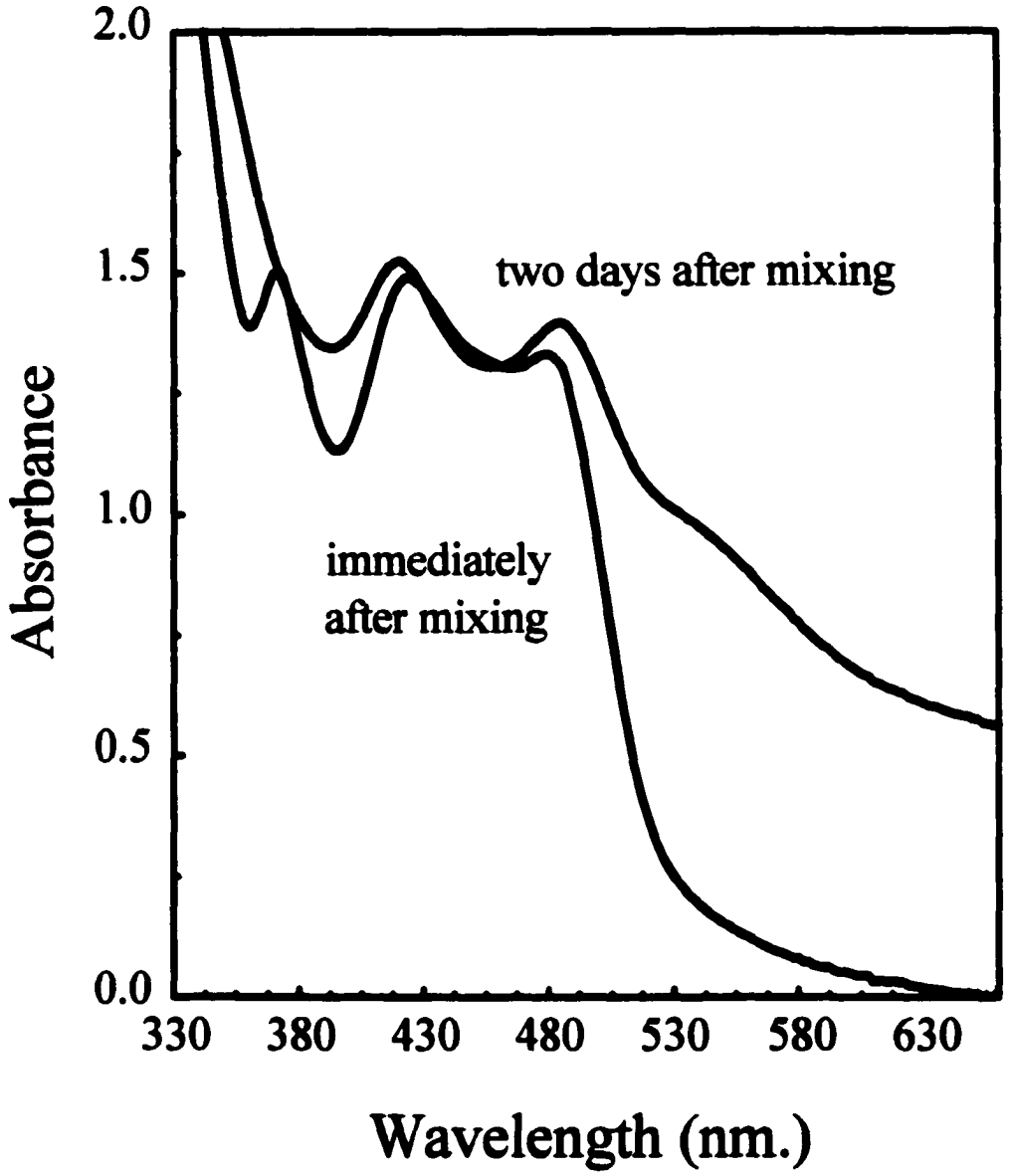

Figure 56. Stern-Volmer plot for intensity (●) and lifetime (■) quenching of $Ru(bpy)_2dpp^{2+}$ by $OsCl_6^{2-}$ in 5.0 M NaCl.

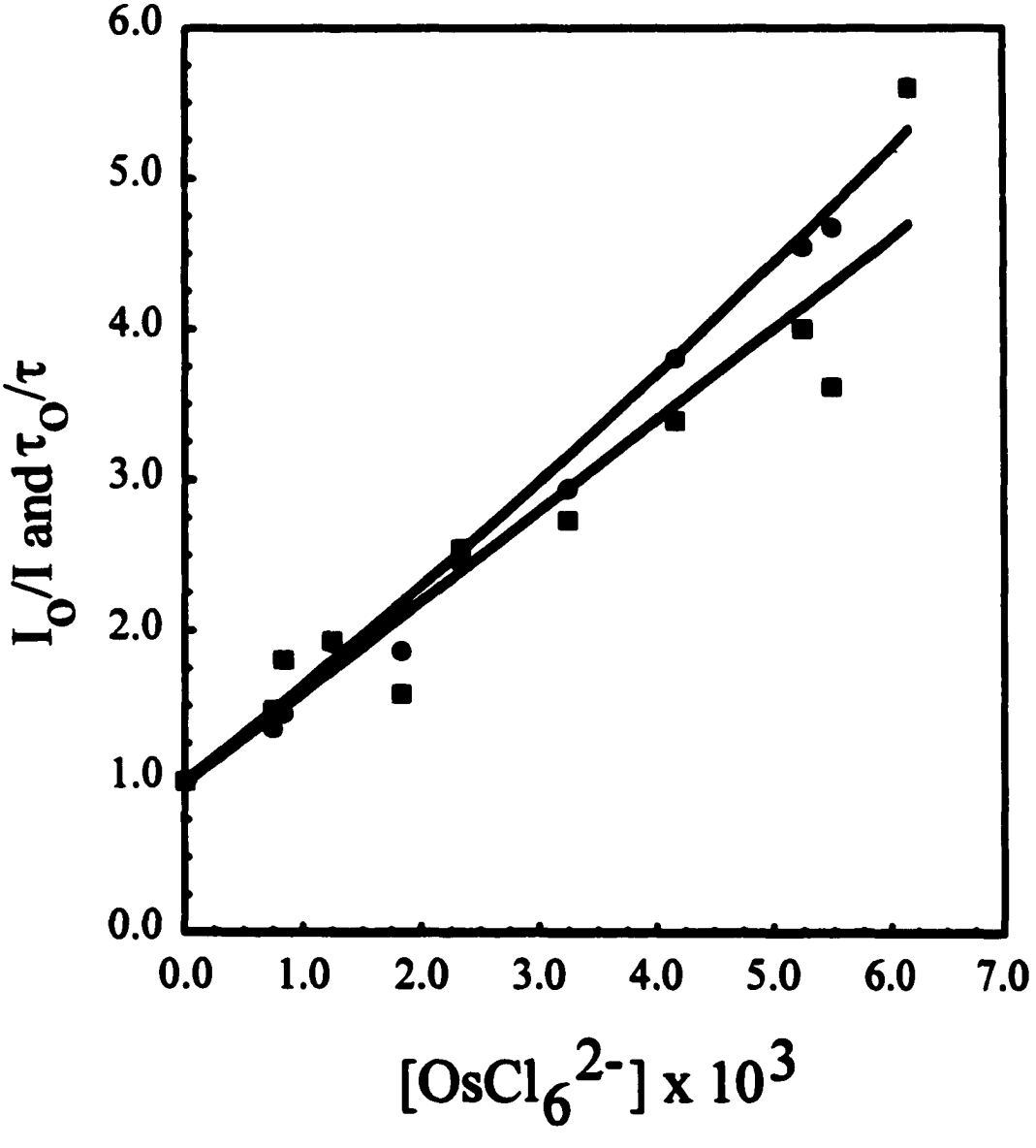

Figure 57. Spectral change for a solution 5.0×10^{-5} M in $Ru(bpy)_2dpp^{2+}$ and 6.6×10^{-4} M $IrCl_6^{3-}$ refluxed in 5.0 M NaCl.

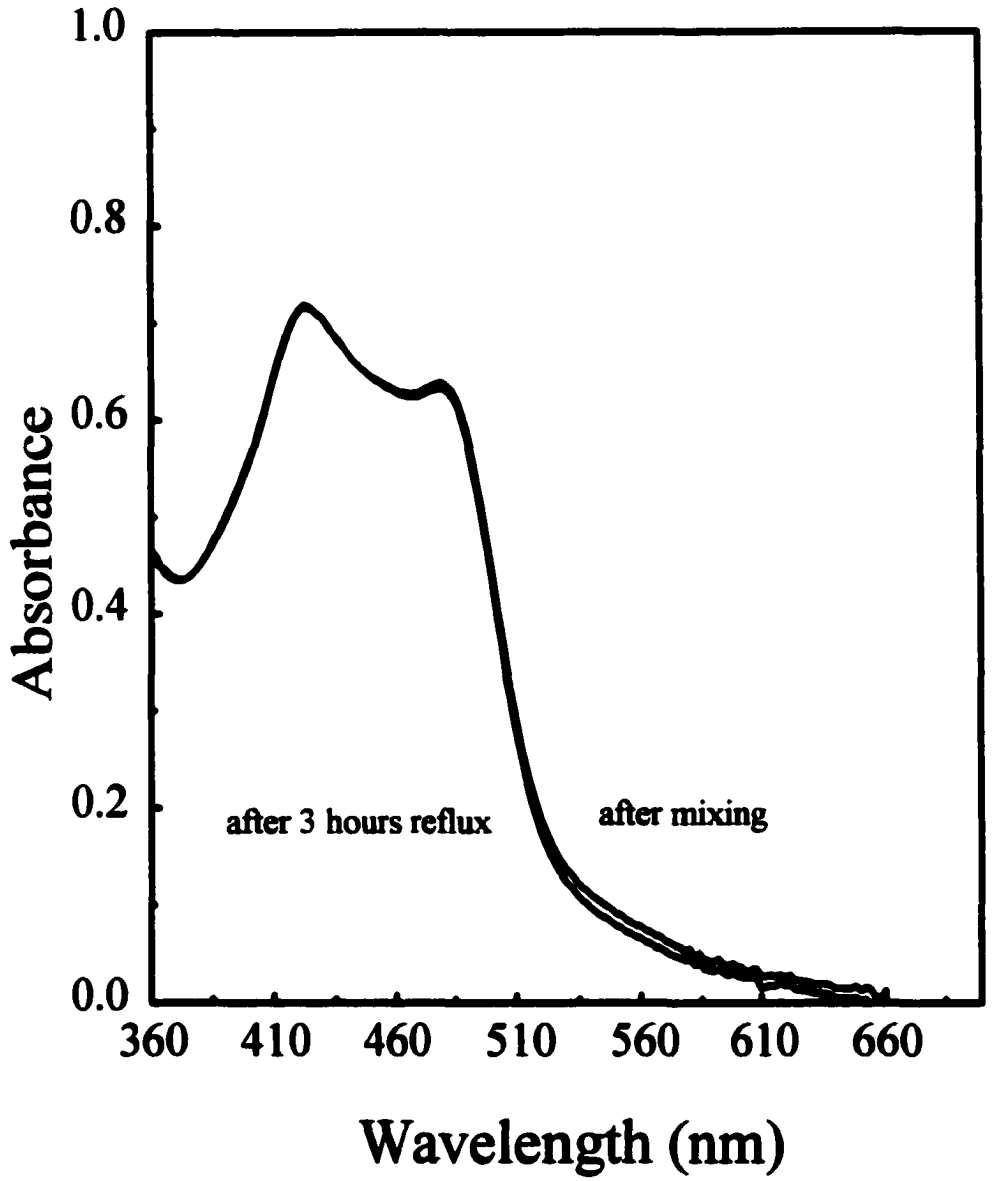

Figure 58. Emission spectrum of $Ru(bpy)_2dpp^{2+}$ with increasing concentration of Ag^+ in water. Intensities are decreasing with increased concentration of Ag^+. Shown are solutions 0, 8.0×10^{-3}, 6.0×10^{-2} and 1.5 M in Ag^+.

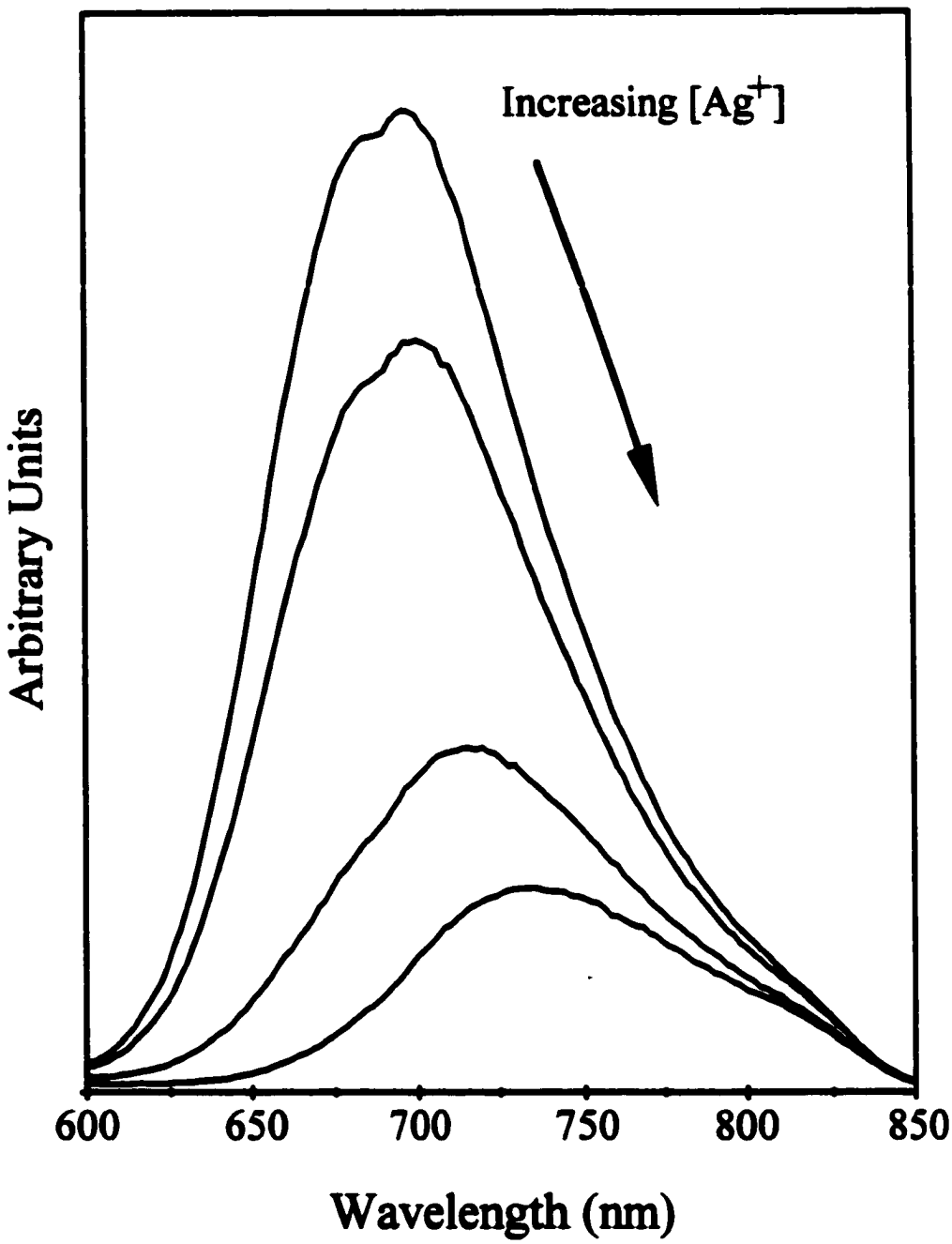

Figure 59. Absorption spectrum of $Ru(bpy)_2dpp^{2+}$ with increasing concentration of Ag^+ in water.

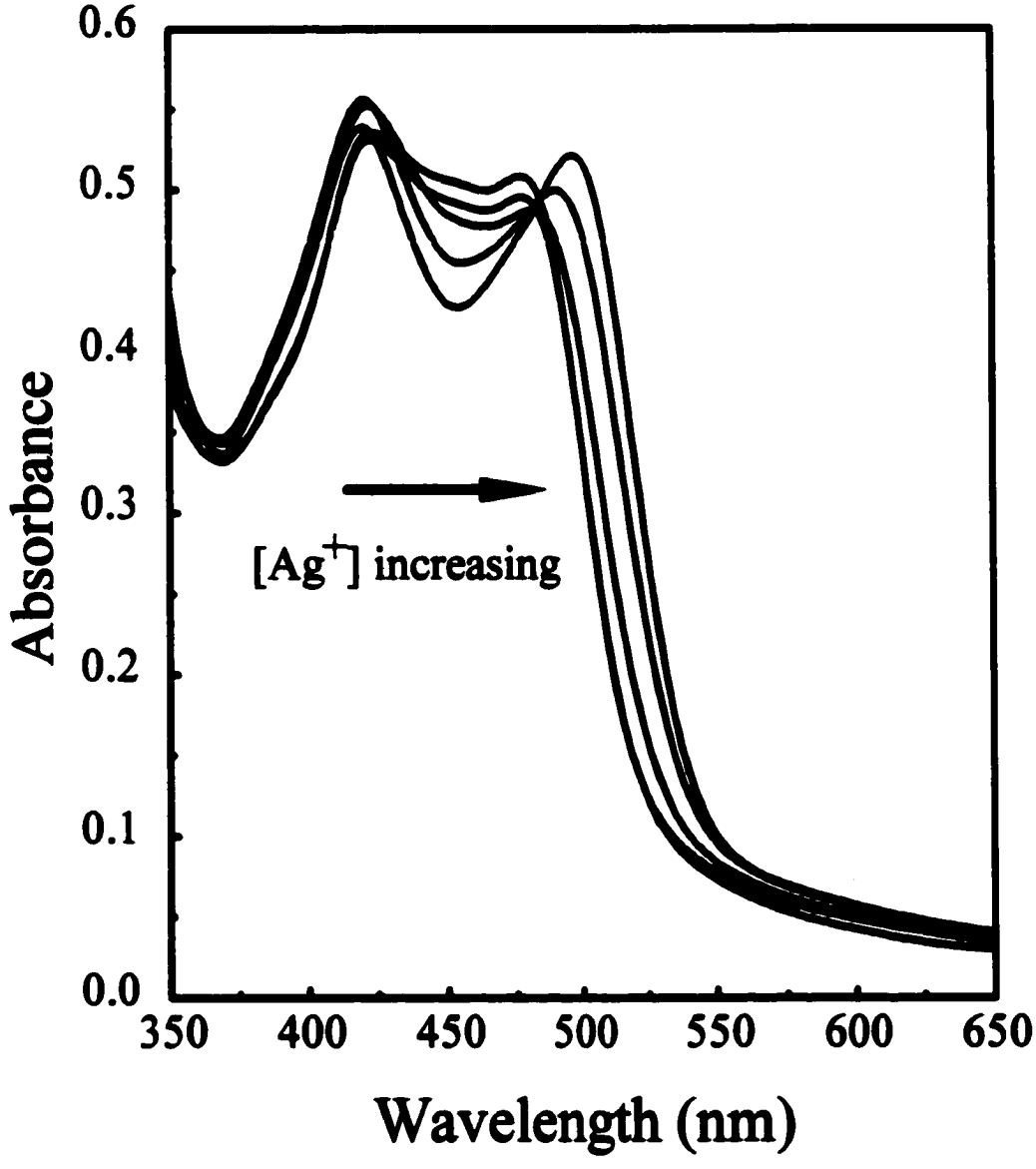

Figure 60. ^{1}H NMR spectrum of $Ru(bpy)_2dpp^{2+}$ in D_2O.

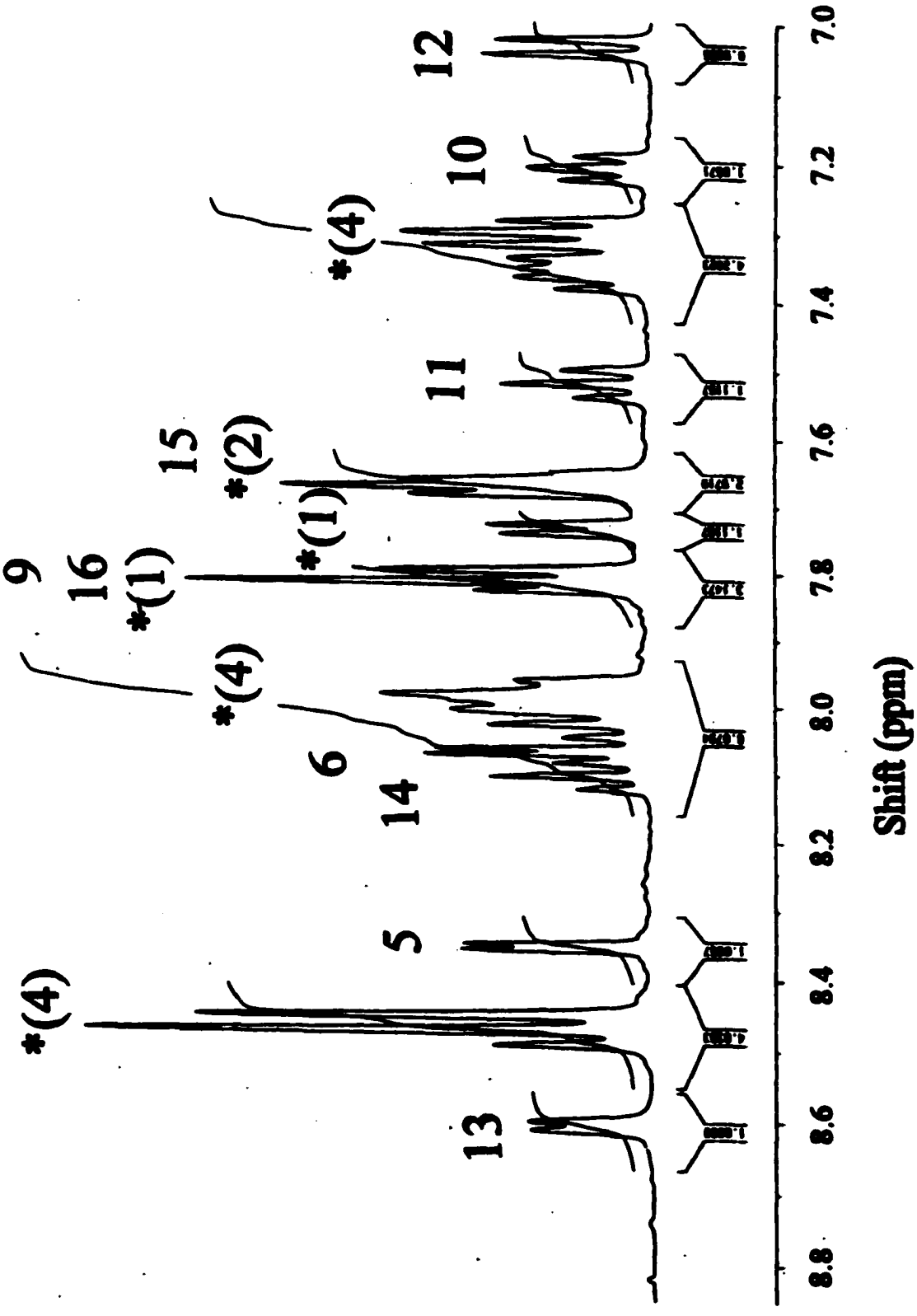

Figure 61. ^{1}H NMR spectrum of $Ru(bpy)_2dpp^{2+}$ in D_2O at concentration of Ag^+ of 0.14 M.

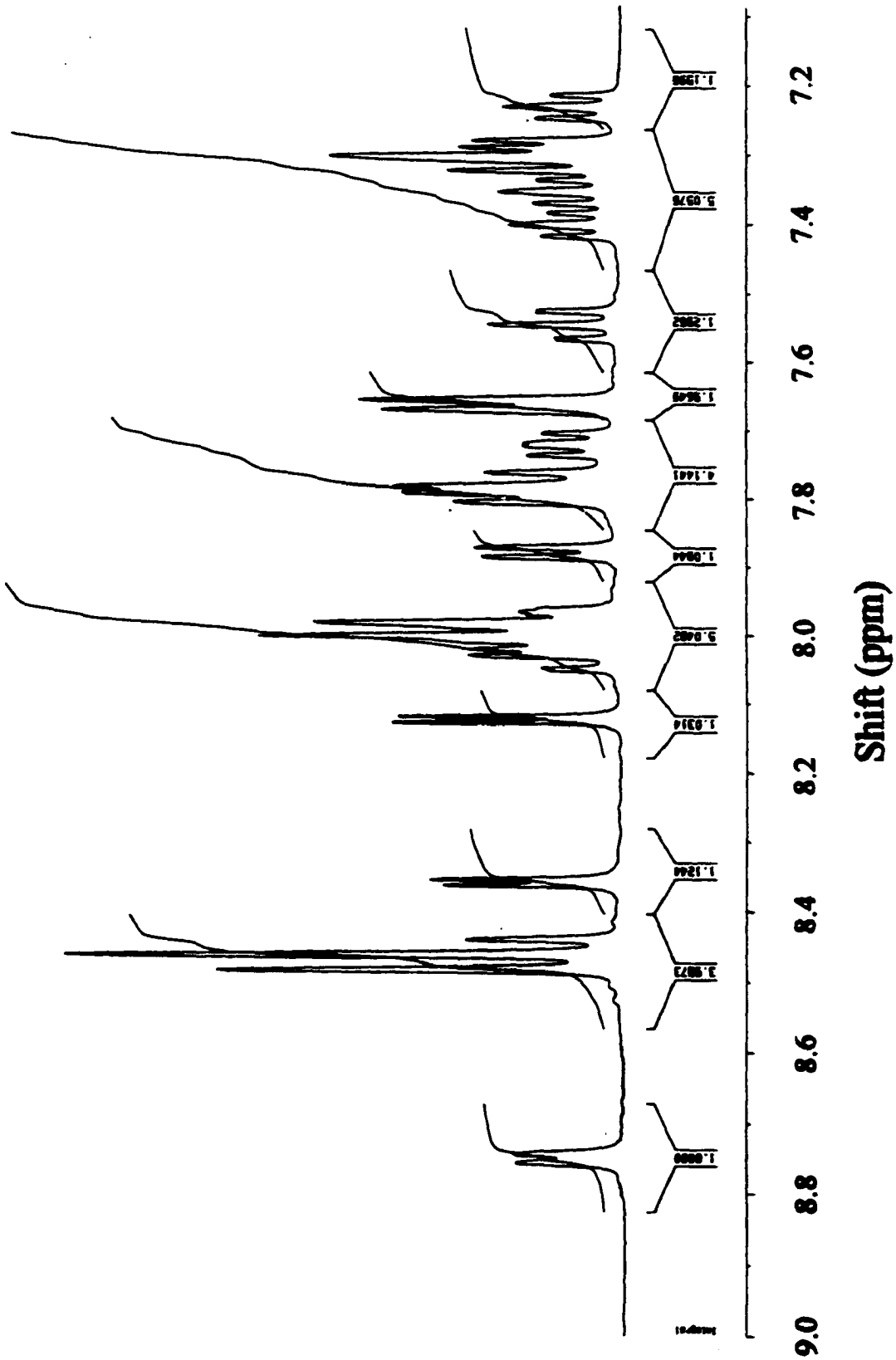

Figure 62. COSY NMR spectra of $Ru(bpy)_2dpp$ in D_2O.

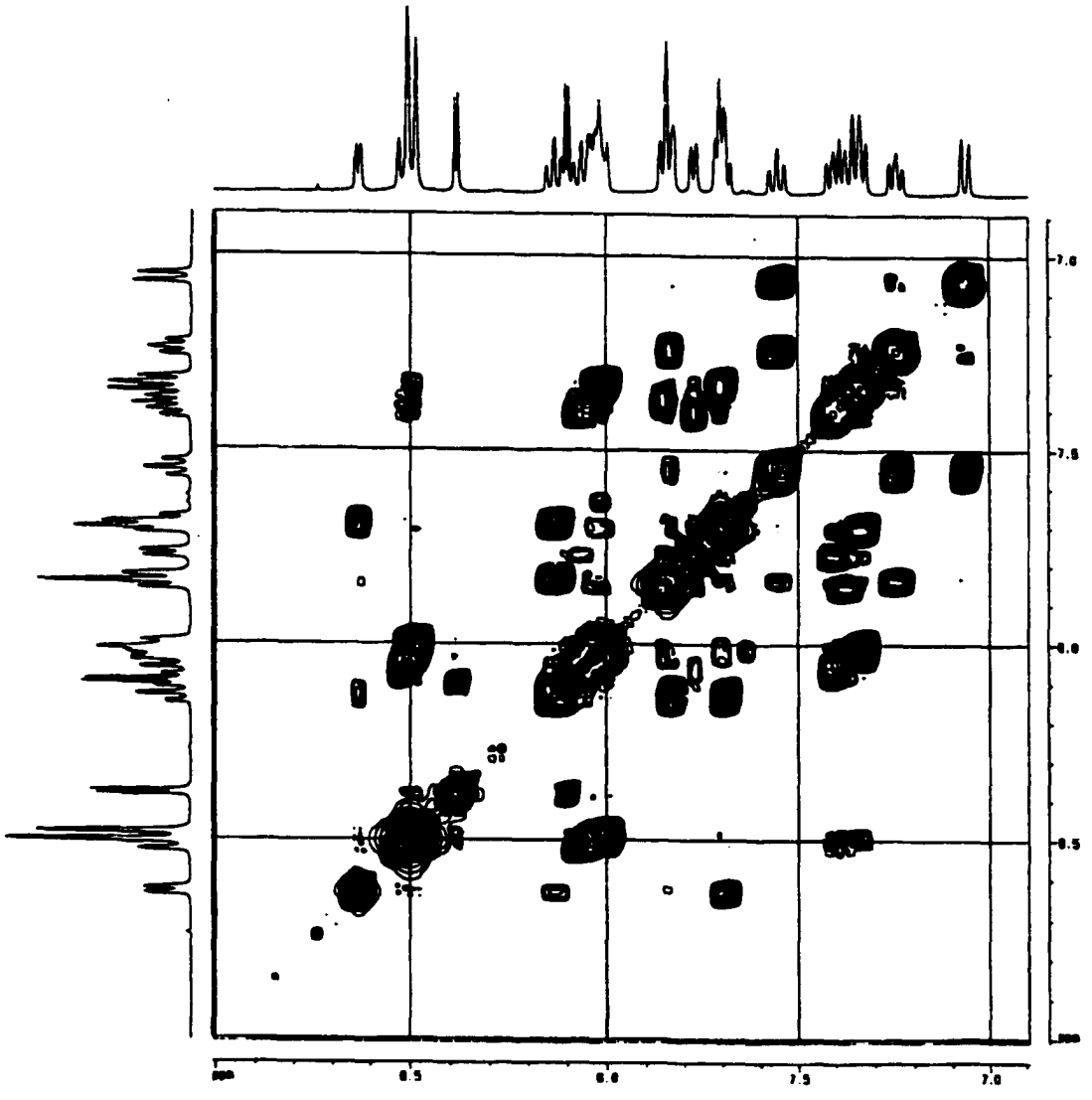

Figure 63. Assignment of the ^{1}H NMR spectrum of $Ru(bpy)_2dpp^{2+}$.

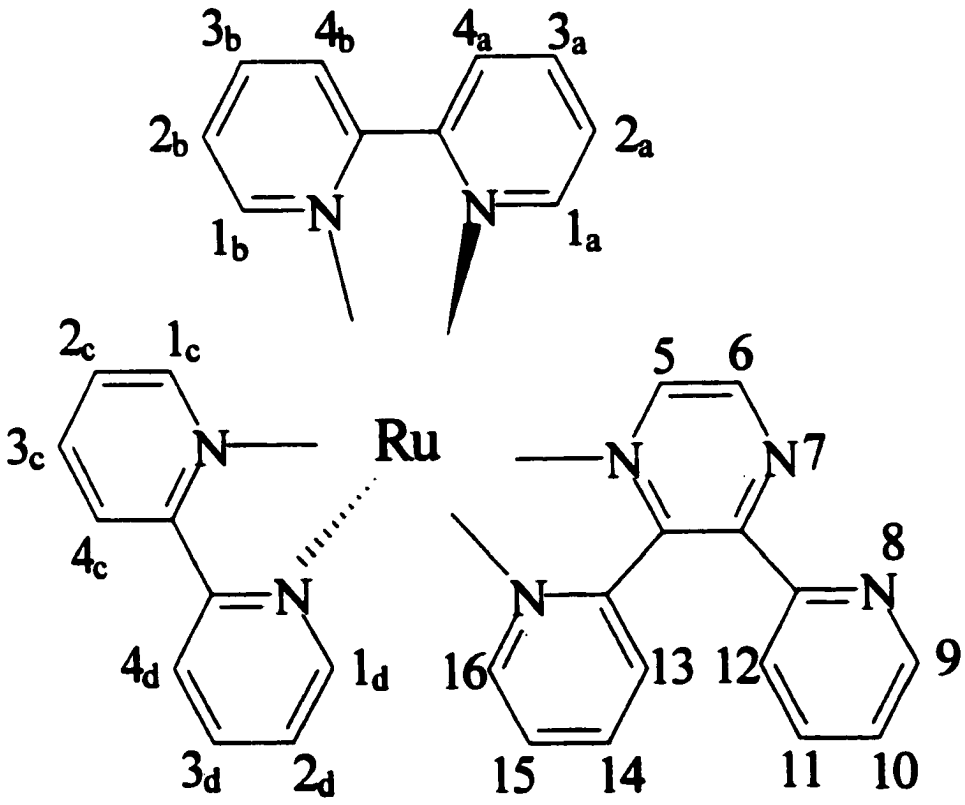

Figure 64. ^{1}NMR shift versus concentration of Ag^+, peak 12 (▲), peak 13 (●), peak 6 (◆) and the 2,2'-bipyridine peak at 7.75 tentatively assigned to position 1c (■).

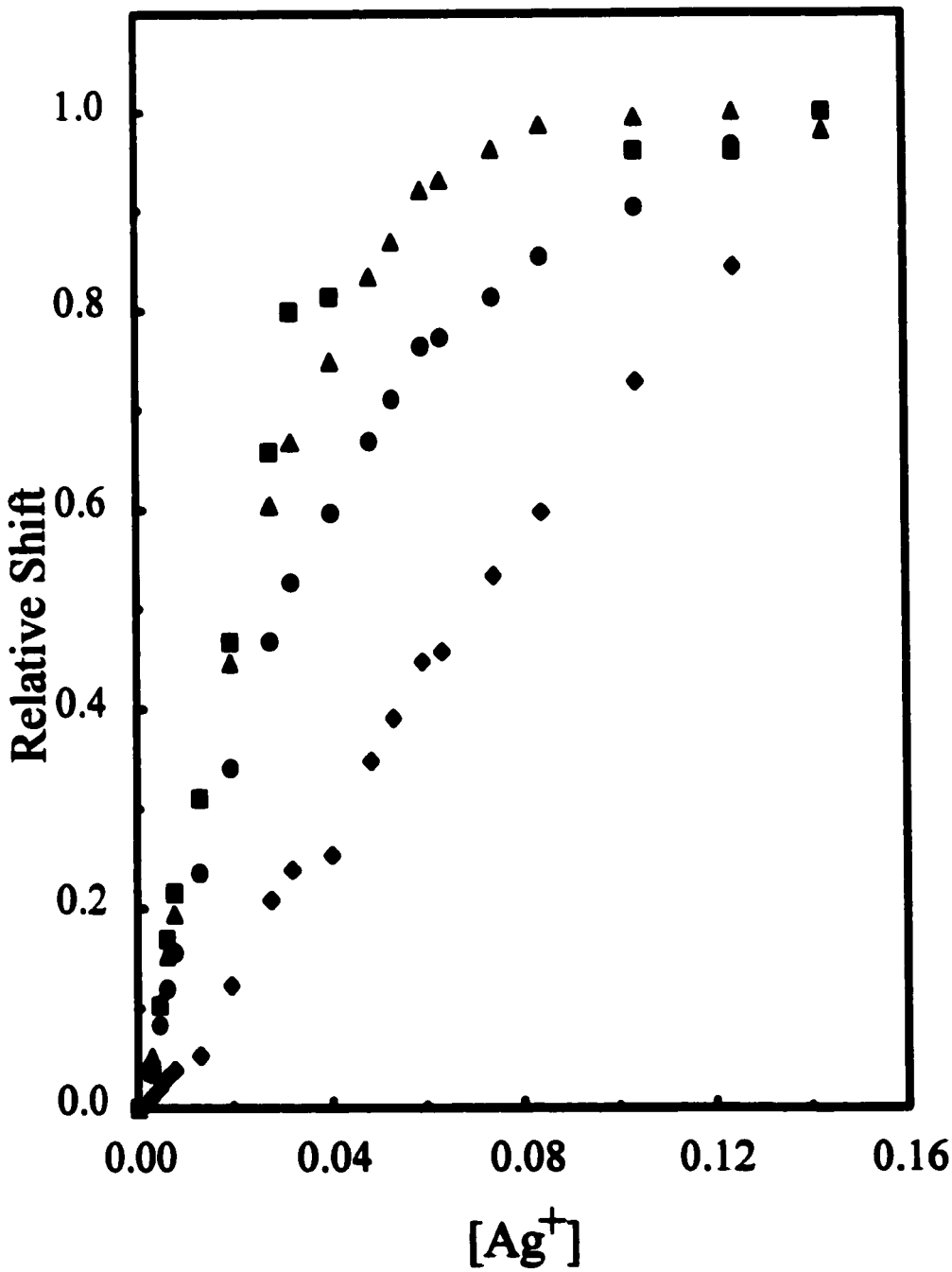

Figure 65. Experimental (■) and best fit (—) data for the change in absorbance at 510 nm vs. concentration of Ag^+, for a solution 5.0×10^{-5} M in $Ru(bpy)_2dpp^{2+}$.

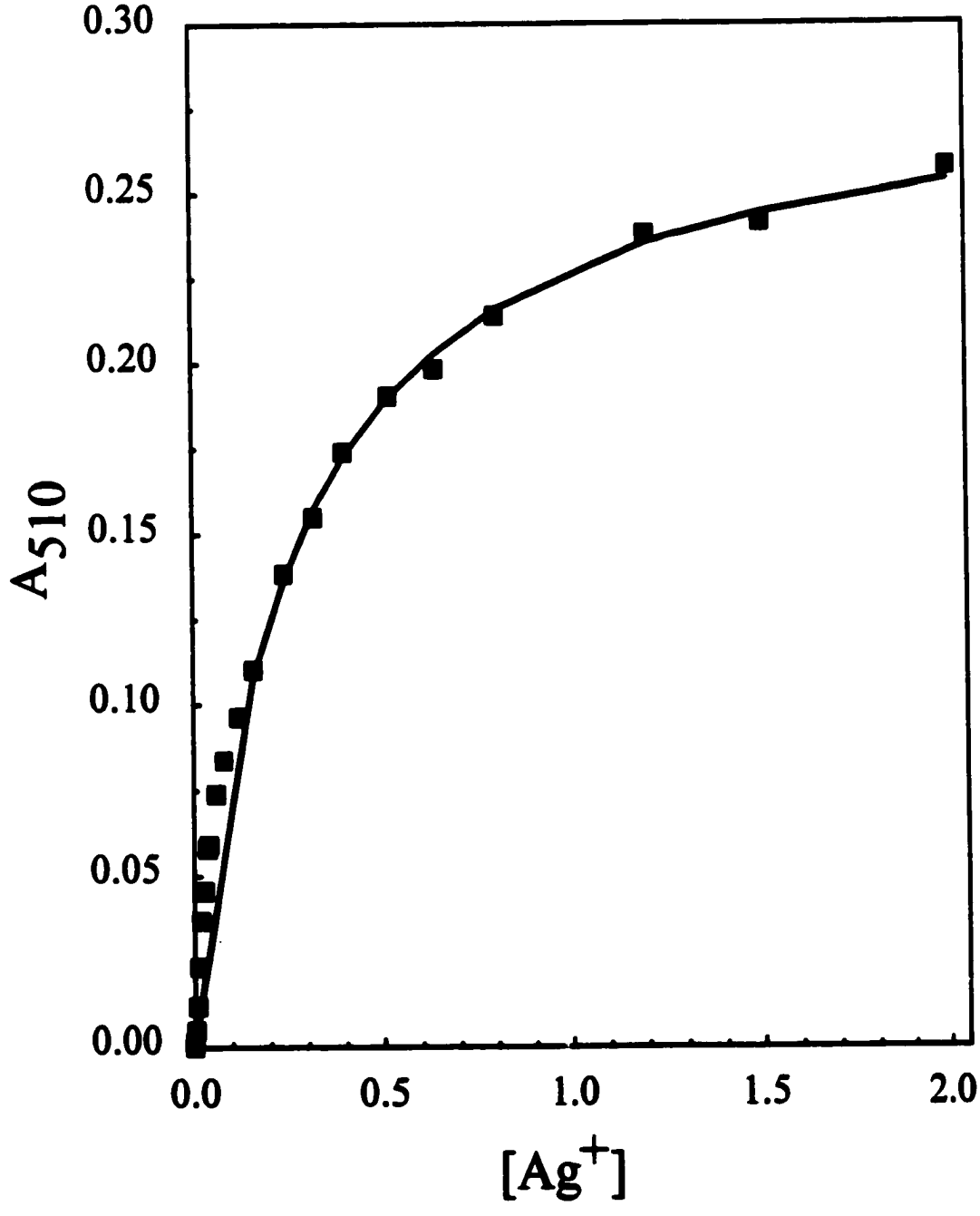

Figure 66. Sigmoidal titration curve of the absorption titration curve for the reaction of $Ru(bpy)_2dpp^{2+}$ with Ag^+.

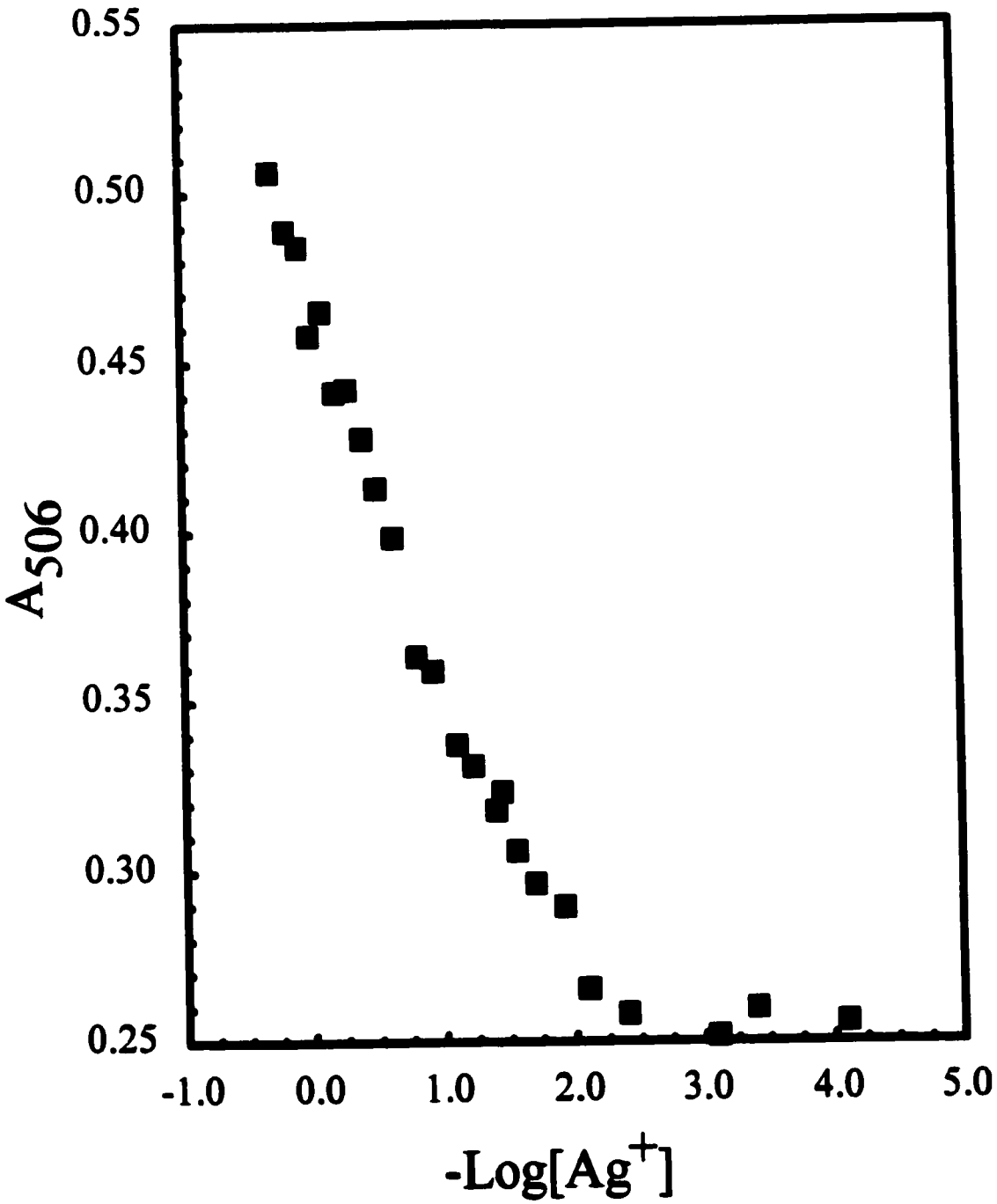

Figure 67. Apparent values of K_{eq} vs. maximum concentration of Ag^+ from ^1H NMR data.

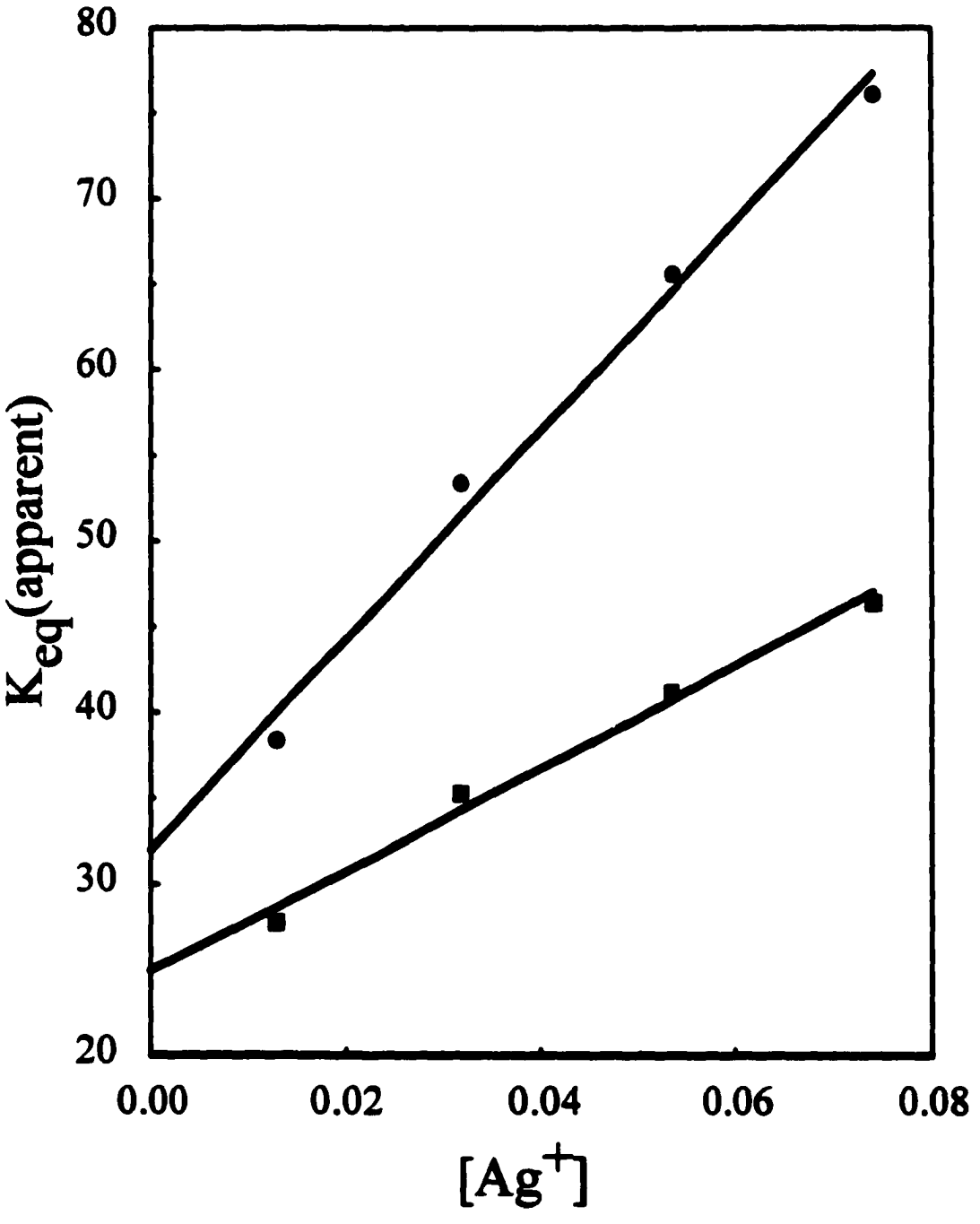

experimental data could not be obtained assigning the maximum spectral change to complete reaction. Therefore, the value of the epsilon of the product was varied as a best fit parameter, in addition to the value of the equilibrium constant. In both ^{1}H NMR and absorbance spectra, the spectral changes were assumed to be proportional to the concentration of the bimetallic product. Fitting the data to eq 26, with a non-linear minimization routine, yields $K_{eq} = 5 \pm 2$ from the absorbance data. (Figure 65). Using the same absorbance data, but analyzing it by a sigmoidal titration plot (i.e. a plot of – log[Ag+] versus Absorbance at 510 nm), yielded a sigmoidal curve that does not reach an endpoint at the highest concentration of Ag^+ used. This agreed with the results of the fitting that acceptable fits could not be obtained by assuming complete reaction had occurred. The halfway point of this curve in stead of the inflection point yields an upper limit of $K_{eq} \leq 5$ (Figure 66). This is an upper limit because the eventual endpoint of this curve must be on the lhs of Figure 66. This end of the titration curve corresponds to higher concentrations of Ag^+ required to completely complex the $Ru(bpy)_2dpp^{2+}$and therefore smaller values of K_{eq}.

Analysis of the ^{1}H NMR data by a titration curve method yielded a distorted sigmoidal plot. This distortion is due to the fact that the concentration of Ag^+ had significantly changed from its nominal concentration, which is the quantity that is treated as the independent variable in this type of analysis. Fitting of the NMR data yielded values that were determined to reflect non-ideal solution behavior, since the best fit values decreased monotonically with exclusion each data point of a higher concentration. An extrapolation technique was therefore used to determine the apparent value of K_{eq} at infinite dilution. The technique consisted of obtaining fits to the data using lower

Figure 68. Fluorescence titration curve for the excited state coordination of Ag^{+} by $Ru(bpy)_2dpp^{2+}$.

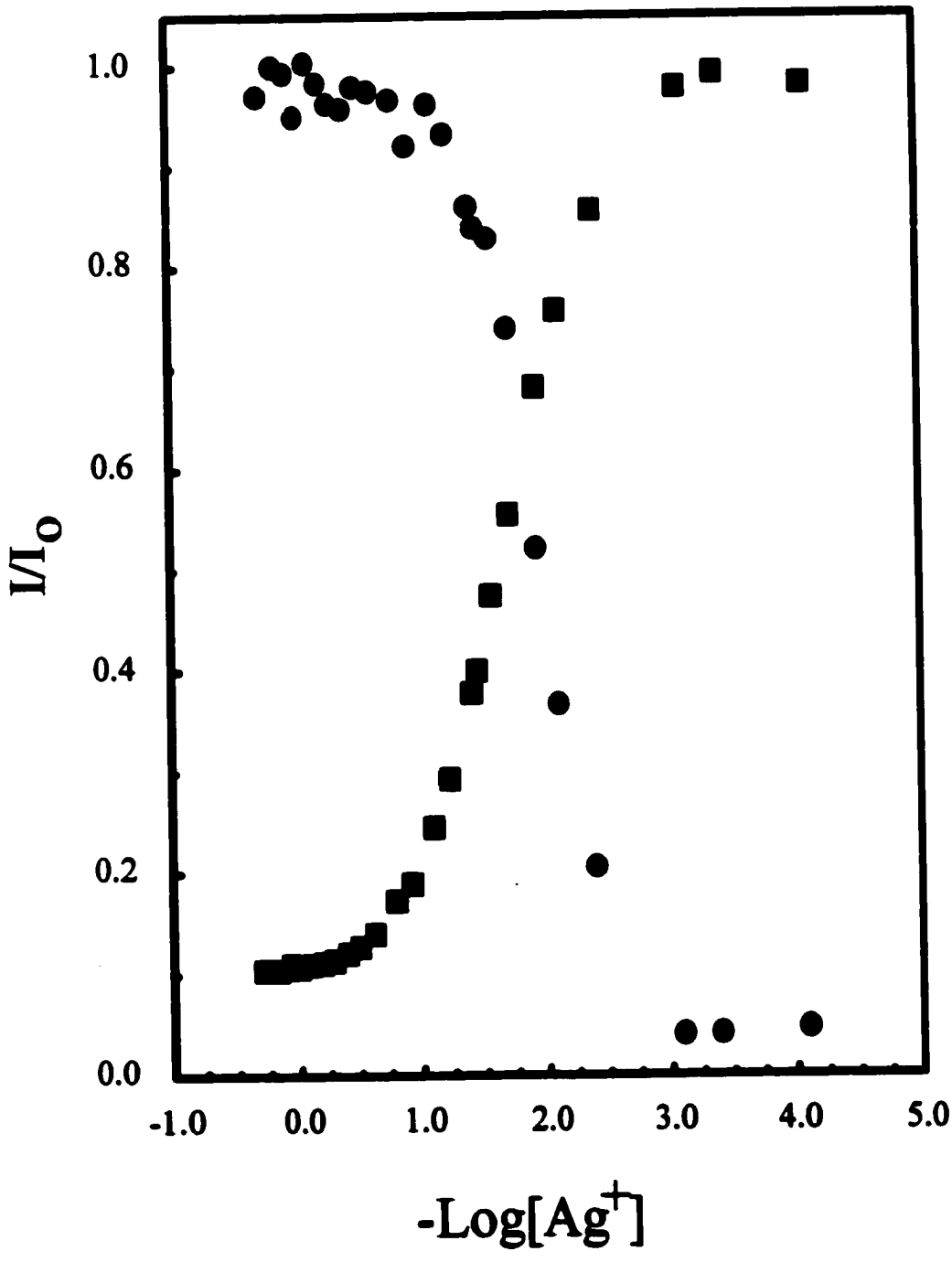

concentration ranges on successive trials. Plots of the apparent value of K_{eq} versus the highest concentration of Ag^+ used in the fitting, yields values of 25 and 32 from the two ^1H NMR resonances monitored (Figure 67). Of the five resonances that shift with addition of Ag^+, this technique was only applied to peaks 12 and 13 (Figure 60). The other resonances were not used for different reasons. Peak 9 was almost completely obscured and monitoring it quantitatively was not possible. The shift observed in the bipyridine doublet at 7.75, was to noisy to successfully apply the extrapolation technique on, and peak 6 was not used due to the inability to assign an extent of reaction to the observed shift, which is explained further in the discussion section.

The fluorescence data was analyzed using the same methods outlined earlier, which are routinely applied to sigmoidal titration plots obtained from emission spectra of the protonated and deprotonated forms of complexes. The emission intensities were monitored at 695 and 732 nm as solid $AgNO_3$ was titrated into a single reaction solution, by weighing small portions and adding them to the NMR tube containing the $Ru(bpy)_2dpp^{2+}$ stock solution. Each spectrum was corrected for the overlap of the other, as outlined earlier for proton-transfer emission spectra. This correction was substantial for the band at 732 nm, due its small intensity relative to the band at 695 nm. The expected "S" shape of this titration curve was still apparent though, despite being somewhat noisier than the band at 695 (Figure 68). The fluorescence titration curves obtained from 732 and 695 nm, intersected within experimental error of their own inflection points at $-\log[Ag^+] = 1.9$. The new emission peak centered at 732 nm decays with first-order kinetics characterized by an excited-state lifetime of $\tau = 75$ ns. Whereas

Figure 69. Spectral change observed upon irradiation of a solution 5.0×10^{-5} M in $Ru(bpy)_2dpp^{2+}$ and 10^{-4} M in trans-$Pt(NH_3)_2Cl_4$. Spectra are displayed as the difference between each spectrum and the first taken, in order to make a very slight spectral change apparent.

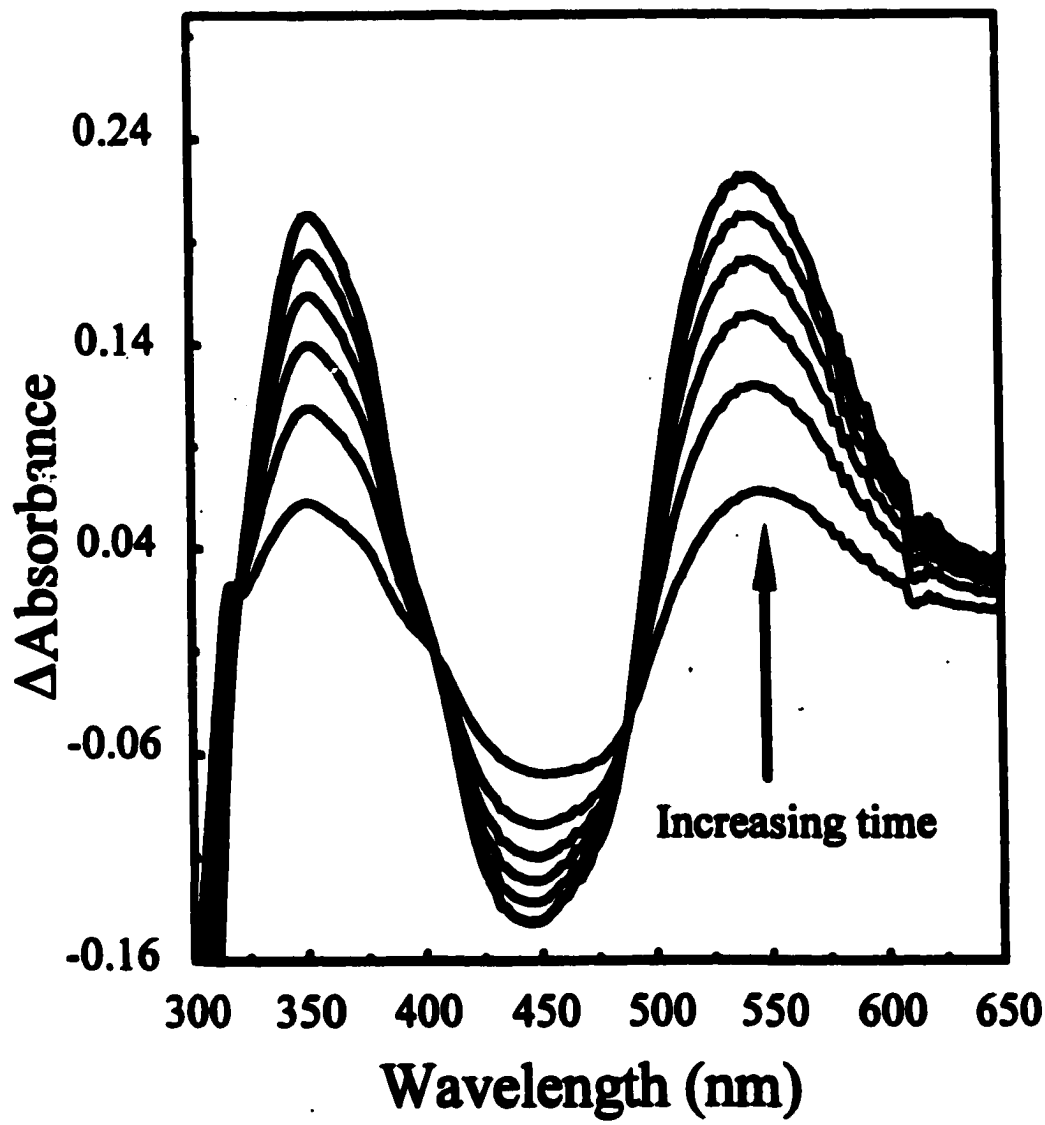

the 695 band, which is assigned to $Ru(bpy)_2dpp^{2+}$ has τ = 125 ns. The lifetime correction factor (eq 57) is calculated to be –log(125/75) = -.22, which gives a value of $^*K_{eq}$ = 48.

(10) Interaction of $[Ru(bpy)_2dpp](ClO_4)_2$ with *cis*-$PtCl_4(NH_3)_2$ and *trans*-$PtCl_4(NH_3)_2$

cis-$PtCl_4(NH_3)_2$ is not reactive thermally with $Ru(bpy)_2dpp^{2+}$ in aqueous solution, as indicated by no change in the visible absorption spectrum over a period of 30 minutes in the dark. Nor is it reactive photochemically, in aqueous solution under conditions of intense 488-nm irradiation. However, monitoring the absorption spectrum of a solution 5.0×10^{-5} M in $Ru(bpy)_2dpp^{2+}$, and saturated in trans-$PtCl_4(NH_3)_2$ (approximately 10^{-4} M) shows that a reaction occurs readily at room temperature in the dark, reaching completion over several hours. An identical spectral change is obtained, and is measurable after 10 minutes of intense 488-nm irradiation of an identical solution (Figure 70). Photochemical and thermal reactions both proceed with maintenance of isosbestic points at 403 nm and 488 nm. The product is quite soluble and its formation is very apparent to the naked eye as the reaction solutions turn an intense purple when the reaction is conducted in water. Figure 67 shows this spectroscopic change as a difference spectra, indicating a new electronic transition growing in at 540 nm, spectra shown are taken every 10 minutes.

While the accumulation of product makes the photochemical reaction of trans-$PtCl_4(NH_3)_2$ easily observable, its poor solubility makes observation of its possible quenching behavior difficult. Saturated solutions appeared to have a solubility of approximately 10^{-4} M in water. These solutions display no measurable intensity quenching of $Ru(bpy)_2dpp^{2+}$. However, over a period of many hours of sitting, or 30

minutes of sonication, excess solid left in the stock vessel dissolves. Use of the molar absorptivity of trans-$PtCl_4(NH_3)_2$ suggests these solutions are 1.5×10^{-3} M in trans-$PtCl_4(NH_3)_2$. Stock solutions of cis-$PtCl_4(NH_3)_2$ show a similar increase in solubility with time, achieving concentration of 10^{-3} M, based on the epsilons of cis-$PtCl_4(NH_3)_2$. Measurement of the intensity quenching of $Ru(bpy)_2dpp^{2+}$ using both of these solutions and the nominal molarities yields values of 448 ± 68 M^{-1} and 315 ± 33 M^{-1}, for the cis and trans isomers, respectively. However, subsequent work casts some uncertainty on how to interpretation of this data. Treatment of the stock solutions of trans-$PtCl_4(NH_3)_2$ and cis-$PtCl_4(NH_3)_2$ obtained by sonication, with silver nitrate, yielded a positive test for free chloride, indicated by its cloudy color. No trace of the intense blue color of $Ag(NH_3)_2^+$ could be detected by the naked eye suggesting no release of coordinated ammonia. We therefore attribute the apparent increase in solubility with a chemical reaction, probably the substitution of a coordinated chloride by an H_2O molecule. Given the known specificity of the thermal substitution chemistry when the trans effect is operative, this data may well represent quenching by cis and trans isomers of $PtCl_3(H_2O)(NH_3)_2$ or $PtCl_2(H_2O)_2(NH_3)_2$.

The poor solubility of cis-$PtCl_4(NH_3)_2$ and trans-$PtCl_4(NH_3)_2$ made it an excellent candidate for measurement of its quenching efficiency, by the technique developed in this work, based upon measurement of the time dependence of the steady-state emission intensity. A decline in the emission intensity from $Ru(bpy)_2dpp^{2+}$ with time, was apparent for solutions containing trans-$PtCl_4(NH_3)_2$. However, attempts to analyze the quenching of $Ru(bpy)_2dpp^{2+}$ by trans-$PtCl_4(NH_3)_2$ by use of the time dependence of the emission intensity, were unsuccessful. Photochemical acceleration of the reaction between trans-

$PtCl_4(NH_3)_2$ and $Ru(bpy)_2dpp^{2+}$ is very apparent under conditions of intense 488-nm irradiation. However, in the time dependent steady-state emission experiment, the source of irradiation is the excitation source of the emission spectrometer. The intensity of this source was only capable of a very slight acceleration of the reaction, relative to an identical solution kept in the dark. Attempts to extract the pure photochemical rate by subtraction of the rate observed for the thermal control, from the photochemical trials, was unsuccessful yielding inconsistent results, upon repetition of identical experiments. Comparison of the experimental conditions of the 488 nm-photolysis that established a photochemical reaction, and the conditions under which the time dependence of the steady-state emission experiments were conducted, shows that a simple explanation can be made. In the photolysis experiment, it was determined by actinometry that $I_o \approx 10^{-5}$ Einsteins/lit-s, compared to a value of $I_o \approx 7.0 \times 10^{-7}$ Einsteins/lit-s, in the emission spectrometer. In addition, the emission experiments were done at lower concentrations of $Ru(bpy)_2dpp^{2+}$, in order to minimize self-absorption of emitted light, while the photolysis of $Ru(bpy)_2dpp^{2+}$ in the prescience of trans-$PtCl_4(NH_3)_2$, had comparatively large absorbance values for $Ru(bpy)_2dpp^{2+}$, in order to harvest a large fraction of the incident light. It was therefore concluded that with the limited light intensity available using the spectrometer as the irradiation source, the photochemical rate was to small too reproducibly measure relative to the thermal rate at room temperature.

In an attempt to find a solvent in which the solubility of cis-$PtCl_4(NH_3)_2$ and trans-$PtCl_4(NH_3)_2$ was sufficient to obtain quenching data, it was observed that the reaction of these two stereoisomers in ethanol leads to different products than are obtained in water. Reaction mixtures with one equivalent of each isomer and

$Ru(bpy)_2dpp^{2+}$ kept at 78 °C for 2 hours turn from the brown color of the $Ru(bpy)_2dpp^{2+}$ to clear, indicating complete conversion to products of the $Ru(bpy)_2dpp^{2+}$ present as a reactant. The reaction products obtained from both isomers are bright orange and are insoluble in ethanol. ^1H NMR spectra of the crude solids obtained without any purification shows that substitution has taken place with very little loss of stereochemistry. The spectra are both shifted downfield consistent with the deshielding associated with the positive charge of the metal center. The ^1H NMR spectrum of both the cis and the trans isomers, each have impurity peaks that correspond to the primary product of the other isomers reaction. These peaks suggest the amount of racemization that occurs with substitution. In the case of the trans isomer (Figure 70) integration of these impurity peaks, suggests less than .6% racemization occurs. In the case of the cis-isomer the extent of racemization is much greater at about 1.6% (Figure 71)

Figure 70. H NMR spectrum in d_6-acetone, of the unpurified products of the reaction of $Ru(bpy)_2dpp^{2+}$ with trans-$PtCl_4(NH_3)_2$ in ethanol.

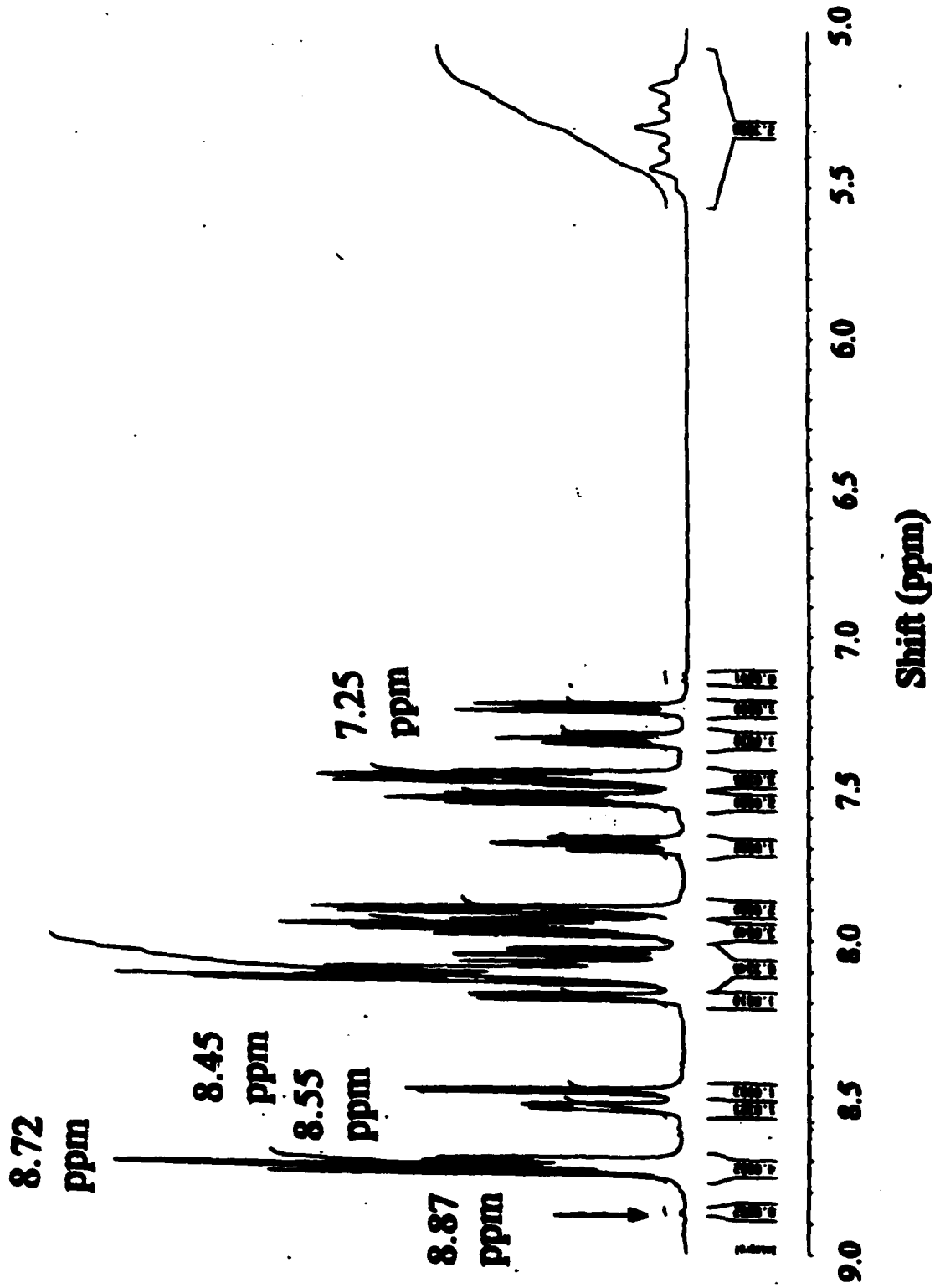

Figure 71. ^{1}H NMR spectrum in d_6-acetone, of the unpurified products of the reaction of $Ru(bpy)_2dpp^{2+}$ with cis-$PtCl_4(NH_3)_2$ in ethanol.

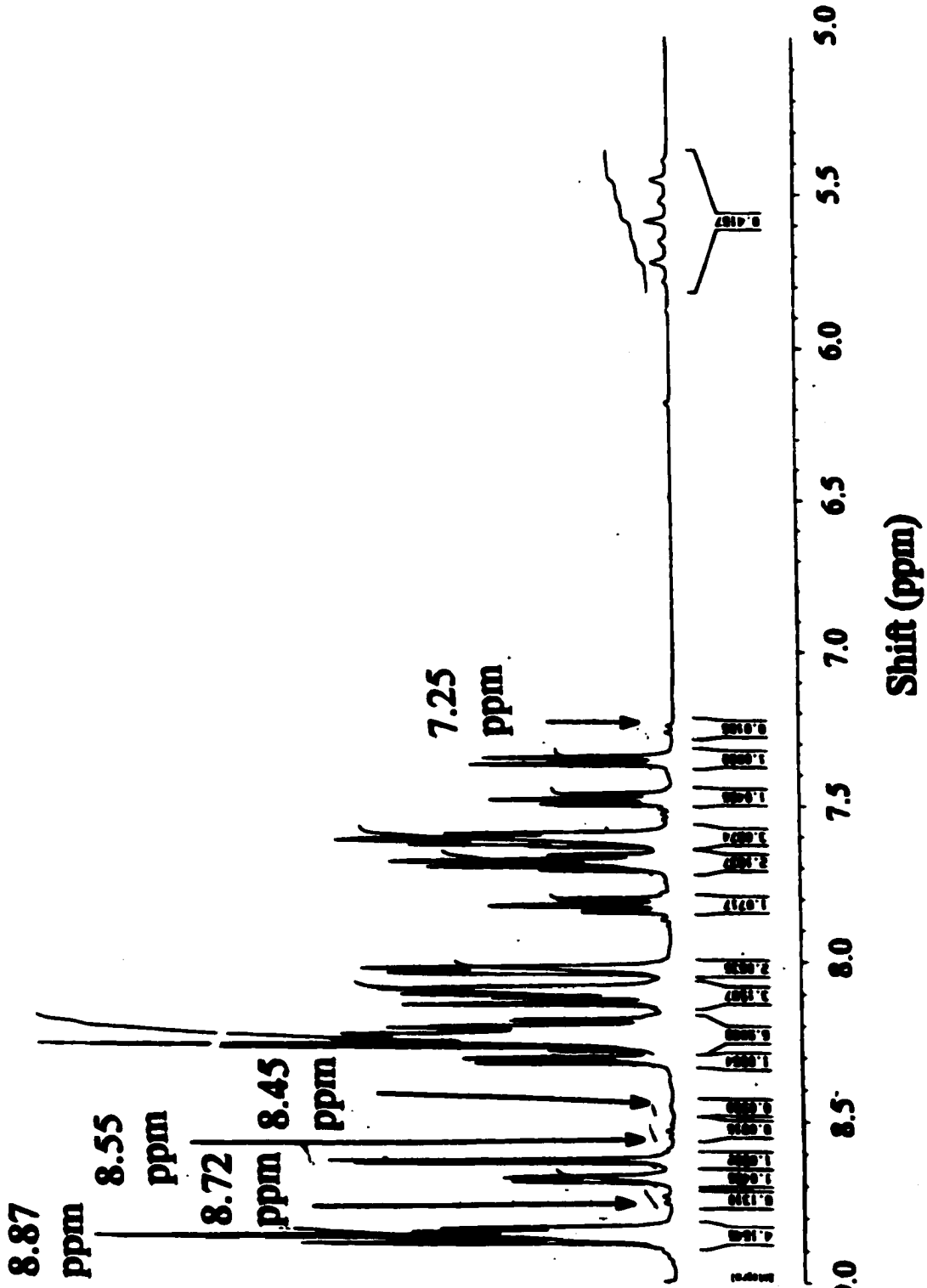

IV Discussion

(1) Reactions of $[Ru(bpy)_2dpp](ClO_4)_2$ with $Na_2[PtCl_6]$

Central to understanding the mechanism of any photochemical reaction is the determination of the initiation step. While the reactant concentrations can be manipulated to make any one component of a solution the dominant absorber, all components of the solution have non-zero fractions of light absorbed. Therefore, amplification of even a small fraction of light absorbed by a chain reaction process is a nagging concern. If the initiation step in the photochemical formation of $Ru(bpy)_2dppPtCl_4^{2+}$, were in fact absorption of light by $PtCl_6^{2-}$ followed by reaction with a ground state molecule of $Ru(bpy)_2dpp^{2+}$ then the rate of product formation would depend upon the ground state concentration of $Ru(bpy)_2dpp^{2+}$. However, our experimental data suggests that this sort of mechanism is unlikely. The sharp reduction observed in the rate of formation of this product in the presence of a competitive quencher, $FeCl_3$, (Figure 27) establishes that reaction occurs via the MLCT of $Ru(bpy)_2dpp^{2+}$, rather than by a mechanism in which the molecule that undergoes substitution is photolyzed to form a coordinately unsaturated intermediate that undergoes substitution by a ground state $Ru(bpy)_2dpp^{2+}$.

The sharp decline in the quantum yield of formation of $Ru(bpy)_2dppPtCl_4^{2+}$establishes that the photochemical reaction between $Ru(bpy)_2dpp^{2+}$ and $PtCl_6^{2-}$ occurs through the MLCT state of $Ru(bpy)_2dpp^{2+}$. Generally, Photochemical reactions are not considered to involve the interaction of two excited species, due to the limitations that both have finite lifetimes and are usually present at concentrations which are tiny fractions of the ground state concentrations they are derived from. The following

discussion shows that a mechanism involving the reaction of $^*Ru(bpy)_2dpp^{2+}$ and a Pt(III) transient is unlikely.

Excitation into the ligand field bands of $PtCl_6^{2-}$ has been shown to lead to aquation and reduction in the presence of suitable reducing agents.

$$Pt(IV) \xrightarrow{h\nu} Pt(III) \qquad \text{rate} = {}^{Pt}I_a\phi_{Pt(III)} \qquad (108)$$

$$2Pt(III) \longrightarrow Pt(II) + Pt(IV) \qquad \text{rate} = k_2[Pt(III)]^2 \qquad (109)$$

Regardless of the details of the initiation step, such as the elementary steps resulting in the change described in eq 108, unless we have a chain reaction, the upper limit on the formation of Pt(III) is equal to I_a, the rate of absorption of photons, if we take $\phi_{Pt(III)}$, the quantum yield of formation the Pt(III) transient, to be unity. This seems reasonable since irradiation with light of wavelength greater than 365 nm has been shown to have quantum yields less than one, in contrast to the use of UV light.[51] Under conditions of constant irradiation, a photostationary state would be set up. An upper limit on the steady-state concentration of the transient could be estimated using $^{Pt}I_a$ and the rate constant $k_2 = 4.6 \times 10^6\ M^{-1}s^{-1}$, for decay of the Pt(III) transient reported by Wright and Laurence.[39]

$$\frac{d[Pt(III)]}{dt} = {}^{Pt}I_a - k_2[Pt(III)]^2 \qquad (110)$$

A steady state approximation can be used to estimate the concentration Pt(III) by requiring

$$\frac{d[Pt(III)]}{dt} = {}^{Pt}I_a - k_2[Pt(III)]_{ss}^2 = 0 \qquad (111)$$

After rearranging this expression, a relation linking the steady state concentration of the transient, to the absorbed light intensity and the rate constant for decay is obtained. Substitution of the value of ${}^{Pt}I_a = 3.38 \times 10^{-7}$ Einsteins·s^{-1}L^{-1}, for $PtCl_6^{2-}$ (the fraction of the total absorbed intensity that was absorbed by $PtCl_6^{2-}$) and the value of $k_2 = 4.6 \times 10^6$ M^{-1}s^{-1} reported by Wright and Laurence yields the steady-state concentration of the Pt(III) intermediate,

$$[Pt(III)]_{ss} \leq \sqrt{\frac{{}^{Pt}I_a}{k_2}} = 7.34 \times 10^{-14}\ M \qquad (112)$$

For [*Ru(bpy)$_2$dpp^{2+}], a similar steady state approximation obtained by setting eq 14 equal to zero and rearranging yields,

$$[*Ru(bpy)_2dpp^{2+}]_{ss} = \frac{{}^{Ru}I_a}{[PtIII)]k_p + 1/\tau} \qquad (113)$$

where τ = 125 ns, is the excited state lifetime of Ru(bpy)$_2$dpp^{2+}. Neglecting [Pt(III)]k_p can only lead to an overestimation of [*Ru(bpy)$_2$dpp^{2+}]$_{ss}$, and only a small one since the [Pt(III)] was less than 10% of the inverse of ${}^{T}K_{sv}$.

$$[*Ru(bpy)_2dpp^{2+}]_{ss} \leq {}^{Ru}I_a\tau = 1.33 \times 10^{-12}\ M \qquad (114)$$

The rate of photochemical product formation in the reaction between Ru(bpy)$_2$dpp^{2+} and $PtCl_6^{2-}$, that these estimates apply to, was 3.93×10^{-8} M·s^{-1}. Assuming a second order elementary step leads to product formation,

$$Ru(bpy)_2dpp^{2+} + Pt(III) \xrightarrow{k_p} \text{bimetallic product} \qquad (115)$$

suggests the rate law.

$$\text{Rate} = k_p[\text{Pt(III)}][^*\text{Ru(bpy)}_2\text{dpp}^{2+}] \quad (116)$$

If the overestimates of the steady-state concentrations of $[\text{Pt(III)}]_{ss}$ and $[^*\text{Ru(bpy)}_2\text{dpp}^{2+}]_{ss}$ are substituted into this rate law and the expression is rearranged to solve for the bimolecular rate constant for product formation (k_p), yields

$$k_p \geq \frac{rate}{[Pt(III)][^*Ru(bpy)dpp^{2+}]} = 2.66 \times 10^{14}\ s^{-1}M^{-1} \quad (117)$$

The direction of the inequality sign, making this value of k_p a lower limit, is due to the fact that the value of k_p is inversely proportional to the steady state concentrations of reactants. Therefore overestimates of the steady state concentrations lead to underestimates of k_p. This value is not within the diffusional limit in aqueous solution, usually taken to be approximately $10^{10}\ s^{-1}M^{-1}$ at 25°C. The significance of this estimate is that this type of mechanism, involving two photochemically generated intermediates cannot lead to large rates of product formation, due to the limited bimolecular rate of collision at such low concentrations of reactants. This conclusion does not depend upon the casting of the rate law, since higher order rate laws could be shown to have upper limits on their rate constants based on similar arguments, and would be further prohibited by their higher molecularity.

While this Pt(III) species has been implicated as long-lived species thought to be the chain carrier responsible for much of the photochemistry of $PtCl_6^{2-}$, the bond homolyis observed by Wrighton and Laurence was initiated by unfiltered UV discharge. It is not surprising that the use of such high energy light might lead to formation of radicals and chain reactions with quantum yields in excess of unity. However, as

mentioned earlier the quantum yields for photoaqution and photoreduction of $PtCl_6^{2-}$ have been shown to be less than unity when light of 365 nm or longer wavelengths is used

Quantum yields are ratios of rates for particular excited state processes, to the sum of the rates of all the deactivation processes rates. It expresses the efficiency of the process to funnel the energy of absorbed photons down a particular pathway. Quantum yields in excess of one reflect chain reactions, while quantum yields less than unity usually reflect the relative efficiency of deactivation by particular pathway. From the experimental standpoint, the quantum yield is the ratio of the rate of a particular deactivation process, to the rate of absorption of photons producing the excited state.

$$\phi(\text{any process}) = \frac{\text{rate of an excited state process}}{\text{rate of all deactivation processes}} \qquad (118)$$

Since the energy of the photons absorbed must eventually be dissipated, the average rate of absorption of photons must be equal to the average of the sum of the rates of all decay processes. The term absorbance must be qualified to mean absorbance by the species presumed to give rise to the transient, the decay of which has been referred to throughout this discussion. Unless an initiator species has a term in the kinetic scheme that contributes to its own decay (i.e. it undergoes self quenching), the quantum yield for any process does not depend upon the concentration of the species assumed to be the initiator. The quantum yield could depend upon any other species, whose interactions with the excited species might lead to deactivation by way of a contribution to the numerator of eq 118. If an erroneous designation of initiator species is made, the apparent quantum yield will not be independent of the concentration of this initiator. This is true because the observed rates in this case will are result of the absorbance of a non-zero

fraction of light by the real initiator. The erroneous initiator assignment can be detected by the dependence of the quantum yield upon its concentration. This is true even if the species erroneously assigned as the initiator does not lead to any deactivation, since it will mediate the fraction of light absorbed by the true initiator and thereby change the observed rate. Therefore, whether the proper assignment of initiator for a photochemical process has been made can be checked, as long as the species is not thought to undergo self-quenching. This is accomplished by demonstration that the quantum yield for the process is independent of the concentration of the initiator. $Ru(bpy)_2dpp^{2+}$ does not undergo any self quenching processes. This is apparent from the data in Figure 22, that shows the value of ${}^{T}K_{sv}$, obtained from lifetime quenching data, is independent of the concentration of $Ru(bpy)_2dpp^{2+}$, at which the experiment is conducted. The independence of the quantum yield of product formation of the concentration of $Ru(bpy)_2dpp^{2+}$, is established by the data in Table 5. The data of Table 5 refers to the photochemical reaction between $Ru(bpy)_2dpp^{2+}$ and $PtCl_6^{2-}$, under conditions of high ionic strength (3.0 M NaCl) and predominant absorption of light by $Ru(bpy)_2dpp^{2+}$.

The independence of ϕ_p for the formation of $Ru(bpy)_2dppPtCl_4^{2+}$ of the concentration of $Ru(bpy)_2dpp^{2+}$, also shows that product formation is not the result of two pathways acting in parallel. The first being a simple quenching pathway, and the second a trivial photolysis of the hexachloride, and subsequent thermal ligation by a molecule of $Ru(bpy)_2dpp^{2+}$ in the ground state. If this type of parallel scheme were operating, the rate of product formation would be sensitive to the amount of light absorbed by the $PtCl_6^{2-}$. So that even if the total fraction of light absorbed by $PtCl_6^{2-}$ were small, and the rate of reaction reflected an extremely efficient conversion of photons, changing the amount of

light absorbed by $PtCl_6^{2-}$, would be expected to mediate the rate. However, examination of the data in Table 5, shows that this is not the case. For instance using the data in the first and last rows of this Table, the fraction of light absorbed by the $Ru(bpy)_2dpp^{2+}$ is .9991 and .9866, making the fractions absorbed by $PtCl_6^{2-}$ 1-.9991=.0009 and .0134. This is roughly a fifteen fold increase, though the rate remains equal well within experimental error. This establishes, at least under conditions where absorption of light by $PtCl_6^{2-}$ can be neglected, the formation of product occurs by a photochemical pathway initiated by absorption of light by $Ru(bpy)_2dpp^{2+}$.

Though the pathway to product formation is initiated by absorption of light by $Ru(bpy)_2dpp^{2+}$ a simple sensitization mechanism,

$$*Ru+Pt \longrightarrow *Pt + Ru \qquad (119)$$

$$Ru + *Pt \longrightarrow Product \qquad (120)$$

could also lead to photochemical product formation by transfer of the excitation energy to $PtCl_6^{2-}$, making it more reactive to ground state molecules of $Ru(bpy)_2dpp^{2+}$. However, our data suggests this type of mechanism is not operating in the photochemical formation of $Ru(bpy)_2dppPtCl_4^{2+}$. If energy-transfer sensitization, as shown in eqs 119 and 120, was the mechanism leading to product formation, such a pathway would lead to differing fractions of excited acceptors subsequently undergoing coordination by a ground state $Ru(bpy)_2dpp^{2+}$, with differing concentration of $Ru(bpy)_2dpp^{2+}$. Therefore, the quantum yield of product formation would depend upon the concentration of the ground state $Ru(bpy)_2dpp^{2+}$, and its efficiency at intercepting *Pt. However, as mentioned earlier, measurements made under conditions where most of the light is absorbed by $Ru(bpy)_2dpp^{2+}$, show that the quantum yield of product formation, is independent of the

concentration of $Ru(bpy)_2dpp^{2+}$ (Table 5). That is not to say that under conditions where a substantial fraction of light is absorbed by the $PtCl_6^{2-}$, that the mechanism is the same, as shown in Figure 24 . This Figure suggests that the rate is being mediated predominantly by the effect of $Ru(bpy)_2dpp^{2+}$ to competitively absorb the light. Therefore, in this concentration range the increase in concentration of $Ru(bpy)_2dpp^{2+}$ leads to a decrease in the rate of product formation, despite the fact that more light is being absorbed by $Ru(bpy)_2dpp^{2+}$ under these conditions. This suggests that in addition to a mechanism involving coordination, that operates under conditions of predominant aborption of light by $Ru(bpy)_2dpp^{2+}$, there is a mechanism initiated by absorption of light by $PtCl_6^{2-}$, that is operating in this concentration range. The simple photolysis mechanism would have to have a higher quantum yield than the mechanism involving coordination, in order to exhibit this dominating effect.

The efficiency of product formation versus reversion to ground state starting materials, is a characteristic derived from varying the concentration of quencher. It therefore does not show a dependence upon the concentration of quencher. Since ϕ_p, for $Ru(bpy)_2dppPtCl_4^{2+}$, is independent of the concentration of $Ru(bpy)_2dpp^{2+}$, this establishes that the value of 5% is intrinsic to the interaction of these two species at least under the conditions of these experiments, since it is independent of each of these species concentrations. This efficiency is the ratio of rate constants, $(k_{qp})/(k_{qp} + k_q)$.

When the data for the quenching of $Ru(bpy)_2dpp^{2+}$ by $PtCl_6^{2-}$ in 3.0 M NaCl, is interpreted in the scheme below, good agreement is obtained between the values of ${}^{T}K_{sv} = (k_q + k_{qp})/(k_r + k_{nr})$, ${}^{P}K_{sv} = (k_{qp})/(k_r + k_{nr})$, obtained from lifetime, intensity, quantum

yield of product formation, and modeling of the time dependence of the intensity quenching.

$$D + h\nu \xrightarrow{h\nu} {}^*D \qquad \text{Rate} = {}^{D}I_a \qquad (121)$$

$${}^*D \xrightarrow{k_r} D + \Delta \qquad \text{Rate} = k_r[{}^*D] \qquad (122)$$

$${}^*D \xrightarrow{k_{nr}} D + h\nu' \qquad \text{Rate} = k_{nr}[{}^*D] \qquad (123)$$

$${}^*D + Q \xrightarrow{k_q} D + Q \qquad \text{Rate} = k_q[{}^*D][Q] \qquad (124)$$

$${}^*D + Q \xrightarrow{k_{qp}} P \qquad \text{Rate} = k_{qp}[{}^*D][Q] \qquad (125)$$

This model is depicted in Figure 72.

An alternate scheme was also considered,

$$D + h\nu \xrightarrow{h\nu} {}^*D \qquad \text{Rate} = {}^{D}I_a \qquad (126)$$

$${}^*D \xrightarrow{k_{nr}} D + \Delta \qquad \text{Rate} = k_r[D] \qquad (127)$$

$${}^*D \xrightarrow{k_r} D + h\nu' \qquad \text{Rate} = k_r[{}^*D] \qquad (128)$$

$${}^*D + Q \xrightarrow{k_E} E \qquad \text{Rate} = k_E[{}^*D][Q] \qquad (129)$$

$$E \xrightarrow{k_q} D + Q \qquad \text{Rate} = {}^{E}k_{nr}[E] \qquad (130)$$

$$E \xrightarrow{k_{qp}} P \qquad \text{Rate} = k_{qp}[E] \qquad (131)$$

This model is depicted in Figure 73.

Figure 72. Mechanism for the formation of $Ru(bpy)_2dppPtCl_4^{2+}$ outlined in eqs 121-125.

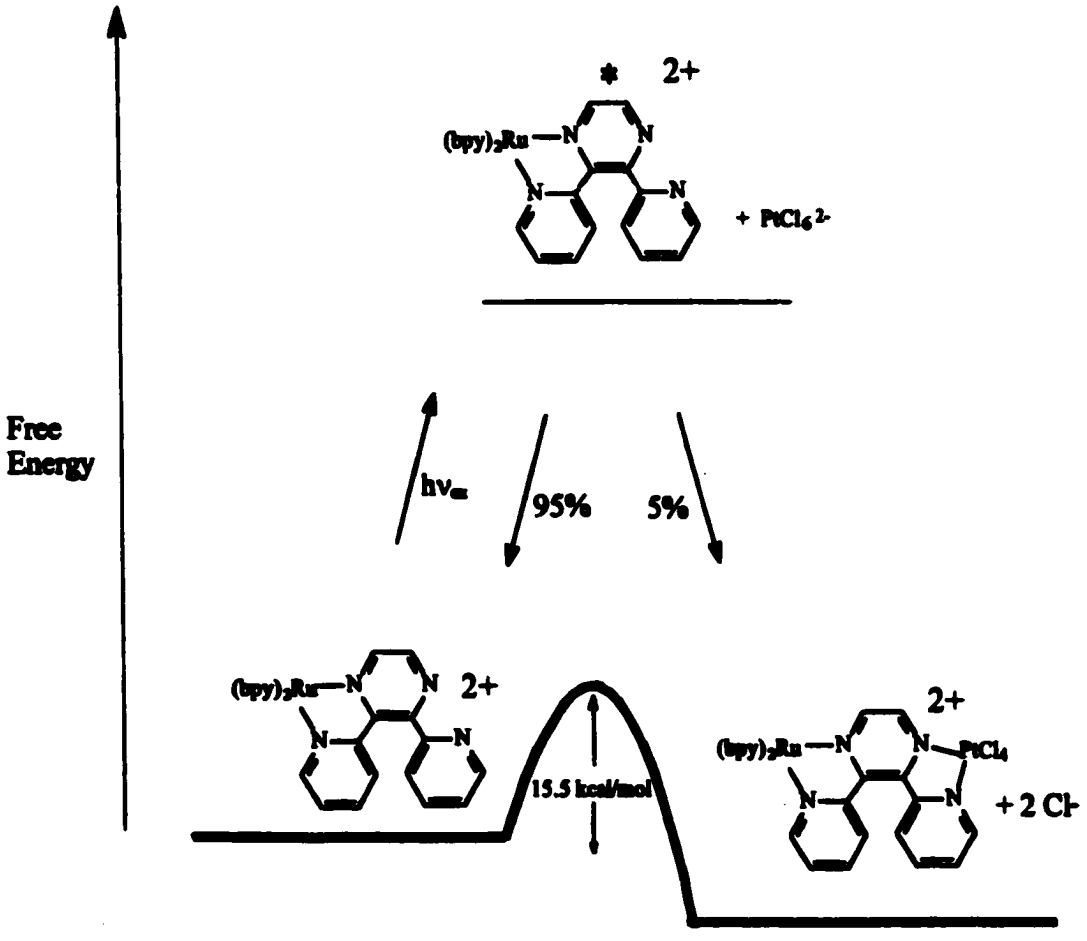

Interpretation of the same data in this model leads to similar results. Instead of ${}^{T}K_{sv}$ the apparent quantity measured is the ratio $k_E/(k_r + k_{nr})$, and in the place of ${}^{P}K_{sv}$ we obtain $k_{qp}/(k_{qp} + {}^{E}k_{nr})$. Though the interpretation above does have an important distinction from the first model, in formation of the encounter pair (E), without deactivation. Since, E is presumed to be non-emissive and formed irreversibly, the two interpretations are not distinguishable based on the available data. They represent different possibilities for interpretation, though both are successful at accounting for all the experimental data. The first model accounts for the 5% efficiency of product formation as being the intrinsic ratio $k_{qp}/(k_{qp} + k_q)$. In the second model the 5% conversion represents the ratio $k_{qp}/({}^{E}k_{nr} + k_{qp})$. However, since it features the formation of E without deactivation, the second model invites the question of whether the 5% could reflect the fraction of species that undergo chelation before deactivation, and as a result relax to products rather than starting materials. The classical interpretation of the chelate effect has been that formation of the first bond is the rate-determining step. The second bond classically is thought to form rapidly due to its very high effective concentration near the reaction center, but there is increasing evidence that this is not always the case.[52] If excited state deactivation were competing with the formation of the second bond, this would be an example of a non- classical chelate effect, due to the limitation that reactions in the excited state must reach completion within the lifetime of the excited state in order to be observed.

The casting of the formation of E in eq 129 as irreversible was based upon the observation that all the lifetime quenching data was linear within experimental error, and the deviations of the intensity quenching data were all positive and attributable to ion

Figure. 73 Mechanism for the formation of $Ru(bpy)_2dppPtCl_4^{2+}$ outlined in eqs 126-131.

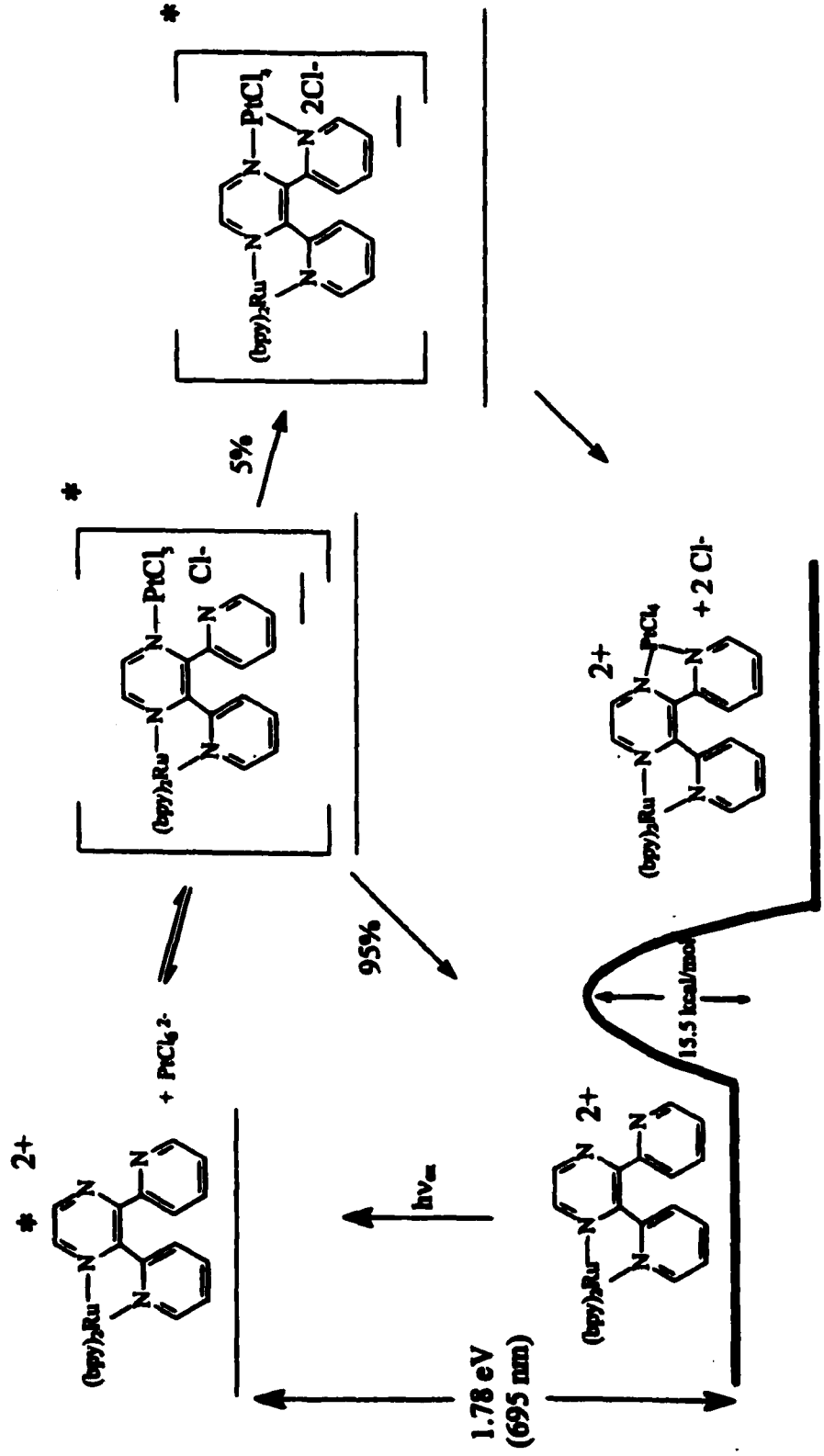

pairing. However in contrast to this, if equilibrium existed, instead of eq 129 we would have

$$D + Q \rightleftharpoons E \qquad K_{eq} = \frac{k_E}{k_{-E}} \qquad (132)$$

which leads to a negative deviation in the Stern-Volmer intensity plots.[8] This type of behavior is observed for the interaction of $Ru(bpy)_2dpp^{2+}$ with Ag^+ and is discussed further below. The failure to observe negative deviations in the intensity data by no means establishes that this data does not reflect equilibrium, since the range of concentration of Q, simply might not have been sufficient to distinguish this behavior. This designation is inconsequential though, since all the lifetime quenching data, with the above exception, obtained in this work was linear within experimental error. This suggests that either the step depicted in eq 131 is irreversible, as it is written, or if an equilibrium exists it is being sampled over a range that $[E] = K_{eq}[D][Q]$ is linear within experimental error. In this model, lack of an emission from the encounter pair is attributed to a chemical change that has taken place in forming E, thereby preventing emission (i.e. E is not an emissive species). The lack of a detectable component of emission with a shifted maximum over virtually the whole range that a measurable emission could be detected, supports this premise. Emission spectra of unquenched solutions, as well those with I_o/I values of 50, were found to be superimposable, when their maxima were normalized.

A prerequisite for efficient energy-transfer quenching is that the process be exergonic. However, a favorable free energy change for the quenching reaction, by no means proves that efficient energy transfer will occur. The data in Table 8 shows some

Table 8. Photophysical properties of some known energy transfer quenchers of $Ru(bpy)_3^{2+}$.

Quencher	E_T (kJmol^{-1})	$k_q \times 10^{-7}$ ($M^{-1}s^{-1}$)	Reference
Anthracene	176	220	53
$Cr(H_2O)_6^{3+}$	179	1.2	54
$Ni(CN)_4^{2-}$	204	560	56
$Ru(terpy)_3^{2+}$	205	150	57
trans-Stilbene	205	0.21	58
$Ti(H_2O)_6^{3+}$	208	0.60	59
trans-2-Styridylpyridine	209	0.45	53

observed rate constants for energy-transfer quenching of $Ru(bpy)_3^{2+}$, which has an excited state energy of 204 kJ. With slightly endergonic free energy changes for quenching, such as the one kJ gap for $Ru(terpy)_3^{2+}$ (terpy = 2,2',2"-terpyridine) values of k_q close to the diffusion limited rate can still be observed. However, exergonicities as large as 5 kJ cause the values of k_q to drop by three orders of magnitude. That is not to say that values of k_q can be predicted by the energetics. For instance, in the case of $Cr(H_2O))_6^{3-}$, the relatively large exergonic free energy change of 25 kJ, corresponds to a rate constant about 100 times smaller than that observed for $Ru(terpy)_3^2$. One clear pattern within this data is that no quenching reactions that are endergonic by more than a few kJ quench with an efficiency close to the diffusion limited rate. In fact, energy transfer that is endergonic by more than a few kJ is rarely observed.[28]

In $Ru(bpy)_2dpp^{2+}$, the excited state localized on the dpp ligand lies 1.78 eV above the ground state. The singlet $^1T_1$ state of $PtCl_6^{2-}$ lies 3.0 eV above the ground state.[60] Lower energy weaker absorption bands, place the spin-forbidden triplet $^3T_2$ at 2.8 eV,[60] while the $^3T_1$ state is calculated to lie 2.0 eV above the ground state (Table 8). The energy of the quintet state $^5T_1$ state is expected to be very close to that of the $^3T_1$ state.[61] This suggests that at very best energy transfer would be endergonic by 0.22 eV. The possible contribution of energy transfer cannot be ruled out altogether, based on simple energy arguments, since the absorption bands for each of these states do overlap even if the maxima are widely separated. An attempt to quantify the possible contribution of energy transfer was made by analysis of the spectral overlap (J), of the emission spectrum of $^*Ru(bpy)_2dpp^{2+}$ and the lowest energy absortion band for $PtCl_6^{2-}$, as discussed below.

Mechanistic distinctions based on energy arguments are fraught with uncertainty. Even in cases unclouded by the possibility of contributions by other mechanisms to the observed quenching, where energy transfer is presumed to be operating, a simple correlation between energy gap and the value of k_q is poor. While energy transfer clearly becomes much less efficient with even small endergonic free energy changes, the possibility of energy transfer through higher vibrational states in the tails of the absorption and emission spectrum of the quencher and donor is a lingering concern. The values of k_q observed for $PtCl_6^{2-}$ is a substantial fraction of the diffusion- limited rate in aqueous solution. If energy transfer quenching were operating through the resonance of upper vibrational states of $^*Ru(bpy)_2dpp^{2+}$, and lower vibrational states of $PtCl_6^{2-}$ for which the process was exergonic or not substantially endergonic, the concentrations of both donor and quencher could be replaced by effective concentrations. These effective concentrations reflect the fraction of the quencher species occupying vibrational states of low enough energy, that energy transfer quenching, from molecules of $Ru(bpy)_2dpp^{2+}$ in higher vibrational states, could be an exergonic process. An attempt was made to estimate each of these fractions from values of the overlap between the emission spectrum of the donor and the absorption spectrum of the quencher. Since the Stern-Volmer analysis is based upon the measurement of quantum yields, it does not depend upon the concentration of the donor, in this case $Ru(bpy)_2dpp^{2+}$. Therefore, even though this analysis assumes an interaction of the quencher with only a fraction of the emitters, the fraction of emitters in no way plays a role in correcting the value of $^TK_{sv}$.

The absorption and emission spectra were treated as if their intensities directly reflect the relative numbers of species of that energy. The interpretation of the spectra in

Table 9. Lowest Energy absorption bands of $PtCl_6^{2-}$, $RhCl_6^{3-}$ $PdCl_6^{2-}$, $PtCl_4^{2-}$, $RuCl_6^{3-}$, $OsCl_6^{2-}$, and $IrCl_6^{3-}$.

Complex	Lowest Energy Transition Observed (eV)	Assignment	Reference
$PtCl_6^{2-}$	2.74	$^3T_1 \leftarrow {}^1A_1$	62,63
$RhCl_6^{3-}$	1.82	$^3T_1 \leftarrow {}^1A_1$	64,65
$PdCl_6^{2-}$	2.57	$^1T_1 \leftarrow {}^1A_1$	66
$PtCl_4^{2-}$	2.21	d-d	67
$RuCl_6^{3-}$	3.17	$2t_{2g} \leftarrow \pi^1 t_{ig}$ (LMCT)	68
$OsCl_6^{2-}$	2.96	$2t_{2g} \leftarrow \pi^1 t_{ig}$ (LMCT)	69
$IrCl_6^{3-}$	2.02	$^3T_1 \leftarrow {}^1A_1$	70,71

this way is not possible if more than one electronic transition must be considered. The simultaneous consideration of more than one electronic transition in this method leads to an ambiguity in the population interpretation of the absorption bands. Since both bands represent populations, elements being molecules in different overall energy states, each absorption band represents a differing possible future for the same ground state population.

In order to implement this method, the absorption spectrum of $PtCl_6^{2-}$, was resolved into gaussian functions centered at the observed maxima, with values of width at half-height determined by best-fitting procedures (Figure 2). However, the rapid fall off of these gaussians, made the use of only the lowest energy band in calculating the overlap, a justified approximation. The values of the overlap of the absorption gaussians for all electronic transitions that were neglected, was in all cases very small, compared to the overlap of the lowest energy band only.

Next, the gaussian functions obtained were normalized. The spectrum of $Ru(bpy)_2dpp^{2+}$ was normalized to unity area, since it represents the totality of the population, and the allowedness of the transition (ε_{488} = 8755 $M^{-1}cm^{-1}$) suggested an oscillator strength not very small relative to unity. Any overestimation in this case seemed reasonable since it would only lead to underestimates of corrected values of k_q, and this analysis is based on showing the apparent value of k_q exceeds the limit imposed by diffusion in solution. The spectrum of $PtCl_6^{2-}$ was also normalized to unity. This was a conservative overestimate, since its oscillator strength was less than 10^{-3}.[72] The correspondence of the oscillator strength, which is the classical transition probability based on treatment of the absorber as a harmonic oscillator interacting with the sinusoidal

electric vector of light, with a the rate of energy transfer from a metal complex in a radiationless process, is not clear. Small values of the oscillator strength reflect many factors that make the transition weak. However, the radiationless interaction presumed to couple the upper and lower states on $PtCl_6^{2-}$, might couple the states substantially better that the oscillating dipole of light. Therefore, we obtained a conservative estimate using this overlap method, since we normalized the absorption band to unity as if it were a fully allowed transition, even though its oscillator strength was small, reflecting it being forbidden by both the Wigner spin selection and the Laporte rule.

A spectrum was then constructed from the emission spectrum of $Ru(bpy)_2dpp^{2+}$, and the gaussian attributed to the lowest energy transition assigned to $^3T_1 \leftarrow {}^1A_1$, for $PtCl_6^{2-}$, which was the union of the two, and the overlap calculated from Union = $E_D + A_Q$ – overlap. The value of the integral of the union spectra was calculated by a numerical integration. For instance, the normalized absorption spectrum of $PtCl_6^{2-}$ intersects the normalized emission spectra of $Ru(bpy)_2dpp^{2+}$, at 17600 cm^{-1}. Numerical integration of this composite spectrum, which was the union of the two, yielded a value of 1.987. Therefore, the overlap was calculated to be 2-1.987 = 0.013. This fraction was interpreted as representing the portion of the ground state population of the quencher that could undergo energy transfer. This value then was used to calculate a corrected value of K_{sv}. This correction can be understood to reflect that equivalent quenching had occurred at lower actual (corrected), values of quencher concentration. This overlap factor was introduced as a correction factor (C_o), multiplying the nominal concentration of quencher,

$$K_{sv}(corrected) = \frac{\tau_o/\tau - 1}{[Q]C_0} \qquad (133)$$

For $PtCl_6^{2-}$ this yielded a corrected value of K_{sv} equal to 31000 M^{-1}. Using the corrected value of K_{sv}, the lifetime of $Ru(bpy)_2dpp^{2+}$, 125 ns, and the relation,

$$K_{sv} = k_q\tau \tag{134}$$

yields a value of $k_q \geq 2.3 \times 10^{11}\ M^{-1}s^{-1}$. This value is substantially greater than the upper limit for diffusional rate constant of $10^{10}\ M^{-1}s^{-1}$, in aqueous solution at room temperature, taken from diffusion of a proton. This means that energy transfer, through higher vibrational states, would have to occur at a rate that is not feasible for a bimolecular process in aqueous solution, in order to account for the observed value of ${}^{T}K_{sv}$. Since the values of ${}^{T}K_{sv}$ are established as diffusional values, from the agreement obtained from lifetimes and emission data, therefore energy transfer alone is unlikely account for the observed quenching.

A prerequisite for efficient electron transfer is the requirement that the overall free energy change be favorable. The excited state reduction potential of $Ru(bpy)_2dpp^{2+}$ is estimated to be .30 V, from the difference between the ground state oxidation potential, and the energy of the excited state. No reversible single electron reduction or oxidation has been observed for Pt(IV). Nonetheless, an alternate mechanism might be proposed in which reductive quenching occurs, forming a reactive Pt(III) intermediate that undergoes coordination. However, our data suggests this is unlikely. The Pt(III) intermediates have been postulated to be either a four or five coordinate. The formation of a coordinately unsaturated intermediate in aqueous solution would lead to coordination of water and a mixture of products with differing equivalents of water, and a variety of stereochemistries. However, the reaction proceeds with maintenance of two isosbestic points at 401 nm and 488 nm, through at least 70% extent of reaction, suggesting that

only a single product is formed. In addition, Pt(III) is known to disproportionate into Pt(IV) and Pt(II) by a second order mechanism. If product formation did occur via a Pt(III) intermediate, its rate would be expected to depend on the concentration of $PtCl_4^{2-}$. However, this is not consistent with the effect of added $PtCl_4^{2-}$. Measurement of the relative quantum yield of product formation shows that addition of $PtCl_4^{2-}$ has no effect on the rate of bimetallic formation.(Figure 28)

Finally, the photochemical reaction observed between $Ru(bpy)_2dpp^{2+}$ and $PtCl_4^{2-}$ shows isosbestic points at 408 and 486 suggesting that a different product is formed with $PtCl_4^{2-}$ than $PtCl_6^{2-}$, inconsistent with the notion that the Pt(III) transient, believed to be the intermediate in the interconversion of $PtCl_6^{2-}$ and $PtCl_4^{2-}$, is in fact the reactive substrate in the overall reactions.

$$Ru(bpy)_2dpp^{2+} + PtCl_6^{2-} \xrightarrow{h\nu} Ru(bpy)_2dppPtCl_4^{2+} + 2Cl^- \quad (135)$$

$$Ru(bpy)_2dpp^{2+} + PtCl_4^{2-} \xrightarrow{h\nu} Ru(bpy)_2dppPtCl_2^{2+} + 2Cl^- \quad (136)$$

Though both thermal and photochemical pathways yield the same product, the photochemical reaction of $Ru(bpy)_2dpp^{2+}$ with $PtCl_6^{2-}$ exhibits a stunning acceleration relative to the thermal pathway. $Ru(bpy)_2dpp^{2+}$ has been shown to be a much stronger base in the excited state with a ΔpK_a greater than 3.[35] We believe that this large change in Bronsted basicity correlates with a large increase in its nucleophilicity and leads to coordination. Perhaps product formation is facilitated by the chelate effect, or secondary events centered on $PtCl_6^{2-}$ after formation or relaxation of the exciplex. The correlation between the inverse of quantum yield of product formation and the inverse of concentration of quencher yield $K_{sv} = 417 + 250\ M^{-1}$, (Figure 21) as the ratio of intercept

to slope. This value is within experimental error of K_{sv} = 403 ± 16 M^{-1}, (Figure 18) obtained from lifetime quenching. The value of the inverse of the slope of this plot also yields $^{P}K_{sv}$ equal to 20 M^{-1}. We interpret this to mean that the quenching encounter consists of formation of a non-emissive exciplex, which in competition with other non-radiative decay processes, roughly 5% of the time relaxes to the ground state bimetallic. Perhaps the velocity of product formation reflects the rate at which the second bond can be formed after relaxation before separation of the ground state pair by diffusion. Alternately, the 5% product conversion could be interpreted as the fraction of exciplexes that undergo formation of a second bond to become fully chelated, before the decay of the excited state occurs. Since no data is available on the lifetime the exciplex, we cannot speculate which of these two pathways is more likely. If the exciplex were very short lived, the latter interpretation would seem less feasible.

(2) Reactions of $[Ru(bpy)_2dpp](ClO_4)_2$ with $Na_3[RhCl_6]$ and $K_2[RhCl_5(H_20)]$

There are no known single electron reduction or oxidation potentials for $RhCl_6^{3-}$ or $RhCl_5(H_2O)^{2-}$. Nor are there any known examples of stable complexes of Rh(IV) or Rh(II), making electron-transfer quenching unlikely for either complex. The absorption spectrum of $RhCl_6^{3-}$ shows the lowest energy transitions is assigned to the $^3T_1$ state which lies 1.77eV above the ground state (Table 8). This makes energy transfer potentially a very viable pathway, at least for $RhCl_6^{3-}$. Corresponding spectral data on $RhCl_5(H_2O)^{2-}$ is not available. We believe energy transfer is the operative pathway and explains why product formation does not occur. Indeed, in all cases we have observed where energy or electron transfer is viable photochemical product formation does not occur. For instance,

Cr(III) is known to form stable diimine complexes, though energy transfer does not lead to product formation.

As discussed earlier, using complexes of $Ru(bpy)_3^{2+}$ as an example, a favorable free-energy change for energy transfer quenching by no means establishes that energy transfer will occur. An alternate explanation for the failure of $RhCl_6^{3-}$ to react photochemically by a mechanism involving coordination is that an exciplex forms, but since it does not have a sufficiently stable bimetallic product to relax to, so no product formation occurs. The result is that from the association in the excited state a chemical quenching has occurred (i.e. a chemical change has taken place, which prevents emission) but since the driving force for association exists only in the excited state, relaxation to starting materials occurs. This alternate explanation is consistent with the observed rates of the thermal reaction between $Ru(bpy)_2dpp^{2+}$ for $RhCl_6^{3-}$ and $RhCl_5(H_20)^{2-}$ which are characterized by rate constants of 5.5×10^{-4} $M^{-1}s^{-1}$ and 3.6×10^{-4} $M^{-1}s^{-1}$, respectively. These rates are slow relative to values of other complexes reported in this work, such as $PtCl_4^{2-}$ and $PdCl_6^{2-}$ for which values of .62 $M^{-1}s^{-1}$ and 75 $M^{-1}s^{-1}$, respectively were obtained. Perhaps more pertinent than the thermal rate constants is that the equilibrium appears to strongly disfavor the bimetallic, as shown by the slight spectral changes observed for a solution $Ru(bpy)_2dpp^{2+}$ in the presence of $RhCl_6^{3-}$ allowed to equilibrate over a period of days (Figure 36).

Our postulation on the mechanism of reaction in the photochemical formation of a rhodium containing bimetallic, evolved from the initial observation that a photochemical reaction occurred in solutions prepared from the hexachloride. The kinetic data showed that the reaction was unlikely to proceed directly with the hexachloride, making the

monoaqua product seemed a likely candidate. The failure of monaqua species to react leads to the conclusion that some intermediate, possibly a photolytic one, is the active form undergoing substitution. This is based on the quantum yield of product data, which established that quenching with product formation for $RhCl_6^{3-}$ is negligible or zero, and the failure of $RhCl_5(H_2O)^{2-}$ to react photochemically at all. Additionally, examination of the preliminary results that showed formation of a bimetallic, suggests that a photolyis of $RhCl_6^{3-}$ might be the photochemical pathway observed. This is suspected since this data was obtained conditions where $RhCl_6^{3-}$ accounted for absorption of 48% of the incident light. Also, the rate was noticeable accelerated relative to the quantum yield data, where absorbance by $RhCl_6^{3-}$ was kept to less than 5%, even though both sets of data were obtained with the concentration of $Ru(bpy)_2dpp^{2+}$ equal to 5.0×10^{-5} M.

(3) Reactions of $[Ru(bpy)_2dpp](ClO_4)_2$ with $Na_2[PdCl_6]$

The rapid thermal chelation of $PdCl_6^{2-}$ by $Ru(bpy)_2dpp^{2+}$ reflects a greater susceptibility to undergo substitution than any of the other complexes studied. At room temperature, for a solution 5.0×10^{-4} M in $PdCl_6^{2-}$and 5.0×10^{-5} M in $Ru(bpy)_2dpp^{2+}$, with 488-nm light with an intensity of 10^{-8} Einsteins/L·s, the photochemical rate is eclipsed by the thermal rate. A photochemical component is suggested by the longer term behavior of the reaction system, as the thermal reaction appears to slow down with equilibration and the photochemical contribution drives the reaction to about 4% greater extent. $PdCl_6^{2-}$ does quench the emission of $Ru(bpy)_2dpp^{2+}$ with K_{sv} estimated to be greater than 400 M^{-1}, from lifetime data collected quickly after preparing the solution directly from weighed solid. This value is only an estimate since the values obtained varied widely with the extent of thermal reaction.

As was observed for all the other complexes that undergo photochemical product formation, $PdCl_6^{2-}$ has no known single electron reduction potential. Examination of Table 8 would suggest that energy transfer is not viable, though the available data could be misleading. The lowest-energy state reported, is the $^1T_1$ state that lies 2.53 eV above the ground state.[73] Energy transfer quenching of $Ru(bpy)_2dpp^{2+}$, with its MLCT state 1.78 eV above the ground state, would seem unlikely. However, examination of a Tanabe-Sugano diagram suggests that there is lower energy $^5T_{2g}$ state that has not been observed. Since there is a photochemical component to the reaction, as discussed earlier, even if energy transfer occurs it appears to be competing with product formation. We are very cautious though to make this assignment without the preponderance of data that was available for $PtCl_6^{2-}$. A highly efficient trivial photolysis of the hexachloride, followed by thermal ligation, could account for the photochemical component.

(4) Reactions of $[Ru(bpy)_2dpp](ClO_4)_2$ with $Na_2[PtCl_4]$

S_N2 nucleophilic substitution reactions of coordination complexes are more facile for 16 electron species that can readily accommodate an incoming nucleophilic ligand. This is apparent in the substitution chemistry of $PtCl_4^{2-}$. The rate constants for thermal substitution of two chlorides by $Ru(bpy)_2dpp^{2+}$ on $PtCl_6^{2-}$ and $PtCl_4^{2-}$ are 1.8×10^{-4} and .63 $M^{-1}s^{-1}$ respectively. $PtCl_4^{2-}$ also undergoes the corresponding photochemical reaction (i.e. formation of a bimetallic), though the rapidity of the thermal reaction certainly makes the system more difficult to disentangle.

Despite this complication, $PtCl_4^{2-}$ has been shown to quench $Ru(bpy)_2dpp^{2+}$ with a value of $^TK_{sv} = 282\ M^{-1}$. $PtCl_4^{2-}$ has no known reversible one-electron oxidation or reduction potential, nor are there any known coordination complexes with Pt(I) or Pt(III).

The lowest energy state of $PtCl_4^{2-}$ assigned to a d-d transition, which lies 2.21 eV above the ground state, while the excited state of $Ru(bpy)_2dpp^{2+}$ lies 1.78 eV. Energy transfer would have to be endergonic by 0.43 ev (24.1 kJ) making it seem unlikely.

We interpret this complex's behavior as an example of a case where the thermal pathway is so facile, that even under the most intense irradiation available, the photochemical rate of product formation is eclipsed by the thermal rate. Therefore, though measurement of the ${}^{P}K_{sv}$ from ϕ_p data was not possible, due to the fast thermal rate of chelation by $Ru(bpy)_2dpp^{2+}$, we suspect that the value of ${}^{P}K_{sv}$ is significantly larger than the 5% found for $PtCl_6^{2-}$, with its saturated coordination sphere.

(5)Reactions of $[Ru(bpy)_2dpp](ClO_4)_2$ with $K_3[RuCl_6]$, $K_2[OsCl_6]$, and $K_3[IrCl_6]$

Like the hexachlorides of Pt^{4+}, Pd^{4+}, and Rh^{3+}, the hexachlorides of Ru^{3+}, Ir^{3+}, and Os^{4+} all undergo some extent of thermal reaction with $Ru(bpy)_2dpp^{2+}$ to form the corresponding bimetallic under reflux conditions in aqueous solution for a sufficient time. The rate constants estimated from absorption spectral changes have been calculated and are collected in Table 9. These complexes all fail to react photochemically. Examination of Table 10 fails to reveal any obvious trend in their lability to undergo either thermal chelation to form a bimetallic, or aquation.

Though these metals do not react photochemically, they all quench the emission of $Ru(bpy)_2dpp^{2+}$ with values of K_{sv} shown in (Table 10) As a class, the unreactive quenchers have rates of aquation, and chelation by $Ru(bpy)_2dpp^{2+}$ to form a bimetallic, that span the range of those that do react photochemically. However, they do have one clear distinction from all of the examples that react photochemically. They all have known reversible one-electron reduction potentials.

The reversible reduction potential of $Ru(bpy)_2dpp^{2+}$ in the ground state is 1.54 eV (vs. NHE). Use of this reduction potential along with the emission maximum of $Ru(bpy)_2dpp^{2+}$, 695 nm, in the Weller equation (eq 42),[74] neglecting the electrostatic term, because of the large dielectric constant of water, yields .30 eV for the excited state reduction potential of $Ru(bpy)_2dpp^{2+}$(Figure 82). Using the reported value for the ground state reduction potential of $OsCl_6^{2-}$,[75]

$$OsCl_6^{2-} + e^- \rightleftharpoons OsCl_6^{3-} \qquad E^\circ = .85\ V \qquad (137)$$

suggests that excited state electron-transfer quenching,

$$*Ru(bpy)_2dpp^{2+} + OsCl_6^{2-} \rightleftharpoons OsCl_6^{3-} + Ru(bpy)_2dpp^{3+} \qquad (138)$$

is exergonic by 1.13 eV.

For $IrCl_6^{3-}$, the situation is more interesting. $IrCl_6^{3-}$ is exceptionally stable, its rate of aquation and thermal chelation are the slowest of all the complexes considered in this work. This is not surprising since complexes of Ir(III) are generally known to be substitution inert. The ground state reduction potential to form Ir(IV)

$$IrCl_6^{3-} \rightleftharpoons IrCl_6^{4-} + e^- \qquad E^\circ = -.867\ V \qquad (139)$$

is very unfavorable at -.867 V.[75] Though no measurement of a reversible ground state oxidation potential for $Ru(bpy)_2dpp^{2+}$

$$Ru(bpy)_2dpp^{2+} + e^- \longrightarrow Ru(bpy)_2dpp^{+} \qquad (140)$$

is available, it has been estimated to be 1.0 V,[76] suggesting oxidative electron transfer,

$$*Ru(bpy)_2dpp^{2+} + IrCl_6^{3-} \longrightarrow Ru(bpy)_2dpp^{+} + IrCl_6^{4-} \qquad (141)$$

Table 10. Collected data for the quenching, ion-pair formation, thermal chelation by $Ru(bpy)_2dpp^{2+}$, and aquation, of the complexes studied.

Complex	$K_{s\text{-}v}(M^{-1})$	K_{IP}	$k_{aq}(s^{-1})$	$k_{bim}(M^{-1}s^{-1})$	E_a(kcal)
$Na_2[PtCl_6]$	407	54	2.6×10^{-4}	1.8×10^{-4}	15
$Na_2[PdCl_6]$	< 400	-	-	75	6.8
$Na_3[RhCl_6]$	417	32	5.5×10^{-4}	5.5×10^{-4}	-
$K_2RhCl_5H_20$	75	20	1.1×10^{-3}	3.6×10^{-4}	-
Na_2PtCl_4	282	104	-	6.3×10^{-1}	-
$K_3[RuCl_6]$	157	994	$\geq 5.6\times10^{-3}$	3.4×10^{-2}	-
$K_2[OsCl_6]$	660	21	-	2.2×10^{-3}	-
$K_3[IrCl_6]$	10	-	-	1.04×10^{-5}	-

Figure 82. Energy diagram of the excited state of $Ru(bpy)_2dpp^{2+}$ relative to the ground state oxidized ($Ru(bpy)_2dpp^{3+}$) and reduced ($Ru(bpy)_2dpp^{+}$) forms.

$$Ru(bpy)_2(dpp)^{2+} \rightleftharpoons Ru(bpy)_2(dpp)^{3+} + e^- \quad E^o = 1.54 \text{ V (vs. NHE}$$

$$^*Ru(bpy)_2(dpp)^{2+} \rightleftharpoons {}^*Ru(bpy)_2(dpp)^{3+} + e^- \quad E^o = 0.30 \text{ V (vs. NHE}$$

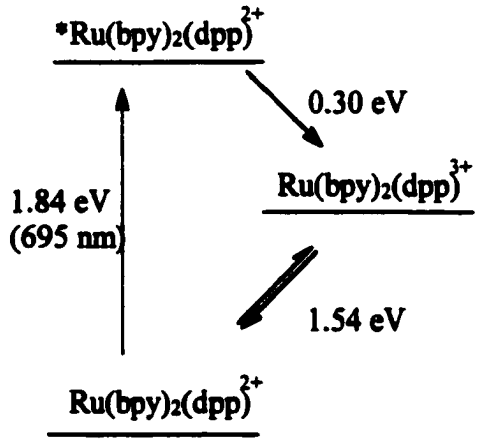

s exergonic by 0.133 V.[75] The observed value of K_{sv} of 10 M^{-1}, reflects this small driving force. The interesting point here is that while Ir(III) is very substitution inert, complexes of Ir(IV) are very labile. If photoproduct formation in the other systems reported on in this work were the result of a labilizing electron transfer, then Ir(III) would seem to be a likely candidate for this type of mechanism. Oxidative electron transfer would result in reactive $IrCl_6^{2-}$ trapped in the solvent cage with a $Ru(bpy)_2dpp^+$. However, no photochemical bimetallic formation is observed. The failure of $IrCl_6^{3-}$ to react photochemically is not due to coordination being eclipsed by electron transfer, given the small value of K_{sv}. An alternate explanation is that $IrCl_6^{3-}$ is just too inert to substitution to undergo it within the excited state lifetime of $Ru(bpy)_2dpp^{2+}$.

Though a reduction potential for $RuCl_6^{3-}$, or $RuCl_5(H_2O)^{2-}$ are not available examination of potentials for a variety of Ru(III) to Ru(II) reductions, suggests the potentials are positive and in the range from 0.10 to 0.6. V. For instance, the reduction

$$Ru(H_2O)_6^{3+} + e^- \longrightarrow Ru(H_2O)_6^{2+} \qquad (142)$$

has E_o = .239 V.[75] Using this value and the excited state energy potential for $Ru(bpy)_2dpp^{2+}$ suggests that electron-transfer quenching is likely to be favorable by about 0.48 eV, making it a viable quenching pathway.

(6) Reactions of $[Ru(bpy)_2dpp](ClO_4)_2$ with $AgNO_3$

Further evidence of excited state Lewis acid-base reactivity is apparent in the interaction of Ag^+ with $Ru(bpy)_2dpp^{2+}$. Ag^+ is known to form exciplexes with a number of Ru(II) diimines. An exciplex is formed between Ag^+ and $Ru(bpy)_2dpp^{2+}$ in aqueous solution, as evidenced by a new emission band growing in at 732 nm (Figure 58). There

is also an interaction between of Ag^+ and $Ru(bpy)_2dpp^{2+}$, in the ground state shown in Figure 59. Both ^1H NMR, and absorption spectroscopy have been used to examine the ground state interaction.

The absorption and ^1H NMR data were analyzed by two independent techniques, the first being the standard sigmoid titration curve presentation, where a parameter proportional to the extent of reaction is plotted on the ordinate versus concentration of titrant, in base 10 logarithmic units on the abscissa. The second type of analysis involved fitting the experimental data to the same model that first method is derived from. However, this method differed by not using the standard approximation of neglecting changes in concentrations which are small relative to the nominal concentrations from which they are subtracted.

Both models are based on a simple equilibrium model for association

$$Ru(bpy)_2dpp^{2+} + Ag^+ \longrightarrow Ru(bpy)_2dpp\text{-}Ag^{3+} \qquad (143)$$

characterized by a single equilibrium constant we designate K_{eq}. The sigmoidal method is based upon a Henderson-Hasselbach type equation derived from the equilibrium expression.

$$K_{eq} = \frac{[Ru(bpy)_2dpp - Ag^{3+}]}{[Ru(bpy)_2dpp^{2+}][Ag^+]} \qquad (144)$$

by taking the logarithm of both sides and rearranging.

$$-\log[Ag^+] = pK_{eq} + \log\left(\frac{[Ru(bpy)_2dpp - Ag^{3+}]}{[Ru(bpy)_2dpp^{2+}]}\right) \qquad (145)$$

Using the stiochiometric relationships implied by eq 143, and casting the associated species, $Ru(bpy)_2dpp\text{-}Ag^{3+}$, as the independent variable and labeling it P, with the initial concentrations of $Ru(bpy)_2dpp^{2+}$ and Ag^+ denoted as $[D]_o$ and $[Ag^+]_o$, respectively, yields

$$-\log([Ag^+]_o - [P]) = pK_{eq} + \log\left(\frac{[P]}{[D]_o - [P]}\right) \qquad (146)$$

This equation is gives rise to the sigmoidal shape of a titration curve usually presented graphically with the lhs is regarded as the independent variable, and either [P] or $[D]_o$-[P], are regarded as the dependent variable. Equation 138 can be rearranged to express either [P] or $[D]_o$-[P], as the dependent quantity.

The data were also analyzed by a best fitting procedure using the exact solution to equilibrium problem of eq 143.

$$[P] = \frac{1}{2}\left([Ag^+]_o + [D]_o + \frac{1}{K_{eq}} - \sqrt{\left([Ag^+]_o + [D]_o + \frac{1}{K_{eq}}\right)^2 - 4[Ag^+]_o[D]_o}\right) \qquad (147)$$

and allowing K_{eq} to vary as the best fit parameter. In this equation as above P is the associated $Ru(bpy)_2dpp\text{-}Ag^{3+}$ species, and D is $Ru(bpy)_2dpp^{2+}$. The negative root must be the solution in this system, since the stoichiometry dictates

$$[P] \leq [D]_o \text{ or } [Ag^+]_o \qquad (148)$$

and choice of the positive root can yield values of [IP] as large as $[D]_o + [Q]_o + 1/K_{eq}$

The absorption spectral changes were characterized by a red shift of the MLCT state terminating on the dpp, from 488 to 532 nm. The spectra were analyzed using Beers

law and the methods outlined in the experimental section. The presence of a second species was not necessary in order to obtain satisfactory agreement between with the experimental data, when analyzed by presentation as sigmoidal titration curves, or by the best fitting method. The spectral change does not reach complete saturation in 2.0 M Ag^+, and attempts to fit the data based upon assignment of the greatest extent of reaction to complete conversion, failed to yield satisfactory solutions. Therefore, it was necessary to vary the molar absorptivity of the product (ε_p), as a fitting parameter. This fitting procedure suggests in that solutions 1.6 M in Ag^+, and 5.0×10^{-5} M in $Ru(bpy)_2dpp^{2+}$, approximately 50% of the $Ru(bpy)_2dpp^{2+}$ were associated, yielding a value of $K_{eq} = 5 \pm 2$. (Figure 65)

Figure 66 shows the full range of absorbance data presented as sigmoidal titration curve. The endpoint of this curve, at low values of $-\log[Ag^+]$ has not been reached, in agreement with the determination made with the fitting method. Taking the halfway point of this curve can only lead to an overestimation of the value of the equilibrium constant, since it would assign complete conversion to some smaller extent of reaction. Taking the halfway point of this curve yields $K_{eq} = 5$. This agreement between the two methods of analysis of the same data, was expected since the absorbance experiments were performed with the nominal concentration of $Ru(bpy)_2dpp^{2+}$ equal to 5.0×10^{-5} M and the Ag^+ ranging up to 1.5 M. Over this concentration regime the extent of reaction was negligible when the concentration of Ag^+ was on the order of the concentration of $Ru(bpy)_2dpp^{2+}$. Therefore, the sigmoidal method was a sound approximation. This is not the case with the ^1H NMR data, as is discussed in detail below.

An unambiguous assignment of the ^{1}H NMR spectrum is a formidable task since $Ru(bpy)_2dpp^{2+}$ has 26 non-equivalent protons, in seven isolated spin systems. Six of the seven spin systems have four protons each, with identical multiplicities expected. The seventh system has been assigned unambiguously based on it having only two spins. Peaks 5 and 6 in (Figure 60 and 63) have identical coupling constants, and each appear as cross peaks to each other in the COSY spectrum (Figure 62). Based on previous assignments,[77] peak 5 is assigned to the position significantly more deshielded, since it is closer to the Ru^{2+} center. COSY NMR spectra were used to distinguish which peaks were coupled to each other, allowing for assignment of which peaks were part of the same spin system, though the absolute assignment of each spin system cannot be confirmed at this point. However, an assignment has been made based upon similar spectra for which complete assignments have been made, and the assumption that the observed chemical change with titration of Ag^+, would be expected to only have a specific effect if it involved the lone pairs of the periphery nitrogens of dpp. This seemed reasonable since most of the peaks in the ^{1}H NMR spectra were unaffected suggesting the interaction was very specific. The number of positions on the bipyridines that are chemically similar would suggest that many shifting peaks would be observed if Ag^+ interacted with the π system of one or more of the rings. However, only five peaks are observed to change upon titration with Ag^+.

Upon titration of solid $AgNO_3$ directly into the NMR tube, the shifting of four doublets, numbers 6, 9, 12, 13, and the bipyridine peak at 7.73 ppm, is apparent in the spectrum. Of these four doublets, peaks 12 (▲), 13 (●) and the bipyridine peak at 7.73 (■), saturate in a parallel fashion (Figure 64). Plots of shift versus concentration of Ag^+,

appear to grow almost independent of concentration of Ag^+, as the concentration approaches 2.0 M. Peak 9 does appear to move, but two overlapping peaks make it difficult to determine its exact field position. Peak 12 is also obscured through part of the titration by overlap with bipyridine resonances in the 7.3 - 7.4 ppm range. Peak 5 shifts but does not become independent of the concentration of Ag^+. The parallel nature of the change in the peaks 12, 13, and the unassigned bipyridine peak, is due to coordination at the free pyridyl ring followed by rotation of the pyridyl ring to chelate the Ag^+ at the pyrazyl nitrogen. The ring flip causes a steric clash between 12 and 13, resulting in the observed shift for both. This is corroborated by similar changes observed in the ^1H NMR for 2,2'-bipyridine, when it coordinates to Ru^{2+}. When the ligand is free it adopts the conformation,

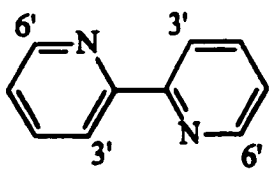

to avoid steric clash between the 6 and 6' positions.[78,79,80] Upon coordination to Ru^{2+} rotation must occur, forcing the 3 and 3' positions to clash. This type of clash has been cited as the reason that these protons are the most deshielded protons in $Ru(bpy)_3^{2+}$.[81, 82] The mechanism is believed to be the diamagnetic interaction which occurs as they approach closer than their van der Waals radii.[83] It has been reported that the free pyridyl ring of $Ru(bpy)_2dpp^{2+}$ adopts a non-planar conformation to avoid a similar steric clash.[84] Therefore, it is not surprising that the largest shifts observed are for peaks 12 and 13 which, are forced into a configuration, which judging from a molecular model, appears to be more strained than the bipyridine 3 and 3' positions experience in $Ru(bpy)_3^{2+}$.

The unassigned bipyridine peak that undergoes a shift during the Ag^+ titration, we assign to the peak 1_c (Figure 63) that faces the ring system of dpp and is closest to the position of coordination. Judging from a molecular model its through space distance is close enough to experience a substantial change in environment. The assignment is therefore based on this factor alone, since no other bipyridine peak appear close enough to the presumed site of interaction to be shifted as a result of it.

The shifts of the resonances assigned to peaks 12 and 13, were used to measure the equilibrium constant under the assumption that the degree of deshielding was proportional to the concentration of associated species. Implicit in this is also the assumption that the exchange rate of Ag^+ is rapid relative to the T_1 relaxation times limiting the ^1H NMR time resolution. This was assumed due to the shifting of the peak, rather than the formation of a new peak. The ^1H NMR data were analyzed by the methods that were used for the absorption data, both inspection of sigmoidal titration curves, and also by a best fit parameter method.

Implicit to the use of titration curves is the familiar assumption that the quantities subtracted from nominal concentrations are negligible, making the algebra somewhat easier. This assumption breaks down in the case that the neglected quantity becomes significant relative to the nominal concentration from which it is subtracted. This is what we observe in the NMR experiments. Presentation of the data in the familiar sigmoidal fashion shows distortion of the sigmoidal shape above values of $-\log[Ag^+]$ corresponding to concentrations of Ag^+ as small as 10^{-2} M. The inherent sensitivity the ^1H NMR experiment requires that the concentration of $Ru(bpy)_2dpp^{2+}$ be on the order of 10^{-2} M. The concentration of $Ru(bpy)_2dpp^{2+}$ is 8.0×10^{-3} M in the data shown in Figure 64.

Therefore under conditions where significant fractions of $Ru(bpy)_2dpp^{2+}$ have become associated the concentration of Ag^+ has been substantially changed. This is the reason for the distortion of the data from the expected $y = c_1+\log(x/c_2-x)$ dependence predicted from eq 145. In light of this, the data were handled by a slightly more sophisticated technique using the exact solution to the equilibrium of eq 143, obtained by use of the quadratic formula.

Fitting of the data to this solution with one parameter, K_{eq} yields values that are very sensitive to the inclusion or exclusion of a single data point. This sensitivity was determined to be systematic in the sense that the apparent value of K_{eq} obtained declined monotonically with exclusion of each data point of higher concentration of Ag^+. A plot of K_{eq}(apparent), versus highest concentration of Ag^+ used, was quite linear and was extrapolated back to an apparent value of $K_{eq} = 25 \pm 2$ at infinite dilution.(Figure 67).

The data on the shift of peak 6 was not used since it did not appear to saturate and therefore attempts to fit two parameters (K_{eq} and a parameter to determine the extent of reaction), to this data would be pointless. This can be understood in terms of the degree of saturation, which is related to the curvature of the data. The extent of reaction can clearly be inferred to have reached completion if the parameter that characterizes concentration becomes independent of the titrant. In other words the data is scaled by a parameter so as to assign complete reaction to the saturation point. Analysis of the absorbance data to determine both K_{eq} and ε_p was successful because it showed a degree of saturation Although satisfactory fits could not be obtained by assigning the greatest extent of reaction to complete conversion to products the extent of reaction was assigned

indirectly by obtaining a best fit value of the molar absorptivity of the product (ε_p). As a parameter it served to scale the function, since it multiplied across the whole expression.

$$A = \frac{1}{2\varepsilon_p B}\left\{[Q]_o + [D]_o + \frac{1}{K_1} + \sqrt{\left([Q]_o + [D]_o + \frac{1}{K_{eq}}\right)^2 - 4[Q]_o[D]_o}\right\} \qquad (149)$$

where A is absorbance, ε_p is the molar absorptivity of the product, and B is the path length derived from the use of Beers law. This scaling property leads to a more limited path of analysis for the ^{1}H NMR that had not begun to saturate. If there is no discernible saturation within experimental error, then the function that the data represents is approximately linear

$$E = m[Ag^+] \qquad (150)$$

where E is any parameter proportional to extent of reaction, m is the apparent slope of the line (under conditions of higher concentrations of Ag^+ m does have a dependence on Ag^+), and the intercept of this line is zero, since the extent of reaction under conditions where one reactant is absent, is equal to zero. The introduction of a second parameter as a scaling function, which was successful in the case of the absorbance measurements, will not work here since its distribution across the data leads to

$$f = smx \qquad (151)$$

Making a distinction between values of s and m in this equation is impossible, without consideration of another independent measurement. This result is intuitively plausible, since the failure of the data to begin to saturate even slightly, leaves no suggestion as to how soon it will begin to saturate. In light of the above analysis, the data collected for

peak 6, while corroborating the rotation of the pyridyl ring, cannot be used to obtain a value of K_{eq}.

While the equilibrium constant does not depend on the concentrations of Ag^+ or $Ru(bpy)_2dpp^{2+}$, the activities of both Ag^+ and $Ru(bpy)_2dpp^{2+}$ depend upon the ionic strength which is principally determined throughout these experiments by the amount of Ag^+. The increase in concentration in going from the absorbance to the ^1H NMR experiments leads to smaller concentrations of Ag^+ required to reach any extent of reaction. Therefore, the activity coefficient corrections, for both $Ru(bpy)_2dpp^{2+}$ and Ag^+, are larger for the solutions used in the absorbance experiments, at any extent of reaction, leading to smaller apparent values of the equilibrium constant at lower concentrations of $Ru(bpy)_2dpp^{2+}$. We believe this is sufficient to account for the discrepancy observed between the values of K_{eq} obtained from absorbance and ^1H NMR techniques.

Analysis of this system as undergoing a change in Lewis acid-base properties in the excited state, suggests methods similar to conventional excited state acid-base chemistry. Therefore, using emission data collected at 695 and 732 nm, fluorescence titration curves were constructed using Ag^+ as the titrant. The intensities were corrected for overlap as outlined for proton transfer fluorescence curves earlier (eq 53 and 54). Both curves have the usual sigmoidal profile commonly observed for excited-state proton transfer equilibrium. The inflection points of both curves are within experimental error of each other, at a value of $-\log[Ag^+] = 1.82$. The value of the rate constant for the forward reaction (k_f), shown below

$$*Ru(bpy)_2dpp^{2+} + Ag^+ \rightleftharpoons *Ru(bpy)_2dpp\text{-}Ag^{3+} \qquad (152)$$

Figure 75. Stern-Volmer intensity quenching plot for the quenching of $Ru(bpy)_2dpp^{2+}$ by Ag^+ in water.

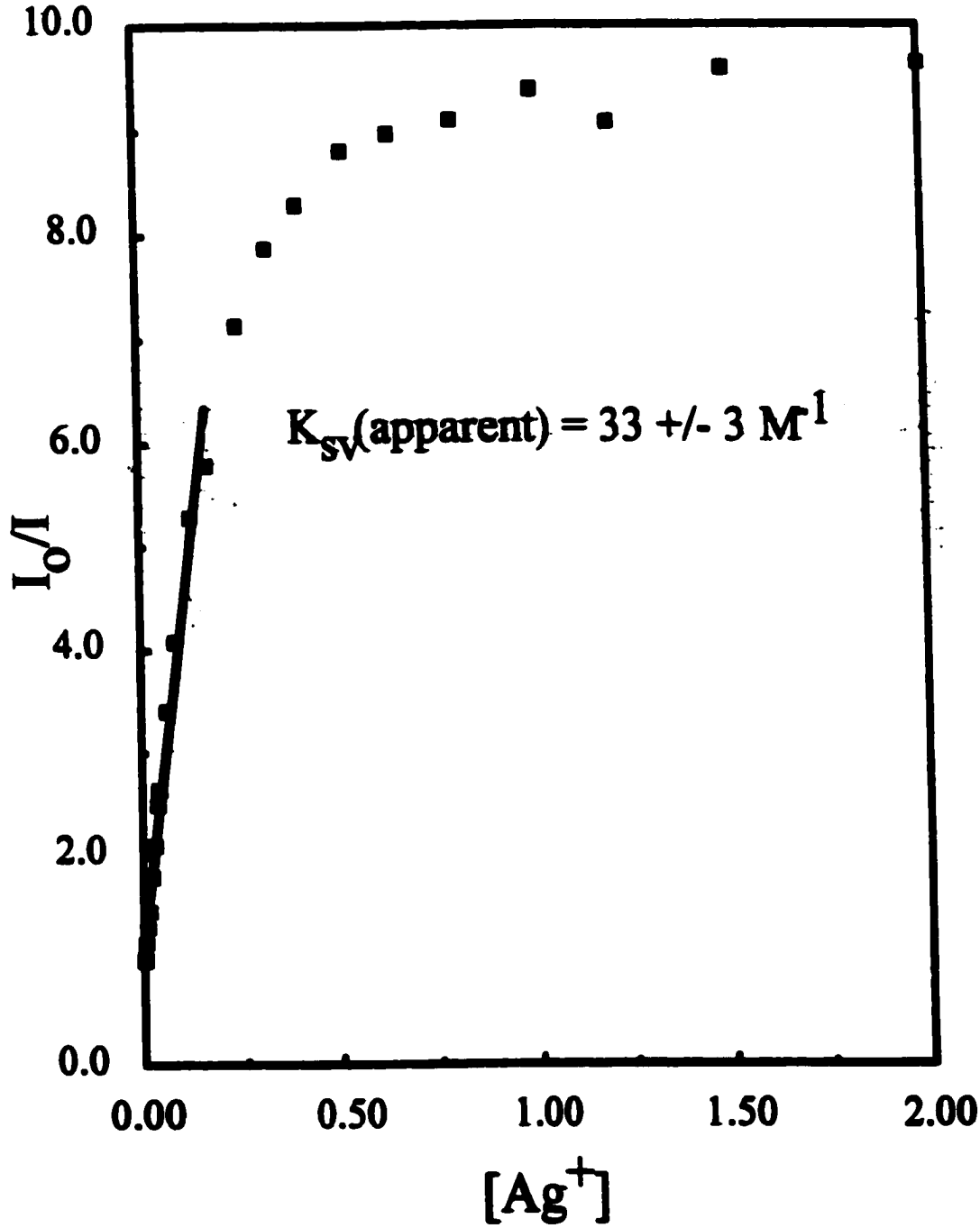

Figure 76. Stern-Volmer intensity quenching plot for the quenching of $Ru(bpy)_2dpp^{2+}$ by Ag^+ in water. The range of data shown ($[Ag^+] < .15$ M) quenching appears to obey the Stern-Volmer quenching law.

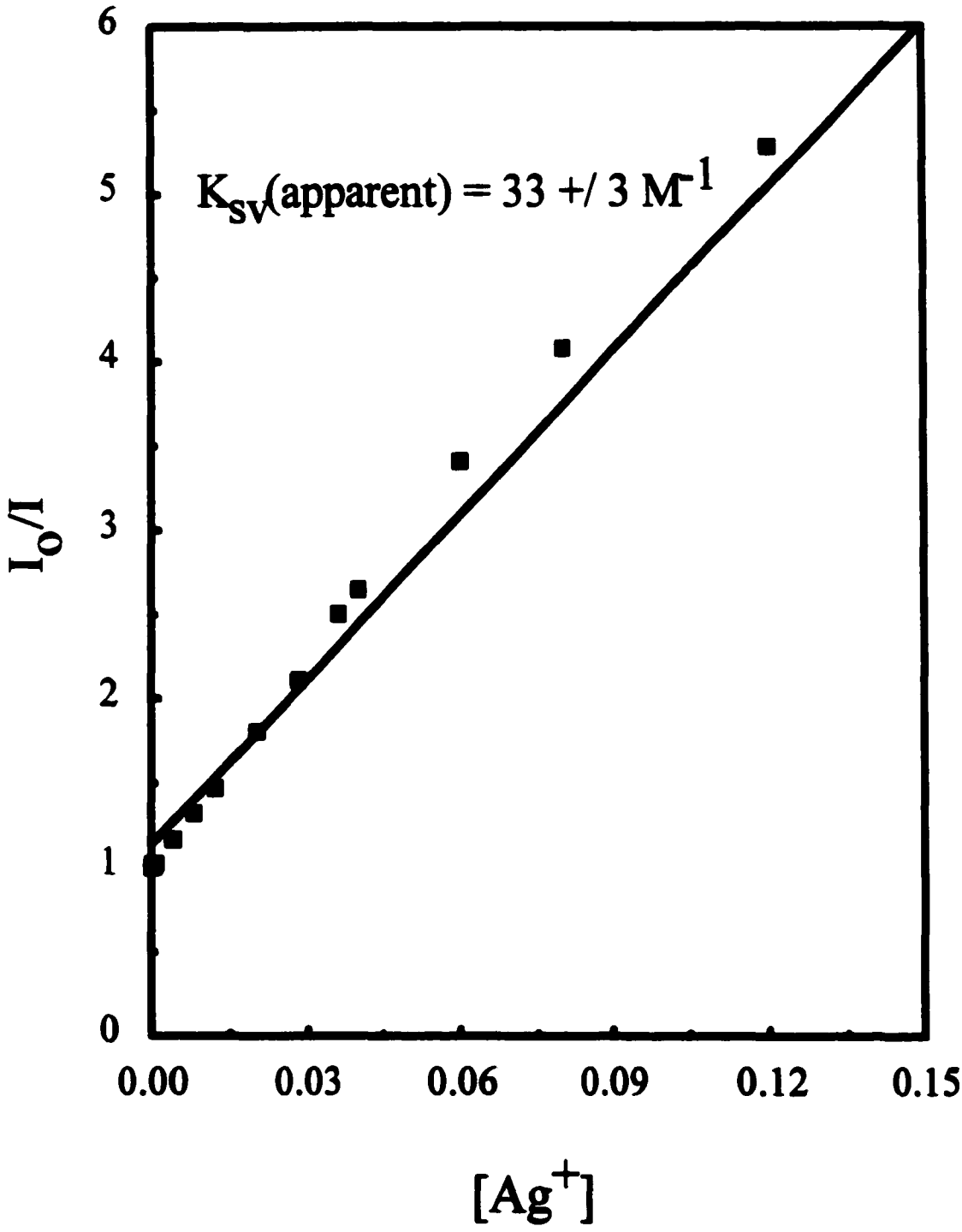

was obtained from a plot of I_o/I, by restricting the line fit to the region over which the plot was linear. (Figures 75 and 76) The initial slope of this Stern-Volmer plot yielded $K_{sv} = 33 \pm 3\ M^{-1}$. Using this value of K_{sv}, the lifetime of $Ru(bpy)_2dpp^{2+}$ of 125 ns, and the relation $k_q = K_{sv}/\tau$, yields the value $k_f = 2.71 \times 10^8\ M^{-1}s^{-1}$. The region where negative deviations from the Stern-Volmer quenching law occur, is an indication that the quenching is occurring by an equilibrium process, rather than an irreversible quenching step.[8] A steady-state analysis leads to an expression for the emitted light intensity from $Ru(bpy)_2dpp^{2+}$,

$$I^{em} = \frac{\left(I_a + k_{-f}[{}^*Ru(bpy)_2dpp - Ag^{3+}]\right)k_r}{k_r + k_{nr} + k_f[Ag^+]} \qquad (153)$$

Comparison of this expression, to the expression derived earlier for irreversible quenching (eq 24), shows that this expression differs only in having the term $k_{-f}[Ru(bpy)_2dpp\text{-}Ag^{3+}]$. As mentioned earlier in the discussion of ion pairing, the fraction of associated species in an equilibrium such as this must approach zero at infinite dilution. Therefore, the term $k_{-f}[Ru(bpy)_2dpp\text{-}Ag^{3+}]$, is negligible at low concentration of Ag^+, and the low concentration regime of a Stern-Volmer plot will reflect the forward rate of association, whether a backward rate exists or not. Treatment of the initial part of the curve as if the quenching were not an equilibrium event is valid then, since whether or not the process depicted in eq. 151 is reversible (i.e. if eq. 151 actually lead to deactivation the reverse reaction would not exist), the observed forward rate would be unchanged. In other words at low concentration of Ag^+, the contribution of the reverse rate in eq 152, would be small in the reversible case, or zero if deactivation occurs. Even, if the contribution of the reverse rate in eq 152 were not small, it would lead to

underestimates of k_f and therefore not alter the direction of the inequality in eq. 153. Consideration of eq 49 suggests the criterion for the excited state equilibrium of eq. 151 should be

$$k_1[Ag^+] >> 1/\tau_{Ru} \quad (154)$$

where τ_{Ru} is the lifetime of $Ru(bpy)_2dpp^{2+}$ which is 125 ns. Use of this value, the data for Ag^+, and in place of the inequality, requiring that the lhs of eq 154 be 10 times larger than the rhs, and rearranging for the concentration of Ag^+ suggests

$$[Ag^+] \geq 1/ k_1\tau_{Ru} = .26\ M \quad (155)$$

What this means is that at concentrations of Ag^+ greater than .26 M, the forward rate of eq. 136 is 10 times greater than the rate of deactivation of $Ru(bpy)_2dpp^{2+}$, by other pathways. This value of .26 M corresponds, on the logarithmic scale used in Figure 68, to a value of $-\log[Ag^+] = 0.59$. However at this point in the titration curve all of the measurable change has already taken place. This would suggest that excited-state equilibrium is far from being established due to the competition of radiative and non-radiative decay with the coordination process. This can be explained by considering the encounters between these two like-charged species, and eq 12. While the establishment of equilibrium relies on the occurrence of a sufficient number of encounters, which is determined by k_{dif}, the efficiency of conversion to is determined by the first order rate constant for conversion of the encounter pair to the exciplex. We interpret this value of $k_f = 2.71 \times 10^8\ M^{-1}s^{-1}$ not as a diffusion limited rate, but rather as reflecting the difficulty in converting the encounter pair into an exciplex. Use of $k_{dif} = 10^{10}\ M^{-1}s^{-1}$, in eq 12 suggests that the corrected value of $k_f = 2.79 \times 10^8\ M^{-1}s^{-1}$. This reflects that the rate of diffusion is

not limiting the rate of reaction very much. This small value relative to the metal complexes studied in this work, is a reflection of the difficulty in bringing $Ru(bpy)_2dpp^{2+}$and Ag^+ sufficiently close together to undergo formation of the exciplex.

The emission centered at 732 nm was found to have an excited state lifetime of 75 ± 10 ns. The change monitored by the fluorescence titration has been assigned to the chelation of an Ag^+ at the pyridyl and pyrazyl nitrogens of dpp, in an excited state coordination reaction. If the exciplex were structurally very different from the ground state species time would be required in order to reorganize from the ground state species into the exciplex. This would lead to a delayed emission, as the emissive species after the pulse would initially be at zero concentration. Attempts were made to detect a reorganization, indicated by the presence of a rising component early in the intensity decay for a solution with greater than 50% of the $Ru(bpy)_2dpp^{2+}$ associated with an Ag^+ in the ground state These attempts failed to show any rising component after the excitation pulse, which might indicate reorganization from the ground state species was necessary to form the exciplex. A rising component would also be expected simply based on the increase in K_{eq} if the rate of re-equilibration were rapid relative to the lifetime of $Ru(bpy)_2dpp\text{-}Ag^{3+}$. This would be due to the re-equilibration populating the exciplex concentration more rapidly than it was decaying. We infer this to mean that equilibration is not rapid relative to the lifetime of $Ru(bpy)_2dpp\text{-}Ag^{3+}$. This is an indirect confirmation of the conclusions drawn earlier based on the rather small value of k_f for formation of the exciplex. An alternate explanation for the failure to detect a rising component in the intensity decay is the substantial overlap of the two emissions, and the fact that the quantum yield of emission of the exciplex judging from Figure 58, is about 20% of the

quantum yield of emission of $Ru(bpy)_2dpp^{2+}$. Therefore detection of this component might be beyond the sensitivity and time resolution of our detection system.

Use of the lifetime of the exciplex of 75 ns, and the inflection point of both fluorometric curves of 1.82 in eq 57, suggests a value of $^*K_{eq} = 48$. Comparison of this value to the values of 5 ± 2, obtained from absorption seems more appropriate since the experimental conditions were identical. Regardless of the variations in activity between the absorbance and ^1H NMR data, comparison of the absorbance and emission data is justified since both were collected under the same conditions. The excited-state of K_{eq} represents an enhancement relative to the ground state value. The increase in Bronsted basicity of the peripheral nitrogens, due to MLCT excitation, leads to an enhanced coordinating ability, and in turn leads to increased equilibrium concentrations of the bimetallic complex in the excited state,

$$^*Ru(bpy)_2dpp^{2+} + Ag^+ \rightleftharpoons {}^*Ru(bpy)_2dpp\text{-}Ag^{3+} \qquad (156)$$

Upon deactivation, reversion to the ground state equilibrium position occurs, resulting in no net chemical change. The change in K_{eq} appears to be much more moderate than the enhancement of basicity observed, reflecting slower diffusion of Ag^+ and the difficulty in bringing these two like charged species together. It also might reflect the underestimation $^*K_{eq}$, since equilibration appears not to be rapid relative to the lifetime of $^*Ru(bpy)_2dpp^{2+}$. As discussed earlier the value of $k_f = 2.71 \times 10^8\ M^{-1}s^{-1}$ for Ag^+ reflects the difficulty of bringing the encounter pair together. However, it could also be interpreted as inhibiting equilibrium. That is to say, repulsion of Ag^+ and $Ru(bpy)_2dpp^{2+}$ prevents a close enough encounter from occurring such that the effective

number of encounters which get close enough to form the exciplex is so reduced that as a result equilibrium is not approached in the excited state.

This represents an example of an excited state acid-base interaction, in which the products are so readily formed thermally that equilibration in the ground state exists before excitation. Even though the excited state population might rest at a position of equilibrium much further towards the products than the ground state, after relaxation the thermally driven re-equilibration to the ground state equilibrium position results in no net chemical change. The ease with which this is observed is in part due to the fact that an emissive exciplex is formed, so that the process is easily monitored. It is also in part due to the less hindered nature of Ag^+ as an acceptor of an incoming group. It is tetrahedrally coordinated to four water molecules making it substantially less hindered than the octahedral complexes.

(7) Reactions of $[Ru(bpy)_2dpp](ClO_4)_2$ with *cis*- $PtCl_4(NH_3)_2$ and *trans*-$PtCl_4(NH_3)_2$

Of this pair of stereoisomers, the trans isomer may be exhibiting a trans effect in its excited state substitution chemistry, when the reaction is conducted in water. Though the data is limited, this is suggested by the apparent preference for the trans isomer to react photochemically over the cis isomer, which appears to be completely inert. Although the trans isomer reacts photochemically in water, in 0.10 M HCl, where $Ru(bpy)_2dpp^{2+}$ is completely proton quenched the reaction does not occur photochemically. Therefore, the photochemical reaction proceeds through the MLCT state of $Ru(bpy)_2dpp^{2+}$.

The trans-directing effect of Cl ligand is considered stronger than the trans-directing effect of an NH_3 ligand. While the cis and trans isomers of $PtCl_4(NH_3)_2$ have

chloride ligands positioned trans relative to other chloride ligands, the trans isomer has two features that favor it undergoing chelation. It has all four of its chloride ligands labilized by virtue of their trans stereochemistry relative to other chlorides, while the cis isomer has only two of its chlorides positioned trans, relative to other chloride ligands. Furthermore, in order for chelation to occur a second ligand must be displaced. In the case of the trans isomer, chlorides occupy all four equatorial positions and each has 2 adjacent chlorides that are trans effect favored. In the cis isomer on the other hand, the two axial chloride ligands, only adjacent chlorides are trans-effect disfavored. In other words, if stereochemical integrity is maintained, chelation displacing two chlorides cannot occur for the cis isomer, without substitution of at least one trans-effect disfavored chloride. While the evidence presented for this speculation is limited, it is consistent with the well-established thermal chemistry of platinum complexes, which offer classic examples of the trans effect.

Reaction of cis-$PtCl_4(NH_3)_2$ and trans-$PtCl_4(NH_3)_2$ with $Ru(bpy)_2dpp^{2+}$ in ethanol leads to different products than are obtained in water. The lack of 2 adjacent trans-effect labilized chlorides in the cis isomer prevents it from readily undergoing substitution by a chelating ligand, unless it undergoes rearrangement. In ethanol relatively little rearrangement occurs, and the formation of two isomers is established by the ^1H NMR. (Figures 70 and 71). The isomeric nature of the two products is suggested by the potential to form isomers given the starting materials, the observation that the two ^1H NMR spectra obtained are very similar, and that each spectrum has a small fraction of the other apparent in it as an impurity. Integration of these impurity peaks suggests that the trans isomer is 99.4% pure and the cis isomer is 98.4 % pure. These spectra are taken without

any purification and represent the percent yield of the reaction. The product is inferred to be a Ru(II)-Pt(IV) bimetallic, since no isomeric pair of square planar Pt(II) complexes with a chelating ligand are possible. The substitution must then occur with loss of a single NH_3 ligand. This is corroborated by the integration of the protons of the coordinated ammonia, though they were exchangeable and did not appear in D_2O, the ^1H NMR in d_6-acetone has this peak integrating to between two and three protons for the trans isomer.(Figure 70) Perhaps formation of the more polar intermediate associated with the loss of two chlorides is responsible for the change in the mode of reaction, when the solvent is changed from water to the less polar ethanol. In this case, loss of only one chloride, would have in its favor the milder charge buildup, as well as the possibility of both leaving ligands being trans-effect labilized.

(8) Quenching by Deactivation or Chemical Change

While the theories of the rates energy and electron-transfer quenching center attention on deactivation of the excited state, the theory that rationalizes proton transfer does not depend on the ability of the quencher to accept energy or an electron. Proton transfer effects quenching by formation of the conjugate acid of the excited donor species. The result is a profound change in the molecules inherent properties, either causing changes in k_r, or by improved solvent coupling, reflected in an increase in k_{nr}. Fundamentally, the chemical change itself leads to the decline in the quantum yield of emission, so there is no necessity to characterize the pathway by which the quenched excited state is deactivated. This is in contrast to the theories of electron and energy transfer, where the focus of explanation is on deactivation itself. Whether or not proton transfer occurs adiabatically, in many cases of proton quenching of metal complexes, is

unknown. However, the preponderance of data shows that the protonated form of most metal complexes is not emissive, even if it is the form that undergoes excitation. This implies that the failure to observe emission is not necessarily due to deactivation by the event of proton transfer, but rather by a chemical change, since emission would not be observed even if the molecule was protonated upon excitation.

In order for a chemical change in the excited state to be feasible, the process of reorganization of the coordination sphere must take place within the lifetime of the excited state. In this respect, an aqueous proton has an advantage which makes it very singular. The reorganization for a proton involves only solvent reorganization. However, in order for a substitution to take place on a metal complex, diffusion of the incoming ligand, formation of an encounter pair, and its rearrangement to the product, must all occur rapidly enough to compete with relaxation of the excited state. In particular, the rearrangement of the encounter pair into the product might be the most difficult to overcome, since formation of a bond to a proton in the excited state is well established. In addition, if a product that is not thermodynamically stable in the ground state forms in the excited state, its existence is itself transient. Or, if a stable product does exist between the donor and acceptor, and equilibrium is established readily in the ground state, any shift in equilibrium for the excited state population is erased after relaxation, when the ground state equilibrium is quickly re-established. So in this case, even though a stable product is available to the pair of reactants, no net shift of the equilibrium towards products is achieved by a transient shift of equilibrium in the excited state. Therefore, if a chemical change is to be observed as a result of an excited state interaction, a delicate balance must be struck between stability with respect to thermal formation of the product, and

susceptibility of a substrate to substitution by an excited state molecule. On one hand, a substrate very susceptible to substitution is desirable so that its rate of reaction is within the lifetime constraints of the donor. However, the existence of a stable product, and a fast thermal pathway to form that product, suffer the risk that the photochemical component might be overlooked, or simply obscured by the rate of thermal product formation.

In addition, the protonation process itself has a special advantage in its favor. The mobility of the proton is tremendous in aqueous solution, where in addition to diffusion it can migrate by a hopping mechanism. This has been critical in the observation of excited state acid-base properties, which were first made in systems where the excited state species were organic singlets, with lifetimes of a few nanoseconds or less. In some of these systems, despite the rapid diffusion of the proton, excited state equilibrium is not be fully established. Therefore, it is not surprising that a more complex chemistry, involving a slower diffusing substrate than a proton, and requiring greater reorganization energies, is not observed for short-lived organic singlets. The failure to observe more complex chemical changes than protonation, among excited organic triplets, which are much longer lived, is due to much smaller changes in acid-base properties in the excited state.

Furthermore, quenching by a process involving coordination is inherently slower than either energy or electron-transfer mechanisms. Therefore, in addition to requiring that its rate be fast enough to be competitive with relaxation of the unquenched excited state, coordination must also be rapid enough to be competitive with other mechanisms of quenching. These mechanisms might be occurring in parallel, or with such great efficiency as to preclude coordination altogether.

The orchestration of a complex chemical change within the excited state lifetime of $Ru(bpy)_2dpp^{2+}$, such as the reorganization of the coordination sphere, we feel is likely aided by ion-pairing. The establishment of diffusional quenching by the agreement obtained between lifetime and intensity quenching data, implies that formation of an encounter pair by diffusion and eventual deactivation, accounts for all quenching. However, it does not give any detailed information on the encounter or ion pair itself. The strong electrostatic interaction between $Ru(bpy)_2dpp^{2+}$ and all of the –2 or –3 anionic complexes leads to long encounter times before the pair diffuses apart. This probably plays an important role in the chemical change reaching completion, before deactivation by other pathways occurs.

(9) Summary

The pattern of reactivity, the energetics, and the magnitude of the values of k_q observed, suggest quenching does not occur by energy or electron-transfer mechanisms. Instead, quenching occurs by means of excited-state coordination in the cases of, $PtCl_6^{2-}$, $PtCl_4^{2-}$, and $PdCl_6^{2-}$, and is possibly a factor with $RhCl_5(H_20)^{2-}$ and $RhCl_6^{3-}$. The failure of $RhCl_6^{3-}$ and $RhCl_5(H_20)^{2-}$ to lead to a bimetallic product, we attribute to competitive energy transfer quenching. Alternately, in the latter 2 cases, if energy transfer is not operating, quenching by coordination might be occurring. If this is the case, relaxation to a stable product is prevented by the fact that the resulting bimetallic product is not stable, as suggested by minimal formation when reacted thermally.

We consider the event that results in quenching upon coordination to be a chemical change. This is suggested by the failure of most known structurally similar bimetallics to be emissive in fluid solution. We view this as an example of an excited-

state coordination reaction. $Ru(bpy)_2dpp^{2+}$ undergoes a tremendous change in basicity of greater than 3 pKa units, upon promotion of an electron into the ligand localized, MLCT state. This large increase in basicity translates into improved coordinating ability in the excited state and facilitates product formation. It is not that surprising that the addition of a single electron to the π-system results in such a tremendous change in basicity. For instance, the radical anion of bpy, which could be viewed as a model of the MLCT state $Ru(bpy)^2dpp^{2+}$, has been reported to have a pKa's of 24 and 8.[85]

While basicity, a thermodynamic quantity, need not correlate with kinetic ability to coordinate efficiently, a correlation appears to exist between the ground and excited states of $Ru(bpy)_2dpp^{2+}$ enhancement of basicity and ability to chelate. This is because the ground and excited states are like members of a homologous family, being structurally identical, with different electron distributions. Given this structural similarity it is not surprising that enhancement of basicity leads to enhanced coordinating ability, since a somewhat similar kind of correlation is known to exist in thermal chemistry for diimine ligands. For example, depicted in Figure 77, is the relationship between ground state acidity constant and the formation constant K_1, for coordination to Fe^{3+} and Zn^{2+} by a series of phananthroline derivatives. Using this empirical correlation between basicity, and equilibrium constant for coordination, obtained for this set of phenanthroline derivatives,

$$\log(K_1) = .51pK_a + .33 \qquad (157)$$

with the $\Delta pKa \geq 3$ for $Ru(bpy)_2dpp^{2+}$, suggests that the K_1 for coordination of $Ru(bpy)_2dpp^{2+}$ to Fe^{2+} would increase by a factor of 34.

Figure 77. Dependence of the equilibrium constant for coordination to either Zn^{2+} or Fe^{2+} of a series of phenanthroline derivatives, upon the pKa for the free ligand. Abbreviations used are: Phenanthroline (phen), 5-Methyl-Phenanthroline (5-me-phen), 5-Bromo-Phenanthroline (5-br-phen), and 5-Nitro-phenanthroline (5-NO_2-phen).

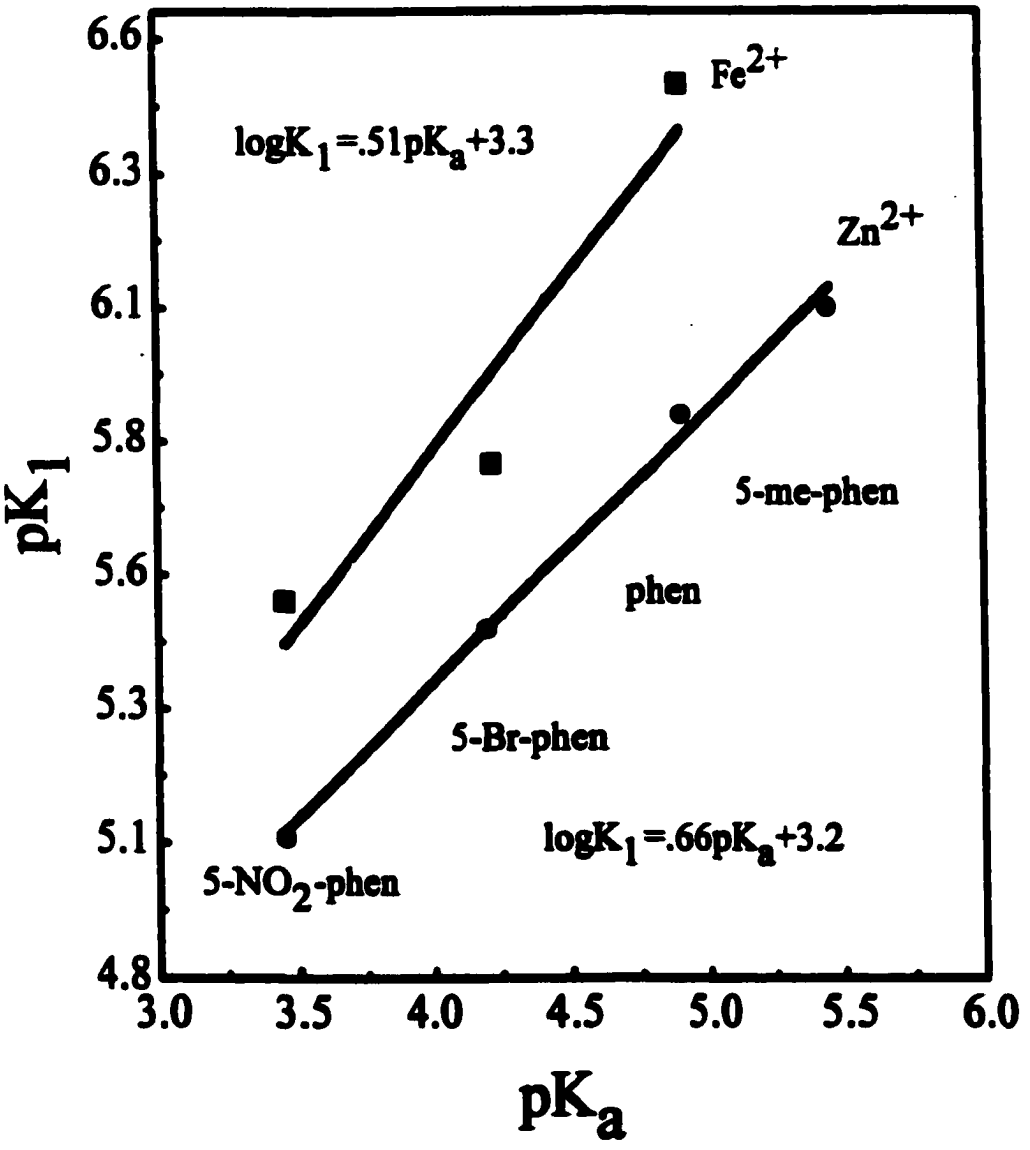

Excited state coordination as a mode of chemical quenching, is indirectly suggested by the observation that thermal preparation of many bimetallic species derived from $Ru(bpy)_2dpp^{2+}$ fail to be emissive. Despite Ru^{2+} having a microenviroment very similar to that of $Ru(bpy)_3^{2+}$, many bimetallic complexes of the form $(bpy)_2RuBLM(bpy)_n$, are not emissive (BL = 2,2'-bipyrimidine, 4,4'-dimethyly-2,2'bipyrimidine) fail to be emissive.[86,87,88,89,90]. In this work the bimetallic, $Ru(bpy)_2dppPtCl_4^{2+}$, was prepared and was found not to be emissive. Emission spectra taken of thermal reaction mixtures of $Ru(bpy)_2dpp^{2+}$ with $RhCl_6^{3-}$, $PdCl_6^{2-}$, $RuCl_6^{3-}$, $OsCl_6^{3-}$, $IrCl_6^{3-}$, all fail to show any new emissive species. The failure of many metal complexes to emit in a protonated form parallels the failure of many bimetallics to be emissive. We believe this parallel behavior between protonated complexes and complexes with second metals coordinated, indicates chemical quenching between monometallic species and other metals ions, is just as plausible as quenching by protons. We also recognize that it is not known in many cases if proton transfer occurs adiabatically or with quenching. We believe that quenching by metal ions also can occur by both pathways. These pathways involve coordination leading to immediate deactivation, and coordination resulting in a non-emissive species in the excited state.

One important exception to the observation that bimetallic species are not emissive is cis-$Ru(bpy)_2Cl_2$, whose symmetric bimetallic $Ru(bpy)_2dppRu(bpy)_2^{4+}$ is emissive.[91] However, irradiation of a solution 10^{-4} M in cis-$Ru(bpy)_2Cl_2$ and 10^{-4} M in $Ru(bpy)_2dpp^{2+}$ in acetone, does not show any new emissive species attributable to $^*Ru(bpy)_2dppRu(bpy)_2^{4+}$ to be present, after correction of the spectra for the inner filter effect. Unlike many complexes considered in this work though, cis-$Ru(bpy)_2Cl_2$ is

uncharged and therefore cannot form an ion pair with $Ru(bpy)_2dpp^{2+}$. Perhaps the attraction of these oppositely charged ions plays an important role in assisting in formation of the encounter pair, and subsequent product formation, within the lifetime of the excited state. As a result, the failure of cis-$Ru(bpy)_2Cl_2$ to react precludes reaction from occurring with a great enough efficiency to observe.

The failure of $OsCl_6^{2-}$, $IrCl_6^{3-}$ and $RuCl_6^{3-}$ to react by a photochemical pathway offers an excellent example of an important distinction between thermal and excited state chemistry. $OsCl_6^{2-}$, $IrCl_6^{3-}$, and $RuCl_6^{3-}$ are all likely to participate in electron-transfer mechanisms, which can occur much more rapidly than the processes necessary for formation of an exciplex, and relaxation to products. In these systems the electron transfer occurs rapidly enough that it precludes excited-state coordination. Therefore, no product formation is observed. So the distinction is that though all the types of pathways of reaction which are available to a ground state in principle may be available, every process' efficiency is scaled by the rapidity with which it occurs. Events which take substantially longer than the lifetime of an excited-state species will not reach completion before relaxation, so might be initiated over and over but never completed. One exception to this occurs in the case that formation of a thermodynamically stable product is an available pathway.

While thermal chemistry is governed by the Hammond postulate, which ensures that equilibrium can exist no matter how high the energy and correspondingly low the concentration of any intermediate is, the observable chemistry of the excited state has a different, but corresponding principle. In the ground state inefficient formation of a product can be overcome by its accumulation over a correspondingly long period of time,

if that product is thermodynamically favored. The products of excited state reactions are usually transients themselves. In order for their formation to be feasible, they need only to be stable with respect to the excited state from which they are being produced. However, their accumulation is competitive with further relaxation and thermal processes to reform the starting materials. In general this leads to the observation that any process which cannot occur within the lifetime of the excited state is not observed. Though in principle the outlying possibility of survival significantly longer than τ is realized by a small number of molecules, and represents a pathway to accumulation of products, albeit an inefficient one, the inability to accumulate these products, since they themselves are transient, erases this pathway.

The systems reported on in this work in which photochemical product formation occurs despite competition with relaxation processes is due to the availability of a product that is stable, not just with respect to the parent excited state, but also with respect to the starting materials. The relatively small values of ϕ_p over the accessible range of quencher reflect this, in that they are very small values in an absolute sense. For instance, a value of ϕ_p is equal to 10^{-5} for the formation of $Ru(bpy)_2dpp^{2+}$, at concentrations of $PtCl_6^{2-}$ equal to 2.0×10^{-4} M. Without accumulation of product as a way to measure this pathway, detection of 1 transient molecule in every 10000 excited states would be a formidable task. It is the ability to measure the rate by integrating it over an extended period of time, to a substantial accumulation of product, that makes detection feasible. The availability of a stable ground state product makes the chemistry of the excited state obey the Hammond Postulate. In the sense that the high-energy low-concentration intermediate, of the Hammond postulate is the fraction of the excited-state

population which survives substantially longer than its own value of τ. In doing this, these excited states become able to participate in reactions requiring times substantially longer than τ, and can succeed in product formation.

V Appendices

Appendix 1- Solution of Ordinary Differential Equations

The numerical solutions to eqs 35-37 were solved using the ordinary differential equation solver in Psiplot,[40] using a Runga-Kutta method. A typical set of data is shown below. This data generated the solution shown in Figure 14.

```
[MODEL NAME]: vii-p45trial4.ode
[INDVAR]: T
[DEPVAR]: Ru,P
[PARAMS]:Io,tau,Qo,Ro,kq,kqp
[EQUATIONS]:
// comment line
Ru=Ia*(1-10^(-7400*(Ro-P))  )-(Ru/tau)-(Ru*(Qo-P)*(kq+kqp))
p'=Ru*(Qo-p)*kqp
END OF EQUATIONS
[PARAMS VALUES]:
// go to a new line
Io=1.759e-6
tau=135e-9
Ro= 5.41e-5
Qo=.00131
kq=2.908e9
kqp=2.92e8
[INIT CONDITION]:
// go to a new line
T=0
Ru=0
p=0
// specify the step size to collect data:
[STEP SIZE]: 1
// specify the stop value for independent variable:
[STOP VALUE]:100
```

Apendix 2-Error Analysis

The values of the error ranges reported throughout this work represented two standard deviations, corresponding to a 95% confidence level. They were calculated using Psi-Plot.[40] The software in most cases calculated best-fit parameters by standard linear least-squares analysis.

VI References

1) Ford, P. *Coord. Chem. Rev.* **1982**, 44, 61.

2) Woodward, R. B.; Hoffman, R. *J. Am. Chem. Soc.* **1965**, 87, 395.

3) Kirk, A. D. *J. Chem. Ed.* **1983**, 60, 843.

4) Talebinesab-Sarvari, M; Ford, P. *Inorg. Chem.* **1980**, 19, 1835.

5) McCosker, J. K.; Damrauer, N.H. *J. Phys. Chem. A* **1999**. 103, 8440

6) Balzani, V.; Scandola, F. *J. Chem. Ed.* **1983**, 60, 814.

7) Smoluchowski, M. *Z. Phys. Chem.* **1917**, 92, 129. b) Debye, P., *Trans. Electrochem. Soc.* **1942**, 82, 265, c) Wagner, P. J.; Kochevar, I. *J. Am. Chem. Soc.* **1969**. 91, 2232.

8) Balzani, V.; Moggi, L.; Manfrin, F.; and Bolleta, F. *Coord. Chem. Rev.* **1975**, 15, 321.

9) Turro, N.; Kavarnos, G. *Chem. Rev.* **1986**, 86, 401-449.

10) Parker, C.A. *Photoluminescence of Solutions* 2nd ed., **1968**, Elsevier, New York.

11) Wayne, R. P. *Photochemistry* 1st ed., **1970**, Butterworth, London, Chapter 6.

12) Nazeeruddin, Md. K.; Kalyanasundaram, K. *Inorg. Chem.* **1989**, 28, 4251.

13) Giordano, P.; Bock, C. R.; and Wrighton, M.; Interrante, L.V.; Williams, R. *J. Am. Chem. Soc.* **1977**, 99, 3187.

14) Lay, P.; Sasse, W. *Inorg. Chem.* **1984**, 23, 4123.

15) Kirsch-De Mesmaeker, A.; Jacquet, L.; Nasielski, J. *Inorg. Chem.* **1988**, 27, 4451.

16) Crutchley, R. J.; Kress, N; Lever, B. *J. Am. Chem. Soc.* **1983**, 105, 1170.

17) Weber, K. *Z Physik. Chem.* (Leipzig) **1931**, B15, 18.

18) Weller, A. *Z. Phys. Chem.* (Frankfurt), 3, 238, **1955**, and Weller, A. *Discussions Faraday Soc.* **1959**, 27, 28 ; see for earlier references

19) Jackson G.; Porter, G. *Dis. Fara. Soc.* **1958**, 27, 103 b) Jackson, G.; Porter, G. *Proc. Roy. Soc. (London)* **1961**, *A260*, 13.

20) Forster, T. *Z. ElectroChem.* **1950**, 54, 42 b) ibid **1950**, 54, 531.

21) Ireland, J. F.; Wyatt, P. A. *A. Adv. Phys. Org. Chem.* **1976**, 12, 131.

22) Schulman, S.G.; Capomacchia *J. Phys. Chem.* **1975**, 79, 1337.

23) Weller, A. *Prog. React. Kinet.* **1961**, 1, 189.

24) Hicks, C.; Ye, G.; Levi, C.; Gonzalez, M.; Rutenberg, I.; Kassis, A.; Helmy, R.; Fan, J.; Gafney, H. D. *Coord. Chem. Rev.* **2000**, 1, 78.

25) Calder, C. V.; Barton, J.; *J. Chem. Ed.*, **1971**, 48 338.

26) Demas, J. N.; Peterson, S. *J. Am. Chem. Soc.* **1976**, 101, 22, 6571.

27) a) Caswell, D.S.; Spiro, T. *Inorg. Chem.* **1987**, 26, 18. b) Ferguson, J.; Sasse, W. H. F. *Chem. Phys. Lett.* **1979**, 68, 21. c) Rillema, D. P.; Allen, G.; Meyer, T.J.; Conrad, D. *Inorg. Chem.* **1983**, 22, 1617.

28) Turro, N. *Modern Molecular Photochemistry* 1st ed., Benjamin/Cummings, Menlo Park, **1978**, Chapter 5.

29) Ayala, N. P.; Flynn Jr., C. M.; Sacksteder, L.; Demas, J. N.; DeGraff, B. A. *J. Am. Chem. Soc.* **1990**, 112, 3839.

30) Tsubomara, T.; Igarashi, O.; Norita, M. *Chem. Lett.* **1992**, 385.

31) Lever, A.B.P.; Seymour, P.; Auburn, P. *Inorg. Chim. Acta*, **1988**, 145, 43, 48.

32) Horvaith, A.; Stevenson, K. L. *Coord. Chem. Rev.* **1996**, 153, 57.

33) Gafney, H. D.; Adamson, A. *J. Am. Chem. Soc.* **1972**, 94, 8238.

34) Casalboni, F.; Mullazzini, Q. G.; Clark, C. D. Hoffman, M. Z.; Orizondo, P. L.; Perkovic, M. W.; Rillema, D. P. *Inorg. Chem.* **1997**, 36, 2252

35) Hosek, W.; Tysoe, S. A.; Baker, A. D.; Strekas, T. C.; Gafney, H. D. *Inorg. Chem.* **1989**, 28, 1228.

36) Jolly, W.L. *Modern Inorganic Chemistry* 2nd ed., MacGraw-Hill, New York, **1991**, Chapter 19.

37) Balzani, V.; Carassiti, V. *Photochemistry of Coordination Compounds*, 1st ed., **1970**, Academics Press, New York, Chapter 19.

38) Rich, R. L.; Taube, H. *J. Am. Chem. Soc.* **1954**, 76, 2608.

39) Wright, R.C.; Laurence, G.S. *J.C.S. Chem. Comm.* **1972**, 132.

40) *Psiplot Version 4.5 for Windows*, 32 bit edition, **1995**, Poly Software International, Salt Lake City.

41) Ginzburg, S.I. *Analytical Chemistry of the Platinum Metals* 1st ed. **1975**, Wiley, New York, p 68.

42) Roundhill, M. *J. Am. Chem. Soc.* **1985**, 107, 6284.

43) Archibald, E.H. *J. Chem. Soc. Trans.* **1920**, 117, 1104.

44) Griffith, W.P. *The Chemistry of the Rarer Platinum Metals* 1st ed., **1967**, Interscience Publishers, New York, Chapter 4.

45) Cady, A. H.; Connick, R. E. *J. Am. Chem. Soc.* **1958**, 80, 2646. b) Connick, R. E. *Advances in Chemistry of Coordination Compounds* (Ed. S. Kirschner), MacMillan New York, **1961**, Chapter 1. c) Connick, R. E.; Fine, D. A. *J. Am. Chem. Soc.* **1961**, 83, 3414.

46) Quanta-Ray DCR2A Pulsed Nd-YAG Laser Instruction Manual, **1982**, Spectra-Physics.Mountain View.

47) Robb, W.; Harris G. M. *J. Am. Chem. Soc.* **1965**, 87, 4472.

48) Cotton, A.; Wilkinson G. *Advanced Inorganic Chemistry* 5th ed., **1988**, Wiley, New York

49) Miano, R.; Garner, C. S. *Inorg. Chem.* **1965**, 4, 337.

50) Ingeborg, A.; Garner, P.; Garner, C. S. *J. Am. Chem. Soc.* **1961**, 84, 2032.

51) Cameron, R. Ph.D. Dissertation, Princeton Univerity, **1986**.

52) Jordan, R.B. Reaction *Mechanisms of Inorganic and Organometallic Systems* 2nd ed., Oxford Unviversity Press, New York, **1998**.

53) Wrighton, M.; Markham, J. *J. Phys. Chem.* **1973**, 77, 3042.

54) Lin, C.; Botcher, W; Chou, M.; Creutz, C.; Sutin, N. *J. Am. Chem. Soc* **1976**, 98, 6536.

55) Robb, W.; Harris, G.M. *J. Am. Chem. Soc.* **1965**, 87, 4472.

56) Demas, J. N.; AddingtonJ. *J. Am. Chem. Soc.* **1976**, 98, 5800.

57) Demas, J. N.; Adamson, A. *J. Am. Chem. Soc.* **1971**, 93, 1800.

58) Demas, J. N.; Adamson, A. *J. Am. Chem. Soc.* **1973**, 95, 5159.

59) Brunschwig, B. S.; Sutin, N. *Inorg. Chem.* **1979**, 18, 1731.

60) Martin, D.S. *Adv. Ser. Chem.* **1971**, 98, 74.

61) Tanabe, Y.; Sugano, S. *J. Phys. Soc. Japan.* **1954**, 9.

62) Jorgenson, C. K. *Acta. Chem. Scand* **1956**, 10, 518.

63) Schlesinger, H.; Tapley, M. *J. Am. Chem. Soc.* **1924**, 46, 276.

64) Jorgenson, C. K. *Acta Chem. Scand* **1956**, 10, 500.

65) Jorgenson, C. K. *Acta Chem. Scand* **1957**, 11, 355.

66) Cohen, A.J.; Davidson, N. *J. Am. Chem. Soc.* **1951**, 73 1955.

67) Elding, L.I.; Olssen, L.F.; *J. Phys. Chem.* **1978**, 8269.

68) Jorgenson, C. K.; Brinen, J.S. *Mol. Physics* **1962**, 5, 535.

69) Piepho, S. B.; Dickinson, J.R.; Spenser, J.A.; Schatz, P.N. *Mol. Phys.* **1972**, 24, 609.

70) Jorgenson, C. K. *Acta Chem. Scand* **1956**, 10, 500.

71) Jorgenson, C. K. *Acta Chem. Scand* **1957**, 11, 151.

72) Engleman, R *J. Am. Chem. Soc.* **1962**, 84, 345.

73) Schlesinger, H. Tapley, M *J. Am. Chem. Soc.* **1924**, 46, 276.

74) Rehm, D.; Weller, A. *Isr. J. Chem.* **1970**, 8, 259.

75) Bards, A.; Parsons, R.; Jordan, J. *Standard Potentials in Aqueous Solution* 1st ed, Marcel Dekker, New York, **1985**.

76) Based upon the value for $Ru(bpz)_3^{2+}$, Hoffman, M. Private Communication, **1999**.

77) Lytle, F. E.; Petrovsky, L. M.; Carlson, L. R. *Anal. Chim. Acta* **1971**, 57 239.

78) Castellano, S.; Gunther, H.; Ebersole, S *J. Phys. Chem.* **1965**, 69, 4166.

79) Kramer, F. A.; West, R. *J. Phys. Chem.* **1965**, 69, 673.

80) Calder, I. C.; Spotswood, T.; Tanzer, C. I. *Aust. J. Chem.* **1967**, 20, 1195.

81) Cheney, B.V. *J. Am. Chem. Soc.* **1968**, 90, 5083.

82) Bryant, G. M.; Ferguson, J. E. *Aust. J. Chem.* **1971**, 24, 441.

83) Castellano, H; Gunther, H. *J. Phys. Chem.* **1965**, 69, 4166.

84) Nakomoto, K. *J. Phys. Chem.* **1960**, 64, 1420.

85) Krishnan, C. V.; Creutz, C.; Schwartz, H. A.; Sutin, N *J. Am. Chem. Soc.* **1983**, 105, 5617.

86) Rillema, D. P.; Mack, K. B. *Inorg. Chem.* **1982**, 21, 3849.

87) Rillema, D. P.; Callahan, R.W.; Mack, K.B. *Inorg. Chem.* **1982**, 21, 2589.

88) Hunziker, M.; Ludi, A. *J. Am. Chem. Soc.* **1977**, 99, 7370.

89) Dose, E.; Wilson, L. J. *Inorg. Chem.* **1978**, 17, 2660.

90) Haga, M. A. *Inorg. Chim. Acta* **1980**, 45, L183.

91) Braunstein, C.; Baker, A. D.; Strekas, T. C.; Gafney. H. D. *Inorg. Chem.* **1984**, 23, 857.